Petrogenesis of anorthosites of the Mesoproterozoic Kunene Intrusive Complex, NW Namibia: evidence from stable and radiogenic isotope and lithophile and highly siderophile trace element composition

vorgelegt von
Diplom-Geowissenschaftler
Philipp Gleißner
aus Berlin

Von der Fakultät VI – Planen Bauen Umwelt
der Technischen Universität Berlin
zur Erlangung des akademischen Grades
Doktor der Naturwissenschaften
Dr. rer. nat.

genehmigte Dissertation

Promotionsausschuss:

Vorsitzender: Prof. Dr. rer. nat. Wilhelm Dominik
Berichter: Prof. Dr. rer. nat. Gerhard Franz
Berichter: Dr. rer. nat. Kirsten Drüppel
Berichter: Prof. Dr. rer. nat. Rolf L. Romer

Tag der wissenschaftlichen Aussprache: 08.07.2010

Berlin 2011

D 83

Table of contents

Zusammenfassung

Anorthosit-Massive (so genannte *massif-type* anorthosites) sind charakteristische Bestandteile der proterozoischen Kruste. Anorthosit-Komplexe sind gewöhnlich großflächige Intrusionen, die aus Plagioklas-Kumulatgesteinen und kleineren Volumen assoziierter mafischer und granitischer Gesteine bestehen. Ihre Verbreitung ist auf das Proterozoikum beschränkt. Dies deutet darauf hin, dass zu dieser Zeit von heute abweichende tektono-thermale Bedingungen herrschten. Die dabei aktiven Krustenbildungsprozesse, die zur Bildung von *massif-type* Anorthositen geführt haben, sind jedoch noch Gegenstand der wissenschaftlichen Diskussion. Ihre Entstehung wird im Allgemeinen als partielles Schmelzen des oberen Erdmantels oder Aufschmelzung mafischer Unterkruste diskutiert, um das aluminiumreiche basaltische oder ferrodioritische Stammmagma zu erzeugen, dass für die Kristallisation großer Mengen Kumulus-Plagioklas notwendig ist.

Der 18.000 km^2 große Kunene-Intrusiv-Komplex erstreckt sich von Nordwest Namibia nach Südwest Angola und ist einer der größten *massif-type* Anorthosit-Komplexe weltweit. Die Gesteine des Kunene-Intrusiv-Komplexes intrudierten während des Mesoproterozoikums in das paleo- bis mesoproterozoische Basement des südlichen Kongo-Kratons. Die Anorthosite wurden nicht prograd metamorph überprägt und ermöglichen somit die direkte Erforschung der magmatischen Prozesse die während ihrer Entstehung aktiv waren. Zwei nacheinander folgend intrudierte Anorthosit Varietäten wurden im Arbeitsgebiet in Nordwest Namibia identifiziert. Der ältere Weiße Anorthosit besteht aus pyroxenführendem Anorthosit und Leukogabbronorit assoziiert mit Fe-Ti Oxid Erz. Der jüngere Dunkle Anorthosit wird durch olivinführenden Anorthosit und Leukotroktolith dominiert. Die Spurenelementgehalte und isotopische Zusammensetzung der beiden unterschiedlichen Anorthosit Varietäten geben neue Hinweise auf die Quelle und Zusammensetzung des Stammmagmas, ihre magmatische Entwicklung und die Rolle krustaler Kontamination während der Entstehung des Kunene-Intrusiv-Komplexes und proterozoischer *massif-type* anorthosite in allgemeinen.

Die Gesteine des Kunene-Intrusiv-Komplexes zeichnen sich durch gut erhaltene Kumulat-Texturen und ursprüngliche Mineralzusammensetzungen aus. Der ältere Weiße Anorthosit ist durch die magmatische Mineralvergesellschaftung Kumulus-Plagioklas (An_{39-64}) ± Kumulus-Orthopyroxen (X_{Mg} 0.57 – 0.72) + interstitiellen Ortho- und Klinopyroxen (X_{Mg} 0.57 – 0.78) + Ilmenit ± Magnetit gekennzeichnet. Spätmagmatischer Biotit und Amphibol umgeben Pyroxen und Fe-Ti Oxide und enthalten idiomorphe Apatiteinschlüsse. Häufige akzessorische Gemengteile sind Zirkon und Sulfide. Die jüngeren Dunklen Anorthosite zeigen ein primär magmatische Zusammensetzung aus Kumulus-Plagioklas (An_{53-65}) + Olivin (Fo_{56-74}) + interstitieller Ortho- and Klinopyroxen (X_{Mg} 0.64 – 0.74) + Ilmenit ± Magnetit ± Biotit. Die chemische Zusammensetzung der Weißen und Dunklen Anorthosite ist reich an Aluminium, Kalzium, Natrium, Eisen und Magnesium und spiegelt unterschiedliche Mengen von Plagioklas, Fe-Mg Silikaten und Fe-Ti Oxiden wieder. Beide Varietäten sind Plagioklas-

Kumulatgesteine, aber der Unterschied im Anorthitgehalt der Plagioklase und das Auftreten von entweder Pyroxen oder Olivin als Mg-Fe Hauptsilikatphase weisen auf einen signifikanten Unterschied in der Zusammensetzung des Stammmagmas hin.

Mit dem Ziel Hinweise auf die Quelle des Stammmagmas und den Einfluss krustaler Kontamination zu finden, wurden Mineralseparate und Gesamtgesteine der beiden Anorthosit Varietäten untersucht. Es wurden Gehalte lithophiler und hoch siderophiler Spurenelemente und Sauerstoff-, Strontium-, Neodym-, Blei- und Osmiumisotopie bestimmt.

Die Gesteine der Weißen Anorthosite sind angereichert an inkompatiblen lithophilen Spurenelementen. Die Chondrit-normierten Seltenerdelementmuster zeigen eine relative Anreicherung der LSEE über die MSEE und SSEE, und positive Europium-Anomalien, wie sie typisch für Plagioklas-Kumulatgesteine sind. Die initiale isotopische Zusammensetzung von Strontium ($^{87}Sr/^{86}Sr$ 0.7031 – 0.7043), Neodym ($^{143}Nd/^{144}Nd$ 0.5110 – 0.5107; εNd +2.1 – -3.1), und Blei ($^{206}Pb/^{204}Pb$ 16.21 – 17.09) überlappt zum Teil mit Mantelwerten und zeigt einen zunehmenden krustalen Einfluss. Das ist in guter Übereinstimmung mit der Sauerstoffisotopie von Plagioklasseparaten im Bereich von 6.2 bis 6.8 ‰ $\delta^{18}O$. Die hoch radiogene initiale Osmiumisotopie ($^{187}Os/^{188}Os$ 5 ± 2; γOs +3982) spiegelt die Assimilation von hoch radiogenem krustalen Material wieder. Im Gegensatz dazu, zeigen die Dunklen Anorthosite niedrigere absolute Konzentrationen lithophiler Spurenelemente. Ähnlich den Weißen Anorthositen zeigen ihre Chondrit-normierten Seltenerdelementmuster eine Anreicherung der LSEE über die MSEE und SSEE, und positive Europium-Anomalien. Die initialen Isotopien von Strontium ($^{87}Sr/^{86}Sr$ 0.7028 – 0.7036) und Neodym ($^{143}Nd/^{144}Nd$ 0.5112 – 0.5109; εNd +6.4 – +0.8) fallen in den Bereich eines verarmten bis nicht verarmten Mantel, wohingegen die Bleiisotopie ($^{206}Pb/^{204}Pb$ 16.18 – 16.94) von krustaler Kontamination dominiert wird. Übereinstimmend überlappt die Sauerstoffisotopie von Plagioklasseparaten von 5.6 bis 6.2 ‰ $\delta^{18}O$ mit Mantelwerten. Die initiale Osmiumisotopie ($^{187}Os/^{188}Os$) reicht von 0.2 ± 0.1 (γOs +48), im Rahmen der Unsicherheit überlappend mit Mantelwerten, bis zu radiogenen krustalen Werten von 1.14 ± 0.05 (γOs +872).

Haupt- und Spurenelementzonierung magmatischer Phasen, die während aufeinander folgenden Stadien der Kristallisation und Kumulation kristallisierten, wurden in situ analysiert um die magmatische Entwicklung während fraktionierter Kristallisation und krustaler Kontamination zu rekonstruieren. Neue Erkenntnisse über die Zusammensetzung des Stammmagmas wurden durch die Gehalte lithophiler Spurenelemente in Plagioklas gewonnen. Um Informationen über Kristallisationsprozesse vor dem Beginn der Plagioklaskristallisation zu gewinnen, wurde weiterhin die Konzentrationen hoch siderophiler Spurenelemente in den Anorthositen und ihren Oxidmineralen sowie in assoziierten Fe-Ti Erzen gemessen.

Plagioklas zeigt mehrheitlich einen weitständig-oszillierenden Zonarbau mit Variationen im Anorthitgehalt zwischen 3 und 5 mol.%, der durch die Bewegung der kristallisierenden Plagioklase in einem Magmareservoir mit periodischen Veränderungen der physiko-chemischen Bedingungen zu erklären ist. Die Plagioklase der Weißen Anorthosite sind durch variable aber hohe Konzentrationen

inkompatibler Spurenelemente charakterisiert. Die Chondrit-normierten Seltenerdelementmuster zeigen in allgemeinen eine Anreicherung der LSEE und starke positive Europium-Anomalien. Vereinzelt zeigt Plagioklas einen Zonarbau mit von Kern zum Rand zunehmenden Spurenelementkonzentrationen, verursacht durch zeitgleiche Kristallisation und krustale Kontamination. Die Plagioklase der Dunklen Anorthosite sind durch geringere Spurenelementkonzentrationen als die der Weißen Anorthosite gekennzeichnet. Gleichzeitig zeigen sie auch eine geringere Anreicherung der LSEE und weniger ausgeprägte Europium-Anomalien. Alle Plagioklase zeigen abnehmende Sr-Konzentrationen von grob- zu den mittelkörnigen Kristallen, in Übereinstimmung mit einer allmählichen Verarmung von Sr in der Schmelze während der Plagioklasfraktionierung. Das Spurenelementbudget der interstitiellen Phasen in beiden Anorthosit Varietäten spiegelt die Entwicklung des Magmas während der Plagioklasfraktionierung wieder. In Übereinstimmung mit vorhergehender extensiver Plagioklasfraktionierung zeigen interstitielle Phasen wie Pyroxen negative Europium-Anomalien. Zeitweilige krustale Kontamination, wie sie sich im Zonarbau einiger Plagioklase des Weißen Anorthosit manifestiert, kann jedoch diese fraktionierte Kristallisations-Signatur der Restschmelze überlagern. In Übereinstimmung damit zeigen sukzessive kristallisierte intercumulus Phasen wie Klinopyroxen und Apatit im Weißen Anorthosit keine negativen Europium-Anomalien.

Die hoch siderophilen Elemente in den Anorthositen des Kunene-Intrusiv-Komplex zeigen fraktionierte Chondrit-normalisierte Muster mit, von den Leukotroktolithen der Dunklen Anorthosite zum Leukogabbronorit der Weißen Anorthosite, zunehmender Anreicherung von Pt, Pd und Re über Ir, Os und Ru. Die zunehmend radiogene initiale Osmiumisotopie ist mit der zunehmenden Konzentration von Re korreliert und bestätigt eine zunehmende Kontamination mit krustalem Material. Die generell niedrigen Konzentrationen von Ir, Os und Ru weisen deutlich auf eine Fraktionierung von Olivin, Cr-spinell und Platingruppen-Mineralen während eines frühen Stadiums der magmatischen Entwicklung hin. Diese Interpretation ist in Übereinstimmung mit der Herkunft des Stammmagmas aus dem Mantel und seiner Akkumulierung in einer tief gelegenen Magmenkammer, wo sie sich durch fraktionierte Kristallisation von mafischen Mineralen zu einer aluminiumreichen basaltischen Zusammensetzung entwickelt. Nach diesem Model sind die beobachteten Mantel- bis Krustenwerte der Osmiumisotopie durch ist die sukzessive Kontamination mit radiogenem Osmium während des Aufstiegs und der Platznahme des fraktionierten Magmas zu erklären.

Zusammenfassend konnte festgestellt werden, die Spurenelement-Zonierungsmuster von Plagioklas und Interkumulusphasen zeigen, dass die älteren Weißen Anorthosite durch simultane fraktionierte Kristallisation von Plagioklas, Pyroxen und Fe-Ti Oxiden aus differenzierterer Schmelze mit signifikant krustalen Charakteristika entstanden sind. Der anschließend intrudierte Dunkle Anorthosit wurde durch fraktionierte Kristallisation von Plagioklas, Olivin und Fe-Ti Oxiden bei magmatischen Temperaturen über 1150°C aus Mantelschmelze, die nur geringe krustale Kontamination erfahren hat, gebildet.

Abstract

Massif-type anorthosite complexes that commonly form huge intrusions composed of plagioclase cumulate rocks with minor volumes of associated mafic and granitic suites are characteristic features of the Proterozoic crust. Their apparent temporal restriction to the Proterozoic suggests unique tectono-thermal conditions during this period, although the specific crust-forming processes that lead to their formation are still subject to debate. Their petrogenesis is generally discussed in terms of partial melting of upper mantle or melting of a mafic lower crustal source to generate high-Al basaltic or ferrodioritic parental melts, necessary for the formation of the high amounts of cumulus plagioclase.

The 18,000 km^2 Kunene Intrusive Complex extends from northwest Namibia into southwest Angola and is one of the largest massif-type anorthosite complexes in the world. The rocks of the Kunene Intrusive Complex intruded the Paleo- to Mesoproterozoic basement at the southern margin of the Congo Craton during the Mesoproterozoic. The anorthosites themselves were not subject to prograde postmagmatic metamorphism and hence allow the direct investigation of igneous processes active during their formation. Two successively emplaced anorthosite varieties have been recognized in the study area in NW Namibia. The older white anorthosite suite consists of pyroxene-bearing anorthosite and leucogabbronorite associated with Fe-Ti oxide ores, whereas the younger dark anorthosite suite is dominated by olivine-bearing anorthosite and leucotroctolite. The trace element and isotopic composition of the two anorthosite varieties put new constraints on the source and composition of the parental melt, its magmatic evolution and the role of crustal contamination during the formation of the Kunene Intrusive Complex and of Proterozoic massif-type anorthosites in general.

The rocks of the Kunene Intrusive Complex display well preserved magmatic cumulate textures and original mineral compositions. The rocks of the older white anorthosite suite are characterized by the igneous mineral assemblage of cumulus plagioclase (An_{39-64}) ± cumulus orthopyroxene (X_{Mg} 0.57 – 0.72) + interstitial ortho- and clinopyroxene (X_{Mg} 0.57 – 0.78) + ilmenite ± magnetite. Late magmatic biotite and amphibole surround pyroxene and Fe-Ti oxides and contain euhedral inclusions of apatite. Common accessories are zircon and sulfides. The younger dark anorthosite suite displays the primary magmatic assemblage of cumulus plagioclase (An_{53-65}) + olivine (Fo_{56-74}) + interstitial ortho- and clinopyroxene (X_{Mg} 0.64 – 0.74) + ilmenite ± magnetite ± biotite. Regarding their major element composition the anorthositic rocks of the white and dark anorthosite suite are rich in aluminium, calcium, sodium, iron and magnesium reflecting variable amounts of cumulus plagioclase, Fe-Mg silicates and Fe-Ti oxides. Although both units represent plagioclase cumulate rocks the difference in anorthite content of plagioclase and the occurrence of either pyroxene or olivine as major Mg-Fe silicate indicate a significant discrepancy in their parental melt compositions.

In order to constrain the source of the parental melt and the impact of crustal contamination mineral separates and bulk rocks of the two anorthosite varieties were investigated for their lithophile and

highly siderophile trace element composition and their oxygen, strontium, neodymium, lead and osmium isotopic composition.

The rocks of the white anorthosite suite are enriched in incompatible lithophile trace elements. Chondrite-normalized patterns display relative enrichment of LREE over MREE and HREE, and positive europium anomalies, typical to plagioclase cumulate rocks. The initial isotopic composition of strontium ($^{87}Sr/^{86}Sr$ 0.7031 – 0.7043), neodymium ($^{143}Nd/^{144}Nd$ 0.5110 – 0.5107; εNd +2.1 – -3.1), and lead ($^{206}Pb/^{204}Pb$ 16.21 – 17.09) overlap in parts with mantle values and display increasing crustal influence. This is in good agreement with the oxygen isotopic composition of separated plagioclase that ranges from 6.2 to 6.8 ‰ $\delta^{18}O$. The initial osmium isotopic composition is highly radiogenic ($^{187}Os/^{188}Os$ 5 ± 2; γOs +3982) and reflects the assimilation of highly radiogenic crustal material. The dark anorthosites, on the other hand, display lower absolute concentrations of lithophile trace element. Their chondrite-normalized REE patterns, like those of the white anorthosites, also display enrichment of LREE over MREE and HREE, and positive europium anomalies. The initial isotopic composition of strontium ($^{87}Sr/^{86}Sr$ 0.7028 – 0.7036) and neodymium ($^{143}Nd/^{144}Nd$ 0.5112 – 0.5109; εNd +6.4 – +0.8) falls in the compositional range of strongly depleted to undepleted mantel whereas the isotopic composition of lead ($^{206}Pb/^{204}Pb$ 16.18 – 16.94) is dominated by crustal contamination. This is in excellent agreement with the of oxygen isotope composition of separated plagioclase that ranges from 5.6 to 6.2 ‰ $\delta^{18}O$ and hence overlaps with mantle values. The initial osmium isotopic composition ($^{187}Os/^{188}Os$) ranges from 0.2 ± 0.1 (γOs +48), which overlaps in uncertainty with the composition of the mantle, to more radiogenic crustal-like values of 1.14 ± 0.05 (γOs +872).

Magmatic phases that crystallized during successive stages of crystallization and cumulate formation were analysed in situ for major and trace element zoning to constrain the magmatic evolution during fractional crystallization and crustal contamination. New insights into the composition of the parental melt were gained from the abundance of lithophile trace elements in cumulus plagioclase. In addition, the abundance of highly siderophile elements in anorthositic rocks and their oxide minerals, as well as of associated bodies of Fe-Ti ore was measured to obtain information on fractional crystallization processes prior to the onset of plagioclase formation.

The majority of plagioclase displays large-scale wavy oscillatory zoning with variations in anorthite content between 3 and 5 mol.%, reflecting movement of crystallizing plagioclase in the magma reservoir during recurrent changes of the physico-chemical conditions. Plagioclase of the white anorthosite suite is characterized by variable but high concentrations of incompatible trace elements. In general, their chondrite-normalized REE patterns display enrichment of LREE and strong positive europium anomalies. Occasionally, plagioclase display zoning in their trace element contents with increasing overall concentrations from core to rim, reflecting its crystallization contemporaneously with crustal contamination. Plagioclase of the dark anorthosite suite has lower concentrations of incompatible trace elements than that of the white anorthosite, shows less enrichment of the LREE and less accentuated positive europium anomalies. All plagioclases display

decreasing Sr concentrations from coarse- towards medium-grained crystals, consistent with the successive depletion of Sr in the melt during plagioclase fractionation. The trace element record of the interstitial phases in both anorthosite varieties reflects the evolution of the magma during plagioclase fractionation. In general, the interstitial phases like clinopyroxene display negative europium anomalies consistent with previous extensive plagioclase fractionation. Intermittent crustal contamination, as evident from trace element zoning of plagioclase of the white anorthosite, can superimpose this fractional crystallization signature of the residual melt. Accordingly, the successively crystallized intercumulus phases like clinopyroxene and apatite of the white anorthosite lack negative europium anomalies.

The highly siderophile element abundances of anorthositic rocks of the Kunene Intrusive Complex display fractionated chondrite-normalized patterns with increasing enrichment of Pt, Pd and Re over Ir, Os and Ru from leucotroctolite of the dark anorthosite suite towards leucogabbronorite of the white anorthosite suite. The more radiogenic initial composition of Os is correlated with the increasing abundance of Re and agrees well with increasing contamination by highly radiogenic crustal material. The general low concentrations of Ir, Os and Ru strongly suggest fractionation of olivine, Cr-spinel and platinum group minerals in an early stage of the igneous evolution. This interpretation is in agreement with a mantle origin of the parental melt and ponding in a deep seated magma chamber, where the magma evolved to high-Al basaltic upon fractional crystallization of mafic minerals. In this model, successive contamination with highly radiogenic crustal osmium during ascent and subsequent emplacement of the fractionated magma might be responsible for the observed elevated isotopic composition from mantle-like to crustal values.

To summarize, the trace element zoning patterns of plagioclase and intercumulus phases demonstrate that the older white anorthosite was derived by simultaneous fractional crystallization of plagioclase, pyroxene and Fe-Ti oxides from evolved melt that had significant crustal characteristics. In contrast, the subsequently emplaced dark anorthosite was formed by fractional crystallization of plagioclase, olivine and Fe-Ti oxides at magmatic temperatures above 1150°C from a mantle-derived parental melt that experienced only minor crustal contamination.

Acknowledgements

First of all, I wish to thank my advisors Prof. Dr. Gerhard Franz and Dr. Kirsten Drüppel for their guidance during this thesis. Prof. Dr. Gerhard Franz is thanked for his guidance through my study from the very beginning and interesting discussions during the last years. Dr. Kirsten Drüppel initiated and lead the project 'Genese der Anorthosite des Kunene Intrusive Complex, Namibia/Angola'. Many thanks for introduction into the subject-matter and accompaniment during the field work. Her patience during long walks in the field as well as during the last three years is greatfully acknowledged.

Cooperation, access to laboratories, introduction to measuring methods and help during interpretation of the results by Dr. Heinrich Taubald (Universität Tübingen), Prof. Dr. Rolf L. Romer (GFZ) and Prof. Dr. Harry Becker (FU-Berlin) is acknowledged. Dr. Heinrich Taubald guided the stable isotope analyses. Prof. Dr. Rolf L. Romer introduced me into the work in the clean room and the technique of mass spectrometer measurements. Prof. Dr. Harry Becker introduced me to the techniques of high-pressure digestion and the extraction of osmium and highly siderophile elements and their measurements.

I thank the staff of the Institut für Angewandte Geowissenschaften and Zentraleinrichtung Elektronenmikroskopie at Technische Universität Berlin, Arbeitsbereich Geochemie at Freie Universität Berlin and Sektion 4.2: Anorganische und Isotopen Geochemie at Deutsches Geoforschungszentrum. In particular I thank Christa Zecha (TU-Berlin) for careful sample preparation, Petra Marsiske (TU-Berlin) for XRF measurements, Ona Appelt (GFZ) and Francois Galbert (TU-Berlin) for assistance with electron microprobe analyses, Jörg Nissen (TU-Berlin) for scanning electron imaging, Sabine Rautenberg (TU-Berlin) for gas chromatrography, and Marc Weynell and Mario Fischer-Gödde (FU-Berlin) for help during the work in the clean room. Special thanks to Dr. Helene Brätz (University of Erlangen) for LA-ICP-MS measurements, Gabriele Stoschek (University of Tübingen) for O-isotope measurement and Dr. Knuth Hahne (GFZ) for ICP-MS analyses. During mineral separation Olesja Terre, Andreas Hertwig, Astrid Kowitz and Henrike Franke (TU-Berlin) were skilful assistants. Dr. Sönke Brandt (University of Kiel) provided samples from the Epupa Complex basement in NW Namibia and I wish to thank him for his unselfish support.

This project was part of the project 'Genese der Anorthosite des Kunene Intrusive Complex, Namibia/Angola' founded by the Deutsche Forschungsgemeinschaft (grant numbers DR 744/1-1 and DR 744/1-2). Two month founding by Fakultät VI of the Technische Universität Berlin is acknowledged.

Published parts

Parts of this thesis were prepared for publication in international journals and are either published, under review or in preparation. These parts are included as specific manuscripts except for layout and numbering of pages, figures and tables.

Chapter 2: Philipp Gleißner[1], Kirsten Drüppel[1] (2009). Spurenelementzonierung von Plagioklasen des Kunene-Intrusiv-Komplexes (NW-Namibia). *Zentralblatt für Geologie und Paläontologie*, Teil I VIII, 3/4, 267-286.

Chapter 3: Philipp Gleißner[1], Kirsten Drüppel[1], Heinrich Taubald[2] (2010). Magmatic evolution of anorthosites of the Kunene Intrusive Complex, NW Namibia: evidence from oxygen isotope data and trace element zoning. *Journal of Petrology* Vol. 51, Nr. 4, 897-919.

Chapter 4: Philipp Gleißner[1], Kirsten Drüppel[1], Rolf L. Romer[3] (in press). The role of crustal contamination in massif-type anorthosites, new evidence from Sr-Nd-Pb isotopic composition of the Kunene Intrusive Complex, NW Namibia. *Precambrian Research,* DOI: 10.1016/j.precamres.2010.11.004

Chapter 5: Philipp Gleißner[1], Kirsten Drüppel[1,4], Harry Becker[4] (in preparation). Osmium isotopes and highly siderophile element fractionation in the massif-type anorthosites of the Mesoproterozoic Kunene Intrusive Complex, NW Namibia. *Chemical Geology*

[1]Technische Universität Berlin, Institut für Angewandte Geowissenschaften, Ackerstr. 71-76, 13355 Berlin, Germany

[2]Universität Tübingen, Institut für Geowissenschaften, Wilhelmstr. 56, 72074 Tübingen, Germany

[3]Deutsches GeoForschungsZentrum, Telegrafenberg, 14473 Potsdam, Germany

[4]Freie Universität Berlin, Institut für Geologische Wissenschaften, Malteserstr. 74-100, 12249 Berlin, Germany

Chapter 1
Introduction

1.1 General characteristics of Proterozoic massif-type anorthosites

1.1.1 Nomenclature and some historical aspects of anorthosite research

Anorthosites are igneous rocks that consist of ≥90 % plagioclase (Fig. 1.1). The term ‘anorthosite’ derives from the dominance of triclinic (anorthose) feldspar and was first used by T. S. Hunt as early as 1863. A classification of anorthosites and anorthositic rocks was first introduced by Buddington (1939) and later adopted by the IUGS Subcommission on the Systematics of Igneous Rocks (Streckeisen, 1976). Rocks that consist of more than 65 % plagioclase are termed leucotroctolite, olivine leucogabbro (norite) and leucogabbro (norite), depending on whether the dominant mafic mineral is olivine or clinopyroxene (orthopyroxene). Although not specified in the IUGS nomenclature, they are referred as ‘anorthositic rocks’ in much of the present literature. Oxide minerals, mostly ilmenite and magnetite, occur and the prefix ‘oxide-rich’ is used if their modal amount exceeds 10 vol.%.

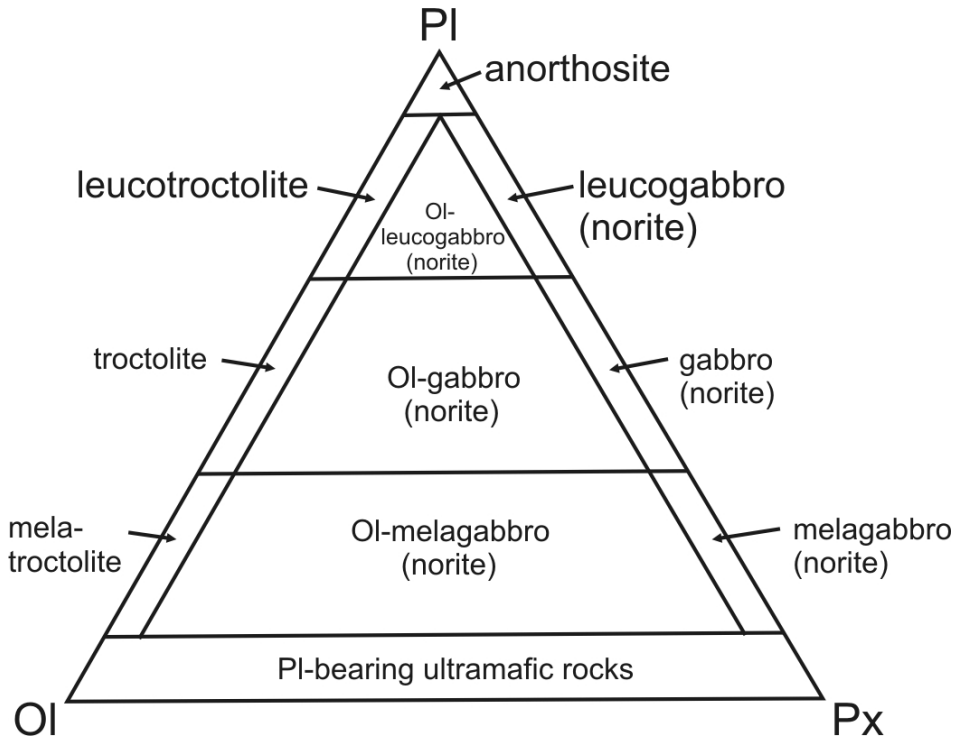

Fig. 1.1. Classification of anorthositic rocks after Streckeisen (1976).

The peculiarity of the nearly monomineralic anorthosites together with their often enormous intrusion size (up to 18,000 km^2) attracted scientists since more than 100 years. After discovery in the early seventies that anorthosites are a major component of the lunar highlands, the investigation of terrestrial anorthosites was intensified, both in their own right and as a lunar analogue (e.g. Emslie, 1978, 1985; Morse, 1982; Duchesne, 1984; Wiebe, 1992). Terrestrial anorthosites are nowadays not longer recognised as lunar analogues but as important features related to the differentiation of the earth (and possibly other planets) and the formation and evolution of the continental crust (Taylor & McLennan, 1985).

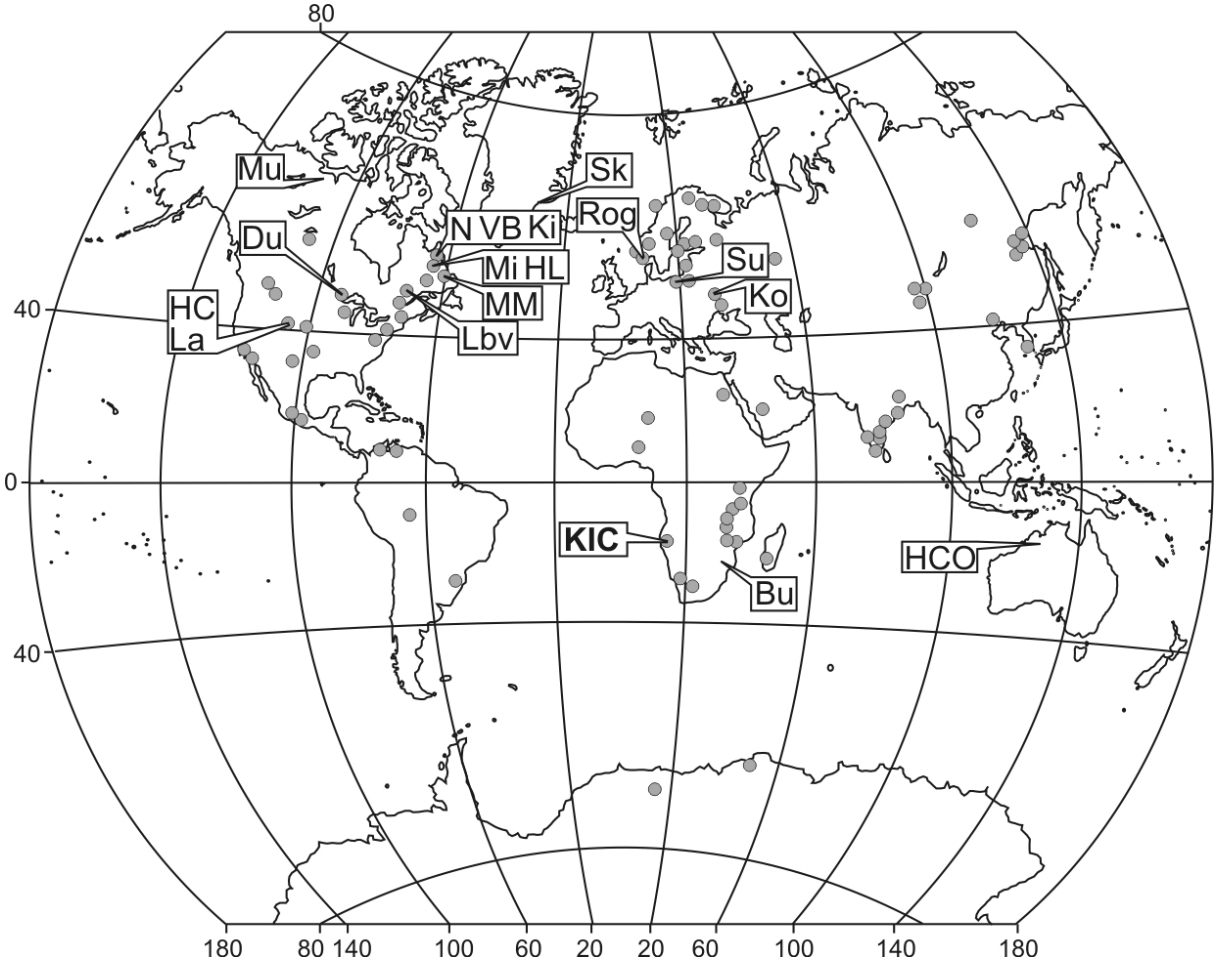

Fig. 1.2. World map showing locations of Proterozoic massif-type anorthosites (taken from Ashwal, 1993). The locations of the Kunene Intrusive Complex (KIC) and several other massif-type anorthosite occurrences and layered intrusions, mentioned in this study, are indicated. Anorthosite massifs: HC Horse Creek; HL Harp Lake; Ko Korosten; La Laramie; Lbv Labreville; Mi Michikamau; MM Mealy Mountains; N Nain; Rog Rogaland; Su Suwałki. Layered mafic intrusions: Bu Bushveld; Du Duluth; HCO layered intrusions in the Halls Creek orogen; Ki Kiglapait; Mu Muskox; Sk Skaergaard; VB Voisey`s Bay.

Different anorthosite types occur over the entire range of the geological timescale but all are remarkably plagioclase cumulate rocks and all lack volcanic equivalents. Based on age and features like composition and associations with other rock types Ashwal (1993) distinguished six basic anorthosite types. 1) The ***Archean anorthosites*** which display equidimensional, clacic plagioclase megacrysts in a fine-grained groundmass of broadly basaltic composition. They are restricted to Archean terranes and many are highly metamorphosed. 2) The ***Proterozoic massif-type anorthosites*** are the most voluminous anorthosites on earth and differ from the Archean by the lower anorthite content of their plagioclases (usually 40-60 mol.%) and the absence of a fine-grained groundmass. 3) ***Anorthosites in layered mafic intrusions*** are discrete layers of significant thickness. The anorthosites together with other plagioclase cumulate rocks usually occur in the upper zone of mafic layered intrusions overlying an ultramafic lower zone. 4) Minor ***anorthosites in oceanic settings*** are interpreted as cumulates formed from the crystallization of basaltic magmas in the lower oceanic crust. 5) ***Anorthosite inclusions in other igneous rocks*** were found in varying compositions from basalt to granite to kimberlite. They represent either accumulations of plagioclase from the same magmas as their host (cognate inclusions) or fragments of older anorthosite (xenolithic inclusions). 6) The ***extraterrestrial anorthosites*** are major component of the lunar highlands and possibly other inner planets of the solar system.

The Proterozoic massif-type anorthosites which are subject to this study are the most abundant of the terrestrial types and are restricted to the Proterozoic continental crust. They occur as small plutons to huge composite complexes on all continents (except Australia) with predominance on the northern hemisphere (Fig. 1.2). Ashwal (1993) gives a number of 131 occurrences in total. As important constituents of the Proterozoic crust they reach up to ~10 % of the exposed surface in the Grenville and the Nain/Churchill Provinces of eastern North America.

1.1.2. The problem of Proterozoic massif-type anorthosites

Several periods of the earth history are characterized by the occurrence of specific rock types, for instance the mafic magmas that formed komatiites and the felsic magmas of the tonalite-trondhjemite-granodiorite suite in the Archean and the S-type granites after the Archean. The restrictions of these rocks to limited periods of the earth history is widely believed to reflect changing conditions for differentiation and crust forming processes in the dynamic earth system. Since the current oceanic crustal record does not persist beyond about 200 million years, except for small fragments, the memory of such early events will be found only in the continental crust.

The temporal restriction of Proterozoic massif-type anorthosites to a particular, although long, period of geologic time suggests unique tectono-thermal conditions during the time of their formation, which is directly related to the enduring problem of mantle-crust interaction and the growth rates of the continental crust. The source and origin of Proterozoic anorthosites is therefore relevant to any

discussion of the evolution of the continental crust. Moreover, Taylor & McLennan (1985) elevated the question of the origin of massif-type anorthosites to a status close to that previously occupied by the 'granite problem'. In terms of their strong restriction to a particular period of the earth history the massif-type anorthosites are similar to the megacrystic anorthosites which are restricted to the Archean but their textural features are more similar to the anorthosites in layered intrusions, which notably occur throughout the entire earth history.

A fundamental unanswered question about anorthosites relates to the tectonic environment of their origin, which is considered as one of the key issues in future research (Ashwal, 2004). The typical association of massif-type anorthosites with high-grade metamorphic rocks is interpreted to reflect their intrusion into older, already stabilized cratonic crust (see reviews by Emslie, 1978; Morse, 1982; Wiebe, 1992). The apparent chemical bimodality of coeval anorthositic and granitoid suites has further been used to argue for a continental rift or incipient rift setting (e.g. Emslie, 1978; Windley, 1993; Corrigan & Hanmer, 1997; Mukherjee & Das, 2002a). The latter concept is also favored because it provides room for the voluminous plutons (Morse, 1982). In more recent years, the geometry and scale of the anorthosites of eastern North America were tentatively interpreted as a time and depth-stretched analogue to the large scale, repeated Cenozoic magmatic activity of the plume derived Cameroon Line (Morse, 2006). In contrast to the proposed anorogenic within-plate settings, the spatial relation of many anorthosite complexes with deep lithospheric structures, like Archean-Proterozoic craton boundaries (e.g. Nain, Laramie, Rogaland), is interpreted as controlling factor for the emplacement of anorthosites (see Duchesne et al., 1999 for a review). The reactivation of pre-existing anorthosite-bearing terranes (e.g. Horse Creek and Laramie Complex; Frost et al. 2000) put further question marks on this issue but may be interpreted in support of the model of a structural controlled emplacement.

Massif-type anorthosites comprise mainly anorthosites *sensu stricto* and other anorthositic rocks of which no volcanic equivalent is known. Together with the lack of ultramafic counterparts this mode of occurrence is often described as the 'anorthosite problem' (see Ashwal, 1993 for a review). From the petrographic point of view it was N. L. Bowen who stated already in 1917, that:

'Seldom can it be truly said that the puzzling feature of any object is its simplicity, yet of all the problems that the anorthosites present to us for solution the most difficult is their simple mineralogical composition.'

It is nowadays widely accepted that the coarse-grained igneous textures present in massif-type anorthosites as well as their huge intrusion size reflect crystallization from a melt volume of considerably size followed by plagioclase accumulation. Older theories like meteorite impacts, a metasomatic origin by 'anorthositization' or their origin as a residual after removal of felsic melt during deep crustal anatexis were not accepted as a viable explanation of anorthosite petrogenesis (see Ashwal, 1993 for a review). Whether these plagioclases sink (e.g. Scoates, 2000) or float (as assumed

for most petrogenetic models) on the magma from which they crystallized and of which we still don't know the chemical composition is still matter of discussion (e.g. Mukherjee & Das, 2002b; Scoates, 2002). The formation of the almost monomineralic plagioclase-rocks is further discussed in terms of crystal mush intrusion, syn-emplacement deformation and recystallization, and trapped melt fractions (for further discussion of petrogenetic models see section 1.1.6).

In as much as the tectonic setting is important, which allows the delivery of large volumes of primitive parental magma, it is the question were do the magmas comes from and how do they evolve to form the massif-type anorthosites. An increasing number of chemical and isotopic studies on anorthosites were published in the last 40 years. The results are subject to ongoing debate and were sometimes considered ambiguous or conflicting in resolving the problem. The interpretation of the petrographic and geochemical features of massif-type anorthosites as well as the origin of associated rocks and the tectonic setting largely depends on the position of the particular author to the main question: What was the composition and source of parental magma? i.e. basaltic vs. ferrodioritic and mantle vs. crust. The problem can also be reduced to the question: Was anorthosite formation a crust-forming process or simply a recycling process of pre-existing crustal material? However, the composition and source of the parental magmas, capable of crystallizing large amounts of relatively homogeneous plagioclase, is indispensable for further progress in tectonic and petrogenetic models but has remained an enduring problem in igneous petrology.

1.1.3 General field relations and associated rocks

Proterozoic massif-type anorthosites are intrusive complexes that cover hundreds to thousands of km^2 surface area. They are dominated by anorthositic lithologies with minor volumes of comagmatic mafic and intermediate to granitoid rocks (Wiebe, 1992; Ashwal, 1993). Fe-Ti ore bodies of variable composition and size occur in many anorthosite complexes and can reach economic importance (Ashwal, 1993; Charlier et al., 2006). Late-stage magmatism in anorthosite complexes occasionally involves the emplacement of high-Al gabbros and dolerite dykes (e.g. Mitchell et al., 1995; Evans et al., 1999; Scoates & Mitchell, 2000).

Most anorthosite complexes are composed of several individual plutons that span a structural range from massive to layered to diapiric (Wiebe, 1992). The dominant plagioclase-rich plutons in anorthosite complexes consist of anorthosite *sensu stricto* and anorthositic rock suites like leucotroctolite, leuconorite or leucogabbronorite. Gravity and seismic studies on massif-type anorthosites suggest that they are thin, slab-like or 'pancake'-shaped bodies of broad horizontal extent (see reviews in Wiebe, 1992 and Ashwal, 1993). Gravity studies also demonstrate the scarcity of ultramafic counterparts underlying the plagioclase cumulate rocks (Morse, 1982, and references therein). However, local positive Bouguer anomalies over massif-type anorthosite suggest that mafic

rocks may reside deeper in the lower crust or at shallow mantle depths (see discussion in Morse, 1982).

The associated mafic suite commonly includes norite, gabbro and troctolite whereas larger volumes of ultramafic rocks, although present in some massifs in minor amounts, are notably absent. The spatially associated felsic suite ranges in composition from monzonite (or mangerite/adamellite) to granite (or charnockite). The common association of anorthositic cumulate rocks and intrusive felsic rocks in the Grenville and Labrador Provinces is termed anorthosite-mangerite-charnockite-granite (AMCG) suite (Emslie & Hegner, 1993; Emslie et al., 1994). Whereas the more mafic rocks are easily identified as cumulate rocks that belong to the 'anorthosite suite' (e.g. Ashwal, 1993; Vander Auwera et al., 2006) the origin of the intermediate to felsic suite is more controversial. The root of the matter is whether the felsic suite is consanguineous with the anorthosites or represents a separate magmatic unit that evolved from intracrustal partial melting. Ferrodiorite (also termed hypersthene monzodiorite or jotunite) occurs as dykes and marginal facies in many complexes and displays chemical and petrographic characteristics of both suites. These rocks are interpreted as ferrodioritic melts that are derived by intracrustal melting of mafic lower crust. The most primitive ferrodiorite varieties are regarded as parental melts to the associated anorthosites (e.g. Vander Auwera et al., 1998; Bolle et al., 2003). Other authors interpret ferrodioritic rocks as residual melts after plagioclase fractionation and at the same time parental to the more evolved felsic suite (e.g. Emslie et al., 1994; Mitchell et al., 1996; Scoates et al., 1996; Markl, 2001).

Fe-Ti ore bodies occur in massif-type anorthosites as gradual layers within oxide-rich gabbros or massive ore bodies with sharp, irregular contacts to surrounding anorthosite (Ashwal, 1993). They are composed of variable amounts of magnetite, ilmenite, apatite, plagioclase and Mg-Fe silicates. Ores containing significant silicates are classified as gabbroic Fe-Ti oxide ores and silicate-free, apatite-rich varieties as nelsonites (Kolker, 1982; Duchesne, 1999). Fe-Ti oxide ores associated with andesine massif-type anorthosite are currently exploited in the Tellnes deposit (Rogaland, Norway) and the Tio Mine (Lac Allard, Canada) for Fe and Ti but may also contain significant resources for V (Ashwal, 1993; Charlier et al., 2006).

The discovery of the Voisey's Bay Ni-Cu-Co magmatic sulfide deposit, hosted by a troctolitic-gabbroic intrusion within the Nain Plutonic suite, triggered intensive investigation on the evolution of such high-Al basaltic magmas and their sulfide deposit potential. Based on sulfur and Ni contents and osmium isotopic composition a model of high-Mg parental magma and an external source of sulfur is suggested for the formation of such massif-type anorthosite related sulfide deposits (Lambert et al., 2000; Scoates & Mitchell, 2000). However, yet no comparable sulfide deposit was found in other anorthosite complexes and the economic important Voisey's Bay deposit probably represents a petrologic oddity.

Late stage gabbros, characterized by high Al_2O_3 content (15 - 20 wt.%), form intrusions that crosscut anorthositic rocks and associated felsic rocks and are considered to represent younger

samples of the anorthosite parental magma (Ashwal, 1993, and references therein; Mitchell et al., 1995; Scoates & Mitchell, 2000). Dolerite dykes were reported from several anorthosite complexes. Available isotopic data are interpreted as reflecting nearly uncontaminated mantle-derived parental melts (Evans et al., 1999) or primary melts of lower crustal origin (Shumlyanskyy et al., 2006).

1.1.4 Petrography and geochemistry

Massif-type anorthosites generally display well-preserved magmatic features like cumulus textures and igneous layering. The term *'massif-type'*, although ingrained in the literature, is unfortunate and refers to a 'plutonic mass of moderate size' not to the internal texture (Ashwal, 1993). Anorthosites that have been affected by metamorphism and deformation commonly preserved relict igneous features. Unmetamorphosed massif-type anorthosites as for example the Rogaland Complex and the Kunene Intrusive Complex are characterized by coarse grain size, with plagioclase commonly in the range of 1-10 cm. The plagioclase and Mg-Fe silicates occur in a wide variety of textures ranging from orthocumulate to adcumulate with subophitic to intergranular textures. Igneous lamination of euhedral plagioclase crystals is as common as randomly oriented or polygonal plagioclase in adcumulus textured anorthosite *sensu stricto*.

Plagioclase of massif-type anorthosites falls in the compositional range of An_{35-70}. Individual anorthosite occurrences display relatively uniform anorthite contents of their plagioclase (Ashwal, 1993). Compositional zoning is described in few publications but was not studied systematically. Wiebe (1990) interpreted oscillatory zoning in the anorthite content of plagioclase as reflecting growth in a convecting magma chamber during several episodes of replenishment with fresh magma. Reversed rims on plagioclase are a general feature observed in many massif-type anorthosites and layered intrusions. From their occurrence in linear networks Morse & Nolan (1984) suggested that they are the last trace of the intercumulus liquid.

Mafic silicates in massif-type anorthosites are mainly orthopyroxene and olivine. Both occur as cumulus and interstitial phases together with clinopyroxene and Fe-Ti oxides. Their X_{Mg} values range from 0.50 to 0.75 and were interpreted to reflect crystallization from fractionated magmas (Ashwal, 1993, and references therein). Minor amounts of amphibole, biotite, apatite and accessory zircon and sulfides might be present. Although the anorthosite classification based on anorthite content of plagioclase is not generally accepted a trend can be observed whereby the so called 'andesine-type' anorthosites tend to contain orthopyroxene whereas the 'labradorite-type' anorthosites often show olivine. Because both types can be closely associated in a single anorthosite complex, either more advanced fractionation of the magmas in the deep crustal magma chamber (Emslie, 1978) or crustal contamination is considered as a controlling factor (Ashwal, 1993).

Bulk compositions of anorthositic rocks primarily reflect the variable amount and composition of their cumulus phases. On the basis of major elements data petrogenetic trends (e.g. fractionation of a

parental melt) remain almost unclear, because discrimination diagrams are based on volcanic rocks which represent crystallized melt compositions but are not suitable for cumulate rocks. On the other hand the modal accumulation and ratio of cumulus phases like plagioclase and Fe-Mg silicates is visible in variation diagrams (e.g. Markl & Frost, 1999). Intermediate X_{Mg} values of the rocks (usually <0.60) are interpreted to imply crystallization from fractionated melts (Ashwal, 1993) but in parts also reflect variable abundances of Mg-Fe silicates and Fe-Ti oxides.

All types of anorthosites are enriched in trace elements compatible in the plagioclase structure (i.e. Sr and Eu) and are depleted in all other lithophile trace elements (Ashwal, 1993). An inverse correlation between strontium concentration and anorthite content of plagioclase is observed in more detailed studies and is attributed to co-crystallization of clinopyroxene (e.g. Wiebe, 1990). A similar correlation is commonly observed in mafic layered intrusions were it is attributed to plagioclase fractionation (e.g. Ashwal, 1993). Massif-type anorthosites are characterized by light REE enrichment when compared to the middle and heavy REE, and conspicuous positive europium anomalies which certainly rules out substantial fractionation of plagioclase prior to the anorthosite formation.

1.1.5 Crystallization conditions

High-alumina orthopyroxene megacrysts (5 - 12 wt.%), that are present in many massif-type anorthosites, constrain their early crystallization at pressures of 10 - 13 kbar (Ashwal, 1993, and references therein). Based on thermobarometric studies of contact areoles and mineral equilibria of lately crystallized anorthosite phases (mainly pyroxene), on the other hand, a shallow-level emplacement of anorthosites is postulated (e.g. Valley & O'Neil, 1982; Markl et al., 1998). Ashwal (1993) summarizes middle to upper crustal pressures from 3 to 6 kbar although higher pressures (6 - 8 kbar) were estimated for several anorthosites (e.g. Wilmart et al., 1994; Drüppel et al., 2001).

Temperature estimates for the crystallization of massif-type anorthosites are scarce but believed to be in the range of mafic plutonic rocks (Taylor, 1968). Farquhar et al. (1993) reported temperatures of 1000 - 1080°C for the Sybille intrusion of the Laramie Anorthosite Complex. Markl et al. (1998) obtained similar results from pyroxene equilibrium thermometry in anorthositic rocks from the Lofoten. The oxygen fugacity during crystallization increases from ~FMQ in olivine-bearing anorthosites and leucotroctolites to ~NNO in pyroxene-bearing anorthosites and leucogabbronorite (Morse, 2006) towards >NNO in the intermediate and felsic suite (Scoates, 2000).

1.1.6 Petrogenetic models and problems

A petrogenetic model for the formation of massif-type anorthosites is necessarily not only an attempt to explain the formation of the anorthosites itself but also the origin and formation of the associated felsic suite and Fe-Ti ore. Regarding the anorthosite petrogenesis, the following key issues have to be

evaluated: 1) The composition of the parental melt (basaltic vs. ferrodioritic), 2) The source of the parental melt. (mantle vs. lower crust), 3) The magmatic evolution of the parental melt, 4) The role of crustal contamination, 5) The crystallization and emplacement conditions, 6) The tectonic setting in which the anorthosite petrogenesis took place, and regarding to their temporal restriction: 7) Is there a petrogenetic feature, e.g. chemical or physical conditions, that is unique to the Proterozoic?

Many authors favour the model of Ashwal (1993; Fig. 1.3a) which assumes plagioclase fractionation from mantle-derived high-Al basaltic parental melt in a lower crustal or upper mantle magma chamber (e.g. Scoates & Frost, 1996; Morse, 2006). The Fe-rich nature of mafic minerals within anorthosite is consistent with parental magmas that fractionated considerably mafic silicates prior to the fractionation of the anorthosites. The maintenance of plagioclase saturation is assumed by some authors by periodical assimilation of plagioclase restitic crust or by continued recharge with high-Al magma (e.g. Emslie et al., 1994). Under conditions at the mantle-crust boundary plagioclase is believed to float on this Fe-rich melt, producing anorthositic flotation cumulates at the top of the magma chamber. The plagioclase-rich crystal mushes are gravitationally unstable, rise through the crust as diapirs and coalesce in the upper crust. According to this model, crustal contamination of the parental magma accounts for chemical and isotopic variations of different massif-type anorthosites. Heat from the crystallizing mafic magmas is expected to cause lower to middle crustal anatexis, thereby producing silicic melts parental to the intermediate to felsic suite. In contrast, several recent studies propose a consanguineous relation of anorthositic and felsic suites (e.g. Mitchell et al., 1996; Scoates et al., 1996; Markl, 2001). An interesting but seldom persecuted version of this model, with regard to the extremely high amount of modal plagioclase of the rocks, is the expulsion of some of the transporting melt during emplacement of a low-Al basalt into higher crustal levels (Miller & Weiblein, 1990).

As noted by Scoates (2000), however, plagioclases in massif-type anorthosites show a limited range of plagioclase compositions and lack normal zoning which would be expected in case of factional crystallization from a basaltic melt. In addition, experimental liquidus equilibria of synthetic high-Al gabbro cannot produce the full range of rocks observed in massif-type anorthosites (Longhi et al., 1999). Furthermore, there is no evidence of voluminous ultramafic cumulates complementary to exposed anorthosites (Wiebe, 1992; Ashwal, 1993). An increasing number of authors therefore support the alternative model of Duchesne et al. (1999), in which the parental magma is ferrodioritic in composition and evolves from melting of a tongue of suitable composition within underthrusted lower crust (Fig. 1.3b). The fundamental differences to the mantle model are the mafic lower crustal source and the necessity for a special tectonic setting in which partial melting of lower crust is possible. The anorthosite formation is interpreted in a similar way like the mantle model of Ashwal (1993), the plagioclase floats to accumulate at the roof of a deep-seated magma chamber and mafic silicates sinks. Anorthosite diapirs rise through the crust, channelled by crustal structures, generated during the ancient stacking of terranes, instead of rising vertically. The mafic cumulates sink and become

indistinguishable from the mantle. Isotopic and chemical variations between and within massif-type anorthosites are interpreted to reflect lower crustal heterogeneity and previous complex crustal history. According to this model acidic melts are produced during a first step of mafic lower crust melting and also by later differentiation of the mafic magma.

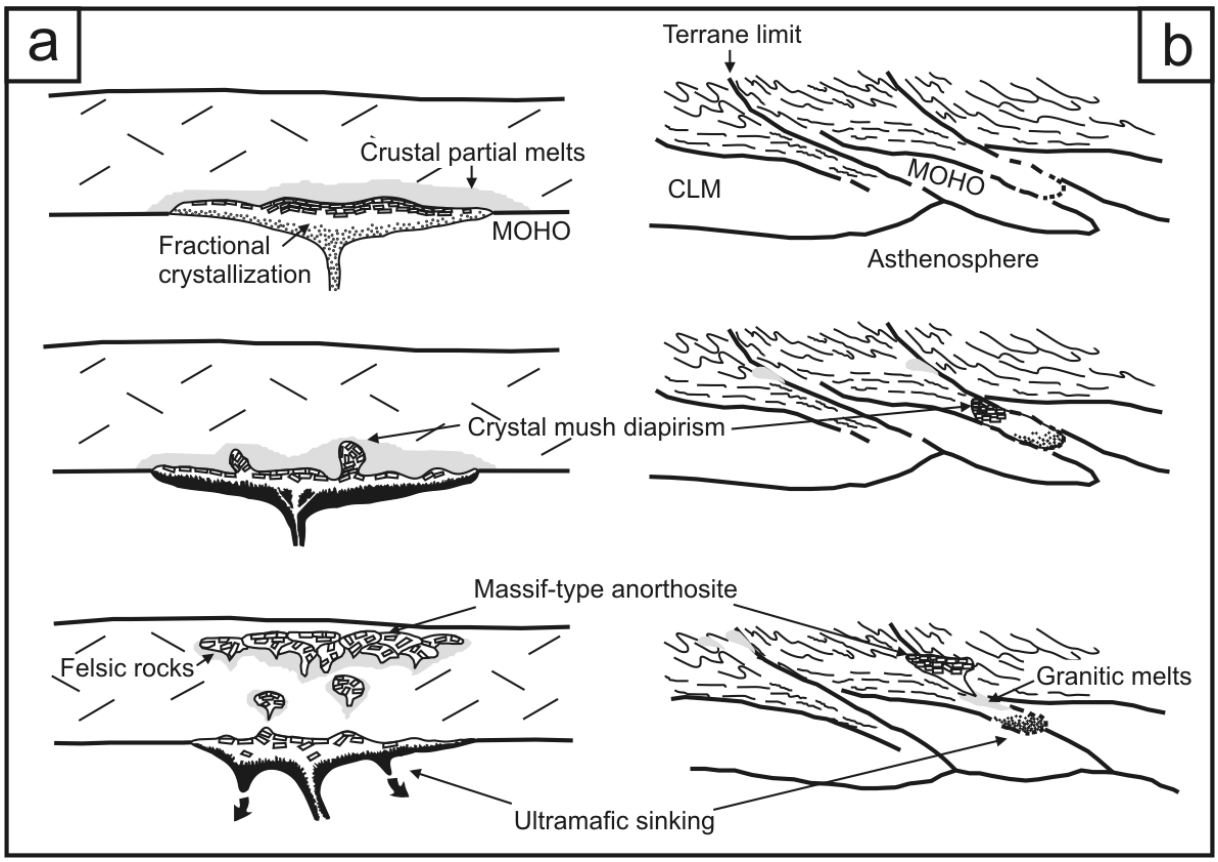

Fig. 1.3. Models of massif-type anorthosite petrogenesis. (a) The two stage mantle model after Ashwal (1993). Mantle-derived mafic melts are ponded at the crust-mantle boundary, where mafic silicates crystallize and sink. Residual melts become enriched in Al and Fe/Mg. Plagioclase is buoyant in these dense melts, producing anorthositic cumulates at the top of the magma chamber. The plagioclase-rich mushes are gravitationally unstable, rises through the crust as diapirs and coalesce in the middle-upper crust. Heat from crystallizing mantle-derived magma causes crustal anatexis to form granitoid magma. (b) The crustal tongue melting model after Duchesne et al. (1999). Collision stacking of terranes produces underthrust lower crust tongues; granitic liquids produced by anatexis of mid-crustal material intruded at higher levels along the terrane boundaries; due to linear delamination along the zone of weakness, the rise in temperature melts a tongue of suitable composition some ten Ma later, and a deep-seated magma chamber develops in which plagioclase floats to accumulate at the roof; a mafic cumulate sinks; anorthosite diapirs rise through the crust, channelled by the zone of weakness, and coalesce higher at mid-crust level to constitute a province of anorthosite massifs; granitic melts are also produced and follow the same path; the mafic cumulate, left behind, becomes indistinguishable from the mantle; a Moho offset in the only scar of the former magma chamber. CLM = continental lithospheric mantle.

Both models concur in that they assume polybaric crystallization, starting in a deep seated magma chamber followed by crystal mush diapirism and crystallization of the residual melt at the emplacement level. Intermediate plagioclase (An_{40-60}) is less dense than the proposed liquids

composition at high pressures and hence have strong tendency to float at the roof of the magma chamber (Kushiro, 1980). There is, however, little direct evidence for plagioclase flotation cumulates either in massif-type anorthosites or anorthosites in layered intrusions (Scoates, 2000; Cawthorn & Ashwal, 2009). The contradiction between the theoretical consideration and the lack of unambiguous evidence of plagioclase flotation in observed field relations is known as the 'plagioclase-magma' density paradox (Morse, 1973; Scoates, 2000). If plagioclase sinks or floats has important consequences for the formation of anorthosites, for instance the question if diapiric emplacement of crystal mushes is a viable process (Mukherjee & Das, 2002b; Scoates, 2002).

An alternative version of the basaltic parental melt model is suggested by Wiebe (1980, 1990, 1992). Plagioclase in a basaltic magma chamber in the deep crust might be remelted upon periodical replenishment with hot, primitive magma. This results in a vertically stratified magma chamber in which the uppermost liquids are oversaturated in plagioclase component. Such 'hyperfeldspatic liquids' are mentioned as possible precursors of stratified anorthosite plutons (Wiebe, 1990) and anorthositic dykes (Wiebe, 1980, 1990; Ashwal, 1993). This model gains its attraction from the minor need of the polybaric crystallization and plagioclase flotation concept. However, experimental investigation of natural anorthositic dykes reveals excessively high liquidus temperatures (1220 - 1420°C) and inappropriate mineralogy (Fram & Longhi, 1992).

For the formation of associated Fe-Ti ore bodies two processes are commonly invoked, segregation of an immiscible Fe-Ti-(P)-rich liquid during plagioclase fractionation from broadly Al-basaltic melt (e.g. Philpotts, 1981; Kolker, 1982; Morais et al., 1998) or fractional crystallization of Fe-Ti oxides, silicates and apatite accompanied by density driven crystal sorting during accumulation (e.g. Charlier et al., 2006, 2007; Tollari et al., 2008; Cawthorn & Ashwal, 2009). The interpretation of ferrodioritic rocks and Fe-Ti ore as a product of liquid immiscibility is abandoned in the recent literature due to the unrealistically high temperatures of such melts and the failure to produce such pure Fe-Ti oxide liquids experimentally (Charlier et al., 2006, and references therein).

Whereas the mantle model of Ashwal (1993) do not refer to a particular tectonic setting the crustal model of Duchesne et al. (1999) includes reactivation of large lithospheric discontinuities during the post-collisional period and linear lithospheric delamination along the shear zone allowing an asthenospheric uprise. Other models suggest orogenic to post-orogenic (Corrigan & Hanmer, 1997; Scoates & Chamberlain, 1997; Lundmark & Corfu, 2008) or anorogenic (Miller & Weiblen, 1990; Windley, 1993) decompression melting of upwelling mantle in an extensional setting. The presence of pre-existing crustal structures, especially Archean/Proterozoic boundaries, is interpreted to strongly influence the generation and emplacement of many Proterozoic anorthosite complexes (Wiebe, 1992; Scoates & Chamberlain, 1997; Scoates & Mitchell, 2000). Alternative interpretations are thermal insulation by a supercontinent or plume related continental break-up to produce upwelling of mantle material that produced magmas to generate anorthosites (see Ashwal, 1993 for a review).

1.2 The Kunene Intrusive Complex

1.2.1 Geographic overview of the Kunene Intrusive Complex and the study area

The Kunene Intrusive Complex is a 350 km long and 30 - 80 km wide composite, N-S elongated anorthosite complex that extends from SW Angola into NW Namibia. With a surface area of 18,000 km^2 it is one of the world's largest occurrences of anorthositic rocks (Ashwal & Twist, 1994). The Kunene River is the natural border between Angola and Namibia and gives the name to the complex. About 15 % (~2500 km^2) of the Kunene Intrusive Complex are situated in Namibia.

Fig. 1.4. Geographic overview map of Namibia. The location of the study area in the Kunene Region is marked.

The study area is located in the Kunene Region (former Kaokoland) of Namibia, extending between 13°10´ - 13°55´ East and 16°58´ - 17°35´ South (Fig. 1.4). The study area is restricted to the West by the Baynes Mountains, to the North and North-East by the Kunene River and to the South-

East by the Ehomba Mountains (Fig. 1.5). The region is poorly accessible and the population density is very low. The country road C43 connects the small villages of Swartbooisdrif, Okangwati and Epupa with the regional capital Opuwo. The study area comprises the anorthositic rocks of the Kunene Intrusive Complex (KIC) and the metamorphic basement of the Epupa Complex (EC). The central part is dominated by the 'Zebra Mountains', a local term derived from the alternating talus slopes and belts of vegetation covering the flanks of massive east-west striking anorthosite ridges (Fig. 1.6a). In contrast the north-western part is a hilly terrain with only isolated massive anorthosite mountains (Fig. 1.6b). Morphologically the metamorphic basement to the south of the Zebra Mountains is a relatively plain area with isolated hills formed by satellite intrusions of the KIC (Fig. 1.6c). The total study area is about 2500 km^2 in size of which a part was inaccessible due to the craggy topography of the central Zebra Mountains.

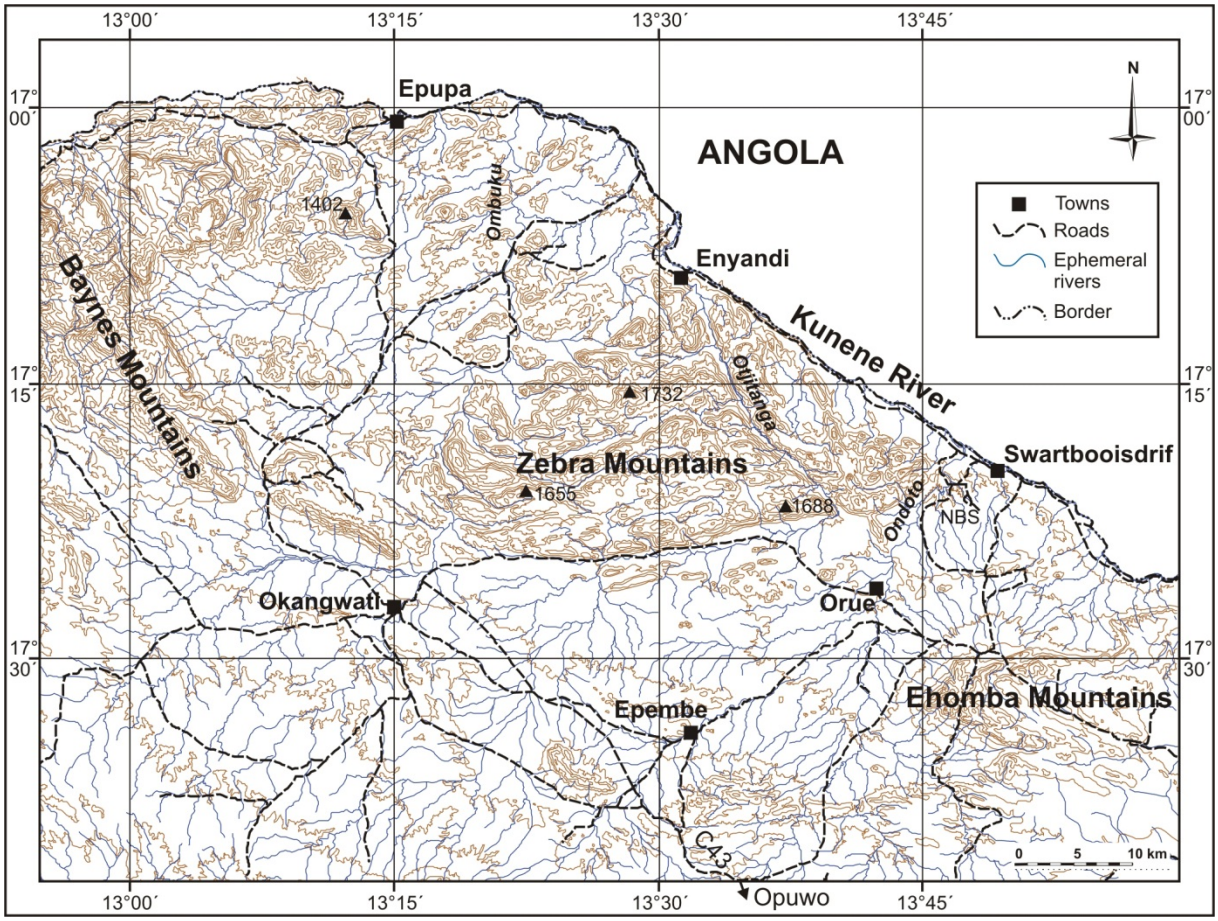

Fig. 1.5. Topographic map of the study area (based on sheet 1712-Swartbooisdrif).

The climate in NW Namibia is subtropical semiarid and the vegetation comprises scrubland dominated by small bushes and trees. Numerous ephemeral rivers flow towards the Kunene River. The courses of the arroyos and of the perennial Kunene River itself are mainly controlled by a NE- and SE-trending fault system. As a result of physical weathering of the anorthosites and a radial drainage

system, huge talus slopes, interrupted by belts with soil and vegetation, cover the flanks of the Zebra Mountain ridges. The valleys between the massive heights are often covered with alluvial sediments of the ephemeral rivers (Fig. 1.6d).

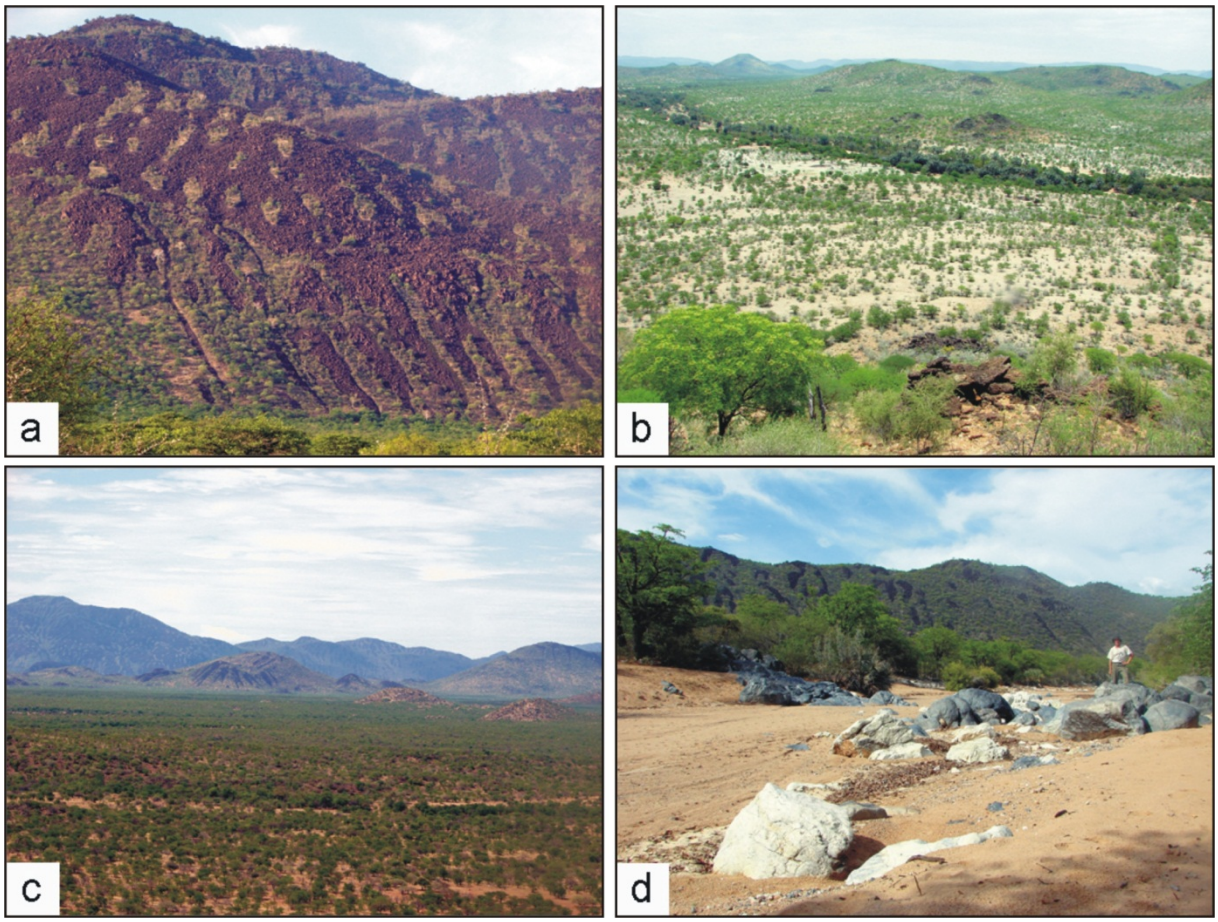

Fig. 1.6. (a) Photography of a massive anorthosite ridge in the Zebra Mountains. Alternating talus slopes and belts of vegetation cover nearly the whole flank of the mountain ridge and give him a striped (Zebra) appearance. (b) View from the height of a massive anorthosite onto the hilly terrain in the north-western study area. The terrain displays the typical scrubland vegetation of the study area, dominated in this area by mopane trees. The strip more abundantly covered with vegetation in the middle of the photograph is the arroyo of the ephemeral Ombuku River. (c) View from the South towards the North on the Zebra Mountains. In the foreground the plain area of the Epupa Complex basement is covered by scrubland vegetation. The two bright-coloured hills on the right hand side are syenite satellite intrusions. (d) Photography of the arroyo of the Otjitanga River within the Zebra Mountains. An outcrop of dark coloured anorthosite (middle left) and displaced boulders of pale and dark anorthosite in parts are covered by alluvial sediments.

1.2.2 Previous work on the anorthosites of the Kunene Intrusive Complex

Despite the early reconnaissance of the Precambrian anorthosite mass of southern Angola (Simpson & Otto, 1960) and more detailed mapping and petrographic work of Köstlin (1967; 1974) and Silva (1972), little was known about the Kunene Intrusive Complex for a long time. C. F. Vermaak stated in 1981:

'The mountainous remoteness of the Kunene Area, poor access and outcrop paucity within the flat-lying desert to semi-desert environment to the north, have precluded detailed mapping or systematic geological-petrological studies of the entire complex'.

In Angola, the KIC was investigated mainly by geologists of the Serviços de Geologia è Minas of the former Portuguese government. After independence in 1975 a nearly 20 years lasting civil war started in which neighbouring South-West Africa (under South-African mandate, today: Namibia) was involved. Scientific investigation was minor during this period and was mainly based on sampling and field observations done before 1975.

Carvalho & Alves (1990), Silva (1992) and Menge (1998) compiled older data and mappings in Angola and NW Namibia, respectively. All recognised two different anorthosite varieties, a 'white' and 'massive' anorthosite, which occurs in the southern portion of the KIC, and a 'dark coloured' fresh anorthosite dominant in the North. Carvalho & Alves (1990) considered the hypothesis of a magmatic chamber that originated from a single intrusion that differentiated to form a zoned 'dome-like' structure. Silva (1992) interpreted systematic variation of the chemistry and mineralogy of the rocks in an east-west section as stratification from base to the top as has been observed in layered intrusions. Similarly, Menge (1998) interpreted the repetitive alternation of anorthosites, olivine anorthosites and troctolites in the Namibian part as upper and lower zone of a repeatedly influxed magma chamber.

Based on comparable magmatic features over large areas of the complex combined with satellite imagery Ashwal & Twist (1994) considered the KIC as a large, composite massif-type anorthosite and overthrew the older assumption of a single or composite mafic layered intrusion. Furthermore they argued that the 'white' anorthosite is not an altered variant of typical 'dark' olivine-bearing anorthositic rock (cf. Silva, 1992) but rather altered pyroxene-bearing anorthosite derived from variable contamination of parental magmas with crustal assimilants. Morais et al. (1998) found that individual plutons of the composite complex are separated by belts of SW-NE tending granitoid bodies and that anorthosites of individual plutons are distinguishable by their chemical composition. From synmagmatic to subsolidus textures they suggested that the anorthosite bodies were formed by shearing of a slowly cooling crystal mush during growth of the complex. They also argued that the granitoids possibly were coeval and transposed and elongated by the same shearing event.

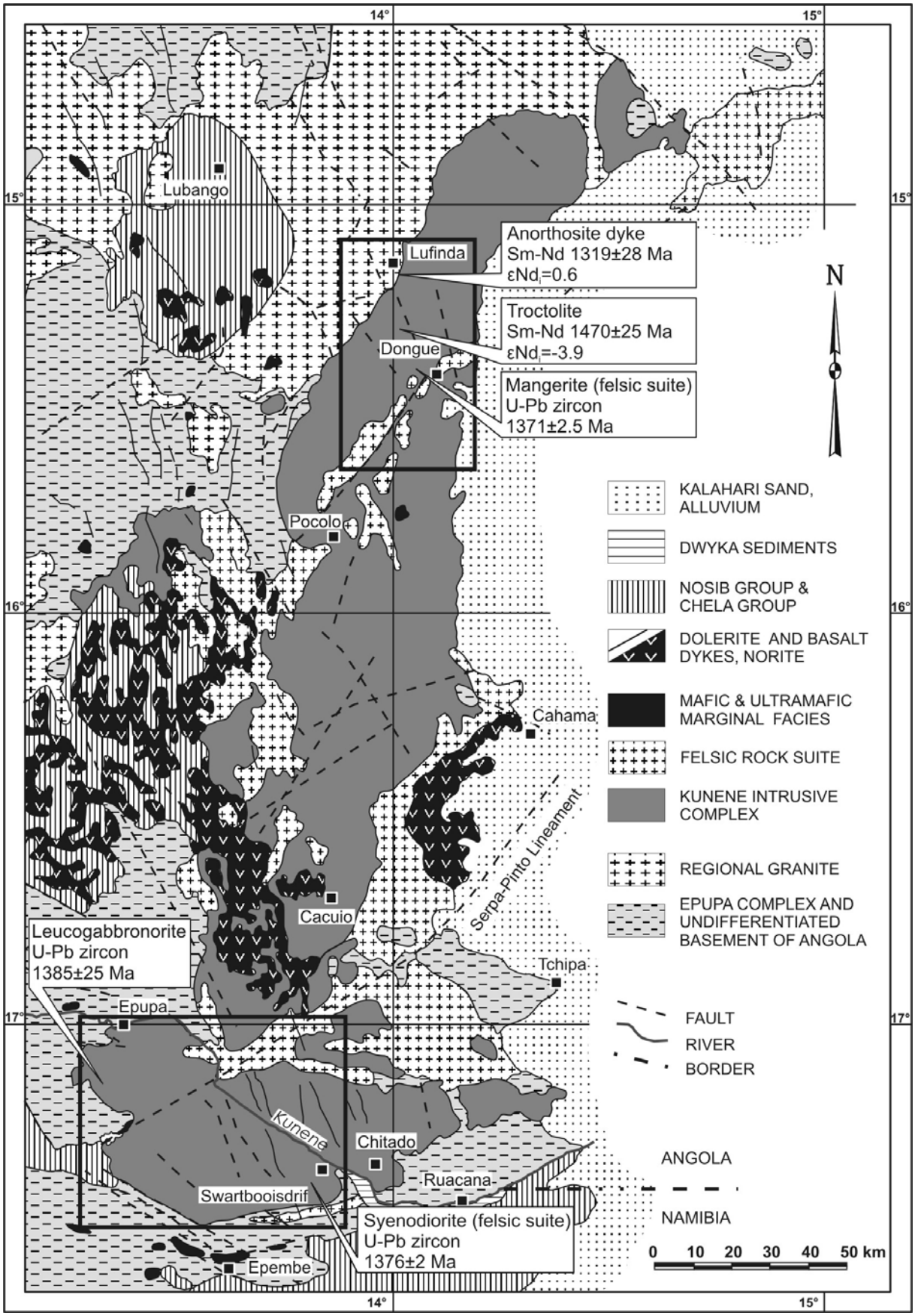
14°
15°
16°
17°
Lubango
Lufinda
Dongue
Pocolo
Cahama
Cacuio
Tchipa
Epupa
Chitado
Ruacana
Swartbooisdrif
Epembe
Kunene
Serpa-Pinto Lineament
Anorthosite dyke
Sm-Nd 1319±28 Ma
εNdi=0.6
Troctolite
Sm-Nd 1470±25 Ma
εNdi=-3.9
Mangerite (felsic suite)
U-Pb zircon
1371±2.5 Ma
Leucogabbronorite
U-Pb zircon
1385±25 Ma
Syenodiorite (felsic suite)
U-Pb zircon
1376±2 Ma
N
KALAHARI SAND, ALLUVIUM
DWYKA SEDIMENTS
NOSIB GROUP & CHELA GROUP
DOLERITE AND BASALT DYKES, NORITE
MAFIC & ULTRAMAFIC MARGINAL FACIES
FELSIC ROCK SUITE
KUNENE INTRUSIVE COMPLEX
REGIONAL GRANITE
EPUPA COMPLEX AND UNDIFFERENTIATED BASEMENT OF ANGOLA
FAULT
RIVER
BORDER
ANGOLA
NAMIBIA
0 10 20 30 40 50 km

The age of the KIC was subject to a long standing discussion. In the earlier literature, based on K-Ar ages on plagioclase, the KIC was assumed to be of Paleoproterozoic or Neoarchean age (Carvalho & Alves, 1990; Carvalho et al., 2000, and references therein). The U-Pb zircon age of 1385 ± 25 Ma of leucogabbronorite of the dark anorthosite suite in Namibia (Drüppel et al., 2000) demonstrates clearly that the KIC is Mesoproterozoic. In addition, the U-Pb zircon ages of felsic dykes of 1376 ± 2 Ma in Namibia (Drüppel et al., 2007) and of 1371 ± 2.5 Ma in Angola (Mayer et al., 2004) reveal that they are coeval and anorthositic and felsic suite intruded during the same magmatic event.

Thermobarometric studies on amphiboles, garnet and orthopyroxene in the Namibian part indicate that the KIC intruded into the lower crust and underwent nearly isobaric cooling from 950 - 985°C/7 - 9 kbar to 790 ± 60°C/8 ± 1 kbar (Drüppel et al., 2001). Similar pressures of 6.5 ± 0.6 kbar were constrained for a contact-metamorphic hornfels by Brandt (2003). Based on subsolidus re-equilibration of clinopyroxene-orthopyroxene pairs, a significantly shallower emplacement depth at 3 - 5 kbar was suggested for the Angolan KIC (Slejko et al., 2002). Regarding the apparent differences in the erosion level of ca. 9 km Drüppel et al. (2007) discussed a continuous gradient in exposed crustal depth or an offset by deep fracture zones as for example the Kunene River fault.

First isotopic studies were published by Slejko et al. (2002) and Mayer et al. (2004) who reported εNd_i values from 0 to -6.4 and $^{87}Sr/^{86}Sr_i$ from 0.7035 to 0.7042 from the Angolan part of the KIC. Both concluded that the KIC may originate from mantle-derived parental melts which underwent distinct cooling histories and crustal assimilation. Trace element and isotope data of the Namibian KIC were reported by Drüppel et al. (2007). They concluded that the general geochemical characteristics (i.e. positive europium anomalies, εNd_i of +1 to +3, $^{87}Sr/^{86}Sr_i$ of 0.7028 to 0.7041, $\delta^{18}O$ of plagioclase of 5.5 to 6.1) of the anorthositic rocks are in agreement with their derivation from mantle-derived magmas.

A suite of ENE tending granitoid bodies of up to 40 km length and smaller NW tending dykes is associated with the anorthosites (Fig. 1.7). From the proximity in time and space of acidic rocks and anorthosites in Angola, Mayer et al. (2004) argued that crustal anatexis occurred concomitantly with the generation of the anorthosites, as suggested for other AMCG complexes (Emslie et al., 1994). The age of 1376 ± 2 Ma for a syenodiorite dyke in NW Namibia demonstrate that felsic and anorthositic suite are coeval but the geochemical data and isotopic signature provide convincing arguments against consanguinity (Drüppel et al., 2007).

Fig. 1.7. (opposite page) Geologic overview map of the Kunene Intrusive Complex in SW Angola and NW Namibia. Map simplified and modified after Carvalho & Alves (1990; taken from Drüppel et al., 2007). Outlined areas mark regions of detailed mapping and geochemical investigation in the Angolan part (Ashwal & Twist, 1994; Morais et al., 1998; Slejko et al., 2002; Mayer et al., 2004) and in the Namibian part of the KIC (Menge, 1998; Drüppel et al., 2001, 2007; Drüppel, 2003). Available age data for the anorthosite and felsic rock suite are displayed (Drüppel et al., 2000, 2007; Mayer et al., 2004).

Massive Fe-Ti oxide ore bodies have been reported from the entire KIC (Vermaak, 1981; Morais et al., 1998; von Seckendorff et al., 2000). They were described as either layered or plug-like titaniferous magnetite occurrences (Vermaak, 1981), Fe-Ti massive ore bodies generally close to granites of the Angolan KIC (Morais et al., 1998) or ellipsoidal magnetite plugs in the white anorthosite variety of the Namibian KIC (von Seckendorff et al., 2000).

The compositional variation and of the mafic satellite intrusions and their magmatic sulfide potential was evaluated by Maier et al. (2008). One troctolite intrusion to the south of the Zebra Mountains was found to host up to 5 vol.% sulfide with 2 - 5 % Ni, 2 - 4 % Cu and 0.5 ppm PGE. The authors interpret these data as sulfide precipitation from moderately fertile magma and argue for the prospect of a Voisey's Bay-type mineralization in the Kunene Intrusive Complex.

Subsequently, the study area in NW Namibia was intruded by nepheline-syenite stocks (1220 - 1210 Ma) along major, deep crustal lineaments (Littmann et al., 2000) and by younger carbonatite and associated nepheline-syenite dykes (1140 - 1120 Ma), emplaced in upper crustal levels (Drüppel et al., 2005). Several crosscutting dolerite dykes were reported from the Namibian (Drüppel, 2003) as well as from the Angolan part of the KIC (Mayer et al., 2004). Their age is assumed to be in the range of 1100 to 1200 Ma, like that of dolerite dykes with similar orientation crosscutting the basement (Mayer et al., 2004, and references therein).

For the emplacement of the KIC at the southern margin of the Congo Craton, an extensional setting and a significant thermal anomaly during the early Kibaran cycle was suggested (Morais et al., 1998; Mayer et al., 2004). Drüppel et al. (2007) evaluated two tectonic scenarios for the emplacement of the KIC and the associated granitic rocks. (1) The formation in a major northeast striking extensional belt that formed during the early stages of separation of the Congo and the southern Kaapvaal-Zimbabwe Cratons. (2) A post-orogenic setting, with the mantle and crustal melts being formed by lithospheric delamination during a post-orogenic collapse that followed widespread Palaeoproterozoic orogenic activity.

1.3 Purpose and aims of the present investigation

The Mesoproterozoic Kunene Intrusive Complex is one of the world's largest occurrences of massif-type anorthosites and comprises pyroxene as well as olivine-bearing lithologies. The anorthositic rocks were not subject to postmagmatic metamorphism and hence allow the direct investigation of processes active during their formation. Regarding the key issues important to anorthosite petrogenesis (mentioned in section 1.1.5), this study attempts to give answers to the source and composition of the parental melt, its magmatic evolution and the role of crustal contamination. The origin and magmatic evolution of the parental melt of anorthosites is maybe the most urgent question in anorthosite petrology as resolving this issue is inevitable before progress can be made in petrogenetic and geotectonic models. Of special interest is the question whether the formation of massif-type anorthosites is a crustal growth process (mantle model) or a crustal recycling process (crustal model).

From the geochemical point of view, the problem with anorthosites is in explaining their mineralogical simplicity but the extreme plagioclase-rich composition only adds to the problem of inverting from the rock to the parent melt composition (Bowen, 1917). Whole rock data show that these rocks are cumulates but makes it difficult to derive genetic information or compositions relevant to the parental melt composition. To assess the composition of the parental melt four approaches are described in the present literature. (1) Estimating the bulk composition of the individual complexes or temporally and spatially related layered intrusions (e.g. Nolan & Morse, 1986; Longhi, 2005; Morse, 2006). (2) Investigation of dykes and sills which were assumed to represent chilled melt compositions (e.g. Wiebe, 1990; Vander Auwera et al., 1998; Longhi et al., 1999). (3) Inverting the trace element composition of cumulus phases to melt composition (e.g. Halama et al., 2002). (4) Subtracting the composition of known cumulus phases (olivine, pyroxene and plagioclase) from cumulate rocks (e.g. Morse, 2006).

In the present study both anorthosite units, the white and the dark anorthosite suite, were investigated. In addition, associated Fe-Ti oxide ore bodies were investigated to gain information about both their formation and their petrogenetic relation to the anorthosites. Emphasis is placed on the temporal and genetic links between the different anorthosite intrusions and the origin and magmatic evolution of their parental magmas.

During field work in November/December 2006 samples were obtained that cover the full compositional range of anorthositic rocks of the KIC. An existing sample stock from a detailed mapped area near Swartbooisdrif (Drüppel, 2003) was extended and further samples from the southern Zebra Mountains and the north-western study area were taken. The sample set comprises anorthosite and leucotroctolite of the white anorthosite suite, anorthosite, gabbroic anorthosite and leucotroctolite of the dark anorthosite suite, troctolite, leucogabbro and oxide-rich diorite which intruded the anorthosites, and Fe-Ti oxide ore samples that crop out within the white anorthosites (see Appendix

A.1 for a full sample list). Additionally, samples of the surrounding Epupa Complex, obtained during mapping by Brandt (2003), were investigated.

The white anorthosite is characterized by a pale whitish to greenish or violet colour due to sericitisation and saussuritisation of plagioclase and uralitisation of Fe-Mg silicate phases (Fig. 1.8a). The dark anorthosites are only weakly or non-altered and characterized by dark greyish colour and higher resistance against weathering (Fig. 1.8b). Rocks of the dark anorthosite suite occasionally contain angular clasts of white anorthosite and constrain their later intrusion (Fig. 1.8c). The Fe-Ti ore bodies of the study area are apparently restricted to the white anorthosite. Their occurrences are noted during field work by the appearance of abundant Fe-Ti oxides in the soil, hard rock outcrops are seldom (Fig. 1.8d). Small troctolite bodies intruded in a major NE-SW-trending ~6 km wide dextral shear zone shear zone within the KIC. Small gabbro and oxide-rich diorite intrusions, several tens of meters in diameter, occur close to the southern margin of the complex. Field relations indicate that they intrude the hosting white anorthosite.

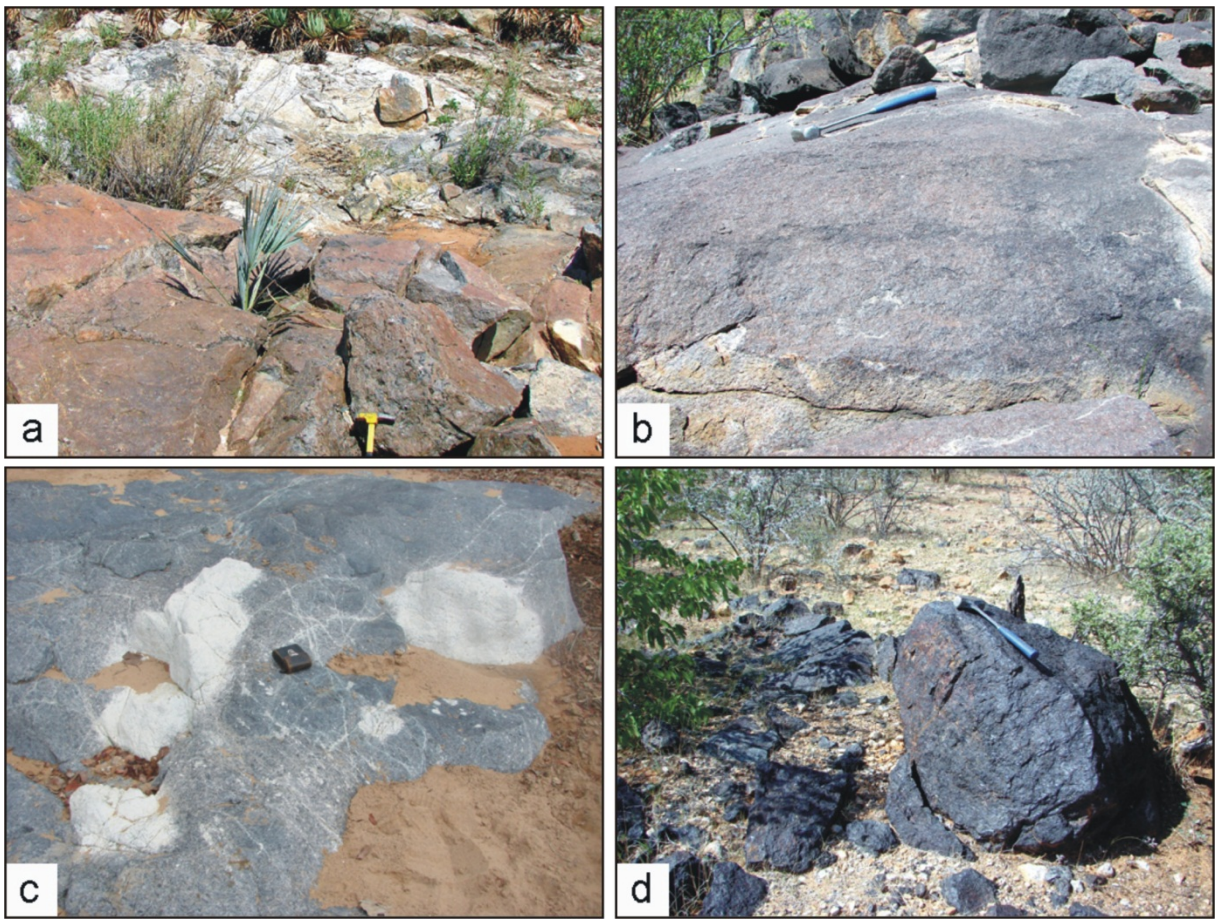

Fig. 1.8. Rocks of the Kunene Intrusive Complex. (a) Outcrop of pale whitish pyroxene-bearing anorthosites of the white anorthosite suite near Swartbooisdrif. (b) Outcrop of grey massive leucotroctolite of the dark anorthosite suite in the southern Zebra Mountains. (c) Xenoliths of pale white anorthosite enclosed by grey dark anorthosite. (d) Outcrop of massive Fe-Ti ore within the white anorthosite near Omuramba. The immediate interface to the anorthosites is covered by soil.

In order to gain information about the source and magmatic evolution of the parental melts of the two anorthosite units and to characterize the nature and amount of crustal contamination the whole sample set was investigated for major element composition, lithophile and siderophile trace elements and its stable and radiogenic isotope composition. The trace element composition of cumulus and intercumulus phases was investigated in situ. For the majority of the isotope analyses mineral separates were used as opposed to whole-rock powders. The use of in situ techniques and mineral separates has several advantages over whole rocks, for instance only fresh mineral grains can be selected for analysis, and the results can be interpreted with more confidence regarding the initial values of the melt they crystallized from. Further it is important to distinguish between primary and secondary effects, which are more abundant in whole rock powders. With this in mind a sample set of mineral separates and corresponding whole rocks was analysed. The following four paragraphs give a short overview of propose and the methods used in each chapter.

Chapter 2: ***Spurenelementzonierung von Plagioklasen des Kunene-Intrusiv-Komplexes (NW-Namibia).*** The chapter focuses on the processes during fractionation of plagioclase and other major to minor phases of the two anorthosite varieties of the Kunene Intrusive Complex.

In situ major and trace element analysis offers the possibility to investigate the trace element budget and zoning of minerals in their particular textural position. Compositional zoning of cumulus plagioclase, for example, provide insight into fractionation processes in the magma chamber and during later adcumulus growth. In representative samples of both anorthosite varieties profiles across centimetre-sized cumulus plagioclase were measured with an electron microprobe (EMP). Afterwards plagioclases with distinct major element composition and zoning patterns were investigated with laser ablation-inductively coupled plasma mass spectrometry (LA-ICP-MS) for their trace element composition along the profiles previous measured with the EMP. In addition, clinopyroxene that crystallized during successive stages of the magmatic evolution was investigated to gain information about the changes in melt chemistry, especially after the fractionation of plagioclase.

Plagioclase of both anorthosite varieties displays variable major and trace element zoning. The majority of plagioclase is characterized by a large-scale wavy oscillatory zoning, reflecting its movement during crystallization in a magma reservoir which was subject to recurrent changes of the physico-chemical conditions. According to the trace element patterns of plagioclase, the white anorthosites derived by simultaneous fractional crystallization of plagioclase, pyroxene and Fe-Ti oxides during and after assimilation of crustal material. The dark anorthosites, on the other hand, were formed by fractional crystallization of plagioclase, olivine and Fe-Ti oxides from an initially uncontaminated magma, derived by partial melting of the upper mantle.

Chapter 3: ***Magmatic evolution of anorthosites of the Kunene Intrusive Complex, NW Namibia: evidence from oxygen isotope data and trace element zoning.*** This chapter focuses on the source of the primary melt and the subsequent magmatic evolution of the parental melt during fractional crystallization of the anorthosites of the Kunene Intrusive Complex.

The oxygen isotope composition of plagioclase in cumulate rocks was used in various studies to constrain the source of the initial melt, crustal assimilation and post-magmatic hydrothermal alteration (Taylor, 1968; Valley & O'Neil, 1982; Morrison & Valley, 1988; O'Connor & Morrison, 1999; Peck & Valley, 2000; Harris et al., 2005). Previous studies have shown that the $^{18}O/^{16}O$ ratio of feldspar in an igneous rock can provide a reasonably good estimate of the $^{18}O/^{16}O$ ratio of the melt from which it crystallized. In basaltic melts the plagioclase is thought to be about 0.3 to 0.5 ‰ richer in $\delta^{18}O$ than the corresponding melt (Taylor, 1968). All common rocks and melts span a narrow range in oxygen concentration and therefore mixing proportions of isotopically distinct components contributing to the chemistry of magmas are more easily defined for oxygen than for most other isotopic systems. Following this, the oxygen isotope geochemistry complements a large number of geochemical tracers involving incompatible trace elements (Eiler, 2001).

The major and trace element composition of bulk anorthosites from Namibia was determined with X-ray fluorescence (XRF) and gave first insights into chemical and mineralogical differences between distinct anorthosite varieties. The oxygen isotope composition of mineral separates (mainly plagioclase) was determined with the laser fluorination technique to constrain the source of the rocks. The magmatic evolution of the parental melt was investigated by combined EMP and LA-ICP-MS major and trace element measurements of the main anorthosite phases. The major and trace composition of cumulus plagioclase (Chapter 2) and phases that crystallized during successive stages of the magmatic evolution (olivine, pyroxene, Fe-Ti oxides, apatite and amphibole) provides important information about the changes in melt chemistry, especially during assimilation and fractional crystallization processes.

In anorthosites, plagioclase is a good proxy for the parental melt $\delta^{18}O$ because of its crystallization early during the magmatic evolution and minor high-temperature fractionations with the melt. The oxygen isotope characteristics of plagioclase and minor phases of the two distinct anorthosite varieties of the KIC are consistent with their derivation from a mantle-derived parental melt that was subject to crustal contamination during the early stages of evolution. Furthermore, the per mill difference in oxygen isotope composition of coexisting plagioclase and olivine of the dark anorthosite was used to constrain their crystallization at magmatic temperatures slightly above 1150°C. By the application of appropriate partition coefficients the trace element composition of plagioclase was used to constrain the trace element budget of the melt they crystallized from. In accordance with the oxygen isotope data, the trace element record of plagioclase and intercumulus phases demonstrate that the white anorthosites crystallized from evolved melt that had significant crustal characteristics. In contrast, the younger dark anorthosites were formed from almost uncontaminated mantle-derived parental melt.

Chapter 4: ***The role of crustal contamination in massif-type anorthosites, new evidence from Sr-Nd-Pb isotopic composition of the Kunene Intrusive Complex, NW Namibia***. The aim of this chapter is to characterise the source and possible crustal contaminants of the different anorthosite varieties in the Kunene Intrusive Complex and to evaluate the amount and timing of crustal contamination.

The isotope compositions of anorthosites and mineral separates, together with the trace element data, provides insights into source characteristics and magmatic processes such as assimilation and fractional crystallization, and the petrogenetic relationship to the chemically evolved rocks. Radiogenic isotope studies of mineral separates have the advantage that no measurable isotope fractionation takes place upon crystallization and the isotopic compositions directly reflect the time integrated values of the melt from which the cumulate phase crystallized. The gained insights are not accessible from major element composition of the cumulate rocks.

Lithophile trace element abundances of plagioclase, pyroxene and bulk rocks of the KIC were determined with inductively coupled plasma mass spectrometry (ICP-MS) and the isotopic composition of strontium, neodymium and lead was measured with isotope thermal ionizations mass spectrometry (TIMS). In addition, the trace element and isotope composition of representative samples from the surrounding Epupa Complex were measured to gain information about the crustal evolution and the composition of potential contaminants.

The Sr and Nd isotopic compositions of the younger dark anorthosite suite of the KIC demonstrate that the parental melt originate from depleted upper mantle. Prior and during the formation of the older white anorthosite the mantle-derived melt was subject to crustal contamination, producing evolved magmas whose isotope and trace element composition was characterized by distinct crustal signatures.

The investigation of spatially related crustal rocks of the Epupa Complex reveals that there trace element and isotopic compositions effectively assign them as likely contaminants. A special advantage especially of the Sm-Nd system in the EC crustal rocks is the lower mobility, when compared to elements like Rb and Sr, during high-grade metamorphism, hydrothermal alteration and chemical weathering. Neodymium model ages, as opposed to an crystallization or metamorphism age, reflect the apparent crustal residence age when the EC rocks had the same isotopic composition like the assumed source (e.g. CHUR or deleted mantle), and give an estimate of the time when the precursor of the particular rock was separated from its source (DePaolo, 1981; Goldstein et al., 1984). Together with the isotopic composition of lead these data provide particularly valuable information on crustal genesis and evolution and can be used to distinguish between old reworked and juvenile crust. Regarding the anorthosites, this is particularly important for the reconstruction of the geotectonic environment. Combining isotope and trace element data of anorthosites and possible crustal contaminants (i.e. the rocks of the Epupa Complex) the successive assimilation can be modelled and the influence of plagioclase crystallization and accumulation can be estimated.

Chapter 5: ***Osmium isotopes and highly siderophile element fractionation in the massif-type anorthosites of the Mesoproterozoic Kunene Intrusive Complex, NW Namibia.*** The purpose of this study is to investigate the early fractional crystallization history of the parental melts of the anorthosites and the influence of the crustal contamination on the Re-Os isotope system. A further subject is the petrogenetic relationship between the associated Fe-Ti ores and the anorthosites of the Kunene Intrusive Complex.

The analysis of highly siderophile element (HSE) abundances and of osmium isotope compositions is a relatively new method in geosciences and provides a powerful tracer of global geochemical processes (cf. Shirey & Walker, 1998). Mantle melting and fractional crystallization of mafic- to intermediate-composition magmas produces Re/Os ratios that are high enough to evolve to very radiogenic Os isotope compositions in only a few million years, providing a sensitive tracer for detecting the involvement of such young crust in magmatic systems. However, the Sr, Nd, and Pb isotope compositions will remain almost constant over such short time intervals due to the lower parent/daughter enrichment during magmatic evolution (e.g. Schiellerup et al., 2000; Hart et al., 2002). The distribution of highly siderophile elements were used to constrain source characteristics and magmatic differentiation of mafic melts in volcanic (e.g. Puchtel & Humayun, 2000, 2001; Pitcher et al., 2009) and plutonic (e.g. Day et al., 2008) settings but only two studies of Os isotope composition of massif-type anorthosite were published so far (Schiellerup et al., 2000; Morgan et al., 2000).

In contrast to the lithophile trace elements the HSE are largely controlled by the occurrence of sulfide phases. In absence of those phases their solubility and partitioning behaviour in oxide and silicate phases are believed to govern the geochemistry of the HSE in magmatic systems. The concentrations in plagioclase cumulate rocks are generally low (Schiellerup et al., 2000; O'Driscoll et al., 2009). With the application of the isotope dilution technique and the use of an appropriate spike for high Re/Os ratios, the HSE concentrations in the sub-ppb range were measurable in samples of the KIC. Highly siderophile element abundances of oxide and sulfide mineral separates and bulk rocks of the KIC were measured with ICP-MS and the isotopic composition of osmium was measured with negative thermal ionization mass spectrometry (N-TIMS).

Oxide mineral separates and bulk rocks of the Kunene Intrusive Complex show highly fractionated HSE patterns and a range of Os isotopic compositions from close to mantle vales up to highly radiogenic crustal values. The new HSE and Os isotope data for the anorthosites of the Kunene Intrusive Complex were interpreted in the light of the results of the previous chapters. In particular, it was important to explain why lithophile isotope systems like Rb-Sr and Sm-Nd indicate clearly a mantle origin of the anorthosites whereas Re-Os do not. The distribution of HSE between different Fe-Ti oxide phases provides information on partition behaviour and post-cumulus re-equilibration processes. The siderophile character of the HSE further provides the possibility to investigate how the fractional crystallization of the associated Fe-Ti oxide ores is related to the anorthosite petrogenesis.

Chapter 2

Spurenelementzonierung von Plagioklasen des Kunene-Intrusiv-Komplexes (NW-Namibia)

Autoren: Philipp Gleißner[1], Kirsten Drüppel[1]

[1]Technische Universität Berlin, Institut für Angewandte Geowissenschaften, Ackerstr. 71-76, 13355 Berlin

Publiziert in: Zentralblatt für Geologie und Paläontologie, Teil I VIII, Nummer 3/4, Seiten 267-286. E. Schweizerbart, Stuttgart (2009)

Eigenanteil:
Probennahme gemeinsam mit Dr. Kirsten Drüppel, selbständige Dünnschliffuntersuchung und EMP-Analytik, LA-ICP-MS-Analytik gemeinsam mit Dr. Helene Brätz, Auswertung und Interpretation der Ergebnisse gemeinsam mit Dr. Kirsten Drüppel, selbständige Ausarbeitung der Publikation.

Zusammenfassung

Plagioklase von zwei unterschiedlichen Anorthosit-Varietäten des proterozoischen Kunene-Intrusiv-Komplexes, NW-Namibia, zeigen übereinstimmend eine Anreicherung der leichten Seltenerdelemente und positive Europium-Anomalien. Ihre Spurenelementzonierungen geben Aufschluss über magmatische Prozesse, die in der Magmenkammer an der Kruste-Mantel-Grenze stattfinden.

Aus den Spurenelementmustern lässt sich ableiten, dass sich die älteren, pyroxenführenden Anorthosite in Folge von simultaner Assimilation von krustalem Nebengesteinsmaterial und fraktionierter Kristallisation von Plagioklas, Pyroxen und Ilmenit bildeten. Die Assimilation fand hierbei sowohl vor als auch während der Kristallisation der Plagioklase statt. Dagegen sind die jüngeren, olivinführenden Anorthosite in Folge einer gleichzeitigen fraktionierten Kristallisation von Plagioklas, Olivin und Ilmenit aus initial unkontaminierter Mantelschmelze entstanden. Die physikochemischen Bedingungen des Magmas während der Kristallisation der Plagioklase dieser Anorthosit-Einheit wurden überwiegend durch die Zufuhr neuer, undifferenzierter Schmelzen verändert. Assimilation krustaler Nebengesteine hatte zu diesem Zeitpunkt der Anorthositgenese nur noch eine untergeordnete Bedeutung.

Abstract

Plagioclase of two distinct Anorthosite varieties of the Kunene Intrusive Complex, NW Namibia display enrichment of the light rare earth elements and positive europium anomalies. The zonation of the trace element contents of plagioclase give insights into magmatic processes in the igneous magma chamber at the mantle-crust boundary.

According to the trace element patterns of plagioclase, older pyroxene-bearing anorthosites derived by assimilation of crustal material and simultaneous fractional crystallization of plagioclase, pyroxene and ilmenite. This crustal assimilation took place before and during crystallization of plagioclase. The younger olivine-bearing anorthosites, on the other hand, were formed by fractional crystallization of plagioclase, olivine and ilmenite in an initially uncontaminated magma derived by partial melting of the upper mantle. The physical and chemical conditions of the magma during the plagioclase crystallization where mainly controlled by replenishing with undifferentiated mantle melts. Assimilation of neighbouring crustal rocks was a subordinate process during this stage of the anorthosite formation.

2.1 Einleitung

Die Ausbildung eines chemischen Zonarbaus in Mineralen magmatischer Gesteine ist eine Reaktion auf Änderungen der physikochemischen Bedingungen innerhalb der Schmelze. Plagioklase sind häufige magmatische Minerale und eignen sich aufgrund ihrer Empfindlichkeit gegenüber Fluktuationen in magmatischen Systemen (Holten et al., 2000) und der langsamen NaSi-CaSi-Diffusion gut zur Untersuchung von Prozessen, die während der magmatischen Differentiation der primären Schmelze bis hin zur endgültigen Platznahme der Magmen stattfinden.

Besondere Bedeutung kommt hierbei den Prozessen der Assimilation von krustalem Nebengestein und der Fraktionierung früh kristallisierender Minerale zu (Taylor, 1980; DePaolo, 1981). Insbesondere partielle Mantelschmelzen, zu denen auch die untersuchten anorthositischen Magmen zählen, haben aufgrund ihrer höheren Temperaturen von ca. 1000 - 1200°C bei ihrem Aufstieg ein hohes Assimilationspotential. Auf der anderen Seite führen die Kristallisation von Mineralen und ihre Fraktionierung zu spezifischen Elementan- und abreicherungen in der Schmelze. Die hierbei entstehenden Kristall-Kumulate unterscheiden sich chemisch nicht nur von der stärker differenzierten Restschmelze sondern auch von der primitiven Ausgangsschmelze. Der Spurenelementeinbau in Plagioklas ist generell abhängig vom Anorthitgehalt des kristallisierenden Plagioklases, der Zusammensetzung der Schmelze und von Druck und Temperatur (Blundy & Wood, 1991; Bindeman et al., 1998; Vander Auwera et al., 2000).

Nach Ashwal (1993) bilden sich die Stammmagmen proterozoischer Anorthosit-Komplexe durch partielles Schmelzen des oberen Mantels und anschließender Ausbildung von Plagioklas-Kumulaten im Dachbereich einer Magmenkammer an der Kruste-Mantel-Grenze. Im Anschluss erfolgt ein diapirartiger Aufstieg des plagioklasreichen Kristallbreis durch die Kruste. Eine Assimilation von krustalem Nebengesteinsmaterial und eine fraktionierte Kristallisation von Plagioklas und weiteren Mineralen könnten somit sowohl innerhalb der Magmenkammer als auch während des Aufstiegs des Magmas erfolgen. Andere Modelle gehen von einer Bildung der anorthositischen Magmen durch partielles Aufschmelzen mafischer bis intermediärer Plutone der Unterkruste aus (Longhi et al., 1999; Schiellerup et al., 2000; Wiszniewska et al., 2002). Hierbei bilden sich die verschiedenen anorthositischen Magmen direkt als Teilschmelzen der Unterkruste. Prozesse wie die Anreicherung von Plagioklas über fraktionierte Kristallisation sowie krustale Assimilation haben nach diesem Modell eine nur untergeordnete Bedeutung.

Im Rahmen dieser Arbeit wurden Variationen in den Spurenelementkonzentrationen von Plagioklasen und weiteren Mineralen zweier Anorthosit-Generationen des Kunene-Intrusiv-Komplexes, NW-Namibia, untersucht. Ziel dieser Untersuchung war die Klärung der Herkunft der Stamm-Magmen der beiden Anorthositkörper sowie eine Beurteilung der magmatischen Prozesse während ihrer Bildung. Im Gegensatz zu anderen proterozoischen Anorthosit-Komplexen wurde der

Kunene-Intrusiv-Komplex im Anschluss an seine Platznahme nicht metamorph überprägt und ermöglicht somit die Untersuchung der bei seiner Entstehung aktiven magmatischen Prozesse. Anhand der gemessenen Spurenelement-Konzentrationen in Plagioklas und ihrer Zonierung war eine Rekonstruktion des Kristallisationsverlaufes der untersuchten Gesteine möglich.

2.2 Geologie

Der Kunene-Intrusiv-Komplex erstreckt sich von SW-Angola nach NW-Namibia (Abb. 2.1). Mit einer Gesamtfläche von ~18000 km^2 gehört er zu den größten Anorthosit-Massiven weltweit (Ashwal & Twist, 1994). Die Intrusion des Anorthositmassivs wurde auf 1,38 Mrd Jahre datiert (Drüppel et al., 2000; Mayer et al., 2004). Seine Intrusion erfolgte am SW-Rand des proterozoischen Kongo-Kratons. Anhand von geobarometrischen Kalkulationen konnte eine Platznahme des Anorthosit-Körpers unter Bedingungen von 7 - 9 kbar in Namibia (Drüppel et al., 2001; Drüppel, 2003) und 3 - 5 kbar in Angola (Sleijko et al., 2002) in der mittleren bis oberen Kruste abgeleitet werden.

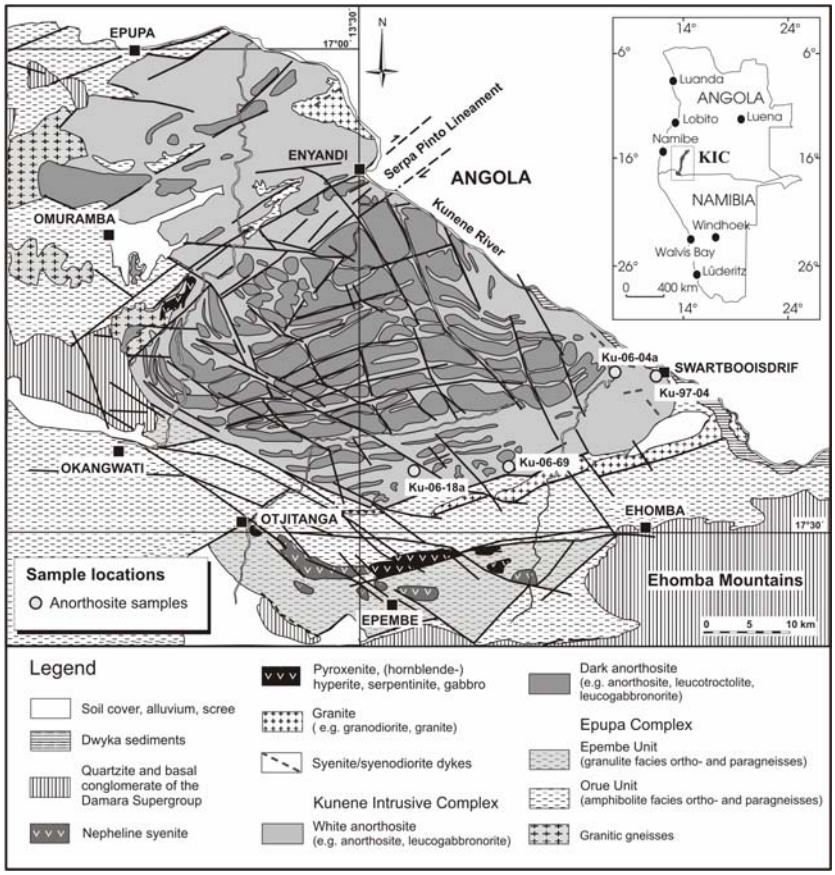

Abb. 2.1. Geologische Karte des südlichen Kunene-Intrusiv-Komplex in NW-Namibia. Karte nach Menge (1998), modifiziert durch Brandt et al. (2003) und Drüppel et al. (2007); die Probenlokalitäten sind markiert.
Fig. 2.1. Geologic map of the southern Kunene-Intrusiv-Complex in NW Namibia. Map after Menge (1998), modified by Brandt et al. (2003) and Drüppel et al. (2007); sample locations are indicated.

Der Kunene-Intrusiv-Komplex in Namibia setzt sich im Wesentlichen aus zwei verschiedenen Anorthosit-Varietäten zusammen, dem stark alterierten „Weißen Anorthosit“ und dem kaum alterierten, dunkelgrauen bis schwarzen „Dunklen Anorthosit“ (Menge, 1998; Drüppel et al., 2001, 2007). Der Weiße Anorthosit dominiert in weiten Teilen des nordwestlichen Arbeitsgebietes (Abb. 2.1). Er besteht hauptsächlich aus unterschiedlich stark alterierten, meist pyroxenführenden Anorthositen. Der Dunkle Anorthosit intrudierte insbesondere im zentralen Bereich des Weißen Anorthosit-Massivs (Drüppel et al., 2001, 2007) und bildet an der heutigen Geländeoberfläche markante Ost-West streichende Bergrücken, die aufgrund ihrer ungewöhnlichen Verwitterungsform auch als Zebraberge bezeichnet werden (Abb. 2.2a). Er besteht vorwiegend aus olivinführenden Lithologien. Bei der Intrusion transportierte der Dunkle Anorthosit Xenolithe des Weißen Anorthosites bis in das Intrusionsniveau (Abb. 2.2b).

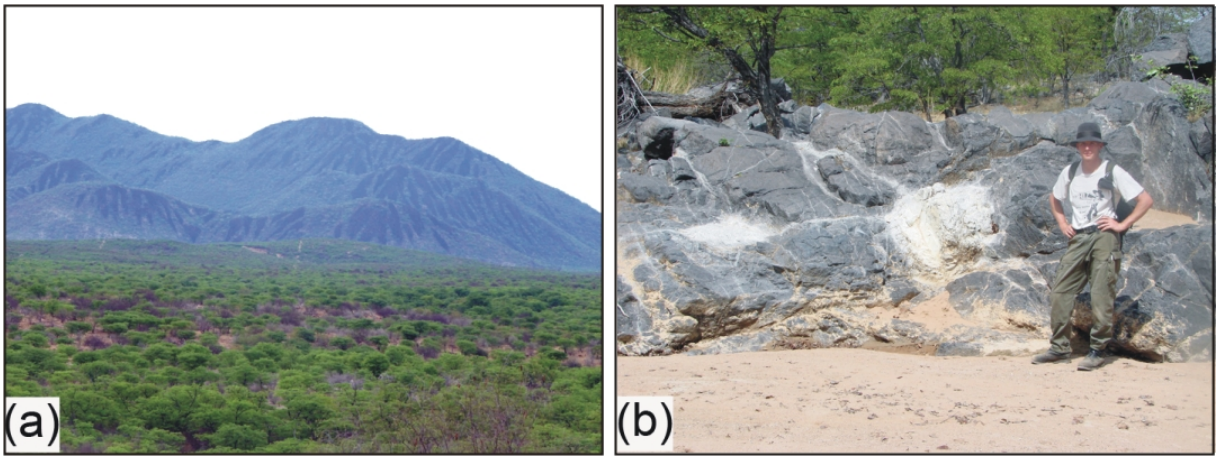

Abb. 2.2. (a) Zebraberge in NW-Namibia. Das Foto zeigt einen markanten Bergrücken des Dunklen Anorthosits. (b) Weiße Anorthosit-Xenolithe im Dunklen Anorthosit in einem Flußaufschluss in den Zebrabergen.
Fig. 2.2. (a) Zebra Mountains in NW Namibia. The photograph shows an elongated mountain of dark anorthosite. (b) Xenoliths of white anorthosite in dark anorthosite in a riverbed outcrop in the Zebra Mountains.

Plagioklas ist ein Hauptgemengteil in allen Gesteinen der anorthositischen Serie (>65 Vol.%). Sowohl der Weiße als auch der Dunkle Anorthosit weisen eine homogen-massige Textur mit riesenkörnigen Plagioklas-Kristallen von bis 8 cm Durchmesser auf. Fein verteilte Eisen-Titanoxid-Einschlüsse im Plagioklas lassen die unalterierten Dunklen Anorthosite nahezu schwarz erscheinen (Morais et al., 1998; Drüppel et al., 2001). Eine späte hydrothermale Überprägung führte in den Weißen Anorthositen zu einer generell starken Serizitisierung und Saussuritisierung der Plagioklase und Alteration der Fe-Mg-Silikate, die in einer weißen bis hellvioletten oder grünlichen Farbe der Gesteine resultieren. Die petrographischen Merkmale des namibischen Teils des Anorthositkörpers wurden im Detail von Drüppel et al. (2001, 2007) beschrieben.

2.3 Untersuchungsmethoden

Die Mineral-Analytik wurde mit Hilfe einer Elektronenstrahlmikrosonde vom Typ Cameca SX 100 mit fünf wellenlängendispersiven Spektrometern am GeoForschungsZentrum Potsdam durchgeführt. Die Messbedingungen waren 15 kV Beschleunigungsspannung, 20 nA Strahlstrom und 2 µm Strahldurchmesser. Die Messgenauigkeit der Mikrosonde beträgt für Hauptelemente ± 1 % relativ. Für Nebenelemente mit Oxidgehalten <1 Gew.% beträgt der relative Fehler ± 5 %.

Die Untersuchung der Spurenelementgehalte von Plagioklas, Pyroxen und Ilmenit wurde an polierten Dickschliffen (ca. 100 µm) mittels Laser Ablation Inductively Coupled Plasma Mass Spectrometry (LA-ICP-MS) am Lehrstuhl für Geodynamik und Geomaterialforschung der Universität Würzburg durchgeführt. Verwendet wurde ein Agilent 7500i ICP-Massenspektrometer das an einen 266 nm Nd-YAG-Laser der Firma Merchantek (Plasmastrom: 1320 W, Trägergasfluss: 1.28 l/min (Ar), Plasmagasfluss: 14.9 l/min (Ar)) gekoppelt ist. Gemessen wurden der Untergrund und die Probe mit jeweils 20 s Messzeit, einem Strahldurchmesser von 50 µm und 10 Hz Wiederholungsfrequenz. Für die externe Gerätekalibrierung wurde das zertifizierte NIST 612 Referenzmaterial mit den Werten von Pearce et al. (1997) verwendet. Als interner Standard dienten mit der Elektronenstrahlmikrosonde erfasste Si- bzw. Mn-Konzentrationen der analysierten Minerale. Die LA-ICP-MS Datenverarbeitung erfolgte mit der Software Glitter 3.0 (interaktive Online Datenverarbeitung für die LA-ICP-MS, Macquarie Research Ltd., 2000). Die Messungenauigkeit beträgt 7 % für Spurenelementkonzentrationen >10 ppm, 10 % für Spurenelementkonzentrationen >5 ppm, 15 % für Spurenelementkonzentrationen >1 ppm und 20 % für Spurenelementkonzentrationen <1 ppm. Das Auflösungsminimum liegt im Bereich von 0,02 - 0,2 ppm für Sr, Y, und die Seltenerdelemente (SEE) und bei 0,1 - 0,5 ppm für Sc, V, und Ba.

2.4 Ergebnisse

2.4.1 Petrographie der mittels LA-ICP-MS analysierten Proben

Untersucht wurden zwei Proben des Weißen Anorthosits (Ku-97-04 und Ku-06-04a) und zwei Proben des Dunklen Anorthosits (Ku-06-69 und Ku-06-18a). Die untersuchten Proben der Weißen Anorthosite zeigen unterschiedlich hohe Modalanteile an Plagioklas. Probe Ku-97-04 enthält ~65 Vol.% an zentimetergroßen, hypidiomorphen Plagioklasleisten. Orthopyroxene und Klinopyroxene in den Plagioklas-Zwischenräumen werden von spätmagmatischer Hornblende und Biotit umgeben. Ilmenit tritt sowohl als Einschluss in Plagioklas und Pyroxen als auch gemeinsam mit spätmagmatischer Hornblende auf. Apatit tritt als Nebengemengteil auf. Probe Ku-06-04a enthält dagegen >85 Vol.% Plagioklas. Große xenomorphe Plagioklaskristalle werden hierbei von kleineren

Plagioklasen umgeben. In den Zwischenräumen werden hypidiomorphe Orthopyroxene von xenomorphen Klinopyroxenen umsäumt. Ilmenit und Apatit treten nur akzessorisch auf. Späte hydrothermale Alteration führte in beiden Proben der Weißen Anorthosite zu einer Serizitisierung der Plagioklase entlang von Rissen (Abb. 2.3a und b).

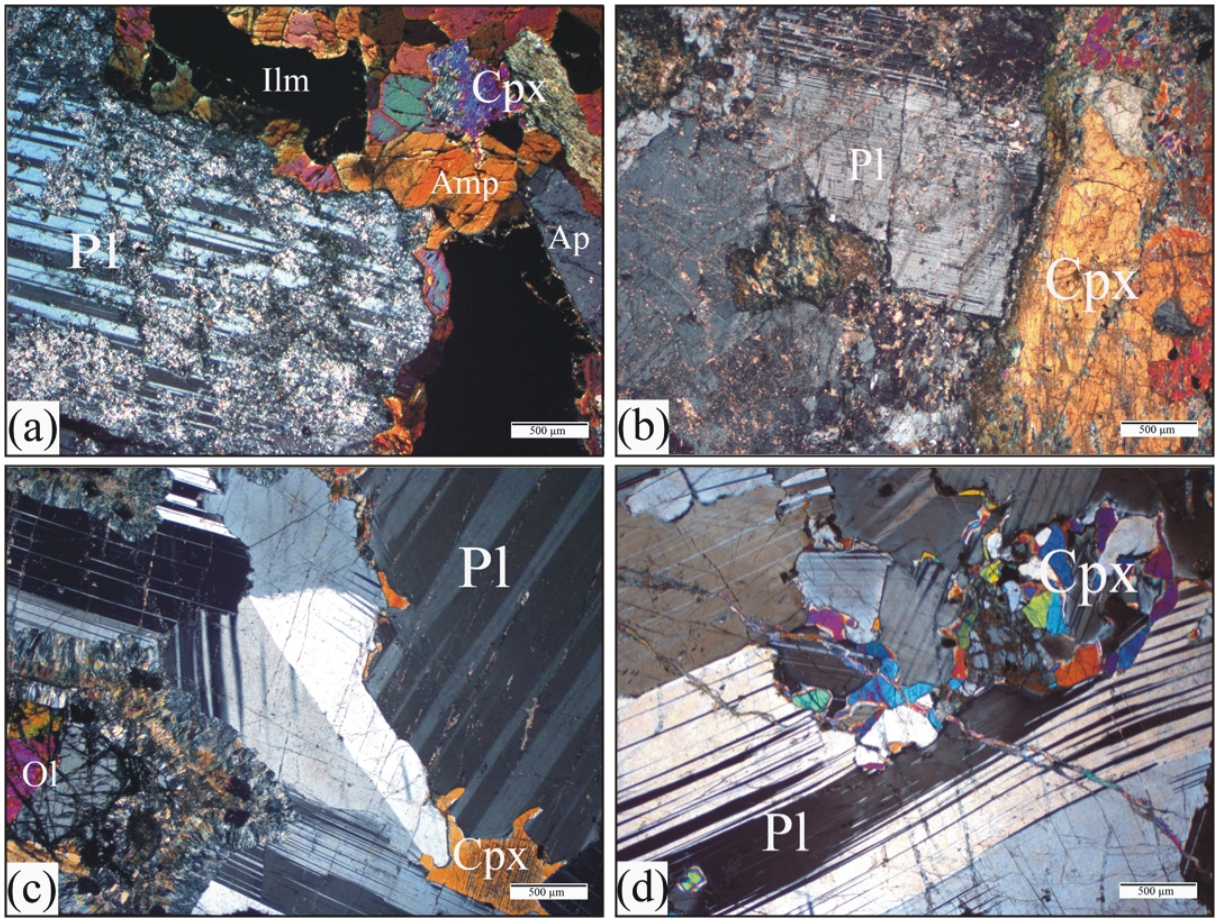

Abb. 2.3. Dünnschlifffotos der untersuchten Proben (gekreuzte Polarisatoren). (a) Ku-97-04: Plagioklas und Klinopyroxen umgeben von spätmagmatishcn Amphibol, Ilmenit und Apatit. (b) Ku-06-04a: Plagioklas neben Klinopyroxen. In beiden Proben der Weißen Anorthosite ist die Serizitisierung des Plagioklases entlang von Rissen zu erkennen. (c) Ku-06-69: Plagioklas, Olivin und später Klinopyroxen in Dunklem Anorthosit. Olivin ist von einem Saum aus Orthopyroxen und Aktinolith umgeben. (d) Ku-06-18a: Ein großer Plagioklaskristall mit Zwickelfüllung aus kleineren Plagioklasen und Klinopyroxen in Dunklem Anorthosit. (Amp-Amphibolit; Ap-Apatit; Cpx-Klinopyroxen; Ol-Olivin; Pl-Plagioklas)

Fig. 2.3. Thin section photographs of studied samples (crossed polars). (a) Ku-97-04: plagioclase and clinopyroxene surrounded by late magmatic amphibole, ilmenite and apatite. (b) Ku-06-04a: plagioclase next to clinopyroxene. Sericitisation of plagioclase along cracks is visible in both samples of the white anorthosite. (c) Ku-06-69: plagioclase, olivine and late clinopyroxene of the dark anorthosite. Olivine is rimed by orthopyroxene and actinolite. (d) A huge plagioclase crystal with smaller plagioclases and clinopyroxene in the interstices.

In den Proben der Dunklen Anorthosite ist der Modalanteil an Plagioklas >80 Vol.%. Probe Ku-06-69 zeigt zentimetergroße idiomorphe Plagioklaskristalle die von kleineren Plagioklasen umgeben

werden. Im Gegensatz dazu sind die großen Plagioklase in Probe Ku-06-18a xenomorph und zeigen buchtige Korngrenzen zu den kleineren Plagioklasen. Olivin und Ilmenit treten in beiden Proben sowohl als Einschluss in Plagioklas als auch als späte Phasen gemeinsam mit Orthopyroxen auf. Klinopyroxen tritt nur als Nebengemengteil in Zwickeln zwischen Plagioklasen auf. Subsolidus-Reaktionen führten in Probe Ku-06-69 zur Ausbildung blockartiger Orthopyroxen-Säume um Olivin (Drüppel et al., 2001). Eine schwache späte Alteration der Dunklen Anorthosite führte zur Serpentinisierung der Olivine in Probe Ku-06-18a und zu Bildung von Aktinolith entlang der Orthopyroxen-Säume in Probe Ku-06-69 (Abb. 2.3c und d).

2.4.2 Hauptelementzusammensetzung der Plagioklase

Repräsentative Haupt und Spurenelementanalysen von Plagioklasen und Klinopyroxenen sind in Tabelle 2.1 aufgelistet. Die Plagioklase der pyroxenführenden Anorthosite (Weiße Anorthosite) zeigen Anorthitgehalte (molares Ca/(Ca+Na)) von 40-50 mol.%. Ein Zonarbau ist häufig nur undeutlich ausgeprägt. Dennoch lassen sich geringfügige oszillierende Variationen der Hauptelementzusammensetzung beobachten (Abb. 2.4a). Der Anorthitgehalt der optisch klaren Plagioklase der olivinführenden Anorthosite (Dunkle Anorthosite) variiert zwischen 47 und 75 mol.%. Es treten hierbei sowohl idiomorphe Plagioklaskristalle mit komplexem oszillierendem Zonarbau und Variationen der Anorthitkomponente von bis zu 10 mol.% (Abb. 2.4c) als auch xenomorphe Plagioklaskristalle mit nahezu homogener Zusammensetzung auf (Abb. 2.4d). Häufig zu beobachten ist eine oszillierende Zonierung mit Wellenlängen von bis zu 2000 µm. Kleine, später gebildete Plagioklase weisen in allen Proben gleiche oder nur geringfügig niedrigere Anorthitgehalte (<10 mol.%) auf.

2.4.3 Spurenelementzonierung der Plagioklase

Die Plagioklase der pyroxenführenden Anorthosite zeigen variable Gehalte der leichten Seltenerdelemente und niedrige Yttrium-Gehalte. Im Gegensatz zu der annähernd homogenen Hauptelementzusammensetzung kann man für die Spurenelemente deutlich einen Kernbereich mit niedrigen und zum Rand hin zunehmenden Gehalten der leichten Seltenerdelemente beobachten, wogegen der Randbereich der Körner variable Gehalte der Seltenerdelemente aufweist (Abb. 2.4a). Andere Plagioklase zeigen variable jedoch kontinuierlich hohe Seltenerdelement-Gehalte (Abb. 2.4b).

Die Plagioklase der olivinführenden Anorthosite weisen generell niedrigere Seltenerdelement-Gehalte bei ebenso niedrigen Yttrium-Gehalten wie die der pyroxenführenden Anorthosite auf. In Proben mit einer deutlichen Variation der Hauptelemente sind auch Variationen der leichten Seltenerdelemente zu beobachten (Abb. 2.4c). Proben mit fast homogener

Hauptelementzusammensetzung zeigen hingegen nur eine geringe Zunahme der leichten Seltenerdelemente zum Rand (Abb. 2.4d).

Tabelle 2.1. Haupt und Spurenelementanalysen von Plagioklasen und Klinopyroxenen des Kunene - Intrusiv-Komplexes.
Table 2.1. Major and trace element analyses of plagioclase and clinopyroxene of the Kunene Intrusive Complex.

	Dark anorthosite				White anorthosite				
sample	Ku-06-18a	Ku-06-69	Ku-06-69	Ku-06-18a	Ku-97-04	Ku-97-04	Ku-06-04a	Ku-97-04	Ku-06-04a
mineral	Pl rim	Pl core	Pl rim	Cpx	Pl core	Pl rim	Pl rim	Cpx	Cpx
[wt.%]									
SiO_2	53.10	52.13	53.59	50.59	54.13	54.78	55.11	52.32	51.16
TiO_2	b.d.l.	b.d.l.	b.d.l.	0.74	b.d.l.	b.d.l.	b.d.l.	0.32	0.31
Al_2O_3	29.75	29.83	29.94	3.36	28.21	27.52	27.07	1.31	1.87
Cr_2O_3	n.a.	n.a.	n.a.	b.d.l.	n.a.	n.a.	n.a.	b.d.l.	b.d.l.
Fe_2O_3	0.36	0.21	b.d.l.	b.d.l.	b.d.l.	b.d.l.	0.29	0.93	b.d.l.
FeO	b.d.l.	b.d.l.	b.d.l.	8.91	b.d.l.	b.d.l.	b.d.l.	11.64	14.02
MnO	b.d.l.	b.d.l.	b.d.l.	0.26	b.d.l.	b.d.l.	b.d.l.	0.30	0.61
MgO	n.a.	n.a.	n.a.	13.87	n.a.	n.a.	n.a.	10.87	10.97
CaO	12.55	12.78	12.34	21.66	10.14	9.51	9.48	21.65	20.34
Na_2O	4.41	4.20	4.69	0.34	5.92	6.42	6.11	0.82	0.39
K_2O	0.27	0.18	b.d.l.	b.d.l.	0.12	b.d.l.	0.24	b.d.l.	b.d.l.
Total	100.42	99.31	100.56	99.73	98.51	98.23	98.26	100.17	99.67
[mol.%]									
An/*Di*	60.17	62.07	59.24	*61.69*	48.31	45.01	45.53	*54.46*	*47.34*
Ab/*Hd*	38.28	36.91	40.76	*22.22*	51.04	54.99	53.12	*32.72*	*33.95*
Or/*En*	1.56	1.02	0.00	*8.53*	0.65	0.00	1.36	*3.99*	*8.42*
[ppm]									
Sc	0.37	b.d.l.	0.99	118	0.58	0.99	0.62	143	95.50
V	3.11	3.46	2.08	446	1.44	0.77	0.50	221	151
Rb	0.92	1.62	1.85	0.14	0.21	0.18	1.19	0.08	b.d.l.
Sr	555	571	750	12.60	683	875	822	44.70	22.80
Y	0.37	0.32	0.89	65.20	0.30	0.47	0.93	15.40	137
Zr	0.08	0.07	b.d.l.	262	0.86	2.96	0.07	69.50	293
Ba	n.a.	n.a.	n.a.	0.61	477	619	379	18.10	3.54
La	2.14	1.68	5.18	1.43	2.19	5.02	16.40	1.30	11.40
Ce	4.07	2.93	9.59	7.41	4.54	8.75	21.80	4.49	45.10
Pr	0.47	0.30	1.08	1.91	0.50	0.95	2.02	0.96	9.12
Nd	1.90	1.10	3.63	14.10	1.45	2.75	5.92	5.45	56.20
Sm	0.32	0.15	0.39	6.80	0.24	0.27	0.63	2.36	18.60
Eu	0.71	0.85	1.06	0.88	1.25	1.58	2.40	0.82	1.87
Gd	0.13	0.16	0.33	10.70	0.18	0.20	0.31	3.51	22.20
Tb	0.04	b.d.l.	0.04	1.59	0.03	0.03	0.02	0.47	3.84
Dy	0.08	b.d.l.	0.23	12.30	b.d.l.	0.10	0.13	3.10	27.10
Ho	b.d.l.	b.d.l.	0.04	2.92	b.d.l.	b.d.l.	0.02	0.61	5.32
Er	b.d.l.	0.08	0.12	7.63	b.d.l.	b.d.l.	b.d.l.	2.07	15.70
Tm	b.d.l.	0.01	b.d.l.	1.09	b.d.l.	b.d.l.	b.d.l.	0.23	2.46
Yb	0.07	b.d.l.	b.d.l.	6.75	b.d.l.	b.d.l.	b.d.l.	1.39	15.10
Lu	b.d.l.	b.d.l.	b.d.l.	0.87	b.d.l.	0.03	b.d.l.	0.33	2.04
Hf	b.d.l.	b.d.l.	b.d.l.	6.00	b.d.l.	b.d.l.	b.d.l.	2.89	10.60
Σ REE	9.93	7.26	21.69	76.38	10.37	19.68	49.65	27.09	236.05
Eu/Eu*	10.58	16.77	9.02	0.31	18.55	21.03	16.61	0.87	0.28
La_N/Nd_N	2.17	2.94	2.75	0.20	2.91	3.52	5.34	0.46	0.20
Gd_N/Yb_N				1.28				2.04	1.19

ΣREE = sum of all rare earth elements; $Eu/Eu^* = Eu_N/(Sm_N \times Gd_N)^{½}$; subscript N = chondrite-normalized value.

Die Vanadium-Gehalte der Plagioklase der pyroxenführenden Anorthosite nehmen vom Kern zum Rand hin ab. Kleinere, spät kristallisierte Plagioklase weisen hierbei die geringsten Gehalte auf. Die Zirkonium-, Strontium- und leichten Seltenerdelement-Gehalte nehmen hingegen vom Kern zum Rand der Plagioklase zu (Abb. 2.5). Diese Zunahme von Strontium vom Kern zum Rand hin ist besonders deutlich in Probe Ku-97-04 ausgeprägt, die im äußersten Randbereich eine sprunghafte Abnahme von Cer aufweist (Abb. 2.5c). In den Plagioklasen aus Probe Ku-06-04a treten starke Variationen der Strontium-Konzentrationen auf, die ebenfalls vom Kern zum Rand der grobkörnigen Kristalle zunehmen und höchste Werte in den kleinkörnigen Kristallen zeigen.

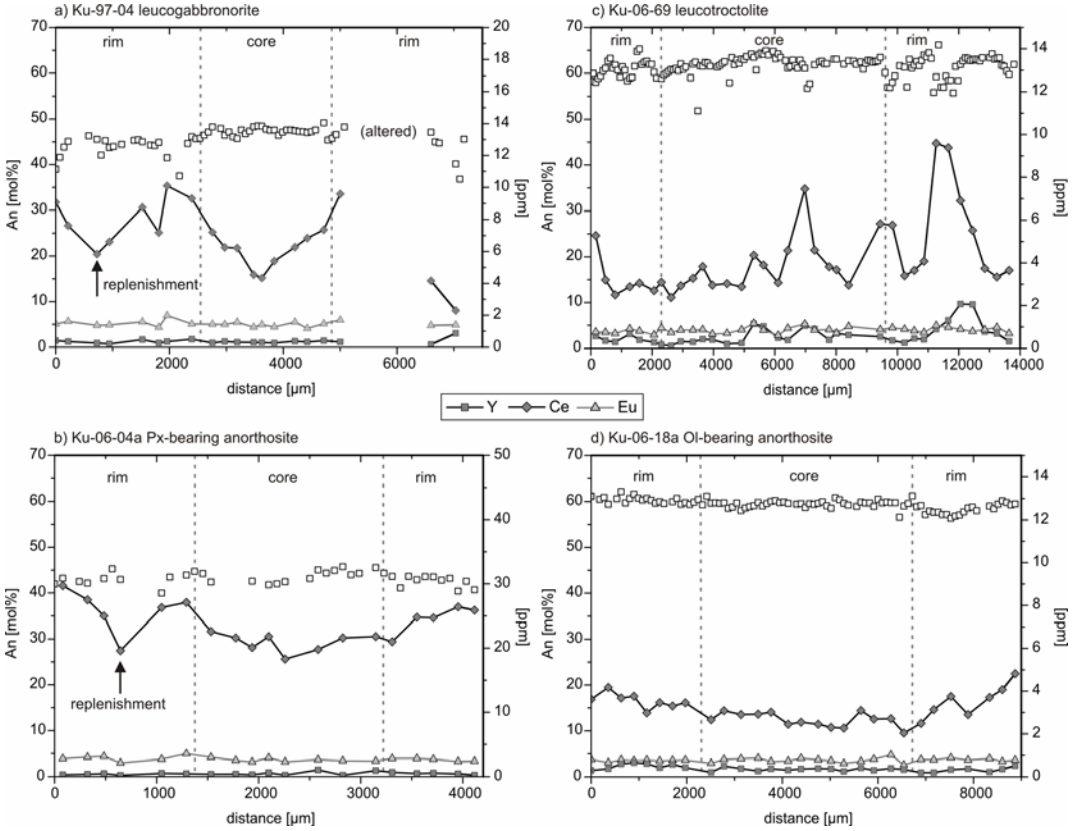

Abb. 2.4. Haupt- und Spurenelementzonierung von Plagioklaskristallen, (a und b) Weißer Anorthosit (pyroxenführend), (c und d) Dunkler Anorthosit (olivinführend). Dargestellt sind der Anorthitgehalt und die Spurenelementkonzentrationen von Yttrium, Cer (stellvertretend für die leichten Seltenerdelemente) und Europium.
Fig. 2.4. Mayor and trace element zonation across plagioclase crystals, (a and b) white anorthosite (pyroxene-bearing), (c and d) dark anorthosite (olivine-bearing). Anorthite content as well as trace element concentration of Yttrium, Cerium (representative for the light rare earth elements) and Europium are displayed.

Die bei den pyroxenführenden Anorthositen beobachtete negative Korrelation von Vanadium und den leichten Seltenerdelementen kann bei den Plagioklasen der olivinführenden Anorthosite noch deutlicher beobachtet werden. Im Gegensatz zu den pyroxenführenden Anorthositen sind hier auch Zirkonium und Strontium negativ mit den leichten Seltenerdelementen korreliert. Während im

Plagioklas aus Probe Ku-06-69 starke Variationen des Cer-Gehaltes auftreten, ist in Probe Ku-06-18a ist eine deutliche Zunahme vom Kern zum Rand der Plagioklas-Kristalle zu erkennen. Die Cer-Gehalte des äußeren Randes entsprechen hierbei denen der kleineren, spät kristallisierten Plagioklase (Abb. 2.5j).

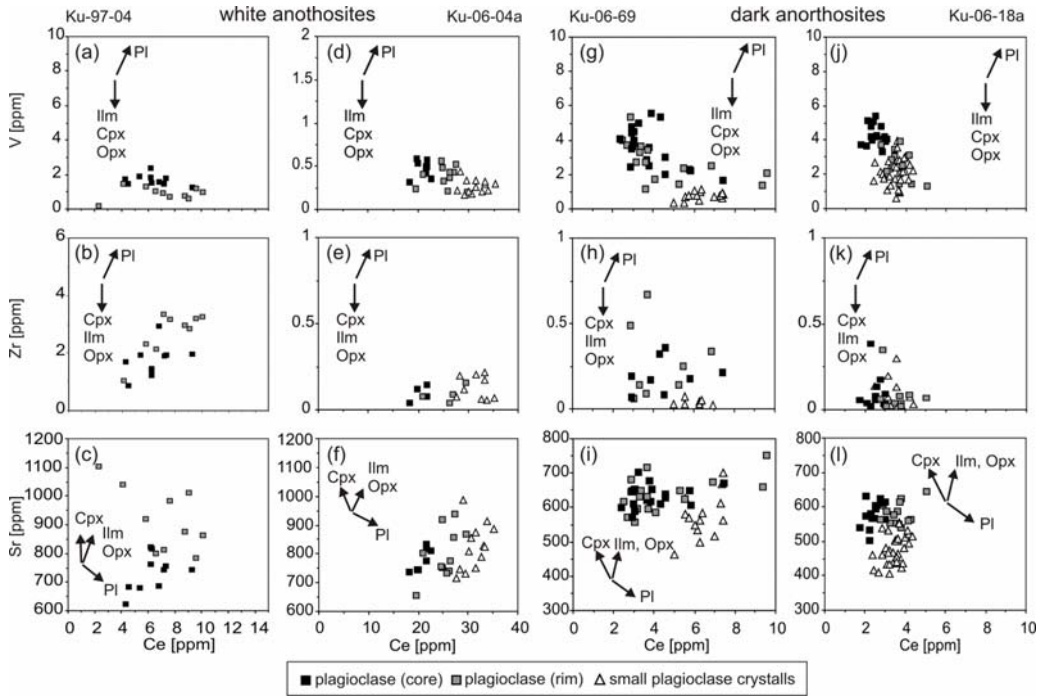

Abb. 2.5. Variationsdiagramme gemessener Spurenelementkonzentrationen in Plagioklas. (a-c) Probe Ku-97-04 und (d-f) Probe Ku-06-04a: Weiße Anorthosite. (g-i) Probe Ku-06-69 und (j-l) Probe Ku-06-18a: Dunkle Anorthosite. Die Auswirkung der gleichzeitigen Kristallisation von Plagioklas (Pl), Ilmenit (Ilm), Klino- und Orthopyroxen (Cpx, Opx) auf den Spurenelementeinbau in Plagioklas ist durch Pfeile gekennzeichnet.
Fig. 2.5. Variation diagrams of measured trace element contents in plagioclase. (a-c) sample Ku-97-04 and (d-f) sample Ku-06-04a: white anorthosite. (g-i) sample Ku-06-69 and (j-l) sample Ku-06-18a: dark anorthosite. The effect of simultaneous crystallization of plagioclase (Pl), ilmenite (ilm), clino- and orthopyroxene (Cpx, Opx) on trace element incorporation in plagioclase is indicated with arrows.

2.4.4 Spurenelementgehalte von Pyroxen und Ilmenit

Die ergänzend zu den Plagioklasen untersuchten Pyroxene und Ilmenite zeigen in allen Proben höhere Konzentrationen inkompatibler Spurenelemente (V: Ilm 200 - 2500 ppm; Opx 55 - 75 ppm; Cpx 150 - 550 Zr: Ilm 2 - 15 ppm; Opx 8 - 12 ppm; Cpx 50 - 300 ppm Y: Opx 2 - 6 ppm; Cpx 10 - 140 ppm). Leichte Seltenerdelemente treten nur in Klinopyroxen in nachweisbaren Konzentrationen auf (Ce: 5 - 65 ppm). Im Gegensatz zu den Plagioklasen sind die Konzentrationen kompatibler Spurenelemente sehr gering (Sr: Ilm <4 ppm; Opx <1 ppm; Cpx 12 - 57 ppm).

2.4.5 Chondrit-normierte Seltenerdelementmuster von Anorthositen, Plagioklasen und Klinopyroxenen

Hinsichtlich ihrer Gesamtgesteinszusammensetzung sind die Anorthosite des Kunene-Intrusiv-Komplexes durch eine Zunahme des X_{Mg} ($MgO/MgO+FeO_{tot}$) von den pyroxenführenden Anorthositen (Ku-97-04: 0,38; Ku-06-04a: 0,55) zu den olivinführenden Anorthositen (0,6 - 0,64) charakterisiert. Die Chondrit-normierten Seltenerdelementmuster (Abb. 2.6a) der Anorthosit-Gesamtgesteinsproben zeigen eine starke Anreicherung der leichten gegenüber den schweren Seltenerdelementen und positive Europium-Anomalien (Eu/Eu*: 1,3 - 11,2), die typisch für Plagioklas-Kumulatgesteine sind (Drüppel et al., 2007). Der Gesamtgehalt an Seltenerdelementen nimmt hierbei von den pyroxenführenden zu den olivinführenden Anorthositen ab, gleichzeitig nimmt die positive Europium-Anomalie zu.

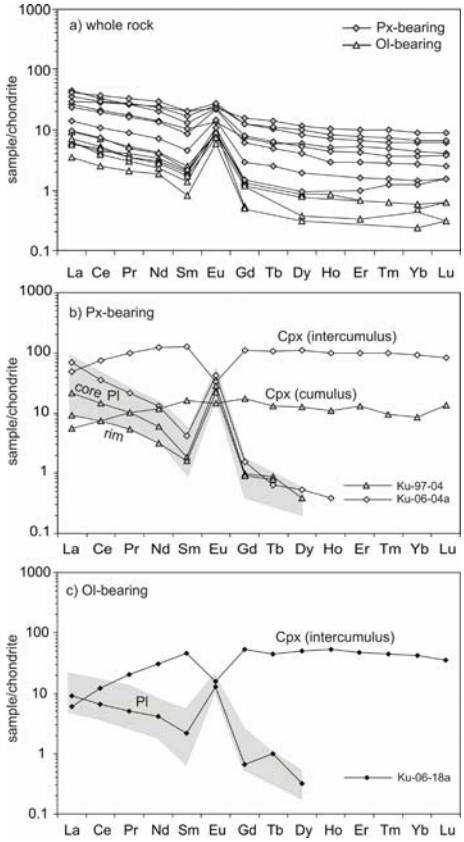

Abb. 2.6. Chondrit-normierte Seltenerdelement-Diagramme. (a) Gesamtgesteine, Daten aus Drüppel et al. (2007). (b) Plagioklas und Klinopyroxen aus pyroxenführenden Anorthositen. c) Plagioklas und Klinopyroxen aus olivinführenden Anorthosit. Die Messwerte sind in Tabelle 2.1 aufgelistet, zur Normierung wurden Chondritwerte von McDonough & Sun (1995) verwendet.
Fig. 2.6. Chondrite normalized REE diagrams. (a) Whole rocks, data from Drüppel et al. (2007). (b) plagioclase and clinopyroxene from pyroxene-bearing anorthosites. c) plagioclase and clinopyroxene from olivine-bearing anorthosite. The measured values are listed in Table 2.1, chondrite values of McDonough & Sun (1995) have been used for normalization.

Die Chondrit-normierten Seltenerdelementmuster der Plagioklase sind durch hohe Konzentrationen der leichten gegenüber den mittleren Seltenerdelementen (La_N/Nd_N: 2,1 - 5,3) und eine positive Europium-Anomalie (Eu/Eu*: 5 - 26) charakterisiert (Abb. 2.6b und c). Diese positive Europium-Anomalie variiert stark und nimmt von den Kernen zu den Rändern der Plagioklase ab. Die Konzentrationen der leichten Seltenerdelementgehalte in Plagioklas der pyroxenführenden Anorthosite variiert stark (Abb. 2.6b). Probe Ku-97-04 weist im Kernbereich Seltenerdelement-Konzentrationen (∑SEE ~10 ppm) und Seltenerdelementmuster (La_N/Nd_N: 2 - 3) ähnlich denen der olivinführenden Anorthosite auf. Zum Rand tritt sowohl eine Zunahme der Gesamtkonzentration an Seltenerdelementen (∑SEE: 15 - 20 ppm) als auch eine stärkere Anreicherung der leichten Seltenerdelemente auf (La_N/Nd_N: 3,5). In Probe Ku-06-04a sind die Konzentrationen der Seltenerdelemente am höchsten (∑SEE: 40 - 70 ppm) und der Konzentrationsunterschied zwischen leichten und mittleren Seltenerdelementen am stärksten (La_N/Nd_N: 4,3 - 5,6).

Die in den gleichen Proben gemessenen Klinopyroxene zeigen hohe Gehalte der mittleren und schweren Seltenerdelemente sowie zu den leichten Seltenerdelementen hin abnehmende Konzentrationen (La_N/Nd_N: 0,2 - 0,5) und negative Europium-Anomalien (Eu/Eu*: 0,2 - 0,3). Der Klinopyroxen im Leukogabbronorit (Ku-97-04) zeigt um eine Größenordnung geringere Konzentrationen und dementsprechend keine negative Europium-Anomalie.

2.5 Diskussion

Die beobachteten Unterschiede in Modalbestand und X_{Mg} der Gesamtgesteine und der Haupt- und Spurenelementzusammensetzung der Plagioklase lassen darauf schließen, dass es eine Änderung der Bildungsbedingungen beim Übergang von den Weißen zu den Dunklen Anorthositen gegeben hat. Die Art der Veränderungen der physikochemischen Bedingungen in der Magmenkammer innerhalb eines Magmenzyklus lassen sich aus den beobachteten Hauptelement-Zonierungsmustern allein nur vermuten. Die beobachteten Spurenelement-Zonierungsmuster der Plagioklase zeigen jedoch, dass in Zuge der Genese der älteren, pyroxenführenden Weißen Anorthosite und der jüngeren olivinführenden Dunklen Anorthosite eine signifikante Änderung in der Schmelzzusammensetzung oder in den Kristallisationsbedingungen erfolgte. Verschiedene Prozesse könnten für derartige physikochemische Änderungen verantwortlich sein, insbesondere (1) zyklische Zufuhr von primitiven Mantelschmelzen, (2) fraktionierte Kristallisation von Plagioklas und assoziierten Mineralen, (3) Assimilation von krustalem Nebengesteinsmaterial und (4) Bewegung der sich bildenden Plagioklase in einer chemisch und thermisch inhomogen Magmenkammer. Diese sollen im Folgenden in ihrer Bedeutung für die Gesteine des Kunene-Intrusiv-Komplexes im Detail diskutiert werden.

Aufgrund der enormen Größe des Kunene-Intrusiv-Komplexes von ~18.000 km^2 und seiner nahezu monomineralischen, plagioklasreichen Zusammensetzung ist anzunehmen, dass mehrere Schübe von

unfraktionierten Mantelschmelzen erforderlich waren um die großen Volumina an plagioklasreichem Schmelzbrei zu bilden. Eine solche zyklische Zufuhr primitiver Magmen hätte bei gleichzeitig erfolgender fraktionierter Kristallisation (von Olivin und Plagioklas) eine Erhöhung der inkompatiblen Elemente (wie z.B. V, Y, Zr, SEE) in der Schmelze zur Folge (O'Hara, 1977).

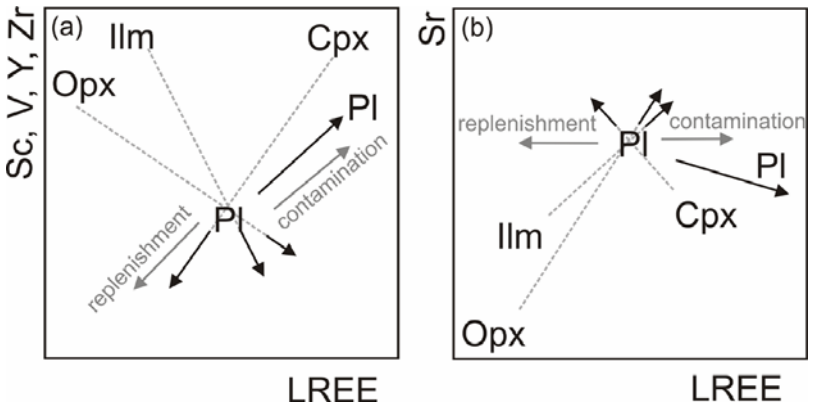

Abb. 2.7. Schematische Darstellung der Auswirkung der Fraktionierung von Plagioklas, Ilmenit, Klino- und Orthopyroxen, der Kontamination mit krustalen Gesteinen und der Zufuhr primitiver Schmelze auf den Spurenelementeinbau in Plagioklas. a) inkompatible Elemente b) kompatible Elemente.
Fig. 2.7. Schematic illustration of the consequences of fractionation of plagioclase, ilmenite, clino- and orthopyroxene, the contamination with crustal rocks and replenishment with primitive melt on the trace element content of plagioclase. a) incompatible elements b) compatible elements.

Die extreme Anreicherung des Ca-Feldspates Plagioklas in allen Gesteinseinheiten des Kunene-Intrusiv-Komplexes lässt sich nur über eine sekundäre Anreicherung von Plagioklas über fraktionierte Kristallisation erklären, da partielle Mantelschmelzen mit einer primären anorthositischen Zusammensetzung nicht bekannt sind. Weitere Minerale, deren frühe fraktionierte Kristallisation eine Änderung der Zusammensetzung der Mantelschmelzen zur Folge hätte sind Olivin, Pyroxen und Fe-Ti-Oxide. Auch die Kristallisation von Apatit, der in den Gesteinen als spätmagmatisches Kristallisationsprodukt auftritt, hat signifikante Auswirkungen auf die Zusammensetzung der Restschmelze. In Abbildung 2.7 sind schematisch die Auswirkungen der gleichzeitigen, sukzessiven Kristallisation von Plagioklas, Olivin, Pyroxen und Ilmenit auf die Zusammensetzung der Schmelze und damit auf den kristallisierenden Plagioklas dargestellt. Die dargestellten Trends unterscheiden sich deutlich: während die Kristallisation von Plagioklas allein eine Erhöhung inkompatibler sowie eine Abnahme kompatibler Elemente zur Folge hat, ergibt sich für die gleichzeitige Kristallisation von Plagioklas, Pyroxen und Ilmenit eine Abnahme der inkompatiblen Elemente. Die zeitgleiche Kristallisation von Plagioklas und großen Mengen an Ilmenit und Pyroxen kann hingegen, entsprechend dem Modell von Blundy & Wood (1991), zu einer Zunahme der Konzentration kompatibler Elemente in der Restschmelze und somit im neu gebildeten Plagioklas führen.

Das Auftreten von krustalen Xenolithen, insbesondere in den älteren Weißen Anorthositen (Drüppel et al., 2001, 2007), deutet zudem darauf hin, dass die Zusammensetzung der Schmelzen signifikant durch Assimilation von Nebengesteinsmaterial verändert wurde. Die Untersuchungen der metamorphen Rahmengesteine des Epupa-Komplexes durch Brandt (2003) zeigen, dass eine Kontamination mit diesen Gesteinen eine Erhöhung der inkompatiblen Elemente (K, Rb, Zr, Ba, SEE) zur Folge hätte. Dagegen sind die Sr-Konzentrationen dieser Gesteine ähnlich denen oder sogar niedriger als die der anorthositischen Magmen und haben somit vermutlich nur eine untergeordnete Bedeutung für die Zusammensetzung der Schmelze. In Abbildung 2.7 ist das schematisch als konstante Strontium-Konzentration bei gleichzeitiger Erhöhung inkompatibler Elemente dargestellt. Eine Zufuhr primitiver Schmelze würde entgegengesetzt dem Trend der krustalen Kontamination auf die Zusammensetzung der anorthositischen Magmen wirken.

Alteration der Gesteine im Anschluss an die Platznahme und unter hydrothermalen Bedingungen kann nachträglich zu einer Mobilisierung von Spurenelementen führen. Die leichten Seltenerdelemente sind hierbei leichter im Fluid mobilisierbar; ihre Konzentration in Plagioklas kann daher durch Interaktion mit hydrothermalen Fluiden stark erhöht werden. Es wurden aus diesem Grund nur optisch intakte Bereiche in Plagioklas analysiert. Analysen mit sehr hohen Konzentrationen an leicht mobilisierbaren Elementen wie z.B. Rubidium und Barium wurden verworfen.

2.5.1 Pyroxenführende Weiße Anorthosite

Generell lassen der niedrigere Anorthitgehalt der Plagioklase (40-50 mol.%), der niedrige X_{Mg} (0,35 - 0,58) und die höheren Gehalte der leichten Seltenerdelemente im Gesamtgestein sowie der hohe Modalanteil spätmagmatischer, wasserhaltiger Phasen wie Biotit und Amphibol darauf schließen, dass die Magmen eine stärkere Kontamination mit krustalem Nebengesteinsmaterial erfuhren (Drüppel et al., 2007). Übereinstimmend zeigen die Chondrit-normierten Seltenerdelement-Muster der Plagioklase aus Weißen Anorthositen eine höhere Konzentration der leichten Seltenerdelemente und eine stärkere Anreicherung der leichten gegenüber den mittleren Seltenerdelementen.

Die Variationsdiagramme für Vanadium (Abb. 2.5a und d) weisen auf eine Kristallisation von Plagioklas gemeinsam mit Ilmenit und/oder Pyroxen in den pyroxenführenden Anorthositen hin. Die in Plagioklas aus Probe Ku-97-04 auftretende Zunahme des kompatiblen Strontium ist durch die geringe Abnahme des Anorthitgehaltes zum Rand und der damit verbundenen Erhöhung des Verteilungskoeffizienten (Blundy & Wood, 1991) nicht erklärbar, sondern vermutlich ebenfalls auf die frühe Kristallisation von Pyroxen und Ilmenit zurückzuführen. Die Kristallisation von Klinopyroxen zu einem relativ frühen Zeitpunkt während der Plagioklasbildung wird auch durch die moderate Anreicherung inkompatibler Elemente, den hohen Strontium-Gehalt von 44 ppm und eine fehlende positive Europium-Anomalie in Klinopyroxen bestätigt. Die beobachtete starke Zunahme des

Zirkonium-Gehaltes im Plagioklas (Abb. 2.5b) ist bei gleichzeitiger Kristallisation von Ilmenit und Klinopyroxen nur durch eine Kontamination mit zirkoniumreichen Material, vermutlich aus der Kruste, möglich. Die deutliche positive Korrelation von Zirkonium und Cer zeigt, dass auch die leichten Seltenerdelemente durch eine Kontamination der Schmelze durch krustales Material angereichert wurden. Die beobachtete sprunghafte Abnahme von Cer am äußersten Rand des Plagioklaskristalls (Abb. 2.5c) wird dagegen vermutlich durch die spätmagmatische Kristallisation von Apatit verursacht.

In Probe Ku-06-04a deutet die hohe Konzentration der leichten Seltenerdelemente im Plagioklas (>20 ppm Ce, Abb. 2.5d-f) auf eine Kristallisation aus einer im Vergleich zu den olivinführenden Anorthositen Seltenerdelement-reicheren Schmelze hin. Die Zirkonium-Gehalte im Plagioklas sind niedrig (<0,5 ppm) und bleiben trotz der aus Abbildung 2.5d ersichtlichen gleichzeitigen Kristallisation von Ilmenit und/oder Pyroxen fast konstant. Im Gegensatz zu Probe Ku-97-04 lässt sich hier nicht zweifelsfrei auf eine krustale Kontamination während der Plagioklas-Kristallisation schließen. Auch die deutlich negativen Europium-Anomalien (Eu/Eu*: 0,28) der Klinopyroxene machen eine stärkere krustale Kontamination während und nach der Plagioklas-Kristallisation unwahrscheinlich. Eine Kontamination der Schmelze vor dem Beginn der Plagioklas-Kristallisation ist somit wahrscheinlich.

Die starken Variationen der Strontium-Konzentrationen der Plagioklase in Probe Ku-06-04a sind nicht mit dem Anorthitgehalt korreliert und können nur durch starke Fluktuationen der Strontium-Konzentration in der Schmelze verursacht worden sein. Die gezeigten Trends im Ce/Sr-Variationsdiagramm (Abb. 2.5f) weisen auf eine Mischung von Prozessen wie Plagioklas-Fraktionierung, Zufuhr primitiver Mantelschmelzen und fraktionierter Kristallisation anderer Phasen wie Ilmenit und Pyroxen hin. Niedrige Konzentrationen der leichten Seltenerdelemente in mittleren Randbereichen der Plagioklase der pyroxenführenden Anorthosite (Abb. 2.4a und b) können hierbei als Folge einer solchen Zufuhr primitiverer Schmelze interpretiert werden. Die Kristallisation größerer Mengen an Apatit zu diesem Zeitpunkt ist unwahrscheinlich, da dies eine dauerhafte Erniedrigung der leichten Seltenerdelement-Gehalte in der Restschmelze zur Folge hätte, die anhand der untersuchten Phasen nicht bestätigt werden kann.

2.5.2 Olivinführende Dunkle Anorthosite

Die Variationsdiagramme der inkompatiblen Elemente (V, Zr) der olivinführenden Anorthosite weisen auf eine gleichzeitige Kristallisation von Plagioklas und Ilmenit hin. Im Gegensatz zu den Weißen Anorthositen sind keine Indizien für eine frühe Kristallisation von Klinopyroxen gegeben, übereinstimmend ist Ilmenit als Einschluss in Plagioklas zu beobachten. Durch den hohen Verteilungskoeffizienten für Strontium zwischen Plagioklas und Schmelze (>1) und die große Menge

neu gebildeter Plagioklase wird die weitere Entwicklung von Strontium in Plagioklas fast ausschließlich durch die fortschreitende Plagioklas-Fraktionierung bestimmt (Abb. 2.5i und l).

Die frühe Kristallisation von Olivin, die in den Proben beobachtet werden kann, hat auf den Spurenelementeinbau in Plagioklas nur insofern eine Auswirkung als durch die Olivin-Fraktionierung eine Erniedrigung des X_{Mg} und eine Erhöhung der Gehalte inkompatibler Elemente erfolgte. Der geringe Modalbestand und die texturelle Position des Klinopyroxens als spätes Kristallisationsprodukt sowie seine sehr niedrigen Strontium-Gehalte (<16 ppm), deutlich negativen Europium-Anomalien (Eu/Eu*: 0,31) und hohen Gehalte an inkompatiblen Elementen lassen ebenfalls auf dessen sehr späte Kristallisation schließen.

Das einzige petrographische Anzeichen für eine krustale Kontamination der Dunklen Anorthosite ist das vereinzelte Auftreten von Biotit. Die im Plagioklas-Zonierungsprofil aus Abbildung 2.4c sichtbaren sprunghaften Anstiege des Cer gehen nicht mit einer deutlichen Abnahme sondern mit fast gleich bleibenden Konzentrationen von Zirkonium und Strontium einher. Diese Trends könnten entsprechend durch kleinere Kontaminationsereignisse und anschließende Zufuhr primitiverer Schmelzen während des Wachstums der Plagioklase verursacht werden. In Probe Ku-06-18a können der kaum merkliche Rückgang der Cer-Konzentration am Übergang von Kern zu Rand und die homogenen Zusammensetzungen spät kristallisierter Plagioklase als Folgen der Zufuhr primitiverer Schmelzen interpretiert werden.

2.6 Schlussfolgerungen

Anhand der Spurenelement-Untersuchung von Plagioklasen und assoziierten Mineralen aus Anorthositen können Rückschlüsse auf den Kristallisationsverlauf und die chemischen Veränderungen der kristallisierenden Phasen und der koexistierenden Schmelze gezogen werden. Alle untersuchten Proben weisen auf eine fraktionierte Kristallisation von Plagioklas als wichtigsten Prozess der Magmengenese hin. Der Einbau von inkompatiblen Spurenelementen in Plagioklas wird hierbei durch Zusammensetzung der Schmelze und die zeitgleiche Kristallisation von Ilmenit und/oder Pyroxen kontrolliert. Auf den Einbau kompatibler Spurenelemente hat deren Kristallisation nur dann einen Einfluss, wenn größere Volumina dieser Minerale gebildet werden. Eine Assimilation krustaler Gesteine während der Plagioklas-Kristallisation ist deutlich von einer Veränderung der chemischen Zusammensetzung des Magmas durch fraktionierte Kristallisation unterscheidbar.

Im Falle der Weißen Anorthosite des Kunene-Intrusiv-Komplexes fand in der Magmenkammer eine beträchtliche Assimilation krustaler Gesteine statt. Diese erfolgte zu einem frühen Zeitpunkt vor und während der Plagioklas-Kristallisation in der Magmenkammer. Die dabei kristallisierten Plagioklase weisen geringere Anorthitgehalte und hohe Konzentrationen inkompatibler Spurenelemente auf. In einigen Fällen fand eine simultane Fraktionierung von Pyroxen und Ilmenit

statt. Die in diesem Fall gebildeten Plagioklase sind durch vom Kern zum Rand hin zunehmende Strontium-Gehalte und höhere Konzentrationen inkompatibler Elemente wie Zirkonium gekennzeichnet, die typisch für die krustale Kontamination sind. Das vermehrte Auftreten der späten Phasen Amphibol, Biotit und Apatit weist auf eine weitere Anreicherung der Restschmelze mit Wasser, Kalium und Phosphor vor deren Kristallisation hin.

Die Verhältnisse in der Magmenkammer müssen sich nach dem diapirartigen Aufstieg der späteren Weißen Anorthosite dahingehend geändert haben, dass während der Genese der Dunklen Anorthosite die Zufuhr primitiverer Schmelze in die Magmenkammer überwog und krustale Kontamination nur eine untergeordnete Rolle spielte. Die bei der fraktionierten Kristallisation von Plagioklas, Olivin und Ilmenit gebildeten Plagioklase weisen einen höheren Anorthitgehalt und niedrigere Konzentrationen inkompatibler Spurenelemente auf. Vereinzelt traten kleinere Kontaminationsereignisse auf, die aber durch anschließende Zufuhr primitiver Schmelze in die Magmenkammer nicht zu einer dauerhaften Veränderung der Spurenelement-Konzentration in der Schmelze und damit in den kristallisierenden Plagioklasen führten. In kleineren, späten Plagioklasen tritt weder eine deutliche Änderung der Hauptelement-Zusammensetzung auf noch weichen sie wesentlich vom Spurenelement-Trend der frühen Plagioklase ab. Ihre Bildung aus einer beim Aufstieg stark kontaminierten Restschmelze ist somit unwahrscheinlich. Die spätesten Phasen der Dunklen Anorthosite sind Klinopyroxen und Ilmenit; eine starke Veränderung der Restschmelze durch krustale Kontamination ist somit unwahrscheinlich.

Chapter 3

Magmatic evolution of anorthosites of the Kunene Intrusive Complex, NW Namibia: evidence from oxygen isotope data and trace element zoning

Autoren: Philipp Gleißner[1], Kirsten Drüppel[1], Heinrich Taubald[2]

[1]Technische Universität Berlin, Institut für Angewandte Geowissenschaften, Ackerstr. 71-76, 13355 Berlin

[2]Universität Tübingen, Institut für Geowissenschaften, Wilhelmstr. 56, 72074 Tübingen

Publiziert in: Journal of Petrology, Volume 51, Number 4, Pages 897-919,
Oxford University Press (2010)

Eigenanteil:
Probennahme gemeinsam mit Dr. Kirsten Drüppel, selbständige Dünnschliffuntersuchung und EMP-Analytik, LA-ICP-MS-Analytik gemeinsam mit Dr. Helene Brätz, selbständige Mineralseparation für die Sauerstoffisotopen Untersuchungen, Auswertung und Interpretation der Ergebnisse gemeinsam mit Dr. Kirsten Drüppel, selbständige Ausarbeitung der Publikation.

Abstract

In the Mesoproterozoic Kunene Intrusive Complex (Angola/Namibia), one of the largest massif-type anorthosite complexes in the world, two successively emplaced anorthosite varieties can be recognized. The older white anorthosite suite consists of pyroxene-bearing anorthosite and leucogabbronorite, whereas the younger dark anorthosite suite is dominated by olivine-bearing anorthosite and leucotroctolite. The oxygen isotope and trace element characteristics of plagioclase and minor phases of the two distinct anorthosite varieties are consistent with their derivation from a mantle-derived parental melt that was subject to crustal contamination during the early stages of evolution. The trace element zoning patterns of plagioclase demonstrate that the older white anorthosite was derived by simultaneous fractional crystallization of plagioclase, pyroxene and Fe-Ti oxides during and after crustal contamination. In contrast, the subsequently emplaced dark anorthosite evolved after replenishment with mantle-derived parental melts by fractional crystallization of plagioclase, olivine and Fe-Ti oxides at magmatic temperatures above 1150°C and experienced less crustal contamination.

3.1 Introduction

Massif-type anorthosites that commonly form large intrusions with minor volumes of mafic and felsic rocks are a prominent feature of the Proterozoic crust. The origin of the parental melts and the specific anorthosite-forming processes remains subject of debate.

Petrography and isotopic compositions, commonly close to mantle values (e.g. Demaiffe & Javoy, 1980; Mitchell et al., 1995; Scoates & Frost, 1996), are consistent with a mantle origin of the parental magma. Plagioclase cumulates fractionated from high-Al basaltic parental melt at the crust-mantle boundary are assumed to float at the top of the magma chamber and ascend as crystal mush diapirs (Ashwal, 1993; Emslie et al,. 1994; Morse, 2006). According to this model, oxygen isotopic compositions exceeding the magmatic anorthosite range (Taylor, 1968) are interpreted to result from crustal contamination of the primitive parental magma (Morrison & Valley, 1988; O'Connor & Morrison, 1999; Peck & Valley, 2000).

Based on Sr isotopic compositions, Taylor et al. (1984) proposed that the parental magma of anorthosites is derived by melting of a mafic lower crustal source. Convincing arguments for this model are provided by the Os isotopic composition of anorthosites from Norway and Poland (Schiellerup et al., 2000; Morgan et al., 2000) as well as phase equilibria and fractional crystallization modelling of designated parental melt compositions (Longhi et al., 1999; Longhi, 2005). According to this model, intracrustal melting is triggered by a mantle plume (Taylor et al., 1984) or by downthrusting of tongues of crustal material along lithospheric-scale weakness zones (Duchesne et al.,

1999) to produce ferrodioritic (jotunitic) parental melts (e.g. Vander Auwera et al., 1998). The anorthosite formation is interpreted in a similar way as the classic model, including polybaric fractional crystallization and plagioclase accumulation (Vander Auwera et al., 1998, 2000; Duchesne et al., 1999).

The Kunene Intrusive Complex (KIC), Namibia, a typical massif-type anorthosite, was not subject to a later metamorphic overprint and hence preserved primary magmatic phases and textures (Ashwal & Twist, 1994; Drüppel et al., 2001, 2007; Mayer et al., 2004). In previous studies of the Namibian KIC, Drüppel et al. (2001, 2007) recognised two major and successively emplaced anorthosite suites. They demonstrate that the geochemical characteristics of the anorthosites are in agreement with their derivation from fractionated basaltic liquids, with the oxygen isotope composition of plagioclase supporting a mantle origin of the magma, whereas Sr and Nd isotope data suggest minor crustal contamination during the early intrusion stages.

In order to gain information about the fractional crystallization, crustal contamination and emplacement processes operative during the anorthosite formation, we analysed the oxygen isotope and in situ trace element composition of plagioclase, olivine, pyroxene, amphibole, apatite, ilmenite and magnetite from the two anorthosite suites. These phases, which crystallized during successive stages of crystallisation and cumulate formation, provide important information on the magma composition and crystallization history, involving assimilation and fractional crystallisation processes. Moreover, the composition of the early liquidus phases enables us to get insight into earlier stages of the magmatic evolution and to constrain the oxygen isotope and trace element characteristics of the parental melt and compositional characteristics of crustal contaminants.

3.2 Geological setting

The approximately 18,000 km^2 Kunene Intrusive Complex extends from NW Namibia into SW Angola (Fig. 3.1) and is one of the largest massif-type anorthosite intrusions of the world (Ashwal & Twist, 1994). The anorthositic rocks were emplaced at the southern margin of the Congo craton during the Mesoproterozoic (Mayer et al., 2004).

In NW Namibia the KIC intruded the high-grade metamorphic Epupa Complex (EC). Neoarchean to Paleoproterozoic protholith ages corresponding to the Eburnian orogeny demonstrate that the EC was part of the Congo craton since the Paleoproterozoic (Tegtmeyer & Kröner, 1985; Seth et al., 2005). The Paleo-Mesoproterozoic rocks of the northeastern EC, including our study area, are overlain by undeformed Neoproterozoic sediments of the Damara Supergroup (Fig. 3.1; Brandt et al., 2007), whereas the south-western part of the EC was reworked during the Pan-African orogeny and incorporated in the Pan-African mobile belt (Seth et al., 2005). In the study area the EC mainly comprises upper amphibolite facies rocks of the Orue Unit and the locally restricted ultrahigh-

temperature granulite facies Epembe Unit (Brandt et al., 2007). The Orue Unit is dominated by large bodies of migmatitic metagranitoids, which intruded a volcano-sedimentary succession of migmatitic metagreywackes, intercalated with mafic metavolcanitic rocks, metapelites, metaarkoses, metaquartzites and rare calc-silicate rocks (Brandt & Klemd, 2008). The Epembe Unit is dominated by intercalated felsic and mafic orthogneisses and subordinate paragneisses (Brandt et al., 2007). Both the Orue and the Epembe Unit were intruded by mafic dykes, which were metamorphosed to amphibolites and two-pyroxene granulites (Brandt, 2003).

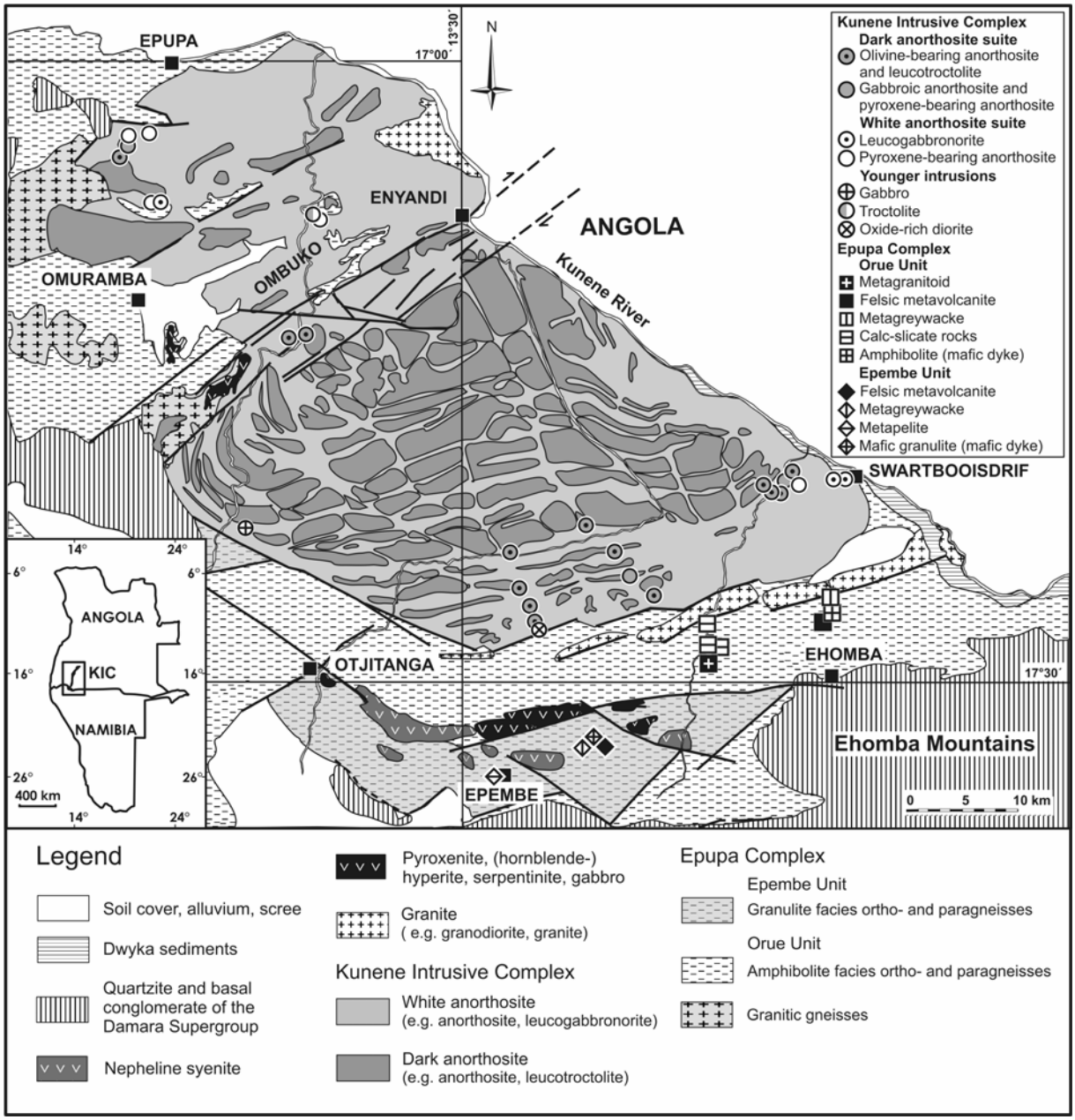

Fig. 3.1. Geological map of the southern Kunene Intrusive Complex and the adjacent Epupa Complex in NW Namibia. Map after Menge (1998), modified by Brandt et al. (2007) and Drüppel et al. (2007). Locations of samples used for oxygen isotope analysis are indicated. Inset shows location of the Kunene Intrusive Complex in SW Angola and NW Namibia.

The contact between the KIC and the surrounding Orue Unit is largely obliterated by broad ductile shear zones and late brittle faults, intruded by syenite and/or dolerite dykes (Drüppel et al., 2007). However, the local occurrence of thermal contact aureoles and the coincidence in pressure of 6 - 8 kbar, determined by Grt-Opx-Pl-Qtz barometry, for subsolidus reaction textures that developed during isobaric cooling of the igneous body (Drüppel et al., 2001, 2007) and metamorphism of the Orue Unit (Brandt & Klemd, 2008) suggest that the latter represents the basement at the intrusion level.

The KIC is a composite massif-type anorthosite that comprises several N-S elongated anorthosite bodies separated by belts of coeval granitoid intrusions in its Angolan part (Ashwal & Twist, 1994; Morais et al., 1998). In the Namibian part of the KIC two anorthosite varieties were distinguished, a tectonized and altered pale 'white anorthosite' and a weakly to non-altered 'dark anorthosite' (Menge, 1998; Drüppel et al., 2001, 2007). The younger dark anorthosite mainly intruded in the form of sheet-like bodies in the centre of the white anorthosite massif and grades into smaller bodies towards the margin of the complex, forming an E-W striking structure (Drüppel et al., 2001, 2007). In NW Namibia a U-Pb zircon age of 1385 ± 25 Ma was obtained for a leucogabbronorite of the dark anorthosite suite (Drüppel et al., 2000). U-Pb zircon ages of cogenetic mangerite in the Angolan part and syenodiorite in the Namibian part of the KIC are 1371 ± 2.5 Ma (Mayer et al., 2004) and 1376 ± 2 Ma (Drüppel et al., 2007), respectively.

The white anorthosite suite mainly comprises pyroxene-bearing anorthosite and leucogabbronorite with well developed cumulate textures. Variable hydrothermal alteration (sericitisation and saussuritisation of plagioclase, uralitisation of pyroxene), induced presumably by interaction with late stage fluids of the younger dark anorthosites, is responsible for their pale colour and higher erodibility (Drüppel et al., 2001, 2007). The dark anorthosite suite mainly consists of leucotroctolite and olivine-bearing anorthosite. The rocks are generally fresh and massive in appearance and display homogeneous cumulate textures. Rare magmatic foliation on the outcrop scale is defined by plagioclase lamination.

Small gabbro and oxide-rich diorite intrusions, several tens of meters in diameter, occur close to the southern margin of the complex. Field relations indicate that they intrude the hosting white anorthosite. A felsic rock suite is associated with the anorthosites and comprises mainly granites, syenites and syenodiorites (Drüppel et al., 2007).

The KIC of our study area is transected by a major NE trending ~6 km wide dextral shear zone (Fig. 3.1). Intermingling zones between structurally isolated slices of Orue Unit crustal rocks and partly foliated anorthosites within and north of this shear zone were occasionally intruded by small troctolite bodies.

3.3 Methods

Major and trace element contents of rock samples were analysed with a PHILIPS PW 2400 wavelength-dispersive X-ray fluorescence spectrometer at the Institut für Angewandte Geowissenschaften, TU Berlin, Germany, using fused glass discs. The approximation of $Fe^{2+/3+}$ was carried out by the method after Wilson (1960) at the GeoForschungsZentrum Potsdam, Germany.

Electron microprobe analyses were performed on a Cameca Camebax instrument at the Zentraleinrichtung für Elektronenmikroskopie, Technische Universität Berlin. Natural and synthetic standards were used for instrument calibration. Mineral analyses were performed with an accelerating voltage of 15 kV, a beam current of 13 nA and an electron beam of 2.5 µm in diameter. Electron microprobe profiles across minerals were analysed using a Cameca SX100 instrument at the GeoForschungsZentrum Potsdam, Germany. Analyses were performed with an accelerating voltage of 15 kV, a beam current of 20 nA and a beam diameter of 2 µm.

In-situ trace element analyses of anorthosite minerals were done on polished ~100 µm thick sections by laser ablation-inductively coupled plasma mass spectrometry (LA-ICP-MS) at the Institut für Geodynamik und Geomaterialforschung of the Universität Würzburg, Germany. A Merchantek 266 LUV laser coupled with an Agilent 7500i ICP-MS device was used (plasma power 1250 W, carrier gas (Ar) 1.28 L/min, plasma gas (Ar) 14.9 L/min, auxiliary gas (Ar) 0.9 L/min). The diameter of the laser beam was 50 µm and the laser repetition rate 10 Hz for all analyses. We measured background and sample 20 s each. Si in silicates, Ca in apatite, and Mn in ilmenite and magnetite were used as internal standards. The glass reference materials NIST 612 (values Pearce et al., 1997) and NIST 614 (values Horn et al., 1997) were used for external instrument calibration and for control of the results. Data processing was realised using GLITTER 3.0 software (On-line Interactive Data Reduction for the LA-ICPMS, Macquarie Research Ltd., 2000). The precision is approximately ± 7 % for element concentrations >10 ppm, ± 10 % for concentrations >5 ppm, ± 15 % for concentrations >1 ppm and ± 20 % for concentrations <1 ppm. The minimum detection limits were in the range of 0.02-0.5 ppm.

The oxygen isotope compositions of whole rock samples and mineral separates were measured at the Institut für Geowissenschaften, Universität Tübingen, Germany. Mineral separation was carried out by standard magnetic separation techniques followed by handpicking. Oxygen from whole rock samples was extracted using a conventional extraction with BrF_5 reagent, according to a method adapted after Clayton & Mayeda (1963). About 7 mg of sample were used and the extracted oxygen was converted to CO_2. The samples were loaded into a Ni-reaction vessel in a dry N_2 stream and pumped for at least 2 h before adding BrF_5. Reaction was performed at 550ºC for 16 - 18 h. Oxygen from mineral separate samples was extracted using a method described by Kasemann et al. (2001 and references therein). Between 2 to 4 mg of sample were loaded onto a small Pt-sample holder. After

preflourination of the sample chamber at a vacuum of ~10^{-6} mbar overnight, the samples were heated with a CO_2-laser at 50 mbar of pure F_2. Excess F_2 was separated from the O_2 produced by conversion to Cl_2 using KCl held at 150°C. The extracted O_2 was collected on a molecular sieve (13X) and subsequently expanded and analyzed using a Finnigan MAT 252 isotope ratio mass spectrometer. Replicate oxygen isotope analyses of the standards (NBS-28 quartz and UWG-2 garnet; Valley et al., 1995) had an average precision of ± 0.1 ‰ for $\delta^{18}O$. The accuracy of $\delta^{18}O$ values is better than 0.2 ‰ compared to accepted $\delta^{18}O$ values for NBS-28 of 9.64 ‰ and UWG-2 of 5.8 ‰.

3.4 Geochemistry of anorthosites and basement rocks

Rocks of the KIC were analysed for their major and trace element composition and compiled with data of Drüppel (2003). Representative analyses are given in Table 3.1. Anorthositic rocks are rich in Al_2O_3 (15 - 30 wt.%), CaO (8 - 14 wt.%), Na_2O (2 - 5 wt.%) and Sr (400-800 ppm), reflecting high amounts of cumulate plagioclase. The bulk cumulate rocks define an overall trend of increasing Al_2O_3 and CaO, with increasing X_{Mg} from the white towards the dark anorthosite suite, reflecting the higher anorthite content of plagioclase and the occurrence of Mg-rich olivine in the dark anorthosites (Fig. 3.2). The concentration of incompatible trace elements like K, Ba and Zr is generally higher in the white anorthosites. Major and trace element composition of younger gabbroic and troctolitic intrusions falls in the overall trend of the anorthosites except for lower Al_2O_3, CaO and Sr, reflecting the lower abundance of cumulus plagioclase.

To characterize possible crustal contaminants, calc-silicate rocks of the neighbouring Orue Unit were analysed for their chemical composition and compiled with geochemical data of the main lithologies of the EC given in Brandt (2003). Paragneisses and felsic orthogneisses are characterized by high concentrations of incompatible trace elements like K, Ba and Zr when compared to the anorthosites. The calc-silicates coincide with the EC paragneisses in major elements but are lower in K, Ba and Zr.

3.5 Petrography and mineral chemistry

Samples from both the white and the dark anorthosite suite commonly display well-preserved primary magmatic assemblages and textures. A detailed petrographic description is given in Drüppel et al. (2001, 2007). Representative chemical analyses of minerals are provided in Table 3.2.

Table 3.1. Representative major and trace element data of Kunene Intrusive Complex anorthositic rocks and Epupa Complex calc-silicate rocks.

	White anorthosite suite				Dark anorthosite suite				Younger intrusions		Epupa Complex		
rock type	Apx	Apx	Apx	LGN	Apx	Aol	LT	LT	Di	G	Cs	Cs	Cs
sample	Ku-06-04a	Ku-06-04b	Ku-06-60	Ku-97-04[D]	Ku-06-06	Ku-06-18a	Ku-06-48	Ku-06-69	Ku-06-20a	Ku-06-31b	B-347-99	B-588-3-99	B-342-6
wt.%													
SiO_2	55.01	56.19	50.99	43.91	50.51	51.39	50.37	48.87	42.88	51.33	69.15	64.77	64.30
TiO_2	0.11	0.06	0.10	4.24	0.18	0.17	0.10	0.30	6.60	0.44	0.36	0.51	0.58
Al_2O_3	22.04	23.98	27.12	15.85	27.35	27.48	24.49	23.72	11.81	17.33	11.23	16.12	16.79
Fe_2O_3	3.50	1.33	1.11	4.00	1.29	1.82	3.62	2.27	7.41	1.97	2.41	2.68	2.84
FeO	0.68	0.50	1.87	9.24	1.14	0.67	2.28	4.25	11.55	3.99	3.90	2.38	2.63
MnO	0.10	0.05	0.05	0.25	0.04	b.d.l.	0.07	0.08	0.25	0.13	0.41	0.40	0.08
MgO	2.61	0.77	3.15	4.42	1.94	1.91	5.40	6.16	5.62	8.35	2.06	2.05	3.17
CaO	7.98	7.55	11.85	10.14	11.72	11.80	10.19	10.44	9.02	13.19	5.08	4.34	1.35
Na_2O	5.82	7.08	3.35	3.35	4.16	3.91	3.46	3.02	2.25	2.36	0.74	0.76	2.99
K_2O	0.62	0.57	0.34	1.27	0.26	0.30	0.30	0.30	0.34	0.18	1.85	3.07	2.33
P_2O_5	b.d.l.	0.03	0.02	0.16	0.02	0.02	b.d.l.	0.02	0.02	b.d.l.	0.05	0.14	0.07
L.O.I.	1.51	1.61	0.63	1.61	1.41	0.66	0.24	1.15	0.20	0.78	1.93	2.81	2.82
Total	99.98	99.96	100.86	98.60	100.28	100.13	100.88	100.58	97.95	100.05	99.17	100.03	99.95
X_{Mg}	0.55	0.45	0.66	0.38	0.60	0.60	0.63	0.64	0.35	0.72	0.38	0.43	0.52
ppm													
V	n.a.	n.a.	b.d.l.	296	n.a.	n.a.	b.d.l.	33.1	n.a.	144	27.3	56.5	66.8
Cr	88.0	b.d.l.	32.7	36.0	36.0	b.d.l.	24.1	33.4	71.7	497	24.6	61.2	75.1
Ni	99.0	61.0	49.3	36.0	31.0	42.0	123.4	127.8	44.0	95.4	18.4	26.9	32.1
Zn	55.0	24.0	17.1	118	26.0	b.d.l.	32.2	43.3	126	31.4	56.0	74.6	104.9
Ga	24.0	26.0	18.0	b.d.l.	20.0	22.0	15.9	19.1	22.0	14.2	13.5	22.3	18.6
Rb	20.0	15.0	23.9	28.0	18.0	15.0	18.9	22.5	b.d.l.	23.0	87.5	163.4	124.4
Sr	791	740	605	447	579	505	446	427	245	296	65.6	120	150
Y	15.0	b.d.l.	b.d.l.	19.0	b.d.l.	b.d.l.	b.d.l.	b.d.l.	14.0	b.d.l.	51.5	29.4	38.6
Zr	29.7	197	b.d.l.	104	b.d.l.	b.d.l.	b.d.l.	b.d.l.	57.9	b.d.l.	248	178	166
Nb	b.d.l.	b.d.l.	b.d.l.	15.0	b.d.l.	b.d.l.	b.d.l.	b.d.l.	b.d.l.	b.d.l.	16.5	17.9	16.1
Ba	570	769	96.4	567	471	184	130	101	361	81.5	194	424	354
Pb	17.0	12.0	b.d.l.	b.d.l.	17.0	b.d.l.	b.d.l.	b.d.l.	b.d.l.	b.d.l.	b.d.l.	15.5	24.5
Th	b.d.l.	b.d.l.	b.d.l.	b.d.l.	b.d.l.	11.3	b.d.l.	b.d.l.	14.8	b.d.l.	b.d.l.	24.3	23.7
Ce	38.0	49.0	b.d.l.	b.d.l.	b.d.l.	b.d.l.	b.d.l.	b.d.l.	60.0	b.d.l.	44.4	90.1	111.7

Aol, olivine-bearing anorthosite; Apx, pyroxene-bearing anorthosite; b.d.l., below detection limit; Cs, calc-silicate rock; Di, oxide-rich diorite; G, gabbro; GA, gabbroic anorthosite; Gn, gneiss; Gran, granulite; LGN, leucogabbronorite; LT, leucotroctolite; L.O.I., loss on ignition; n.a., not analysed; T, troctolite; [D]Drüppel (2003).

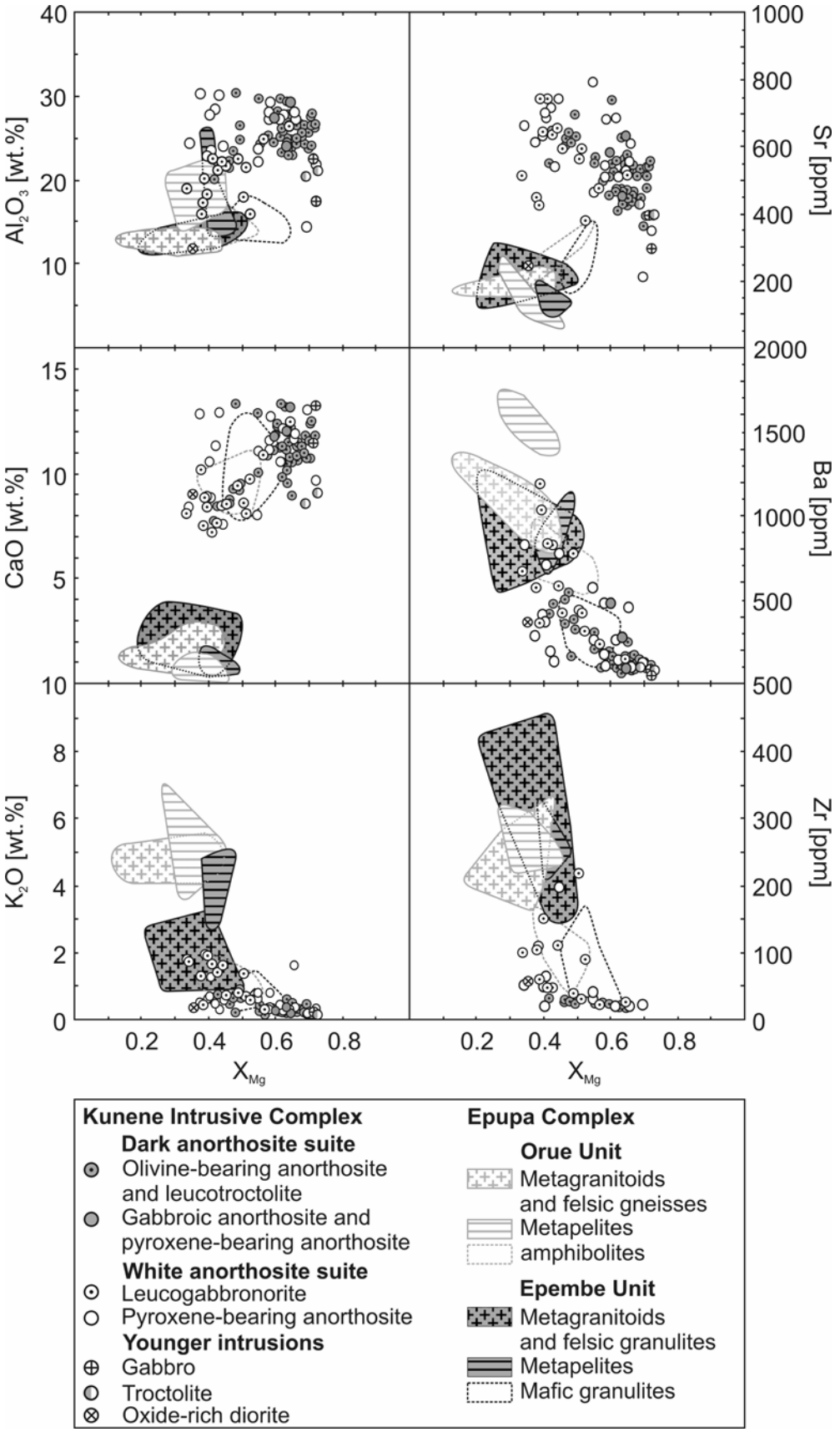

Fig. 3.2. Major and trace element characteristics of anorthositic rocks of the Kunene Intrusive Complex compared to lithologies of the Epupa Complex. Data compiled from Brandt (2003), Drüppel (2003) and this study.

3.5.1 White anorthosite suite

Rocks of the white anorthosite suite display the assemblage of cumulus plagioclase ± cumulus orthopyroxene + interstitial ortho- and clinopyroxene + ilmenite ± magnetite ± biotite ± amphibole ± apatite ± zircon ± sulfides (Fig. 3.3a). Pyroxene-bearing anorthosites are dominated by coarse and anhedral plagioclase without preferred orientation, whereas leucogabbronorites may display laminar textures, weakly defined by a subparallel orientation of euhedral, cm-sized plagioclase. Plagioclase (An_{39-64}) shows minor irregular oscillatory zoning with a variation of the anorthite content of less than 3 mol.%. Thin normal zoned outermost rims occur in euhedral plagioclase of a leucogabbronorite (Fig. 3.4a). Cumulus orthopyroxene (X_{Mg}: 0.57 - 0.72) contains up to 3.5 wt.% Al_2O_3 and occasionally occurs as megacrysts of up to 8 cm in diameter. Coexisting plagioclase and pyroxene (X_{Mg}: 0.57 - 0.78) of the white anorthosite suite display a higher variability in compositions when compared to anorthosite complexes world-wide (Fig 3.5a). Ilmenite ($Ilm_{82-95}Pyr_{3.7-13.9}Hem_{0.7-3.6}$) and magnetite occur as mm-sized inclusions in cumulus plagioclase and also as cm-sized interstitial grains. Late magmatic biotite and amphibole surround pyroxene and Fe-Ti oxides and contain euhedral inclusions of apatite.

Some samples of the white anorthosite suite display unequivocal petrographic indicators for crustal contamination. Drüppel et al. (2007) reported relic xenocrysts of andradite-rich garnet within leucogabbronorite from the south-eastern part of the KIC. The grains occur in the interstices between cumulus plagioclase and are partially replaced by chlorite during later hydrothermal alteration of the rocks (Fig. 3.3b). The occurrence of zircon in anorthosites of the KIC is generally scarce. In rare white anorthosite samples euhedral zircon occurs as inclusion in plagioclase or as anhedral grains together with late orthopyroxene, biotite and anorthite-rich plagioclase (Fig. 3.3c).

3.5.2 Dark anorthosite suite

Rocks of the dark anorthosite suite display the primary magmatic assemblage of cumulus plagioclase + olivine + interstitial ortho- and clinopyroxene + ilmenite ± magnetite ± biotite (Fig. 3.3d). Olivine-bearing anorthosites and leucotroctolites are dominated by subhedral, tabular coarse-grained (commonly 0.5 - 3 cm in diameter) cumulus plagioclase (An_{53-65}). Olivine (Fo_{56-74}) occurs as individual grains and as inclusions in plagioclase, testifying to its early crystallisation contemporaneously with plagioclase. Orthopyroxene and clinopyroxene (X_{Mg}: 0.64 - 0.74) occur as late rims around olivine or as interstitial phases. Ilmenite ($Ilm_{88-98}Pyr_{0.6-12.6}Geik_{0.0-9.7}Hem_{0.2-4.4}$) and magnetite are minor phases and occur as inclusions in cumulus plagioclase and also as anhedral interstitial grains. In general magnetite is more abundant in the dark anorthosite than in the white anorthosite suite, even though ilmenite is always the dominant Fe-Ti oxide. In some samples minor

Table 3.2. Major and trace element composition of plagioclase, pyroxene, amphibole, apatite, olivine, ilmenite, and magnetite from anorthosites of the Kunene Intrusive Complex.

	White anorthosite						Dark anorthosite								
rock type	LGN	LGN	LGN	Apx	Apx	Apx	LT	LT	LT	Aol	Aol	Aol	Apx	Apx	Apx
sample	Ku-97-04	Ku-97-04	Ku-97-04	Ku-06-04a	Ku-06-04a	Ku-06-04a	Ku-06-69	Ku-06-69	Ku-06-69	Ku-06-18a	Ku-06-18a	Ku-06-18a	Ku-06-06	Ku-06-06	Ku-06-06
mineral	Pl	Pl	Pl	Pl	Pl	Pl	Pl	Pl	Pl	Pl	Pl	Pl	Pl	Pl	Pl
position	core	rim	rim	core	rim	matrix	core	rim	matrix	core	rim	matrix	core	rim	matrix
wt.%															
SiO_2	54.67	54.89	57.00	56.57	56.19	56.70	52.33	53.53	54.03	52.91	53.10	53.63	53.20	53.02	53.59
TiO_2	b.d.l.	b.d.l.	b.d.l.	b.d.l.	b.d.l.	b.d.l.	b.d.l.	b.d.l.	b.d.l.	b.d.l.	b.d.l.	b.d.l.	b.d.l.	b.d.l.	b.d.l.
Al_2O_3	28.50	28.49	27.78	27.50	27.56	27.07	30.34	29.77	29.79	29.22	29.75	29.32	29.97	30.18	29.92
FeO	b.d.l.	b.d.l.	b.d.l.	0.24	b.d.l.	0.16	0.28	b.d.l.	b.d.l.	0.39	0.33	0.25	b.d.l.	0.17	b.d.l.
CaO	10.24	10.26	8.65	9.11	9.39	8.76	13.04	12.16	11.89	12.42	12.55	12.05	12.36	12.54	12.34
Na_2O	5.98	6.08	7.39	6.68	6.63	6.60	4.08	4.71	5.05	4.42	4.41	4.74	4.81	4.58	4.88
K_2O	0.12	b.d.l.	0.15	0.23	b.d.l.	0.49	0.20	0.10	b.d.l.	0.36	0.27	0.47	b.d.l.	b.d.l.	b.d.l.
Total	99.50	99.72	100.96	100.32	99.77	99.88	100.27	100.27	100.75	99.72	100.42	100.46	100.34	100.48	100.73
An	48.31	48.25	38.98	42.44	43.91	41.13	63.12	58.45	56.54	59.61	60.17	56.91	58.70	60.24	58.28
Ab	51.04	51.75	60.23	56.28	56.09	56.11	35.73	40.96	43.46	38.35	38.28	40.46	41.30	39.76	41.72
Or	0.65	0.00	0.79	1.27	0.00	2.76	1.15	0.59	0.00	2.04	1.56	2.64	0.00	0.00	0.00
ppm															
Be	0.319	0.529	0.679	1.65	1.02	1.76	0.247	<0.30	0.152	0.257	0.351	0.204	0.260	<0.18	0.244
Sc	0.578	0.639	1.06	0.371	0.357	0.58	b.d.l.	b.d.l.	0.366	0.451	0.367	0.621	0.421	0.572	0.503
V	1.44	1.15	0.567	0.306	0.429	0.298	2.38	1.34	0.485	4.18	3.11	3.00	2.23	3.58	1.82
Rb	0.211	0.066	0.096	1.64	1.34	0.842	1.49	1.85	0.924	7.93	0.915	1.25	2.37	1.95	3.22
Sr	683	784	1011	737	857	828	643	657	498	530	555	485	516	644	500
Y	0.299	0.321	0.41	0.235	0.452	1.95	0.236	1.30	0.266	0.315	0.367	0.416	0.280	0.369	0.308
Zr	0.862	3.18	2.83	0.039	0.085	0.172	b.d.l.	b.d.l.	0.047	0.025	0.083	<0.02	0.037	0.092	0.039
Nb	0.080	0.901	1.14	b.d.l.	0.024	b.d.l.	b.d.l.	0.036	b.d.l.	<0.01	<0.01	<0.02	0.024	b.d.l.	<0.01
Ba	477	586	538	579	352	578	n.a.	n.a.	n.a.	n.a.	n.a.	n.a.	n.a.	n.a.	n.a.
La	2.19	5.14	5.31	12.7	18.0	22.2	1.48	5.01	3.11	1.40	2.14	1.96	0.829	1.36	1.75
Ce	4.54	9.59	9.07	18.3	27.1	33.2	2.88	9.38	6.25	2.45	4.07	3.87	1.60	2.86	3.78
Pr	0.498	0.844	0.757	1.40	2.14	2.96	0.335	1.17	0.654	0.235	0.467	0.415	0.246	0.402	0.384
Nd	1.45	2.77	2.12	4.40	6.29	9.55	1.23	3.89	2.27	1.05	1.90	1.76	0.627	1.46	1.28
Sm	0.237	0.296	b.d.l.	0.426	0.836	0.983	0.222	0.765	0.129	0.093	0.321	0.326	0.334	0.274	0.244
Eu	1.25	1.70	1.45	2.28	3.55	3.29	0.862	0.978	0.757	0.732	0.712	0.838	0.584	0.700	0.816
Gd	0.178	0.191	<0.15	0.171	0.234	0.609	0.097	0.307	0.220	0.116	0.131	0.167	0.098	0.176	0.110
Tb	0.028	<0.02	<0.02	0.015	0.027	0.086	0.028	<0.02	<0.01	<0.02	0.036	0.026	<0.02	0.047	<0.01
Dy	<0.06	0.143	<0.08	0.066	0.153	0.372	0.091	0.373	<0.05	<0.04	0.079	0.095	<0.08	<0.01	0.056
Ho	<0.01	0.041	<0.02	<0.01	<0.02	0.070	<0.02	0.056	<0.01	<0.01	<0.01	<0.01	<0.02	<0.02	<0.01
Er	<0.05	0.063	<0.05	0.046	<0.05	0.146	<0.06	<0.08	<0.03	<0.05	<0.02	<0.03	<0.06	<0.04	<0.05
Tm	<0.02	0.019	<0.02	<0.01	<0.01	<0.02	<0.03	<0.01	<0.01	<0.02	<0.01	<0.01	<0.02	<0.02	<0.01
Yb	<0.07	<0.09	0.134	0.064	<0.08	0.092	<0.12	<0.15	<0.06	<0.07	0.073	<0.06	<0.11	0.122	0.055
Lu	<0.02	<0.02	<0.02	<0.01	<0.02	<0.02	<0.01	<0.03	<0.01	<0.01	<0.02	<0.01	<0.02	<0.03	<0.01
Σ REE	10.37	20.80	18.84	39.87	58.33	73.56	7.23	21.93	13.39	6.08	9.93	9.46	4.32	7.40	8.48
Eu/Eu*	18.55	21.79		25.75	24.47	12.96	17.91	6.15	13.70	21.48	10.58	10.95	9.84	9.72	15.18
La_N/Sm_N	5.77	10.84		18.62	13.45	14.10	4.16	4.09	15.06	9.40	4.16	3.75	1.55	3.10	4.48

Table 3.2. Continued.

	White anorthosite			Dark anorthosite			White anorthosite		
rock type	LGN	LGN	Apx	Aol	LT	Aol	LGN	LGN	Apx
sample	Ku-97-04	Ku-97-04	Ku-06-04a	Ku-06-18a	Ku-06-69	Ku-06-18a	Ku-97-04	Ku-97-04	Ku-06-04a
mineral	Cpx	Cpx	Cpx	Cpx	Opx	Opx	Amp	Ap	Ap
position	cumulus	cumulus	interstital	interstital	interstital	interstital	interstital	interstital	interstital
wt.%									
SiO_2	52.32	52.13	51.16	50.59	53.01	52.87	41.09	n.a.	n.a.
TiO_2	0.32	0.16	0.31	0.74	0.24	0.31	2.62	n.a.	n.a.
Al_2O_3	1.31	1.39	1.87	3.36	1.69	1.62	12.27	n.a.	n.a.
Fe_2O_3	0.93	1.41	0.00	0.00	0.00	0.00	0.34	n.a.	n.a.
P_2O_5	n.a.	n.a.	n.a.	n.a.	n.a.	n.a.	n.a.	40.97	40.83
FeO	11.64	11.36	14.02	8.91	20.22	19.61	18.00	n.a.	n.a.
MgO	10.87	10.60	10.97	13.87	24.20	24.28	8.81	n.a.	n.a.
CaO	21.65	21.98	20.34	21.66	0.85	1.00	10.90	53.75	54.04
MnO	0.30	0.34	0.61	0.26	0.36	0.49	0.17	n.a.	n.a.
Na_2O	0.82	0.80	0.39	0.34	b.d.l.	b.d.l.	2.38	n.a.	n.a.
K_2O	b.d.l.	b.d.l.	b.d.l.	b.d.l.	b.d.l.	b.d.l.	0.98	n.a.	n.a.
F	n.a.	n.a.	n.a.	n.a.	n.a.	n.a.	n.a.	1.51	0.73
Cl	n.a.	n.a.	n.a.	n.a.	n.a.	n.a.	n.a.	b.d.l.	1.18
Total	100.17	100.17	99.67	99.73	100.58	100.17	97.55	96.23	96.78
Wo	46.5	47.2	43.7	45.2	1.7	2.0			
En	32.5	31.6	32.8	40.3	66.9	67.4			
Fs	20.9	21.2	23.5	14.5	31.4	30.6			
X_{Mg}	0.62	0.62	0.58	0.74	0.68	0.69	0.47		
ppm									
Li	7.33	4.74	2.68	1.69	<0.84	<1.4	1.40	2.01	0.353
Be	0.505	<0.23	0.988	<0.31	<0.24	<0.55	<0.30	<0.11	<0.17
Sc	143	90.2	95.5	118	42.6	25.3	65.9	0.353	<0.22
Ti	n.a.	n.a.	n.a.	n.a.	1888	n.a.	n.a.	206	268
V	221	188	151	446	55.3	57.0	166	5.74	2.62
Mn	n.a.	n.a.	n.a.	n.a.	2419	n.a.	n.a.	252	595
Rb	0.080	0.994	<0.06	0.136	<0.08	<0.10	2.47	1.28	0.108
Sr	44.7	40.1	22.8	12.6	<0.07	<0.09	73.8	375	224
Y	15.4	10.2	137	65.2	2.87	6.04	18.6	221	1196
Zr	69.5	39.4	293	262	8.32	11.7	77.0	5.53	4.12
Nb	0.834	0.460	0.559	0.194	<0.07	<0.11	3.29	0.063	0.058
Ba	18.1	59.6	3.54	0.606	<0.56	<0.54	243	11.6	0.648
La	1.30	1.51	11.4	1.43	<0.04	<0.08	3.30	219	336
Ce	4.49	6.97	45.1	7.41	<0.05	<0.08	11.0	552	1468
Pr	0.958	1.23	9.12	1.91	<0.05	<0.05	1.94	72.0	250
Nd	5.45	5.63	56.2	14.1	<0.26	<0.37	11.9	352	1226
Sm	2.36	1.78	18.6	6.80	0.394	<0.42	3.70	72.1	272
Eu	0.824	0.826	1.87	0.879	<0.12	<0.12	1.42	22.8	22.1
Gd	3.51	2.61	22.2	10.7	<0.43	<0.33	4.69	69.5	287
Tb	0.468	0.314	3.84	1.59	0.078	0.095	0.574	7.75	36.3
Dy	3.10	2.39	27.1	12.3	<0.25	0.784	3.89	44.0	214
Ho	0.606	0.401	5.32	2.92	0.115	0.262	0.789	8.39	40.9
Er	2.07	1.09	15.7	7.63	0.459	0.941	1.84	19.3	109
Tm	0.232	0.181	2.46	1.09	0.151	0.177	0.236	2.27	15.3
Yb	1.39	1.24	15.1	6.75	0.724	1.43	1.49	12.9	101
Lu	0.328	0.201	2.04	0.869	0.212	0.196	0.267	1.58	14.2
Hf	2.89	1.47	10.6	6	0.590	0.388	1.99	0.177	0.076
Ta	0.102	0.057	0.095	<0.04	0.100	<0.05	0.143	<0.02	<0.01
Σ REE	27.09	26.37	236.05	76.38	2.13	3.89	47.04	1456	4392
Eu/Eu*	0.87	1.17	0.28	0.31			1.04	0.98	0.24
La_N/Yb_N	0.64	0.83	0.51	0.14			1.50	11.53	2.26
Gd_N/Yb_N	2.04	1.70	1.19	1.28			2.55	4.36	2.30

Table 3.2. Continued.

	Dark anorthosite			White anorthosite		Dark anorthosite				
rock type	LT	Aol		LGN	LGN	LT	LT	Aol		Aol
sample	Ku-06-69	Ku-06-69		Ku-97-04	Ku-97-04	Ku-06-69	Ku-06-69	Ku-06-18a		Ku-06-18a
mineral	Ol	Ol		Ilm	Ilm	Ilm	Ilm	Ilm		Mag
position	cumulus	interstital		in Cpx	interstital	in Pl	interstital	interstital		interstital
wt.%										
SiO_2	36.37	36.40		b.d.l.	b.d.l.	b.d.l.	b.d.l.	b.d.l.		b.d.l.
TiO_2	b.d.l.	b.d.l.		51.16	51.34	51.84	51.33	51.49		0.07
Al_2O_3	b.d.l.	b.d.l.		b.d.l.	b.d.l.	b.d.l.	b.d.l.	b.d.l.		0.15
Cr_2O_3	b.d.l.	b.d.l.		b.d.l.	b.d.l.	b.d.l.	b.d.l.	b.d.l.		0.42
Fe_2O_3	0.00	0.00		2.55	2.26	2.27	3.09	2.33		67.83
FeO	32.14	32.60		44.27	44.04	41.93	44.79	43.88		30.94
MgO	31.38	31.23		b.d.l.	b.d.l.	b.d.l.	0.34	b.d.l.		b.d.l.
CaO	b.d.l.	b.d.l.		b.d.l.	b.d.l.	b.d.l.	b.d.l.	b.d.l.		b.d.l.
MnO	0.33	0.34		1.71	2.10	4.62	0.75	2.40		b.d.l.
NiO	0.18	0.16		n.a.	n.a.	n.a.	n.a.	n.a.		n.a.
Total	100.39	100.72		99.68	99.73	100.66	100.29	100.09		99.40
Fa	36.35	36.79	Ilm	93.89	93.35	88.02	94.20	92.67	Mag	98.82
Fo	63.27	62.83	Pyr	3.68	4.50	9.83	1.60	5.12	Chr	0.65
Te	0.38	0.39	Hem	2.43	2.15	2.14	2.92	2.21	Hc	0.33
ppm										
Li	2.80	4.40		<0.54	<0.70	<0.76	<0.75	<0.52		<0.33
Be	<0.36	<0.50		<0.26	<0.33	<0.57	<0.25	<0.32		<0.21
Sc	1.30	<0.92		21.2	10.8	78.6	38.9	27.9		0.600
Ti	20.7	34.3		n.a.	n.a.	n.a.	n.a.	n.a.		n.a.
V	<0.35	<0.36		254	405	2403	1052	415		2932
Mn	1923	1775		n.a.	n.a.	n.a.	n.a.	n.a.		138
Rb	<0.11	<0.11		<0.05	<0.07	<0.12	<0.05	<0.05		<0.05
Sr	<0.05	<0.06		0.600	0.700	0.600	0.500	0.700		0.500
Y	<0.06	<0.06		0.100	0.100	0.100	0.100	0.100		0.100
Zr	<0.10	0.200		11.7	5.70	1.10	2.00	10.4		0.300
Nb	<0.09	<0.08		105	99.0	351	142	239		<0.04
Ba	<0.56	<0.65		<0.34	<0.57	<0.37	<0.47	<0.42		<0.26
Hf	<0.20	<0.19		3.20	0.600	0.400	0.500	0.400		<0.10
Ta	<0.06	<0.05		9.60	10.0	22.2	11.5	14.3		<0.03
Nb/Ta				10.9	10.0	15.8	12.3	16.7		

Rock types as in Table 3.1; symbols for minerals after Kretz (1983); Geik, geikielite; Pyr, pyrophanite; Te, tephroite; b.d.l., below detection limit; n.a., not analysed; <, gives the minimum detection limit.

biotite and occasionally amphibole occur as late magmatic rims around opaque minerals and pyroxenes.

In plagioclase, large-scale wavy oscillatory zoning with variations in anorthite content of 5 mol.% is common (Fig. 3.4c). Reversed rims on plagioclase (ΔAn 5 - 18 mol.%) were observed sporadically, bordering interstitial mafic silicates. In contrast, anhedral plagioclase in one sample of olivine-bearing anorthosite with a nearly homogeneous composition shows recrystallization microstructures interpreted as a syn-emplacement feature (Fig. 3.4d). The composition of mafic silicates is more restricted, and significant zoning is absent. The range in average compositions of plagioclase and

olivine overlap with those of the northern KIC, although Ashwal & Twist (1994) reported slightly more clacic plagioclase. When compared to other anorthosite complexes the olivine-bearing rocks of the KIC coincide with the anorthosites of Labrador (Fig. 3.5b).

Gabbroic anorthosites and pyroxene-bearing anorthosites of the dark anorthosite suite display a well-preserved cumulate texture of euhedral plagioclase laths and interstitial clinopyroxene. The chemical composition of cumulus and intercumulus phases coincide with those of the olivine-bearing rocks described above.

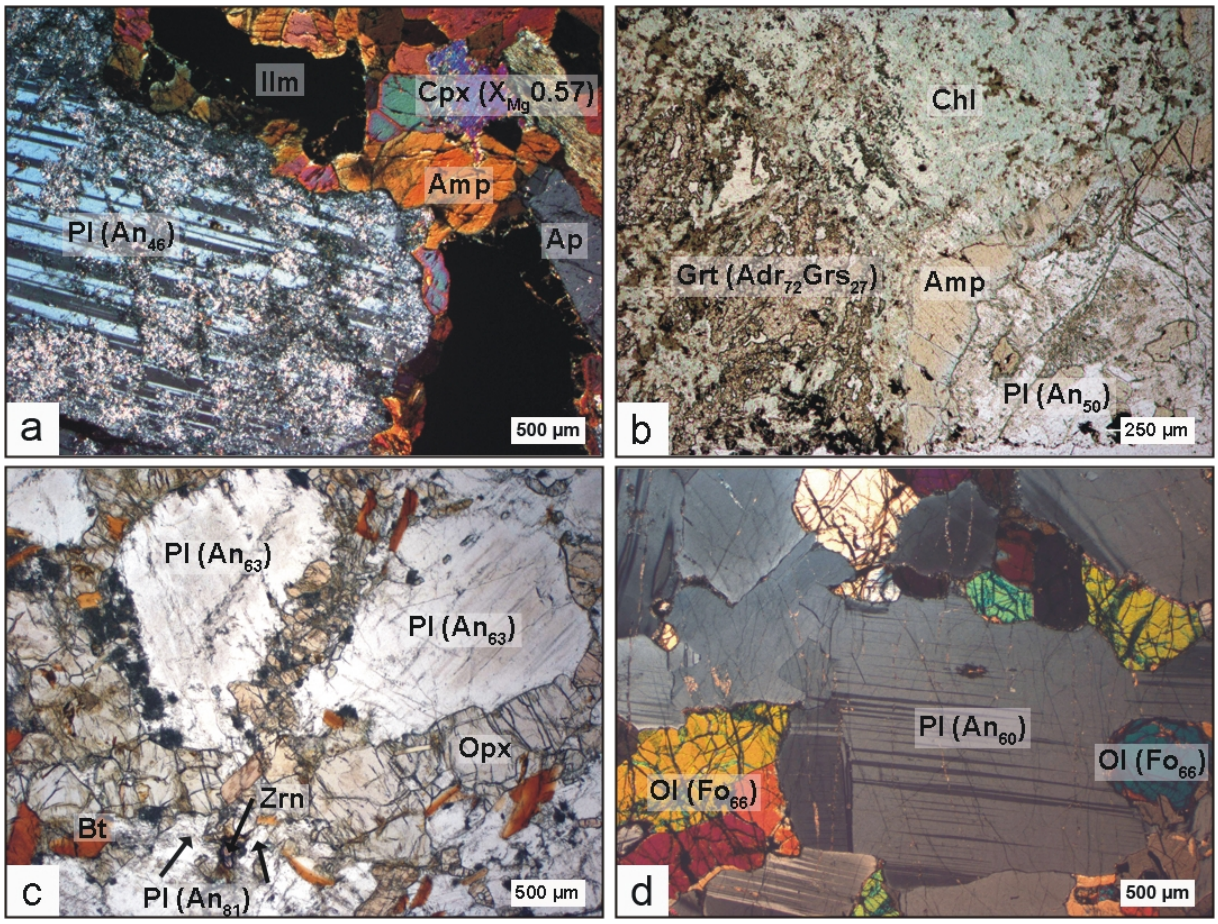

Fig. 3.3. Thin section microphotographs of the (a-c) white anorthosite suite and (d) dark anorthosite suite of the Kunene Intusive Complex (a and d: xpl; b and c: ppl). (a) Leucogabbronorite (Ku-97-04): euhedral cumulus plagioclase and cumulus clinopyroxene are surrounded by ilmenite and amphibole containing apatite inclusions. Plagioclase is sericitized along cracks. (b) Leucogabbronorite (Ku-97-08b): relic xenocryst of andradite-rich garnet adjacent to altered intercumulus phases is surrounded by late magmatic amphibole. (c) Pyroxene-bearing anorthosite (Ku-06-60): orthopyroxene, biotite and anhedral zircon surround cumulus plagioclase crystals. (d) Leucotroctolite (Ku-06-15): subhedral cumulus plagioclase with olivine inclusions and interstitial olivine.

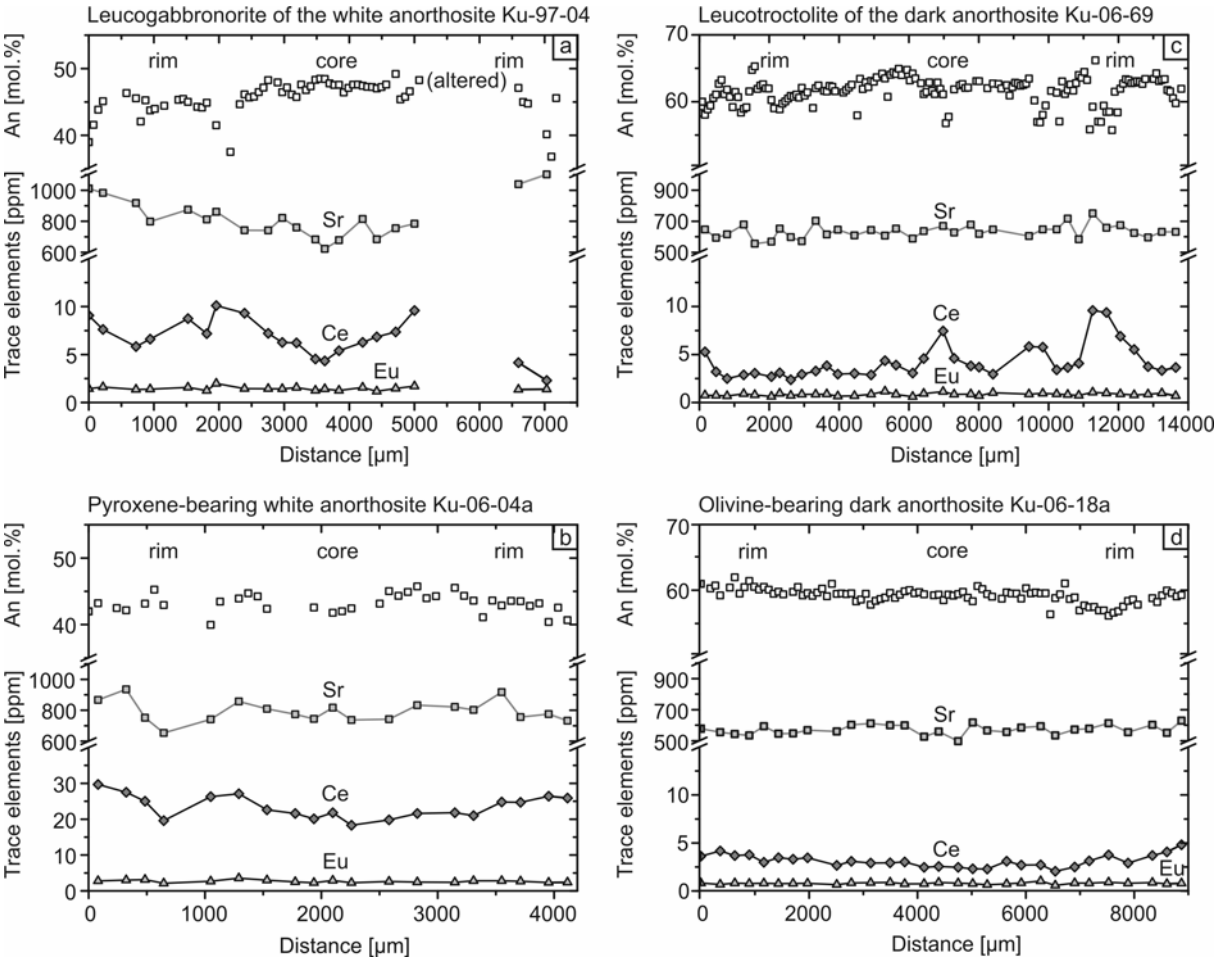

Fig. 3.4. Major and trace element zoning across plagioclase crystals.

3.5.3 Younger intrusions

Oxide-rich diorite intruding the white anorthosite suite consists of cm-sized cumulus plagioclase (An_{42}) + clinopyroxene (X_{Mg}: 0.63) + ilmenite + magnetite + olivine (Fo_{38}). In the gabbro plagioclase (An_{58}) and clinopyroxene (X_{Mg}: 0.73) are the major magmatic phases, whereas ilmenite is an accessory phase. Troctolites intruding the major dextral shear zone display the primary magmatic assemblage of anhedral plagioclase (An_{65}) and olivine (Fo_{74}). The cm-sized olivine is partially serpentinized, leading to radiating expansion cracks in surrounding plagioclase. When compared to the two anorthosite suites, the troctolite phases compositionally coincide with those of the most primitive leucotroctolites of the dark anorthosite suite, whereas the gabbro and oxide-rich diorite phases fall on the chemical trend defined by the white anorthosite minerals (Fig. 3.5).

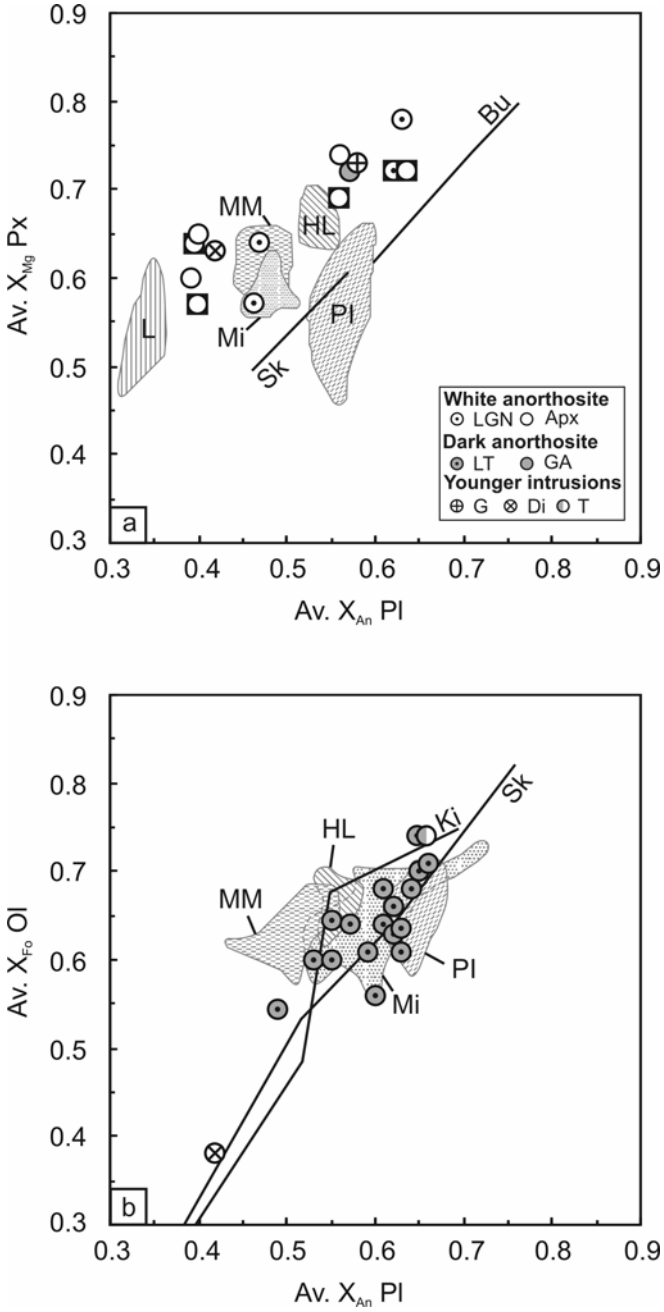

Fig. 3.5. Composition of coexisting plagioclase and (a) pyroxene (Cpx circle; Opx rectangle) and (b) olivine in the KIC compared to other unmetamorphosed massif-type anorthosites and mafic layered intrusion fractionation trends (modified from Ashwal, 1993). Anorthosite massifs: HL Harp Lake, L Labreville, Mi Michikamau, MM Mealy Mountains, PI Paul Island (Nain); Layered intrusion: Bu Bushveld, Ki Kiglapait, Sk Skaergaard.

3.6 Trace element zoning of minerals

In order to gain information about the compositional evolution of the magma from which the anorthosites crystallized, we analysed plagioclase and, if present, pyroxene, olivine, ilmenite, magnetite, amphibole and apatite for their trace element zoning. One leucogabbronorite and a

pyroxene-bearing anorthosite sample from the white anorthosite suite and two leucotroctolites, one olivine-bearing anorthosite and a pyroxene-bearing anorthosite sample of the dark anorthosite suite were chosen for analysis. Representative analyses are listed in Table 3.2 (the full set of LA-ICP-MS analyses is listed in Appendix A.5.4).

3.6.1 White anorthosite suite

Plagioclase of the white anorthosite suite is characterised by high Sr contents (600 - 1100 ppm) and variable concentrations of incompatible trace elements. In general, the trace element concentration of plagioclase increases with decreasing anorthite content. Euhedral cm-sized plagioclase (An_{39-49}) from the leucogabbronorite is zoned; Sr, Ba, Zr and LREE increase by a factor of two from core to rim (Figs 3.4a and 3.6). Coarse plagioclase (An_{35-45}) of pyroxene-bearing anorthosite shows the highest concentrations of Ba, LREE, Y and Be. The concentrations increase from core to rim and toward adjacent medium-sized crystals, except for Ba which decreases in the rim (Figs 3.6f and g). The chondrite-normalized REE patterns of plagioclase (Figs 3.7a and b) display high overall abundances of REE (∑REE: 10 - 75 ppm), enrichment of LREE (La_N/Sm_N: 5 - 22) and strong positive Eu anomalies (Eu/Eu*: 13 - 27).

Clinopyroxene ($Wo_{47}En_{32}Fs_{21}$) in leucogabbronorite displays Sr contents of 40 - 57 ppm, low concentrations of incompatible trace elements (Li: 4 - 7 ppm, Y: 10 - 17 ppm, Zr: 40 - 90 ppm, ∑REE: 25 - 40 ppm) and a flat chondrite-normalized REE pattern without significant Eu anomaly (Eu/Eu*: 0.8 - 1.2; Fig. 3.7a). In contrast clinopyroxene ($Wo_{45}En_{33}Fs_{22}$) in the pyroxene-bearing anorthosite, shows lower Sr concentrations (13 - 22 ppm), higher concentrations of incompatible trace elements (Li: 1 - 3 ppm, Y: 110 - 160 ppm, Zr: 180 - 290 ppm, ∑REE: 200 - 315 ppm), slight enrichment in H+MREE relative to LREE (La_N/Yb_N: 0.4 - 0.7) and a negative Eu anomaly (Eu/Eu*: 0.25 - 0.28; Fig. 3.7b).

Amphibole in leucogabbronorite contains higher concentrations of Ba, Rb and L+MREE than the adjacent clinopyroxene. Their chondrite-normalized REE patterns are sub-parallel (Fig. 3.7a).

Ilmenite in leucogabbronorite displays an increase in V but decreases in Zr and Hf from early ilmenite inclusions in clinopyroxene (V: 250 - 280 ppm, Zr: 6.8 - 11.7 ppm, Hf: 1.9 - 4.0 ppm) towards interstitial ilmenite, associated with late magmatic amphibole (V: 350 - 450 ppm, Zr: 2.6 - 7.0 ppm, Hf: 0.3 - 0.6 ppm). The concentrations of Nb and Ta remain nearly constant with an Nb/Ta ratio of 9.7 - 11.1.

Apatite in leucogabbronorite displays the highest REE concentrations of all minerals, a steep chondrite-normalized REE pattern (La_N/Yb_N: 9.3 - 14.4) and absence of Eu anomalies (Fig. 3.7a). Apatite in pyroxene-bearing anorthosite shows even higher REE concentrations but is less enriched in LREE (La_N/Yb_N: 1.6 - 2.3), with a pronounced negative Eu anomaly (Eu/Eu*: 0.3; Fig. 3.7b).

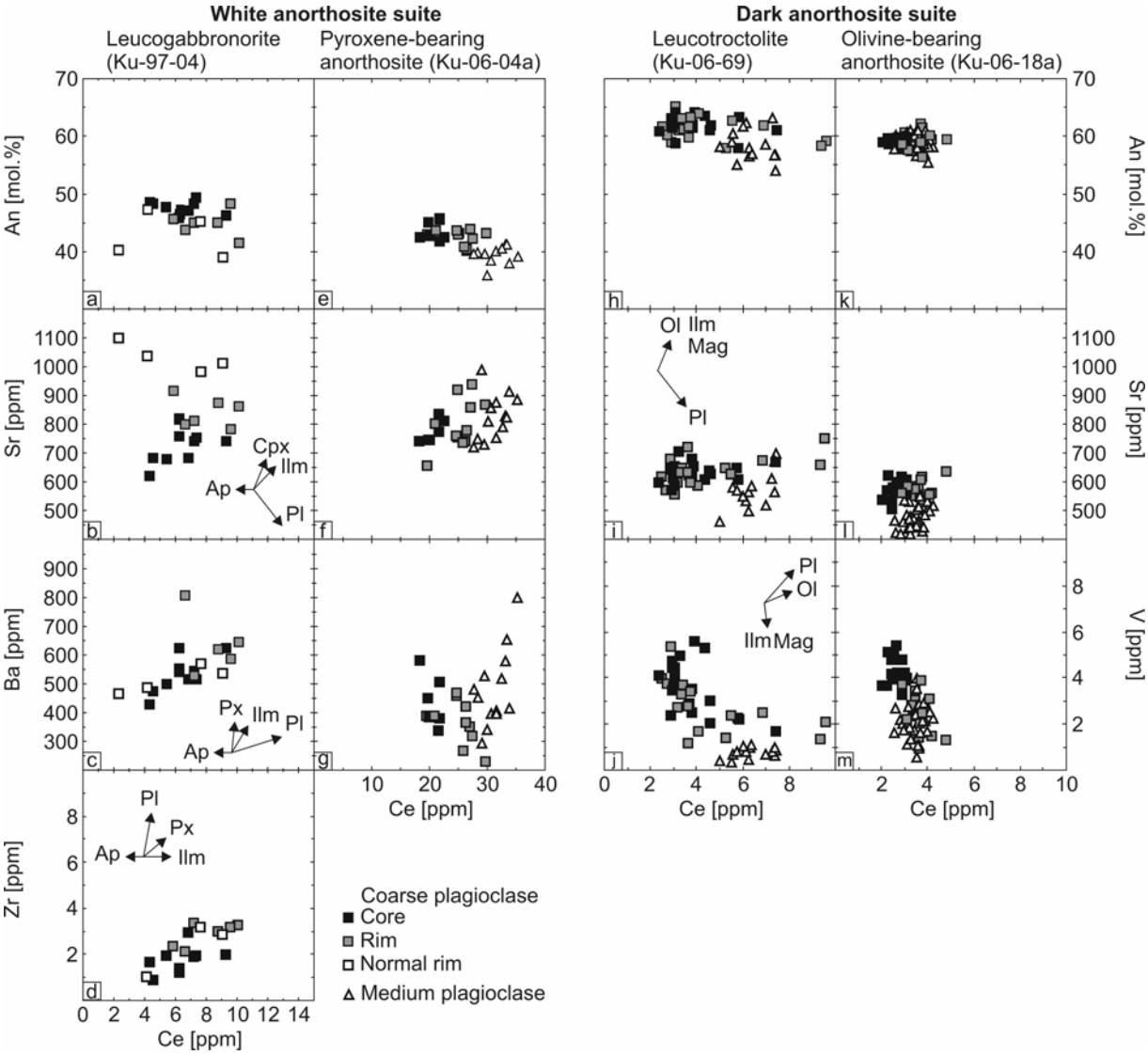

Fig. 3.6. Variation diagrams of measured trace element contents in plagioclase from the white and dark anorthosite suite. Cerium is incompatible to plagioclase and most other phases of the anorthosite assemblage and is therefore used as fractionation indicator. The effect of fractional crystallization of the different minerals on trace element concentration of the residual melt depends on the partition coefficients and is indicated by arrows. The resulting trends for simultaneous crystallisation of different phases depend on modal ratios.

3.6.2 Dark anorthosite suite

Plagioclase (X_{An}: 0.54 - 0.65) of the dark anorthosite suite has lower Sr contents (400 - 750 ppm) and lower concentration of incompatible trace elements than that of the white anorthosite. All plagioclases display decreasing Sr concentrations from coarse towards medium-grained crystals (Figs 3.6i and l). Plagioclase that is oscillatory zoned in its anorthite content also displays variations of the LREE, whereas homogeneous plagioclase shows only a slight increase of the LREE towards the rim (Figs 3.4c and d). The V concentration decreases from core of coarse plagioclase towards the rim and later medium-grained crystals by a factor of ~5 (Figs 3.6j and m). The chondrite-normalized REE patterns of plagioclase reflect the lower and less variable REE values (∑REE: 5 - 22 ppm, La_N/Sm_N: 3 - 10, Eu/Eu*: 7 - 18) when compared to that of the white anorthosites (Fig. 3.7c).

Olivine ($Fo_{63.3}Fa_{33.3}Te_{0.4}$) of the dark anorthosite contains of 10 - 60 ppm Ti and minor concentrations of Li (3 - 5) ppm and Sc (0.8 - 1.4 ppm). No zoning in trace element composition within individual crystals and no differences between early olivine inclusions in plagioclase and interstitial olivine are observed.

Clinopyroxene ($Wo_{44}En_{41}Fs_{15}$) in olivine-bearing dark anorthosite displays low Sr contents (12 - 16 ppm), high concentrations of incompatible trace elements (Li: 2 - 5 ppm, Y: 65 ppm, Zr: 230 - 260 ppm, ∑REE: 69 - 76 ppm), enrichment of M+HREE relative to LREE (La_N/Yb_N: 0.14) and a negative Eu anomaly (Eu/Eu*: 0.3). Late orthopyroxene ($Wo_2En_{67}Fs_{31}$) surrounding olivine is rich in Ti and enriched in the HREE (Fig. 3.7c).

Ilmenite of leucotroctolite shows decreases in V and HFS elements from early ilmenite inclusions in plagioclase (V: 2200 - 2500 ppm, Nb: 320 - 350, Ta: 20 ppm) towards late interstitial ilmenite (V: 1000 - 1200 ppm, Nb: 150 - 230, Ta: 11 ppm). The Nb/Ta ratio ranges from 12.3 to 16.7.

Magnetite inclusions in interstitial orthopyroxene of olivine-bearing anorthosite contain the highest concentration of V (~3000 ppm). REE in opaque minerals of all samples are below detection limit.

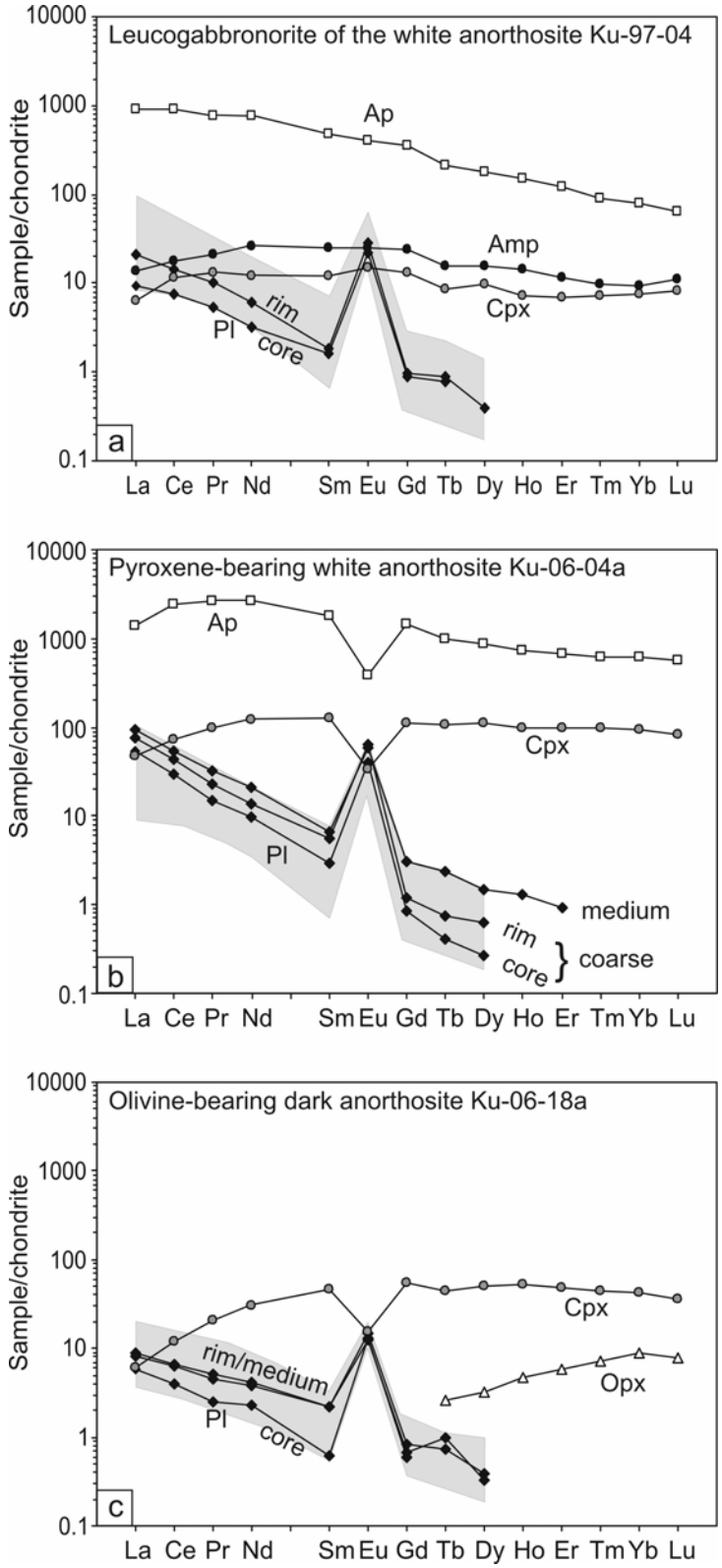

Fig. 3.7. Selected chondrite-normalized REE patterns of plagioclase, pyroxene, amphibole and apatite of the Kunene Intrusive Complex anorthosites. The shaded field outlines the overall ranges of REE patterns in plagioclase of the (a and b) white and (c) dark anorthosite suite. Chondrite values of McDonough & Sun (1995) have been used for normalization.

3.7 Oxygen isotopic composition of the anorthosites and representative basement rocks

To determine the stable isotopic composition of the KIC rocks 30 plagioclase separates were analysed for their oxygen isotopes. In addition, olivine, pyroxene, amphibole, biotite, Fe-Ti oxides and selected anorthosite and basement samples were analysed to test for equilibrium at magmatic temperatures, contamination and subsolidus alteration. The full set of analyses is given in Table 3.3 and shown in Figure 3.8.

3.7.1 White anorthosite suite

Plagioclase of the white anorthosite suite shows variation in $\delta^{18}O$ from 6.2 to 7.6 ‰ with a maximum in the range of 6.2 - 6.8 ‰. These values are in good agreement with data of the previous study by Drüppel et al. (2007). The plagioclase of two leucogabbronorites containing xenocrysts of andradite-rich garnet described by Drüppel et al. (2007) fall to the upper limit of the range (6.7 ‰). No correlation is observed between $\delta^{18}O$ values and either modal amount of plagioclase or its anorthite content.

Cumulus orthopyroxene yield $\delta^{18}O$ values of 4.0 - 4.9 ‰, whereas clinopyroxene have lower values of 3.4 - 4.1 ‰. Late-magmatic amphibole and biotite of leucogabbronorite display $\delta^{18}O$ values of 4.0 and 2.7 ‰, respectively.

3.7.2 Dark anorthosite suite

The $\delta^{18}O$ values of plagioclase of the dark anorthosite suite range from 5.6 to 6.9 ‰. In contrast to the pyroxene-bearing white anorthosites, the olivine-bearing rocks have significantly lower $\delta^{18}O$ values with a maximum in 5.6 - 6.2 ‰. On the other hand, the plagioclase of gabbroic dark anorthosites and the younger gabbro and diorite intrusions range from 6.0 to 6.9 ‰ and coincide with the plagioclase values of the white anorthosites (Fig. 3.9a). Values exceeding the major anorthosite range are observed in rocks located within the major dextral shear zone (troctolite: 7.3 ‰; pyroxene-bearing white anorthosite: 7.5 ‰).

Olivine of leucotroctolite samples yields a narrow range of 3.7 - 4.3 ‰ $\delta^{18}O$, except for one weakly altered sample (3.3 ‰). Orthopyroxene of the dark anorthosite displays $\delta^{18}O$ values of 4.5 and 6.1 ‰, whereas ilmenite yields 2.3 and 4.6 ‰ $\delta^{18}O$.

The $\delta^{18}O$ values of bulk anorthosite rocks range from 5.7 to 7.6 ‰. Lower $\delta^{18}O$ values of the bulk rock when compared to the corresponding plagioclase reflect minor amounts of low $\delta^{18}O$ intercumulus phases. Slightly higher bulk rock $\delta^{18}O$ values, on the other hand, observed in three samples, suggest alteration or heterogeneity within plagioclase.

Table 3.3. Oxygen isotope data of mineral separates and bulk rocks of the Kunene Intrusive Complex and Epupa Complex basement samples.

sample	rock-type	locality	WR X_{Mg}	Pl av. An [mol.%]	oxygen isotope composition [‰]								
					WR	Pl	Ol	Opx	Cpx	Ilm	Mag	Amp	Bt
White anorthosite suite													
Ku-97-03	LGN*	Swartbooisdrif	0.39[D]	47[D]		6.7							
Ku-97-04	LGN	Swartbooisdrif	0.38[D]	46	6.0	6.5			4.1	1.3	1.2	4.0	2.7
Ku-97-08b	LGN*	Swartbooisdrif	0.43[D]	50[D]		6.7							
Ku-06-04a	Apx	Swartbooisdrif	0.55	40		6.1							
Ku-06-04b	Apx	Swartbooisdrif	0.45	39		6.2							
Ku-06-41b	Apx	Ombuko	0.59	62		7.5							
Ku-06-51	Apx	Epupa	0.10	65		7.6							
Ku-06-60	Apx	Epupa	0.66	63		6.2		6.4					4.6
Ku-06-63a	Apx	Epupa	0.65	56		6.3		4.9					
Ku-06-63b	LGN	Epupa	0.70	63		6.8		4.0	3.4				
Dark anorthosite suite													
Ku-98-125	LT	Swartbooisdrif	0.46[D]	53	5.7	6.1[D]	4.1			2.3	0.8		2.6
Ku-98-228	LT	Otjitanga	0.72[D]	65	6.3	5.7	3.7			4.6			
Ku-06-01	LT	Swartbooisdrif	0.70	66		5.9							
Ku-06-02	Aol	Swartbooisdrif	0.43	55		5.8							
Ku-06-06	Apx	Swartbooisdrif	0.60	60		6.0							
Ku-06-07	LT	Swartbooisdrif	0.69	61		5.6							
Ku-06-15	LT	Otjitanga	0.62	60		5.8	3.7						
Ku-06-18a	Aol	Otjitanga	0.60	60		6.0							
Ku-06-18b	LT	Otjitanga	0.65	60		6.1							
Ku-06-19	LT	Otjitanga	0.59	61		5.8							
Ku-06-46	LT	Ombuko	0.64	57		6.2							
Ku-06-48	LT	Ombuko	0.63	60		6.0	4.3	6.1					6.5
Ku-06-59	Apx	Epupa	0.65	66		6.9							
Ku-06-61	Aol	Epupa	0.63	67		6.9							
Ku-06-69	LT	Otjitanga	0.64	61		5.9	4.0						
Ku-06-72	GA	Otjitanga	0.64	57	7.6	6.8			4.0	2.3			
Ku-06-74	LT	Otjitanga	0.66	64		5.8	3.3	4.5					
Ku-06-75	LT	Otjitanga	0.69	65		5.8	4.0						
Younger intrusions													
Ku-06-20a	Di	Otjitanga	0.35	43	6.7	6.4			3.9	1.5			
Ku-06-31b	G	Otjitanga	0.72	58		6.6							
Ku06-41a	T	Ombuko	0.73	64		7.3							
EC metabasites													
B-177-B-98	amphibolite (mafic dyke)	Orue Unit	0.53[B]		5.7								
B-447-1-99	2Px Gran (mafic dyke)	Epembe Unit	0.54[B]		6.4								
EC felsic orthogneisses													
B-174-A-98	Hbl-Bt Gn (metavolcanite)	Orue Unit	0.29[B]		8.2								
B-406-2-99	Hbl-Bt Gn (metagranitoid)	Orue Unit	0.42[B]		8.9								
B-614-2-99	Px Gran (metavolcanite)	Epembe Unit	0.22[B]		7.2								
EC paragneisses													
B-171-A-98	Grt-Bt Gn (metagreywake)	Orue Unit	0.46[B]		8.2								
B-212-A-98	Grt-Sil Gn (metapelite)	Epembe Unit	0.39[B]		9.8								
B-230-A-98	Grt Gn (metagreywacke)	Epembe Unit	0.39[B]		8.3								
B-347-99	Cs	Orue Unit	0.38		11.2								
B-588-3-99	Cs	Orue Unit	0.43		10.7								
B-342-6-00	Cs	Orue Unit	0.52		11.1								

The oxygen isotope compositions are given in the standard δ-notation, expressed relative to VSMOW in per mil (‰). WR, whole rock; Rock types as in Table 3.1; [D]Drüppel (2003), [B]Brandt (2003); * relic xenocrysts of andradite-rich garnet.

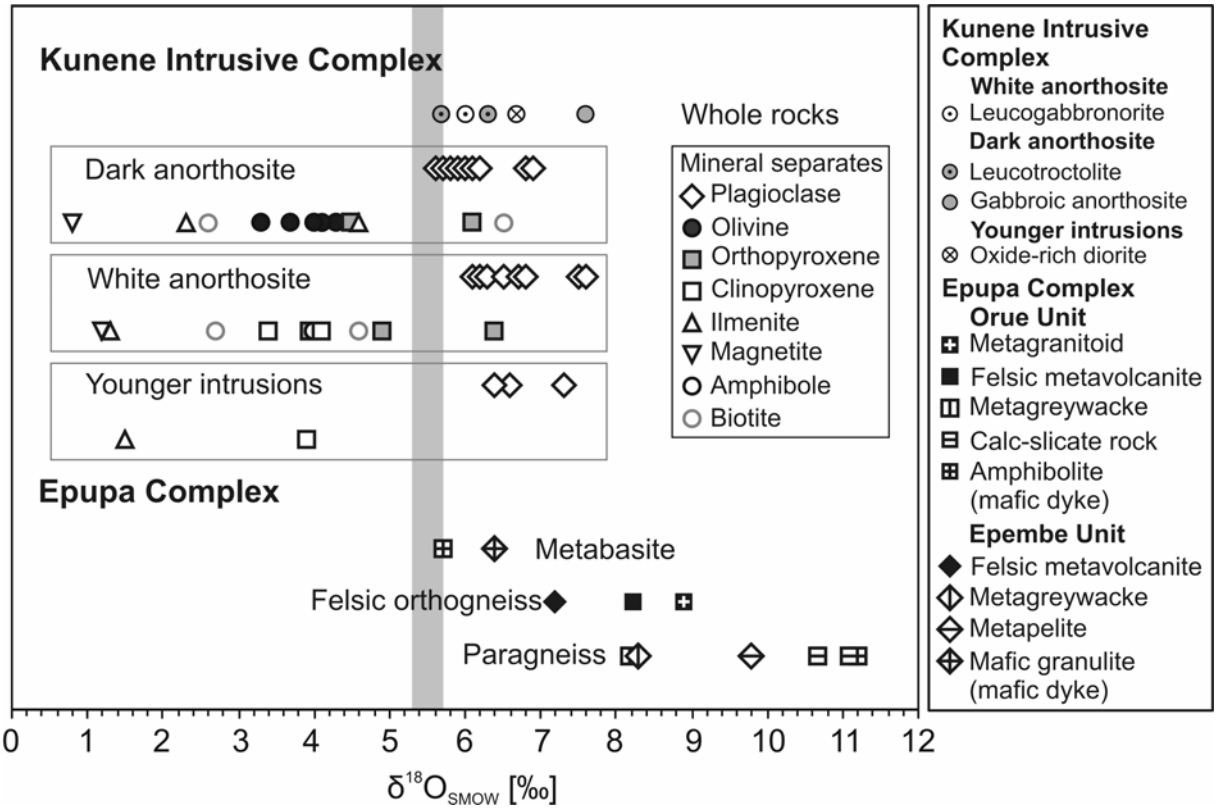

Fig. 3.8. Oxygen isotopic composition of whole rocks and mineral separates from the Kunene Intrusive Complex and the Epupa Complex basement. The shaded field illustrates the range of mantle values after Eiler (2001).

3.7.3 Epupa Complex

Nine representative basement samples of the EC were analysed to characterize the isotopic composition of the crustal reservoir and potential contaminants. Oxygen isotope analyses of the felsic ortho- and paragneisses of the EC yield $\delta^{18}O$ values of 7.2 - 8.9 ‰ and 8.2 - 11.2 ‰, respectively. Metabasite dykes from the EC, on the other hand, yield distinctly lower $\delta^{18}O$ values of 6.4 ‰ in the Epembe Unit and of 5.7 ‰ in the Orue Unit, consistent with their derivation from mantle derived melts.

3.8 Discussion

3.8.1 Magmatic evolution of the white and dark anorthosite suite

The high Sr concentrations, LREE enrichment and positive Eu anomalies in anorthositic rocks of the Kunene Intrusive Complex (Drüppel et al., 2007) agree well with their formation by plagioclase accumulation. In general, the slow CaAl-NaAl diffusion (Grove et al., 1984) and low rates of Sr and REE diffusion (Cherniak, 2003) in plagioclase preserve the element concentrations established during growth from the melt and hence provides them as a good indicator for fractional crystallization, assimilation and trapped liquid processes. The trace element composition of residual liquids, on the other hand, is recorded by interstitial phases.

The large-scale wavy oscillatory zoning of major elements in plagioclase of both anorthosite suites is unlikely to reflect periodic changes in pressure but points to recurrent changes in melt composition due to mixing with new magma pulses, as argued by Wiebe (1990) or, more likely, movement of the crystallizing plagioclases in the magma reservoir (Halama et al., 2002). The occurrence of plagioclase with homogeneous composition, on the other hand, is interpreted to reflect stable physicochemical conditions. The differences in chemical and isotopic composition of cumulus plagioclase of white and dark anorthosite suggest their derivation from distinct melt compositions, either derived by magmatic fractionation, crustal assimilation or both.

3.8.1.1 Magmatic evolution of white anorthosite

In leucogabbronorite the core-rim trace element zoning of plagioclase points to gradual changes in the melt composition during its crystallization (Fig. 3.4a). The slight decrease in the anorthite content of coarse plagioclase from core to rim cannot account for the strong outward increase of compatible Sr from 600 to 1100 ppm (Figs 3.6a and b). The Sr-rich rims adjacent to low-Sr phases (Fig. 3.3a) cannot be interpreted as a consequence of adcumulus growth from trapped liquid or later diffusion either. According to Blundy & Wood (1991), the successive enrichment in Sr can result from simultaneous fractionation of plagioclase and low Sr-phases like pyroxene. The crystallization of pyroxene during plagioclase fractionation is corroborated by the low concentrations of incompatible trace elements and the absence of significant Eu anomalies. The outward increase of the Ba in cumulus plagioclase is consistent with its incompatible behaviour during plagioclase and pyroxene fractionation. The combined decrease of Ba and Ce in the plagioclase outer rim presumably arises from late apatite and biotite crystallization. On the other hand, the high Zr and Hf content of early ilmenite inclusions in clinopyroxene and the strong increase of the Zr concentration from core towards the rim in plagioclase (Fig. 3.6d) argue for successive assimilation of crustal material during growth. The decreases in the Zr

and Hf concentrations in late interstitial ilmenite suggest a contemporaneous crystallization of ilmenite with zircon. Convincing arguments for crustal contamination comes from the REE patterns of late magmatic phases. Both amphibole and apatite lack significant negative Eu anomalies (Fig. 3.7a), demonstrating that they do not reflect characteristics of the residual melt compositions after plagioclase fractionation but rather the contribution by a crustal contaminant. This interpretation is consistent with the high Zr concentration of 104 ppm in the corresponding whole rock and the occurrence of crustal xenoliths in various samples in the outcrop level (Drüppel et al., 2007).

In pyroxene-bearing anorthosite, the lower anorthite content as well as the overall higher concentration of incompatible elements in plagioclase suggest crystallization from a more evolved liquid. The slight increase of compatible Sr from core towards the rim of coarse plagioclase suggests a similar process as in the leucogabbronorite (see discussion above). On the other hand, the strong decrease in Ba (Fig. 3.6g) would require contemporaneous fractionation of a high-Ba phase like biotite, which is regarded as late magmatic. The pretended compatibility of Ba during plagioclase crystallization contradicts its predicted slightly incompatible behaviour (Bindemann et al., 1998) and possibly reflects contamination with exceptionally low-Ba material, like for example calc-silicate rocks. However, the negative Eu anomalies observed in subsequently crystallized clinopyroxene and apatite (Fig. 3.7b) demonstrate the strong influence of plagioclase fractionation on the trace element budget of the residual melt. The flattening of the LREE in the apatite pattern may also result from extensive plagioclase fractionation prior to its crystallization from interstitial liquid.

3.8.1.2 Magmatic evolution of the dark anorthosite

The lower trace element concentrations in plagioclase of the dark anorthosite suite are in good agreement with bulk anorthosite data of Drüppel et al. (2007) and point to fractionation from a homogeneous melt with relatively primitive trace element composition. The decrease in Sr concentration from coarse to medium-grained plagioclases is apparently exclusively controlled by plagioclase fractionation (Fig. 3.6). The observed lower Sr concentrations and less pronounced Eu anomalies of the labradorite plagioclase, when compared to the andesine plagioclase of the white anorthosites, as observed in other massif-type anorthosite occurrences (e.g. Ashwal, 1993), rather results from crystal-chemical control on trace element partition between melt and crystallizing plagioclase (Blundy & Wood, 1991) than from prior plagioclase fractionation. Eu^{2+} under low fO_2 becomes compatible, with an ionic radius slightly higher than Ca^{2+} but similar to Sr^{2+}. The increase in X_{An} from andesine to labradorite yields a stronger decrease in partition coefficients for Sr^{2+} and Eu^{2+} when compared to the REE^{3+} (calculated after Bindemann et al., 1998), resulting in lower Sr incorporation and less positive Eu anomalies in plagioclase. The decrease of V concentrations from the core towards the rim in plagioclase (Fig. 3.6) points to a contemporaneous fractionation of Fe-Ti

oxides. The early crystallization of olivine, evident from its occurrence as inclusion in cumulus plagioclase, presumably increased the concentration of trace elements in the melt but did not result in observable characteristic enrichments or depletions in other phases.

Low concentrations of V and HFS elements in interstitial ilmenite and negative Eu anomalies of clinopyroxene (Fig. 3.7c) reflect the composition of the residual liquid after fractionational crystallization of plagioclase and Fe-Ti oxides. According to Morse & Nolan (1984), the occurrence of reversed rims on plagioclase is interpreted to result from contemporaneous crystallisation of plagioclase rims and mafic silicates from the intercumulus liquid.

3.8.1.3 Temperature conditions during crystallization

Temperatures were calculated based on the oxygen isotope per-mil difference of Pl-Ol, Pl-Px and Pl-Ilm pairs using fractionation factors from literature (Zeng, 1991, 1993; Table 3.4). From textural observations we infer a contemporaneous crystallization of plagioclase and part of the olivine in the dark anorthosite suite. Six plagioclase-olivine pairs with $\Delta\delta^{18}O$ in the range of 1.7 to 2.1 ‰ yield temperatures of 950 - 1150°C (Fig. 3.9b). In general, the inter-mineral and intra-mineral oxygen exchange in anorthosites is dominated by the high modal abundance, grain size and faster rates of oxygen diffusion in plagioclase, which acts as a nearly infinite reservoir. According to the fast grain boundary model of Eiler (1993), the very slow rates of oxygen diffusion in olivine, the low abundance of pyroxene and the almost dry composition of the dark anorthosites support the preservation of equilibrium close to the igneous fractionation between olivine and plagioclase. The obtained values are therefore interpreted to represent equilibrium temperatures, presumably close to the true crystallization temperatures. The temperatures agree well with temperature estimates of 1000 - 1080°C from calculation of oxygen isotope exchange trajectories in the Laramie Anorthosite Complex (Farquhar et al., 1993) and of 1100 - 1185°C from pyroxene equilibrium thermometry in anorthosite rocks from the Lofoten Islands (Markl et al., 1998).

In the white anorthosite suite the use of oxygen thermometry is hampered by the faster oxygen diffusion in cumulus ortho- and clinopyroxene when compared to olivine. Obtained temperatures of 460 - 665 °C from plagioclase-pyroxene pairs therefore most likely represent subsolidus changes in $\delta^{18}O$ values of one or both minerals during slow cooling. This interpretation is consistent with results from other anorthosite complexes (Demaiffe & Javoy, 1980; O'Connor & Morrison, 1999; Peck & Valley, 2000). Higher apparent temperatures of 774 - 985°C were obtained for plagioclase-ilmenite pairs from leucogabbronorite, oxide-rich diorite and one leucotroctolite sample. These estimates agree well with the temperatures of 951 - 986°C determined by Drüppel et al. (2001) for late magmatic amphibole and are interpreted to give an estimation of late magmatic crystallization temperatures.

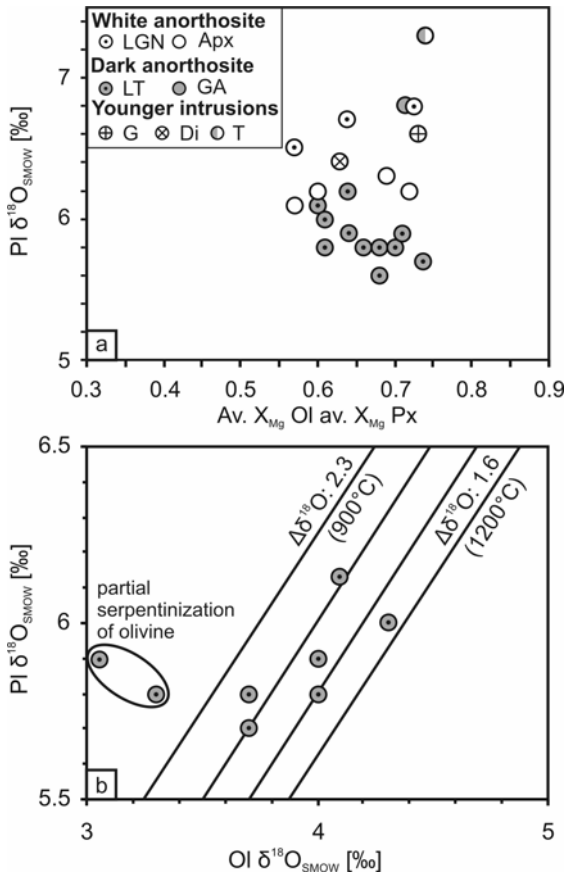

Fig. 3.9. (a) X_{Mg} of mafic silicates vs. oxygen isotopic composition of plagioclase of Kunene Intrusive Complex rocks. (b) Oxygen isotopic composition of coexisting plagioclase and olivine from leucotroctolite samples of the dark anorthosite (including data of Drüppel et al., 2007). Plagioclase-olivine isotherms are calculated for average X_{An} of 0.60 and X_{Fo} of 0.65 after Zeng (1993).

Table 3.4. Temperatures calculated from oxygen isotopic fractionation between mineral pairs of anorthositic rocks of the Kunene Intrusive Complex.

sample	rock-type		Pl-Ol	Pl-Opx	Pl-Cpx	Pl-Ilm
White anorthosite suite						
Ku-97-04	LGN	Di56			463	774
Ku-06-63a	Apx	En70		665		
Dark anorthosite suite						
Ku-98-125	LT	Fo60	1010			985
Ku-98-228	LT	Fo74	1000			
Ku-06-15	LT	Fo66	950			
Ku-06-48	LT	Fo61	1150			
Ku-06-69	LT	Fo64	1040			
Ku-06-74	LT	Fo68	805			
Ku-06-75	LT	Fo69	1080			
Younger intrusions						
Ku-06-20a	Di	Di70			465	953

Rock types as in Table 3.1; the average composition of plagioclase is taken from Table 3.3; temperatures are given in °C.

3.8.2 Composition of the parental and evolved melts

Knowledge about the composition of the melts is crucial for the understanding of the anorthosite-forming processes and the source of the parental magma. Petrographic and geochemical evidence of the anorthosite suites of the KIC argue for a successive contamination of a primitive parental magma producing a more evolved magma that gave rise to the formation of the white anorthosite suite. Contamination with crustal rocks of the EC, dominated by felsic orthogneisses, could be responsible for the observed lower anorthite contents of plagioclase in the white anorthosite suite and the formation of pyroxene instead of olivine as a result of increasing oxygen and silica activities in the contaminated magma.

3.8.2.1 Trace element composition

To convert trace element concentrations in plagioclase to corresponding melt compositions we used the plagioclase-basalt partition coefficients of Bindemann et al. (1998). The mode of calculation accounts for the control of plagioclase crystal chemistry (anorthite content) on partition coefficients (Blundy & Wood, 2003). From our temperature calculations we assume crystallization at ~1200°C. Europium is not considered in the calculation because of the effect of fO_2 on the partition coefficient. The trace element melt composition calculated from plagioclase of the most evolved white anorthosite displays LREE enrichment (La ~80 × primitive mantle, La_N/Sm_N 16) and negative Rb and Sr anomalies. In contrast, the melt composition deduced from plagioclase of four dark anorthosites displays distinctly lower LREE enrichment (La 6 – 10 × primitive mantle, La_N/Sm_N 1 - 3) and lacks significant anomalies (Fig. 3.10).

Since fractionation of silicate minerals does not significantly alter the Nb/Ta ratio of a melt, the Nb/Ta ratios of fractionated ilmenite presumably reflect the original values. Calculation of Nb/Ta ratios using the partition coefficients of Green & Pearson (1987) yields values of 11.5 - 13.0 for the white anorthosite melt and 14.5 - 20.5 for the dark anorthosite melt, overlapping with crustal values of ~11 - 12 and mantle values of ~17, respectively (Sun & McDonough, 1989; Green, 1995).

The reconstructed concentrations and ratios of several key trace elements significantly differ in concentration and corroborate that the two anorthosite varieties did not crystallize from the same magma composition. The observed strong positive Eu anomalies in plagioclase of the white anorthosite rule out the development of the reconstructed negative Sr anomaly in the melt due to plagioclase fractionation and demonstrate that the liquid compositions of white and dark anorthosite were not related by a simple fractional crystallization process. Similar negative Sr anomalies are also observed for mafic rocks derived from basaltic magma contaminated by crustal material (Sun &

McDonough, 1989). The negative anomalies of the white anorthosite melt were therefore interpreted as characteristic features of the assimilated EC crustal rocks.

In order to deduce general characteristics of the anorthosite magmatism we compared the calculated melt compositions to designated parental melt compositions of anorthosites given in the literature (Fig. 3.10). The primitive melt from which the dark anorthosite suite crystallized is enriched in Ba, Rb and K when compared to the fairly primitive high-Al gabbros from the Laramie Anorthosite Complex (Mitchell et al., 1995). If the melt was similar to a high-Al basaltic melt, their steeper trace element pattern requires at least minor contribution from crustal material. The evolved melt of the white anorthosite suite, on the other hand, covers a similar compositional range, except for the MREE and Y, and displays characteristic negative Rb and Sr anomalies similar to those recorded for jotunitic rocks of the Rogaland Complex (Vander Auwera et al., 1998). Significant underestimation of Sr in the evolved melt due to high pressure effects is unlikely because calculation using the equation of Vander Auwera et al. (2000) yields lower but still negative Sr anomalies. The occurrence of late magmatic phases lacking any significant Eu anomaly (Fig. 3.7a) suggests that residual liquids after anorthosite formation do not have to display negative Eu anomalies if they underwent intermittent crustal contamination.

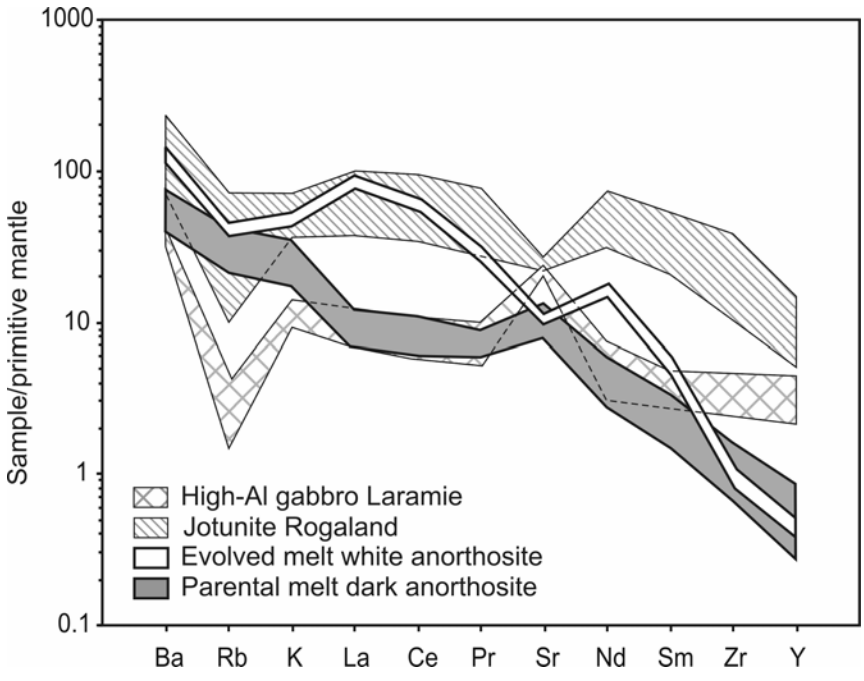

Fig. 3.10. Primitive mantle-normalized trace element compositions of parental and evolved melt, calculated from inverted plagioclase compositions of the white and dark anorthosite suite. The compositional range of high-Al gabbros (Mitchell et al., 1995) and jotunites (Vander Auwera et al., 1998) is given for comparison. Pyrolite values of McDonough & Sun (1995) have been used for normalization.

3.8.2.2 Oxygen isotopic composition

Plagioclase and olivine of most dark anorthosite samples have $\delta^{18}O$ values consistent with oxygen isotopic equilibrium at magmatic temperatures (Fig. 3.9b). Hence the isotopic composition of the magma can be estimated by means of plagioclase-melt fractionation. Assuming a fractionation of + 0.3 ‰ for intermediate plagioclase in basaltic melt (Zhao & Zheng, 2003 and references therein), magma $\delta^{18}O$ values appear to have been between 5.3 and 5.8 ‰, overlapping with mantle values (Eiler, 2001).

In the white anorthosites, the effect of subsolidus diffusion on the oxygen isotopic composition of plagioclase should be stronger when compared to the dark anorthosites, since additional fast diffusing phases like pyroxene, amphibole and biotite are present (Eiler, 1993). However, $\delta^{18}O$ values of orthopyroxene, exceeding those of the corresponding plagioclase of a pyroxene-bearing anorthosite (Ku-06-60), preserved oxygen isotopic disequilibrium and demonstrate that a pervasive subsolidus exchange did not occur. Hence the $\delta^{18}O$ value of 6.2 ‰ of plagioclase is believed to provide a good approximation of the evolved melt.

3.8.2.3 Source of the parental melts and crustal contamination processes

Cumulus plagioclase and minor phases of the dark anorthosite suite display oxygen isotopic compositions, trace element patterns and Nb/Ta ratios of ilmenite consistent with their crystallization from a nearly uncontaminated mantle-derived parental melt. The relatively uniform petrographic and geochemical composition of the dark anorthosite suite on the whole KIC intrusion scale (Ashwal & Twist, 1994; Drüppel et al., 2007) argues for a large and homogeneously composed magma reservoir. Regarding the KIC intrusion size of 18,000 km^2, only partial melting of a mantle source could provide enough primary melt to form the large reservoir that gave rise to the anorthosite formation. Extensive partial melting of lower crust, on the other hand, is unlikely to produce these vast amounts of almost homogeneous parental melts and would also contradict the observation of only minor volumes of associated felsic rocks.

The oxygen isotopic and trace element composition of plagioclase and intercumulus phases also puts constraints on the timing of crustal contamination. The oxygen isotope composition of unaltered plagioclases systematically increases from the most primitive olivine-bearing dark anorthosites towards the pyroxene-bearing white anorthosites and confirms the model of a more pronounced crustal contamination of the latter (Fig. 3.9a). The higher $\delta^{18}O$ values of cumulus plagioclase together with the more evolved trace element compositions of corresponding liquids (Fig. 3.10) of the white anorthosite suite point to crustal contamination prior to plagioclase formation. This model is in agreement with the assumption of early $\delta^{18}O$ enrichment due to crustal contamination prior to

plagioclase fractionation as deduced by Morrison & Valley (1988) and Peck & Valley (2000) for two Grenvillan anorthosites.

The core-rim trace element zoning of cumulus plagioclase and the lack of Eu anomalies in the intercumulus phases of the leucogabbronorite sample demonstrate that crustal contamination also took place during plagioclase formation. Preservation of high $\delta^{18}O$ intercumulus phases exceeding the values of cumulus plagioclase together with the occurrence of zircon (Fig. 3.3c), moreover, argues for occasional crustal contamination after plagioclase formation, presumably during ascent or emplacement of a plagioclase crystal mush.

Assuming the most primitive reconstructed melt to be similar in composition to the parental melt, a contamination in the range of 10 - 30 % average Epembe Unit crust would be necessary to increase the oxygen isotopic composition to the observed $\delta^{18}O$ of 6.2 - 6.8 ‰ and to satisfy the calculated trace element concentration observed for the evolved melt from which the white anorthosite suite crystallized. The lower amount of crustal contamination in the younger dark anorthosite suite most likely arises from the lower availability of crustal partial melts and/or assimilation of previously formed mantle melt-crust mixing zones. A similar process is also suggested for the Laramie Anorthosite Complex, attributed to a reduction of the available low-temperature melts from the lower crust due to the repeated ascent of magma diapirs along the same conduits (Scoates & Frost, 1996).

3.9 Conclusions

Based on oxygen isotopic and trace element compositions of plagioclase and other cumulus and intercumulus phases of the two different anorthosite varieties of the Kunene Intrusive Complex, NW Namibia, we can draw important conclusions on the anorthosite-forming processes and origin and evolution of their parent magmas. According to the oxygen isotope data and trace element zoning patterns of cumulus plagioclase and Nb/Ta ratios of ilmenite, the parental magma was subject to crustal contamination during the early stages of the anorthosite formation. The assimilation of crustal material took place prior to and during plagioclase crystallization and produced an evolved magma that was characterized by higher silica content, higher oxygen isotope values, variable enrichment in LREE when compared to M+HREE, negative Rb and Sr anomalies and crustal Nb/Ta ratios. The white anorthosite suite evolved by fractional crystallization of andesine plagioclase, orthopyroxene and Fe-Ti oxides from the evolved magma. The occasional occurrence of high $\delta^{18}O$ intercumulus phases is interpreted as crystallization from interstitial liquid after crustal contamination of a plagioclase crystal mush.

The oxygen isotopic and trace element compositions of cumulus plagioclase and minor phases of the younger dark anorthosite rocks are consistent with their crystallization from mantle-derived melts and demonstrate that major replenishment with primitive melt preceded their formation. The dark

anorthosite suite was derived by fractional crystallization of labradorite plagioclase, olivine and Fe-Ti oxides at magmatic temperatures above 1150°C from a nearly uncontaminated parental melt. Geochemical evidence together with the size of the Kunene Intrusive Complex are strong arguments for a mantle source providing the huge amounts of melt for the crystallization of vast masses of plagioclase to form the large-scale anorthosite massifs.

Chapter 4

The role of crustal contamination in massif-type anorthosites, new evidence from Sr-Nd-Pb isotopic composition of the Kunene Intrusive Complex, NW Namibia

Autoren: Philipp Gleißner[1], Kirsten Drüppel[1], Rolf L. Romer[2].

[1]Technische Universität Berlin, Institut für Angewandte Geowissenschaften, Ackerstr. 71-76, 13355 Berlin
[2]Deutsches GeoForschungsZentrum, Telegrafenberg, 14473 Potsdam

Im Druck in: Precambrian Research, Elsevier, DOI: 10.1016/j.precamres.2010.11.004

Eigenanteil:
Probennahme gemeinsam mit Dr. Kirsten Drüppel, selbständige Mineralseparation für die Iostopengeochemischen Untersuchungen, Durchführung der Laborarbeiten und Massenspektrometrie unter Anleitung von Prof. Dr. Rolf L. Romer, Auswertung und Interpretation der Ergebnisse gemeinsam mit Prof. Dr. Rolf L. Romer und Dr. Kirsten Drüppel, selbständige Ausarbeitung der Publikation.

Abstract

The Mesoproterozoic Kunene Intrusive Complex (Angola/Namibia), one of the largest massif-type anorthosite complexes of the world, intruded high-grade metamorphic Paleoproterozoic rocks at the southern margin of the Congo Craton. The geochemical characteristics of two successively emplaced anorthosite varieties provide insight into the source and evolution of melts parental to massif-type anorthosites. The older white anorthosite suite consists of pyroxene-bearing anorthosite and leucogabbronorite and is characterized by initial isotopic compositions of $^{87}Sr/^{86}Sr$: 0.7031 – 0.7043, εNd: +2.1 to -3.1 and $^{206}Pb/^{204}Pb$: 16.21 – 17.09. Our data demonstrate that the mantle-derived parental melt of the white anorthosite suite was subject to crustal contamination during the early stages of evolution, producing evolved magma whose isotope and trace element composition shows a distinct crustal influence. In contrast, the olivine-bearing anorthosite and leucotroctolite of the younger dark anorthosite suite show much less crustal influence. These rocks represent the most primitive unit in the Kunene Intrusive Complex and yield initial $^{87}Sr/^{86}Sr$: 0.7028 – 0.7036, εNd: +6.4 to +0.8 and $^{206}Pb/^{204}Pb$: 16.18 – 16.94. The Nd isotopic composition of leucotroctolite provides the best constraint for the depleted upper mantle source of the anorthosites.

4.1 Introduction

Massif-type anorthosite complexes commonly form huge intrusions with minor volumes of mafic and granitoid rocks and are characteristic features of the Proterozoic crust. Their origin is generally discussed in terms of mantle-derived parental melts or partial melting of mafic lower crust (Ashwal, 1993; Duchesne et al., 1999; Longhi, 2005; Morse, 2006). Their apparent temporal restriction to the Proterozoic suggests unique tectono-thermal conditions during this period. However, the specific crust-forming processes that were active during their formation are still a matter of debate.

A general correlation of decreasing εNd with increasing $^{87}Sr/^{86}Sr$ can be observed in many anorthosite complexes worldwide. The isotopic composition of the most primitive end-member is interpreted as source characteristics of either depleted (Ashwal et al., 1986; Emslie & Hegner, 1993) or undepleted mantle (Scoates & Frost, 1996). According to the mantle-source models, anorthosites originate by plagioclase fractionation from a high-Al basaltic parental melt, after extensive fractionation of mafic minerals. The plagioclase cumulates are thought to float on the top of the magma chamber at the crust-mantle boundary and ascend as crystal mush diapirs (for a review see Ashwal, 1993 and references therein; Emslie et al., 1994; Morse, 2006). In this model compositional deviations from mantle values and isotopic variations between different massif-type anorthosite occurrences as well as within individual complexes are interpreted as variable contamination with

crustal material of different ages (Ashwal et al., 1986; Emslie & Hegner, 1993; Emslie et al., 1994; Mitchell et al., 1995; Scoates & Frost, 1996).

A lower crustal source of Proterozoic massif-type anorthosites has been recently suggested based on the broadly crustal Pb, Os and Hf isotopic composition of anorthosites and accessory phases (Schärer et al., 1996; Schiellerup et al., 2000; Morgan et al., 2000; Andersen & Griffin, 2004). Further arguments for a lower crustal origin come from phase equilibria and fractional crystallization modelling of designated parental melt compositions (Longhi et al., 1999; Longhi, 2005). According to this model, intracrustal melting of mafic lower crust is triggered by downthrusting of tongues of crustal material along lithospheric-scale weakness zones (Duchesne et al., 1999; Shumlyanskyy et al., 2006), leading to the formation of ferrodioritic parental melts (Vander Auwera et al., 1998, 2006; Wiszniewska et al., 2002). The formation of anorthosite is interpreted in a similar way as the conventional model of Ashwal (1993), including polybaric fractional crystallization and plagioclase accumulation (Vander Auwera et al., 1998, 2006; Duchesne et al., 1999). The generally variable isotopic composition of many anorthosite complexes is explained by lower crustal heterogeneities (Schiellerup et al., 2000; Wiszniewska et al., 2002) and/or progressive contamination of the primary magmas by isotopically different crustal lithologies (Demaiffe et al., 1986; Vander Auwera et al., 2006).

The Mesoproterozoic Kunene Intrusive Complex (Angola/Namibia) experienced no metamorphic overprint after its emplacement (Ashwal & Twist, 1994; Morais et al., 1998; Mayer et al., 2004; Drüppel et al., 2001, 2007) and hence allows a direct study of the magmatic processes active during its formation. As shown recently by Drüppel et al. (2007), the overall O-Sr-Nd isotopic composition of the anorthosites is in agreement with their derivation from mantle-derived parental magma, whereas the trace element and oxygen isotopic composition of the two subunits of the KIC strongly suggests crustal contamination of the initially primitive parental melt during an early intrusion stage (Gleißner et al., 2010).

We examined the Pb isotope composition in combination with Sr-Nd and trace element characteristics of the anorthosites and possible lower crustal contaminants to characterize the source and evolution of the parental magma. Our detailed isotopic and trace element study of the anorthosites and spatially related crustal rocks, combined with oxygen isotope data (Gleißner et al., 2010) enable us to constrain the amount and timing of crustal contamination during assimilation and fractional crystallization processes. The study improves the knowledge about the magmatic evolution of the anorthosites of the Kunene Intrusive Complex and puts constraints on the petrogenesis of massif-type anorthosites in general.

4.2 Geological setting

The 1.38 Ga Kunene Intrusive Complex (KIC), approximately 18,000 km^2 in size, extends from northwest Namibia into southwest Angola (Fig. 4.1) and is one of the largest massif-type anorthosite intrusions of the world (Ashwal & Twist, 1994). The rocks of the KIC intruded the high-grade metamorphic basement of the Epupa Complex (EC). In NW Namibia the EC mainly comprises upper amphibolite facies rocks of the Orue Unit and locally restricted ultrahigh-temperature granulite facies terranes, the Epembe Unit (Brandt et al., 2007). The Orue Unit is dominated by large bodies of migmatitic metagranitoids which intruded a volcano-sedimentary succession (Brandt & Klemd, 2008). The volcano-sedimentary sequence mainly consists of migmatitic metagreywackes, intercalated with mafic metavolcanic rocks, metapelites, meta-arkoses, metaquartzites and calc-silicate rocks. The Epembe Unit is dominated by intercalated felsic and mafic migmatitic orthogneisses and subordinate migmatitic metagreywackes and metapelites (Brandt et al., 2007). Both units preserve Paleoproterozoic (2.00 - 1.73 Ga) protolith ages and evidence for Mesoproterozoic (1.52 - 1.32 Ga) high-grade metamorphism (Tegtmeyer & Kröner, 1985; Seth et al., 2003, 2005). Paleoproterozoic protholith ages of 2.22 to 1.83 Ga are also constrained for the northern part of the EC, the 'gneiss-migmatite-granite complex' of Angola (De Carvalho et al., 2000) and the southern EC as part of the central Kaoko belt (Seth et al., 1998; Franz et al., 1999; Kröner et al., 2004). These ages correspond to the time of the Eburnean event (1.80 - 2.20 Ga) and demonstrate that the EC was a stable part of the Congo Craton during the emplacement of the anorthosites. The rocks of the north-eastern EC, including our study area, are overlain by undeformed Neoproterozoic (845 - 545 Ma) sediments of the Damara Supergroup (Brandt et al., 2007), whereas the south-western part was reworked during the Pan-African orogeny and incorporated into the Pan-African Kaoko belt (Fig. 4.1; Franz et al., 1999; Seth et al., 2005). Both the Orue and the Epembe Unit were intruded by mafic dykes which were metamorphosed during the Mesoproterozoic high-grade metamorphism to amphibolites and two-pyroxene granulites, respectively (Brandt & Klemd, 2008). The contact between the KIC and the surrounding Orue Unit is largely obliterated by broad ductile shear zones and late brittle faults, intruded by syenite and/or dolerite dykes (Drüppel et al., 2007). However, the local occurrence of thermal contact aureoles with undeformed Grt-Crd-Sill hornfels and the coincidence in pressures of 6-8 kbar for metamorphism of the Orue Unit (Brandt & Klemd, 2008) and anorthosite emplacement (Drüppel et al., 2001) suggest that the Orue Unit represents the metamorphic basement at the intrusion level of the anorthosites, whereas the granulite facies Epembe Unit represents tectonically emplaced slices of the lower crust (Brandt et al., 2007).

The KIC is a composite massif-type anorthosite that comprises several N-S elongated anorthosite bodies separated by belts of coeval granitoid intrusions in the Angolan part (Ashwal & Twist, 1994; Morais et al., 1998). In Namibia two anorthosite varieties were distinguished, a strongly deformed and altered pale 'white anorthosite' and a weakly to non altered 'dark anorthosite' (Menge, 1998; Drüppel

et al., 2001, 2007). The younger dark anorthosite intruded as sheet-like bodies in the centre of the white anorthosite massif and grades into smaller bodies towards the margin of the complex, forming an E-W striking structure (Drüppel et al., 2001, 2007). Crustal xenoliths are found in the white anorthosite suite, whereas the dark anorthosite suite typically contains xenoliths of the white anorthosite (Drüppel et al., 2007).

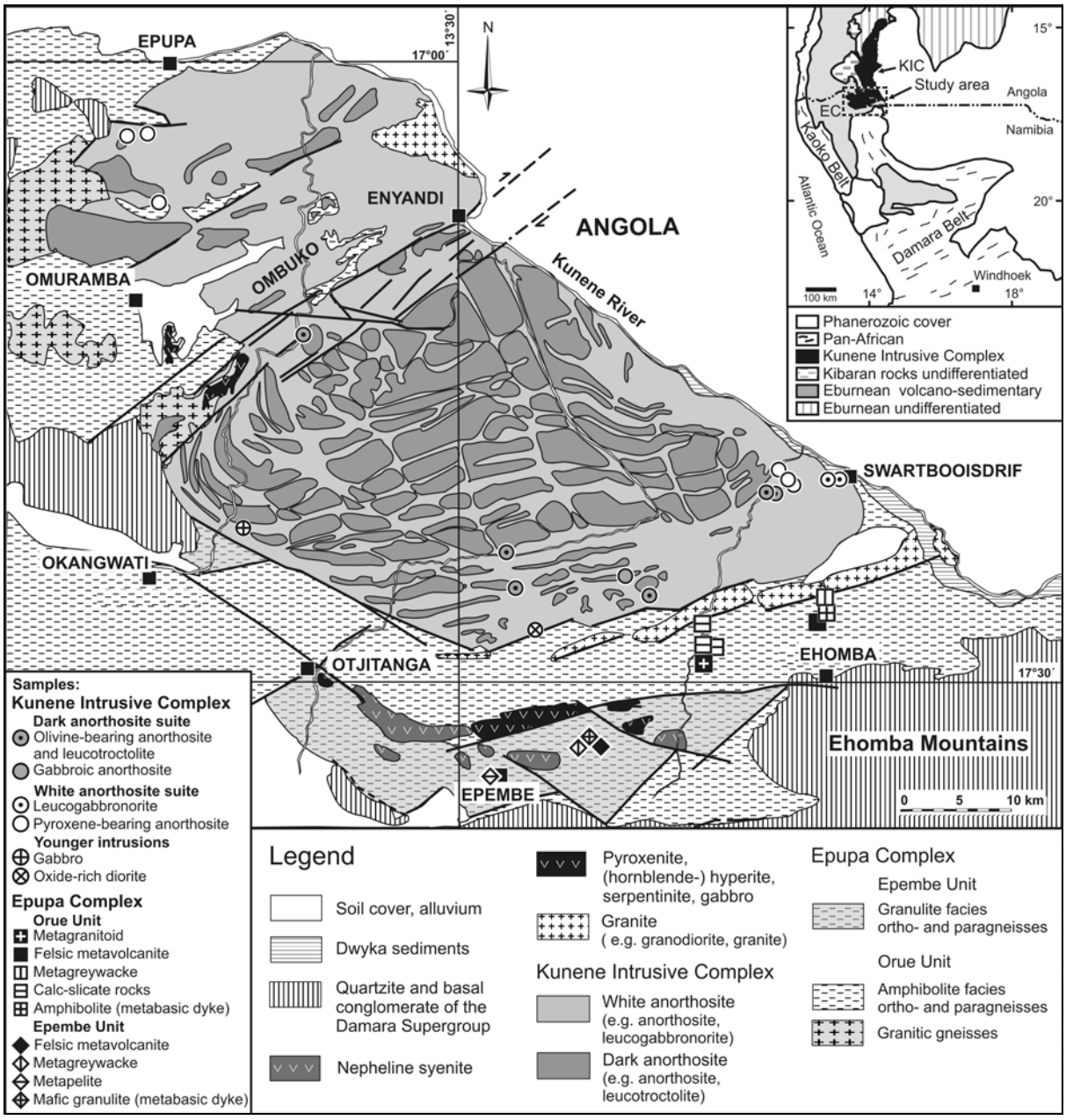

Fig. 4.1. Geological map of the southern Kunene Intrusive Complex and the adjacent Epupa Complex in NW Namibia. Map after Menge (1998) with modifications of Brandt et al. (2007) and Drüppel et al. (2007). Locations of samples used for isotope analysis are indicated. Inset shows location of the Kunene Intrusive Complex (KIC), Epupa Complex (EC) and the Kaoko and Damara belt (Pan-African) in SW Angola and NW Namibia.

The white anorthosite suite mainly comprises pyroxene-bearing anorthosite and leucogabbronorite with well-developed cumulate textures. Rocks of the white anorthosite suite underwent variable hydrothermal alteration, responsible for their pale colour and higher erodibility (Drüppel et al., 2001, 2007). The dark anorthosite suite mainly consists of leucotroctolite, olivine-bearing anorthosite and minor pyroxene-bearing anorthosite to gabbroic anorthosite. The generally fresh and massive rocks display homogeneous cumulate textures. Rare magmatic foliation at the outcrop scale is defined by plagioclase lamination, which occurs in both anorthosite varieties and is also described for the northern KIC (Ashwal & Twist, 1994; Morais et al., 1998; Mayer et al., 2004).

A U-Pb zircon age of 1385 ± 25 Ma dates the intrusion of the dark anorthosite suite in NW Namibia (Drüppel et al., 2000). Small gabbro and oxide-rich diorite bodies intruded the white anorthosite at the southernmost margin of the complex (Gleißner et al., 2010). A felsic rock suite is associated with the anorthosites and comprises granite, syenite and syenodiorite (Drüppel et al., 2007). U-Pb zircon ages of cogenetic mangerite in the Angolan part and syenodiorite in the Namibian part of the KIC are 1371 ± 2.5 Ma (Mayer et al., 2004) and 1376 ± 2 Ma (Drüppel et al., 2007), respectively. Small intrusions of mafic and ultramafic rocks, possibly genetically related to the KIC, crop out within the EC (Menge, 1998; Drüppel et al., 2007). The KIC in the study area is transected by a major NE trending dextral shear zone. Along this lineament isolated slices of Orue Unit and partly foliated anorthosites are intermingled (Fig. 4.1).

4.3 Analytical procedures

Trace element and isotope analysis were performed on a set of 17 bulk samples which cover the full compositional range of the anorthositic rocks in the KIC. Additionally, mineral separates from 10 of these samples were analysed to gain information on fractionation, cumulation and contamination processes. Mineral separation was proceeded by standard magnetic separation techniques and finally by hand-picking under a binocular microscope. Eleven basement samples were analysed to characterize the isotopic and trace element composition of the major lithologies of the EC (see Fig. 4.1 for sample locations).

All laboratory and mass spectrometry work was done at Deutsches GeoForschungsZentrum, Germany. Mineral separates were cleaned in warm 7N HNO_3 for ½ hour and then washed several times in ultra clean water. Whole rock samples and mineral separates were dissolved in hydrofluoric acid (HF) on a hot plate (160°C). After evaporation of the HF, the samples were dissolved in 6N HCl and split into three fractions for trace element analysis, for Sr and Nd isotope analysis and for Pb isotope analysis.

The trace element concentrations of bulk samples and mineral separates were determined by inductively coupled plasma-mass spectrometry (ICP-MS). All mineral separates and part of the whole rock samples were measured from the aliquot after HF-digestion (see above). Additional whole rock

samples were measured from a separate aliquot after HF-$HClO_4$ digestion (in Table 4.4 marked with an asterisk). Dried samples were redissolved in dilute HNO_3. All samples were measured with a Finnigan Element 2 XR ICP-MS instrument. Accuracy was checked with international geological reference material (JB-3). Precision is generally better than ± 10 % for Rb, Sr, Th, U, Pb, Nb, Zr and ± 5 % for REE. Details of sample preparation and long-time reproducibility of concentration data are given in Romer & Hahne (2010).

The Sr, Nd and Pb isotope ratios of bulk samples and mineral separates were determined by thermal ionisation mass spectrometry (TIMS). Sr, Nd and Pb were separated using ion-exchange chromatography described in Romer & Hahne (2010). Total procedural blanks were <50 pg for Sr and <30 pg for Nd and Pb. Sr was loaded on single Ta filaments and measured on a Finnigan MAT262 using static multi-collection and a Thermo Triton mass spectrometer using dynamic multi-collection. All Sr isotopic values were normalized to $^{86}Sr/^{88}Sr = 0.1194$. Repeated measurement of the NBS 987 Sr standard yielded $^{87}Sr/^{86}Sr = 0.710273 \pm 7$ (n = 12) for the MAT262 instrument. Measured values were readjusted to the $^{87}Sr/^{86}Sr$ value of 0.710248 ± 5 (n = 20) obtained with the Triton instrument. Nd was loaded on double Re filaments, and its isotopic composition was measured on the Finnigan MAT262 mass spectrometer in dynamic multi-collection mode. Mass fractionation during Nd measurement was corrected by normalizing to $^{146}Nd/^{144}Nd = 0.7219$. Repeated analyses of the La Jolla Nd standard yielded a value of $^{143}Nd/^{144}Nd = 0.511850 \pm 5$ (n = 20). Pb together with silica-gel was loaded on single Re filaments and measured on the Finnigan MAT262 mass spectrometer using static multi-collection. Values were corrected for instrumental fractionation with 0.1 % per atomic mass unit. Accuracy and precision of reported values are better than 0.1 % at the 2-sigma level.

4.4 Results

4.4.1 Petrography of the anorthosite samples

The rocks of the KIC commonly display well-preserved primary magmatic assemblages and textures dominated by coarse plagioclase. Petrographic as well as geochemical features have been described previously in Drüppel et al. (2001, 2007) and Gleißner et al. (2010). Therefore we only give a short summary here. Rocks of the white anorthosite suite display an assemblage of cumulus plagioclase (An_{39-64}) ± cumulus orthopyroxene (X_{Mg}: 0.57 – 0.72) + interstitial ortho- and clinopyroxene (X_{Mg}: 0.57 – 0.78) + ilmenite ± magnetite ± biotite ± amphibole ± apatite ± zircon ± sulfides. Centimetre-sized cumulus orthopyroxene contain up to 3.5 wt.% Al_2O_3 and display lamellar exsolution of ilmenite (Fig. 4.2a). Biotite, apatite and amphibole are late phases formed from the intercumulus melt. Variable hydrothermal alteration resulted mainly in sericitisation of plagioclase and uralitisation of pyroxene. Xenocrysts of andradite-rich garnet occur in the interstices between cumulus plagioclase within leucogabbronorite from the south-eastern part of the KIC (Fig. 4.2b) and suggest contamination of the

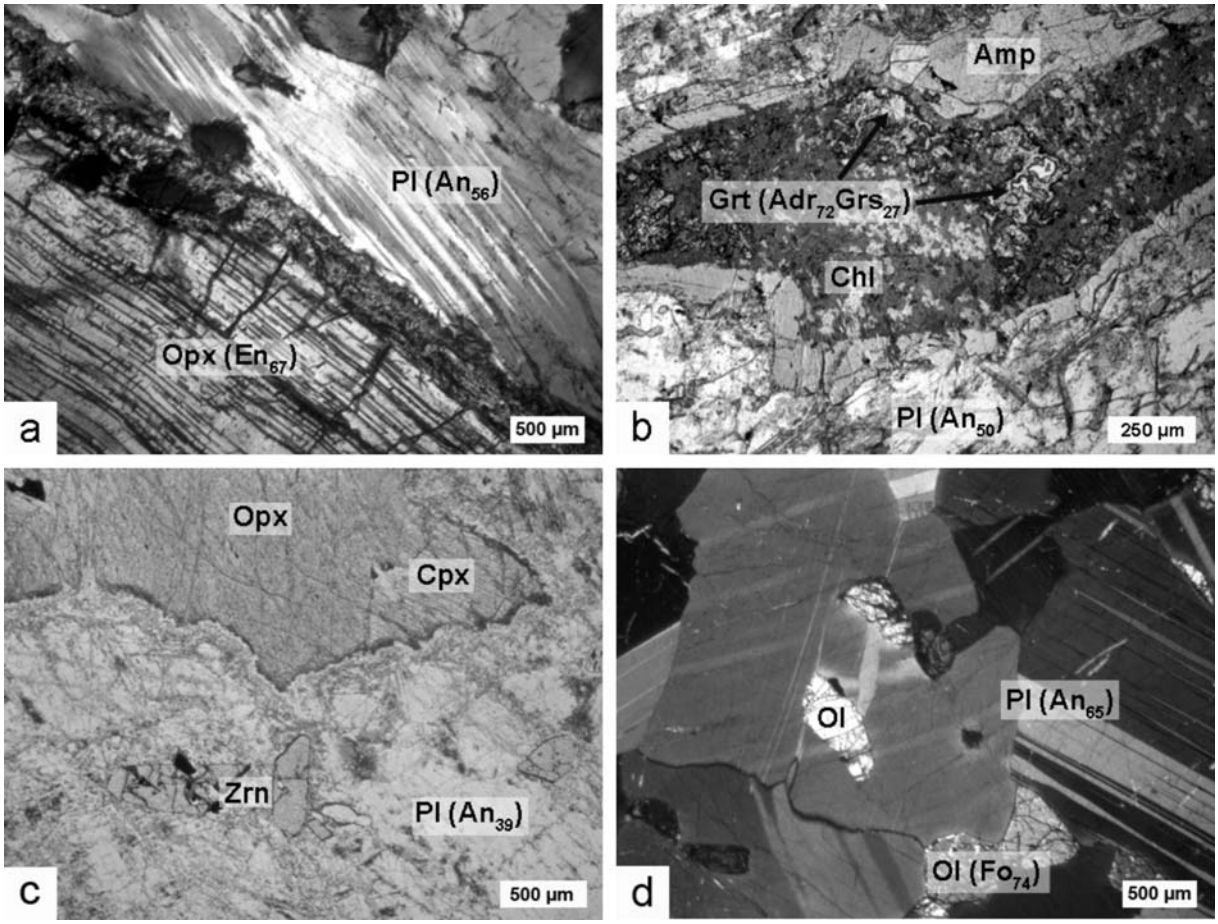

Fig. 4.2. Thin section microphotographs of the white anorthosite suite (a-c) and dark anorthosite suite (d) of the Kunene Intrusive Complex (a and d: crossed polarizers; b and c: parallel polarizers). (a) Pyroxene-bearing anorthosite (Ku-06-63a): Cumulus plagioclase and euhedral orthopyroxene. The cm-sized orthopyroxene displays oriented lamellae of ilmenite and ductile deformation features. (b) Leucogabbronorite (Ku-97-08b): Crustal xenocryst within the interstices of euhedral cumulus plagioclase. Andradite-rich garnet is replaced by chlorite and surrounded by late magmatic amphibole. (c) Pyroxene-bearing anorthosite (Ku-06-04b): Euhedral zircons included in cumulus plagioclase. (d) Leucotroctolite (Ku-98-228): Subhedral cumulus plagioclase with olivine inclusions and interstitial olivine.

parental melt with calc-silicate gneisses of the country rock (Drüppel et al., 2007). Euhedral zircon, occasionally included in plagioclase, also points to assimilation and incomplete dissolution of crustal rocks (Fig. 4.2c).

The dark anorthosite suite displays the primary magmatic assemblage of cumulus plagioclase (An_{53-65}) + olivine (Fo_{56-74}) + interstitial ortho- and clinopyroxene (X_{Mg}: 0.64 – 0.74) + ilmenite ± magnetite ± biotite. The rocks are generally fresh in appearance and show tabular cumulus plagioclase and nearly unaltered olivine, both as inclusion in plagioclase and interstitial phase (Fig. 4.2d). Anhedral ortho- and clinopyroxene fill the interstices between cumulus plagioclase.

4.4.2 Major and trace element composition

4.4.2.1 Anorthosites

Major and trace element data of anorthositic rocks and mineral separates are given in Tables 4.1 and 4.2. The rocks are generally rich in Al_2O_3, CaO and Na_2O, reflecting high amounts of cumulus plagioclase. Al_2O_3 and CaO increase with X_{Mg} from the white to the dark anorthosite suite, reflecting higher anorthite content of plagioclase and the predominance of Mg-rich olivine over pyroxene in the dark anorthosites (Fig. 4.2d).

The white anorthosites are enriched in incompatible trace elements when compared to the dark anorthosites. Chondrite-normalized REE patterns display enrichment of LREE over MREE (La_N/Sm_N: 1.9 – 6.5) and HREE (La_N/Yb_N: 8.2 – 30.6), and positive europium anomalies (Eu/Eu*: 2.0 – 7.0), typical of plagioclase cumulate rocks (Fig. 4.3a). Significant enrichment in other trace elements (Fig. 4.3b) is attributed to the abundance of particular mineral species, e.g. plagioclase (Ba, Sr), clinopyroxene (MREE, Sc), ilmenite (V, Nb) and apatite (Y, REE).

The dark anorthosites display lower absolute trace element concentrations except for Ni, attributed to the presence of abundant olivine in leucotroctolite, and for Cr and Sc, reflecting abundant clinopyroxene in gabbroic anorthosite. The chondrite-normalized REE patterns also display enrichment of LREE over MREE (La_N/Sm_N: 2.1 – 4.3) and HREE (La_N/Yb_N: 3.2 – 29.4), and positive europium anomalies (Eu/Eu*: 3.3 – 7.1). The younger gabbro and oxide-rich diorite intrusions display flatter REE patterns and the lowest positive europium anomalies (Eu/Eu*: 1.6), consistent with the lower modal amounts of cumulus plagioclase.

Plagioclase of the white anorthosite suite shows high concentrations of highly to moderately incompatible trace elements like Rb (0.7 – 5.4 ppm), Pb (0.7 – 10.3 ppm) and Sr (513 – 1220 ppm). In accordance with their whole rock values, plagioclase displays variable but strong LREE enrichment over MREE (La_N/Sm_N: 5.9 – 11.3) and HREE (La_N/Yb_N: 53 – 150), and strong positive europium anomalies (Eu/Eu*: 7 – 29).

Plagioclase of the dark anorthosite suite is lower in Rb (0.5 – 2.8 ppm), Pb (0.4 – 3.4 ppm) and Sr (266 – 907 ppm). The overall REE concentrations are lower, but display nearly homogeneous LREE enrichment over MREE (La_N/Sm_N: 6.1 – 6.7) and HREE (La_N/Yb_N: 53 – 119). As in the white anorthosite suite, all plagioclase samples yield strong positive europium anomalies (Eu/Eu*: 9 – 12), in accordance with their crystallization prior to significant plagioclase fractionation. Clinopyroxene of the dark anorthosite displays higher M+HREE concentrations and negative europium anomalies (Eu/Eu*: 0.2), in accordance with their late crystallization from intercumulus liquid after extensive plagioclase fractionation. Obtained trace element data of mineral separates are in good agreement with in-situ analyses of Gleißner et al. (2010).

Table 4.1. Major and trace element data of representative KIC anorthositic rocks.

	White anorthosite suite					Dark anorthosite suite					Younger intrusions	
rock type	LGN	LGN	Apx	Apx	Apx	LT	LT	LT	Aol	GA	Di	G
sample	Ku-97-03[D]	Ku-97-08b[D]	Ku-06-04a[G]	Ku-06-04b[G]	Ku-06-63a	Ku-98-125[D]	Ku-98-228[D]	Ku-06-69[G]	Ku-06-18a[G]	Ku-06-72	Ku-06-20a[G]	Ku-06-31b[G]
[wt.%]												
SiO_2	45.6	46.1	55.0	56.2	52.1	44.7	49.6	48.9	51.4	51.4	42.9	51.3
TiO_2	2.97	1.78	0.11	0.06	0.11	2.08	0.10	0.30	0.17	0.29	6.60	0.44
Al_2O_3	20.1	21.1	22.0	24.0	29.5	21.4	26.8	23.7	27.5	24.0	11.8	17.3
Fe_2O_3	2.32	9.38	3.50	1.33	0.57	2.55	0.81	2.27	1.82	1.50	7.41	1.97
FeO	6.73	1.38	0.68	0.50	0.46	8.70	3.02	4.25	0.67	2.38	11.6	3.99
MnO	0.21	0.15	0.10	0.05	b.d.l.	0.11	0.05	0.08	b.d.l.	0.07	0.25	0.13
MgO	3.17	4.13	2.61	0.77	0.05	5.33	5.40	6.16	1.91	3.64	5.62	8.35
CaO	8.80	7.62	7.98	7.55	12.3	8.56	11.8	10.4	11.8	12.0	9.02	13.2
Na_2O	3.88	3.71	5.82	7.08	4.19	3.37	3.15	3.02	3.91	3.54	2.25	2.36
K_2O	1.92	1.39	0.62	0.57	0.36	0.47	0.17	0.30	0.30	0.35	0.34	0.18
P_2O_5	0.65	0.05	b.d.l.	0.03	0.02	0.06	0.01	0.02	0.02	0.02	0.02	b.d.l.
L.O.I.	2.20	2.97	1.51	1.61	0.94	1.41	0.23	1.15	0.66	0.48	0.95	0.78
Total	98.6	99.8	99.9	99.8	100.6	98.7	101.0	100.5	100.2	99.7	98.8	100.0
X_{Mg}	0.39	0.43	0.55	0.45	0.08	0.46	0.72	0.64	0.60	0.64	0.35	0.72
[ppm]												
Sc	19	5.0	n.a.	3.1	0.75	4.7	1.7	n.a.	n.a.	16	n.a.	41
V	160	220	n.a.	n.a.	b.d.l.	290	14	33	n.a.	n.a.	n.a.	140
Cr	15	78	88	b.d.l.	26	130	22	33	b.d.l.	280	72	500
Ni	24	110	99	61	b.d.l.	130	200	130	42	53	44	95
Zn	95	100	55	24	b.d.l.	95	30	43	b.d.l.	24	130	31
Ga	19	20	24	26	17	17	26	19	22	19	22	14
Rb	29	26	3.6	2.8	1.0	3.5	0.45	2.4	1.9	1.5	0.42	3.2
Sr	790	680	680	770	650	590	440	420	480	410	190	300
Y	12	8.0	15	b.d.l.	b.d.l.	b.d.l.	b.d.l.	b.d.l.	b.d.l.	12	14	b.d.l.
Zr	60	46	30	200	b.d.l.	27	b.d.l.	b.d.l.	b.d.l.	b.d.l.	60	b.d.l.
Nb	6.1	3.1	n.a.	1.9	0.35	1.3	0.13	n.a.	n.a.	0.41	n.a.	0.39
Ba	1200	820	570	770	180	360	110	100	180	280	360	82
Pb	4.0	4.1	8.7	7.7	0.97	2.7	0.44	1.0	0.92	0.80	2.6	0.50
Th	0.23	0.49	0.60	3.0	0.02	0.15	0.04	0.10	0.09	0.11	0.03	0.05
U	0.06	0.18	0.06	0.14	0.01	0.04	0.01	0.03	0.03	0.03	0.02	0.01
La	8.7	4.6	19	25	1.8	3.4	1.3	2.3	2.0	2.0	2.2	1.2
Ce	20	9.2	30	41	3.6	6.8	2.5	4.5	3.7	4.3	6.2	3.0
Pr	2.8	1.1	3.3	4.2	0.41	0.79	0.27	0.55	0.44	0.56	1.1	0.46
Nd	13	4.0	12	14	1.6	3.2	1.1	2.2	1.8	2.6	6.3	2.6
Sm	2.8	0.83	2.4	2.4	0.27	0.57	0.19	0.43	0.35	0.60	2.1	0.95
Eu	1.9	0.97	2.7	3.4	0.57	0.84	0.42	0.76	0.77	0.77	1.3	0.59
Gd	3.1	0.68	2.4	2.1	0.23	0.51	0.17	0.40	0.34	0.83	2.7	1.3
Tb	0.39	b.d.l.	0.32	0.27	b.d.l.	b.d.l.	b.d.l.	0.06	0.04	0.12	0.46	0.22
Dy	2.2	0.60	2.2	1.8	0.16	0.37	0.11	0.34	0.26	0.86	3.0	1.5
Ho	0.38	b.d.l.	0.42	0.32	b.d.l.	b.d.l.	b.d.l.	b.d.l.	0.05	0.16	0.60	0.31
Er	1.0	0.34	1.3	0.96	0.07	0.17	0.04	0.20	0.14	0.47	1.7	0.89
Tm	0.13	b.d.l.	0.18	0.14	b.d.l.	b.d.l.	b.d.l.	0.03	0.02	0.07	0.24	0.13
Yb	0.72	0.32	1.3	0.88	0.04	0.16	0.03	0.18	0.12	0.43	1.5	0.79
Lu	0.10	b.d.l.	0.21	0.15	b.d.l.	b.d.l.	b.d.l.	0.03	b.d.l.	0.07	0.24	0.13
ΣREE	57	23	78	97	8.8	17	6.1	12	10	14	30	14
Eu/Eu*	2.0	3.9	3.4	4.6	7.0	4.7	7.1	5.6	6.8	3.3	1.7	1.6
La_N/Sm_N	1.9	3.5	4.9	6.5	4.2	3.7	4.3	3.4	3.6	2.1	0.7	0.8
La_N/Yb_N	8.2	9.8	11	20	31	14	29	8.7	11	3.2	1.0	1.0

Major elements taken from [D]Drüppel (2003) and [G]Gleißner et al. (2010). Aol, olivine-bearing anorthosite; Apx, pyroxene-bearing anorthosite; Di, oxide-rich diorite; G, gabbro; GA, gabbroic anorthosite; LGN, leucogabbronorite; LT, leucotroctolite.

Table 4.2. Trace element data of plagioclase and clinopyroxene mineral separates from KIC anorthosites.

	White anorthosite suite		Dark anorthosite suite			
rock type	LGN	Apx	LT	LT	LG	LG
sample	Ku-97-03	Ku-06-63a	Ku-98-125	Ku-98-228	Ku-06-72	Ku-06-72
Min (X_{An})	Pl (0.47)	Pl (0.56)	Pl (0.53)	Pl (0.65)	Pl (0.57)	Cpx
[ppm]						
Rb	5.4	0.67	1.6	0.50	0.44	0.30
Sr	1200	510	910	370	270	26
Y	0.30	0.23	0.35	0.10	0.05	25
Nb	0.43	0.09	0.10	0.06	0.05	0.55
Pb	2.9	0.77	3.4	0.41	0.54	1.6
Th	0.014	0.005	0.052	0.002	b.d.l.	0.44
U	0.005	0.004	0.025	0.004	0.003	0.11
La	4.2	1.2	2.3	0.70	0.70	1.8
Ce	6.6	2.4	4.2	1.4	1.3	8.8
Pr	0.63	0.25	0.43	0.13	0.13	1.8
Nd	2.2	1.0	1.7	0.48	0.48	11
Sm	0.23	0.13	0.23	0.07	0.07	3.8
Eu	2.1	0.32	0.62	0.19	0.26	0.26
Gd	0.21	0.15	0.21	0.07	0.07	4.4
Tb	b.d.l.	0.02	0.02	0.01	0.01	0.83
Dy	0.08	0.07	0.10	0.03	0.02	5.5
Ho	0.01	0.01	0.02	0.005	b.d.l.	1.2
Er	0.03	0.02	0.04	b.d.l.	b.d.l.	3.1
Tm	b.d.l.	0.003	b.d.l.	b.d.l.	b.d.l.	0.43
Yb	0.02	0.02	0.03	0.006	0.004	2.8
Lu	0.003	0.002	b.d.l.	b.d.l.	b.d.l.	0.41
ΣREE	16	5.6	10	3.1	3.0	46
Eu/Eu*	29	7.0	8.6	8.3	11	0.19
La_N/Sm_N	11	5.8	6.2	6.2	6.2	0.30
La_N/Yb_N	143	41	52	79	119	0.43

Apx, pyroxene-bearing anorthosite; GA, gabbroic anorthosite; LGN, leucogabbronorite; LT, leucotroctolite.

4.4.2.2 Epupa Complex

Selection of the samples representative for the major units of the EC was based on the geochemical characterization of the protoliths by Brandt (2003). Major and trace element composition of basement rocks is listed in Table 4.3. Felsic orthogneisses and paragneisses of the EC are characterized by high concentrations of incompatible trace elements (Ba: 200 – 1560 ppm, Rb: 50 – 125 ppm, ∑REE: 167 – 357 ppm). The chondrite-normalized REE patterns display enrichment of LREE over M+HREE and negative europium anomalies (Eu/Eu*: 0.45 – 0.73; Fig. 4.3a). Rocks of the granulite facies Epembe Unit display higher overall HREE concentrations and hence lower LREE enrichment (La_N/Yb_N: 4.3 – 8.9) compared to the amphibolite facies Orue Unit rocks (La_N/Yb_N: 8.3 – 13.8). The mantle-normalized trace element pattern of all felsic orthogneisses and paragneisses show negative Nb, Sr, P, Ti anomalies, typical of average middle crust (Rudnick & Fountain, 1995). Rb depletion, typical of average lower crust (Rudnick & Fountain, 1995), was observed in Epembe Unit rocks and, to a lesser extent, in Orue Unit rocks, except for calc-silicate rocks. The orthogneisses display variable Pb depletion (Fig. 4.3b).

Table 4.3. Major and trace element data of EC ortho- and parageneisses.

	Epembe Unit				Orue Unit				
rock type	mdk	mvolc	mgrw	mpel	mdk	mvolc	mgran	mgrw	cals
sample	B-447-1-99[B]	B-614-2-99[B]	B-230-A-98[B]	B-212-A-98[B]	B-177-B-98[B]	B-174-A-98[B]	B-406-2-99[B]	B-171-A-98[B]	B-588-3-99[G]
[wt.%]									
SiO_2	50.7	75.5	66.4	49.1	48.0	74.6	75.6	67.2	64.8
TiO_2	1.16	0.30	0.93	0.98	1.69	0.20	0.29	0.53	0.51
Al_2O_3	16.0	11.6	14.6	25.5	14.2	11.8	12.3	15.2	16.1
Fe_2O_3	1.20	1.63	0.91	0.98	2.89	1.11	1.00	1.33	2.68
FeO	8.96	1.24	5.89	8.65	8.60	2.05	0.86	2.66	2.38
MnO	0.17	0.04	0.18	0.20	0.21	0.05	0.03	0.12	0.40
MgO	6.55	0.42	2.38	3.37	7.15	0.69	0.73	1.88	2.05
CaO	9.93	1.38	3.06	1.28	10.8	0.64	1.41	1.55	4.34
Na_2O	2.76	3.76	2.94	2.45	2.61	2.78	3.78	3.73	0.76
K_2O	0.72	2.63	1.13	4.74	1.31	5.18	2.60	3.64	3.07
P_2O_5	0.21	0.02	0.05	0.05	0.15	0.04	0.03	0.10	0.14
L.O.I.	0.42	0.65	0.35	1.19	1.21	0.60	0.57	1.49	2.81
Total	98.8	99.2	98.8	98.5	98.8	99.7	99.2	99.4	100.0
X_{Mg}	0.54	0.22	0.39	0.39	0.53	0.29	0.42	0.46	0.43
[ppm]									
Sc	39	12	13	25	34	11	15	12	n.a.
V	260	14	90	140	320	12	15	54	57
Cr	65	b.d.l.	45	110	230	b.d.l.	17	52	61
Ni	63	b.d.l.	b.d.l.	55	75	b.d.l.	b.d.l.	9.0	27
Zn	160	18	56	180	120	49	25	70	75
Ga	32	23	20	38	15	16	13	22	22
Rb	17	27	23	70	11	40	51	98	160
Sr	330	100	190	170	300	180	140	280	120
Y	18	66	84	55	29	38	40	31	29
Zr	49	410	42	320	110	280	330	290	180
Nb	6.0	10	16	30	6.0	9.4	15	15	18
Ba	150	1200	490	1600	720	1200	1000	1600	420
Pb	5.4	3.1	13	23	20	11	11	13	20
Th	0.26	12	5.4	18	1.2	6.6	16	14	17
U	0.14	1.2	0.66	2.9	0.54	1.6	2.0	1.6	3.7
La	24	58	69	76	10	46	70	54	45
Ce	52	120	130	150	22	99	140	110	94
Pr	6.9	16	14	17	3.1	11	16	12	11
Nd	28	61	49	60	15	45	57	44	40
Sm	6.4	13	9.8	12	3.8	9.1	10	7.9	7.7
Eu	1.9	1.8	1.8	2.3	1.4	1.7	1.5	1.4	1.2
Gd	6.3	12	12	11	4.2	7.7	9.2	6.0	6.2
Tb	0.97	2.0	2.1	1.7	0.68	1.0	1.3	0.82	0.86
Dy	6.2	13	15	10	4.1	6.1	7.6	5.2	5.0
Ho	1.3	2.8	3.4	2.1	0.84	1.2	1.5	1.1	1.1
Er	3.6	8.0	10	5.8	2.3	3.5	4.0	3.3	3.0
Tm	0.53	1.2	1.6	0.88	0.32	0.55	0.55	0.50	0.48
Yb	3.5	8.2	11	5.8	2.0	3.7	3.4	3.5	3.2
Lu	0.53	1.3	1.7	0.91	0.30	0.61	0.54	0.56	0.50
ΣREE	142	320	330	355	70	236	321	250	219
Eu/Eu*	0.91	0.44	0.51	0.61	1.1	0.62	0.48	0.62	0.53
La_N/Sm_N	2.3	2.8	4.4	4.0	1.6	3.2	4.4	4.3	3.6
La_N/Yb_N	4.7	4.8	4.3	8.9	3.4	8.4	14	10	9.6

Major elements taken from [B]Brandt (2003) and [G]Gleißner et al. (2010). mvolc, felsic metavolcanite; mgran, metagranite; mdk, metabasic dyke; mgrw, metagreywackes; mpel, metapelite; cals, calc-silicate rock.

The metabasic dykes are characterized by moderate enrichment of LREE over HREE (La_N/Yb_N: 3.4 – 4.7; Fig 3a). The Orue Unit metabasic dyke shows higher concentration in highly incompatible trace elements like Ba, Th, Pb, U and K, but lower REE when compared to the metabasic dyke from the Epembe Unit (Fig. 4.3b).

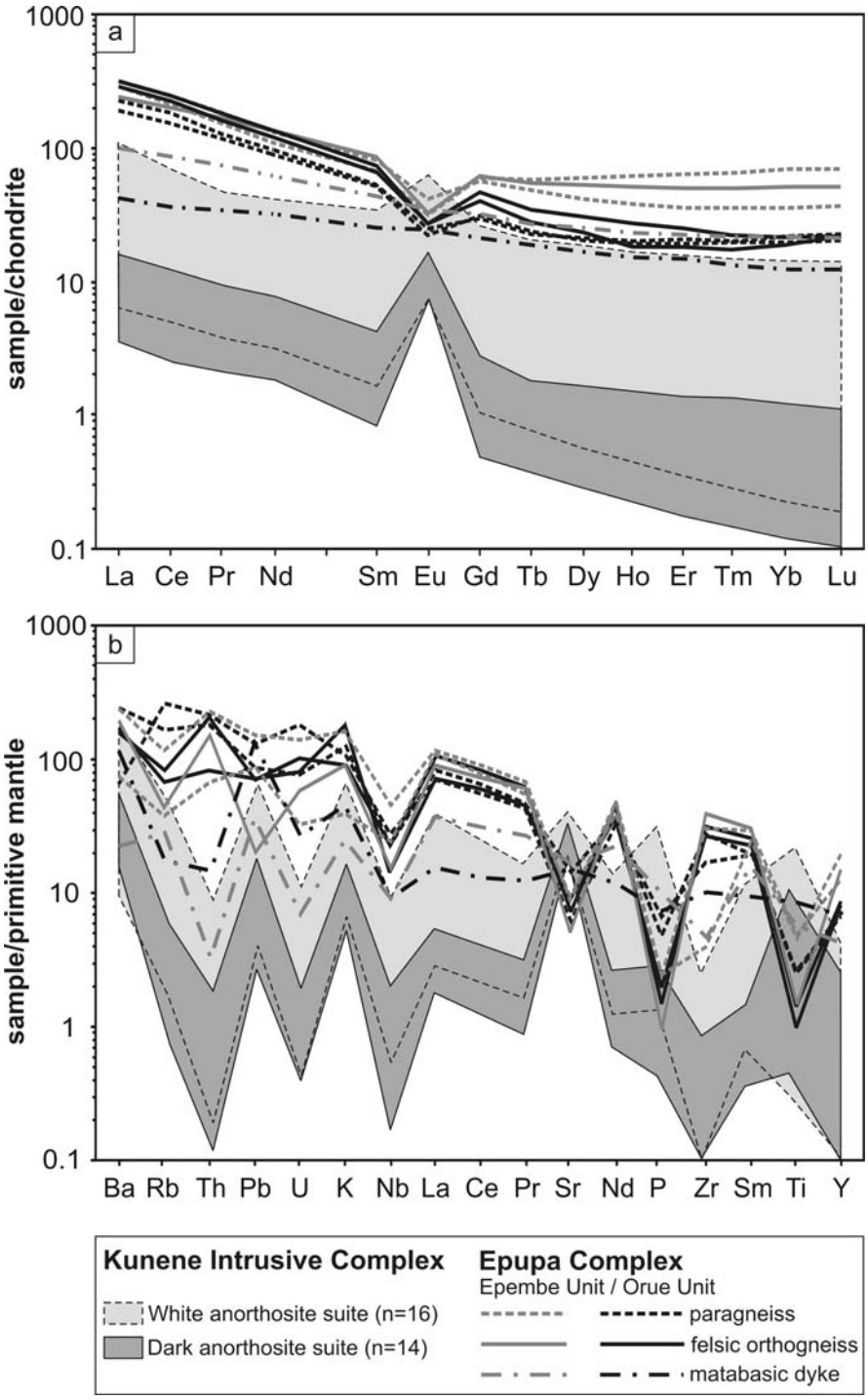

Fig. 4.3. (a) Chondrite-normalized REE composition of anorthosites and representative Epupa Complex (EC) rocks (including data of Drüppel et al., 2007). (b) Primitive mantle-normalized trace element composition of anorthosites and representative EC basement rocks. Chondrite and pyrolite values of McDonough & Sun (1995) have been used for normalization.

4.4.3 Sr, Nd and Pb isotopic composition

Obtained isotopic compositions of KIC rocks and mineral separates were corrected for in-situ decay of Rb, Sm, Th and U to the intrusion age of 1.38 Ga (Drüppel et al., 2000). The isotopic composition of EC rocks was recalculated to the time of anorthosite formation. Measured values and calculated initial values are listed in Tables 4.4 and 4.5.

4.4.3.1 Anorthosites

Sr and Nd isotope ratios of the white anorthosite suite range from the compositional field of slightly depleted mantle to crustal values (Fig. 4.4a). The majority of samples from the southeast of the study area display crustal isotopic ratios ($^{87}Sr/^{86}Sr_i$ 0.70405 – 0.70430, εNd_i -1.0 to -3.1). Samples from the northwest of the study area display more primitive isotopic ratios ($^{87}Sr/^{86}Sr_i$ 0.70312 – 0.70340, εNd_i +2.1 to +0.8). The dark anorthosites fall in the compositional field of strongly depleted to undepleted mantle ($^{87}Sr/^{86}Sr_i$ 0.70284 – 0.70360 and εNd_i +6.4 to +0.8).

All analyses of separated plagioclase fall on the overall trend defined by the whole rock analyses (Fig. 4.4b). However, the isotopic composition of most plagioclase separates differs from that of the corresponding whole rock. Within the range of calculated uncertainties the Sr isotopic composition of plagioclase, with one exception, is less radiogenic than the corresponding whole rock. In contrast, their Nd isotopic composition is commonly identical within error. Three plagioclase separates yield higher εNd_i values than their whole rocks, two of them also display significantly lower $^{87}Sr/^{86}Sr_i$ ratios. The majority of pyroxene separates display age-corrected Nd isotopic compositions which overlap in uncertainty with the corresponding plagioclase and whole rock values, but are significantly lower in $^{87}Sr/^{86}Sr_i$.

The initial Pb isotope ratios of the white anorthosites range from $^{206}Pb/^{204}Pb$ 16.21 – 17.09, $^{207}Pb/^{204}Pb$ 15.39 – 15.49 and $^{208}Pb/^{204}Pb$ 34.85 – 37.13, respectively (Fig. 4.5). Three leucogabbronorite samples, two of them displaying crustal xenocrysts described by Drüppel et al. (2007), approach the Pb isotopic composition of calc-silicate and metapelitic basement rocks (Fig. 4.5b). Plagioclase, separated from two of these samples, yields a significantly less radiogenic composition and falls within the range of the majority of anorthosites (Fig. 4.5b). The initial Pb isotope ratios of the dark anorthosite suite range from $^{206}Pb/^{204}Pb$ 16.18 – 16.94, $^{207}Pb/^{204}Pb$ 15.40 – 15.48 and $^{208}Pb/^{204}Pb$ 35.91 – 36.73, respectively. Most of the plagioclase separates show a Pb isotopic composition similar to the corresponding whole rock samples. Pyroxene separates display the highest measured Pb isotope values. The initial Pb isotopic composition of both anorthosite varieties falls between the mantle and upper crust model reservoir growth curves (Zartman & Doe, 1981).

Table 4.4. Sr and Nd isotope data from KIC anorthositic rocks and EC basement rocks.

sample	rock type[a]	Rb [ppm]	Sr [ppm]	$^{87}Sr/^{86}Sr$[b]	$^{87}Sr/^{86}Sr$ (1.38Ga)[c]	Sm [ppm]	Nd [ppm]	$^{143}Nd/^{144}Nd$[b]	$^{143}Nd/^{144}Nd$ (1.38Ga)[c]	εNd (1.38Ga)[c]	$T_{(DM)}$ [Ga][d]
White anorthosite suite											
Ku-97-03	LGN	29	790	0.706344±4*	0.70434	2.8	13	0.512123±5	0.51094	1.7	1.8
Pl		5.4	1200	0.704131±4	0.70389	0.23	2.2	0.511505±49	0.51093	1.5	1.6
Ku-97-04	LGN	20	430	0.706732±7	0.70420	4.6	17	0.512264±5	0.51078	-1.5	2.4
Pl		5.3	900	0.704123±7	0.70380	0.22	1.8	0.511528±17	0.51086	0.1	1.7
Cpx		1.1	46	0.705213±19	0.70391	4.2	12	0.512667±5	0.51075	-2.1	
Ku-97-08b	LGN	26	680	0.706138±4*	0.70405	0.83	4.0	0.511940±5	0.51080	-1.0	2.0
Ku-06-04a	Apx	3.6	680	0.704469±7	0.70418	2.4	12	0.511758±4	0.51066	-3.8	2.2
Pl		2.0	810	0.704338±7	0.70420	0.72	6.9	0.511269±4	0.51070	-3.1	1.8
Opx		0.16	1.1	0.710084±21	0.70216	1.5	4.1	0.512743±10	0.51074	-2.3	
Ku-06-04b	Apx	2.8	770	0.704497±4*	0.70430	2.4	14	0.511736±5	0.51080	-1.2	1.9
Ku-06-51	Apx	1.5	790	0.703227±4*	0.70312	0.31	2.0	0.511826±6	0.51098	2.4	1.6
Ku-06-60	Apx	2.1	550	0.703581±4*	0.70337	0.55	3.7	0.511736±5	0.51092	1.3	1.7
Ku-06-63a	Apx	1.0	650	0.703490±4*	0.70341	0.27	1.6	0.511823±6	0.51090	0.8	1.7
Pl		0.67	510	0.703228±4	0.70316	0.13	1.0	0.511761±8	0.51105	3.8	1.5
Dark anorthosite suite											
Ku-98-125	LT	3.5	590	0.703915±4*	0.70359	0.57	3.2	0.511870±6	0.51089	0.8	1.8
Pl		1.6	910	0.703714±4	0.70362	0.23	1.7	0.511719±5	0.51098	2.4	1.6
Ku-98-228	LT	0.45	440	0.703147±4*	0.70309	0.19	1.1	0.512128±7	0.51118	6.4	1.4
Pl		0.50	370	0.703104±4	0.70303	0.07	0.48	0.511858±8	0.51106	4.0	1.5
Ku-06-07	LT	2.5	400	0.703172±4*	0.70283	0.34	1.3	0.512259±5	0.51082	-0.6	2.2
Ku-06-48	LT	0.10	440	0.703071±4*	0.70295	0.16	0.98	0.511946±6	0.51105	3.8	1.5
Ku-06-69	LT	2.4	420	0.703458±7	0.70315	0.43	2.2	0.511988±4	0.51092	1.2	1.8
Pl		2.8	570	0.703330±7	0.70306	0.26	1.6	0.511773±8	0.51088	0.5	1.3
Cpx		0.40	19	0.703893±8	0.70275	5.6	14	0.513065±5	0.51087	0.3	
Ku-06-18a	Aol	1.9	480	0.703499±7	0.70328	0.35	1.8	0.512022±7	0.51096	2.0	1.7
Pl		1.6	460	0.703319±7	0.70313	0.19	1.1	0.511838±7	0.51089	0.7	1.7
Cpx		0.45	30	0.703702±7	0.70289	6.1	14	0.513274±5	0.51088	0.6	
Ku-06-72	GA	1.5	410	0.703547±4*	0.70335	0.60	2.6	0.512387±5	0.51112	5.2	1.5
Pl		0.44	270	0.703220±4	0.70313	0.07	0.48	0.511830±5	0.51103	3.4	1.5
Cpx		0.30	26	0.703396±4	0.70277	3.8	11	0.512920±6	0.51103	3.3	
Younger intrusions											
Ku-06-20a	Di	0.42	190	0.703900±7	0.70378	2.1	6.3	0.512808±4	0.51098	2.5	
Pl		1.7	580	0.703620±7	0.70346	0.20	1.5	0.511681±7	0.51095	1.9	1.6
Cpx		0.37	13	0.704338±7	0.70279	5.3	14	0.512971±9	0.51089	0.8	
Ku-06-31b	G	3.2	300	0.703595±4*	0.70301	0.95	2.6	0.512893±6	0.51089	0.7	
Epupa Complex (Epembe Unit)											
B-447-1-99	mdk	17	330	0.707651±7	0.70484	6.4	28	0.512065±5	0.51081	-0.9	2.0
B-614-2-99	mvolc	27	100	0.726072±7	0.71134	13	61	0.511555±5	0.51072	-2.6	2.1
B-212-A-98	mpel	70	170	0.754725±7	0.73219	12	60	0.511548±5	0.51045	-7.9	2.5
B-230-A-98	mgrw	23	190	0.719365±7	0.71276	9.8	49	0.511732±4	0.51064	-4.3	2.2
Epupa Complex (Orue Unit)											
B-177-B-98	mdk	11	300	0.709178±7	0.70718	3.8	15	0.512447±5	0.51106	4.0	1.6
B-174-A-98	mvolc	40	180	0.729218±4	0.71717	9.1	45	0.511776±4	0.51061	-4.7	2.2
B-406-2-99	mgran	51	140	0.727689±7	0.70780	10	57	0.511723±5	0.51076	-1.8	2.0
B-171-A-98	mgrw	98	280	0.723681±4	0.70458	7.9	44	0.511555±5	0.51057	-5.6	2.2
B-347-99	cals	77	65	0.765436±8	0.70053	7.1	30	0.511981±3	0.51068	-3.4	2.3
B-588-3-99	cals	160	120	0.782032±8	0.70886	7.7	40	0.511596±5	0.51054	-6.2	2.3
B-342-6	cals	130	150	0.765883±7	0.71840	8.5	48	0.511595±5	0.51062	-4.5	2.1

[a] Rock abbreviations see Tables 4.1-4.3. [b] Isotope ratios measured on MAT262 (Finnigan) and *on Triton (Thermo). The analytical uncertainties are given at $2\sigma_m$ level. [c] $^{87}Sr/^{86}Sr(T)$, $^{143}Nd/^{144}Nd(T)$ and εNd values were calculated using the age of 1.38 Ga (Drüppel et al., 2000) and the following parameters and constants: $^{147Sm}\lambda = 6.54\times10^{-12}$ y^{-1}; $^{143}Nd/^{144}NdCHUR(0) = 0.512638$; $^{147}Sm/^{144}NdCHUR(0) = 0.1967$; $^{87Rb}\lambda = 1.42\times10^{-11}$ y^{-1}. The Rb/Sr ratios of pyroxene separates are subject to higher uncertainties due to the lower mass of analysed sample. Due to slight Rb/Sr fractionation during sample washing, the calculated $^{87}Sr/^{86}Sr(T)$ ratios tend to be too low. [d] Nd model ages were calculated according to the depleted mantle model of Goldstein et al. (1984). T(DM) was not calculated for samples with $^{147}Sm/^{144}Nd$ close to depleted mantle.

Table 4.5. Pb isotope data from KIC anorthositic rocks and EC basement rocks.

sample	rock type[a]	Pb [ppm]	Th [ppm]	U [ppm]	$^{206}Pb/^{204}Pb$[b]	$^{207}Pb/^{204}Pb$[b]	$^{208}Pb/^{204}Pb$[b]	$^{206}Pb/^{204}Pb$ (1.38Ga)[c]	$^{207}Pb/^{204}Pb$ (1.38Ga)[c]	$^{208}Pb/^{204}Pb$ (1.38Ga)[c]
White anorthosite suite										
Ku-97-03	LGN	4.0	0.23	0.06	17.026	15.462	37.387	16.81	15.44	37.13
Pl		2.9	0.014	0.005	16.541	15.428	36.378	16.52	15.43	36.36
Ku-97-04	LGN	3.4	0.71	0.22	17.424	15.502	37.671	16.47	15.42	36.73
Pl		3.2	0.027	0.017	16.449	15.420	36.109	16.37	15.41	36.07
Cpx					17.710	15.535	37.477			
Ku-97-08b	LGN	4.1	0.49	0.18	17.008	15.455	37.017	16.37	15.40	36.49
Ku-06-04a	Apx	8.7	0.60	0.06	16.333	15.404	36.240	16.24	15.39	35.94
Pl		10	0.039	0.028	16.237	15.417	35.883	16.20	15.41	35.87
Opx					20.005	15.748	40.696			
Ku-06-04b	Apx	7.7	3.0	0.14	16.475	15.417	36.817	16.21	15.39	35.10
Ku-06-60	Apx	2.3	0.24	0.08	17.569	15.533	36.474	17.06	15.49	36.01
Ku-06-63a	Apx	0.97	0.02	0.01	16.460	15.440	36.051	16.31	15.43	35.96
Pl		0.77	0.005	0.004	16.429	15.442	36.027	16.36	15.44	36.00
Ku-06-66b	A	1.3	0.52	0.01	16.707	15.428	36.611	16.60	15.42	34.85
Dark anorthosite suite										
Ku-98-125	LT	2.7	0.15	0.04	16.548	15.436	36.279	16.34	15.42	36.04
Pl		3.4	0.052	0.025	16.454	15.439	36.160	16.35	15.43	36.09
Ku-98-228	LT	0.44	0.04	0.01	16.999	15.482	36.671	16.67	15.45	36.27
Pl		0.41	0.002	0.004	16.583	15.445	36.141	16.44	15.43	36.12
Ku-06-07	LT	0.62	0.05	0.02	16.582	15.433	36.351	16.12	15.39	36.00
Ku-06-48	LT	0.52	0.01	0.01	16.538	15.423	36.044	16.26	15.40	35.96
Ku-06-69	LT	1.0	0.10	0.03	16.877	15.476	36.483	16.44	15.44	36.04
Pl		1.3	0.028	0.016	16.565	15.442	36.128	16.39	15.43	36.03
Cpx					33.252	16.884	57.715			
Ku-06-18a	Aol	0.92	0.09	0.03	17.377	15.515	37.148	16.90	15.47	36.71
Pl		1.5	0.027	0.017	16.700	15.455	36.243	16.58	15.44	36.16
Cpx					60.656	19.339	89.110			
Ku-06-72	GA	0.80	0.11	0.03	16.924	15.480	36.499	16.38	15.43	35.89
Pl		0.54	b.d.l.	0.003	16.513	15.436	36.034	16.43	15.43	<36.03
Cpx					32.897	16.901	54.905			
Younger intrusions										
Ku-06-20a	Di	2.6	0.03	0.02	16.883	15.484	36.294	16.77	15.47	36.24
Pl		4.3	0.015	0.012	16.503	15.432	36.007	16.46	15.43	35.99
Cpx					17.258	15.543	36.843			
Ku-06-31b	G	0.50	0.05	0.01	16.838	15.474	36.463	16.55	15.45	35.99
Epupa Complex (Epembe Unit)										
B-447-1-99	mdk	5.4	0.26	0.14	16.858	15.489	36.185	16.49	15.46	35.97
B-614-2-99	mvolc	3.1	12	1.2	26.069	16.637	49.471	18.63	15.98	26.71
B-212-A-98	mpel	23	18	2.9	18.364	15.600	40.414	16.40	15.43	36.69
B-230-A-98	mgrw	13	5.4	0.66	17.053	15.488	37.801	16.31	15.42	35.93
Epupa Complex (Orue Unit)										
B-177-B-98	mdk	20	1.2	0.54	17.653	15.569	37.320	17.25	15.53	37.05
B-174-A-98	mvolc	11	6.6	1.6	19.232	15.751	40.554	16.93	15.55	37.66
B-406-2-99	mgran	11	16	2.0	20.052	15.831	41.603	17.11	15.57	34.40
B-171-A-98	mgrw	13	14	1.6	17.848	15.585	38.374	16.00	15.42	33.42
B-347-99	cals	3.6	8.8	2.0	26.694	16.313	46.661	16.30	15.40	32.68
B-588-3-99	cals	20	17	3.7	20.030	15.792	40.545	17.08	15.53	36.39
B-342-6	cals	31	18	4.1	18.836	15.680	39.608	16.79	15.50	36.86

[a] Rock abbreviations see Tables 4.1-4.3. [b] Isotope ratios measured on MAT262 (Finnigan). The accuracy and precision of reported values are better than 0.1 % at the 2σ level. [c] Isotopic ratios at the age of KIC formation was calculated using the age of 1.38 Ga (Drüppel et al., 2000) and the constants recommended by IUGS (Steiger & Jäger, 1977). Due to high uncertainties in U/Pb and Th/Pb ratios no age corrected values were calculated for pyroxene separates.

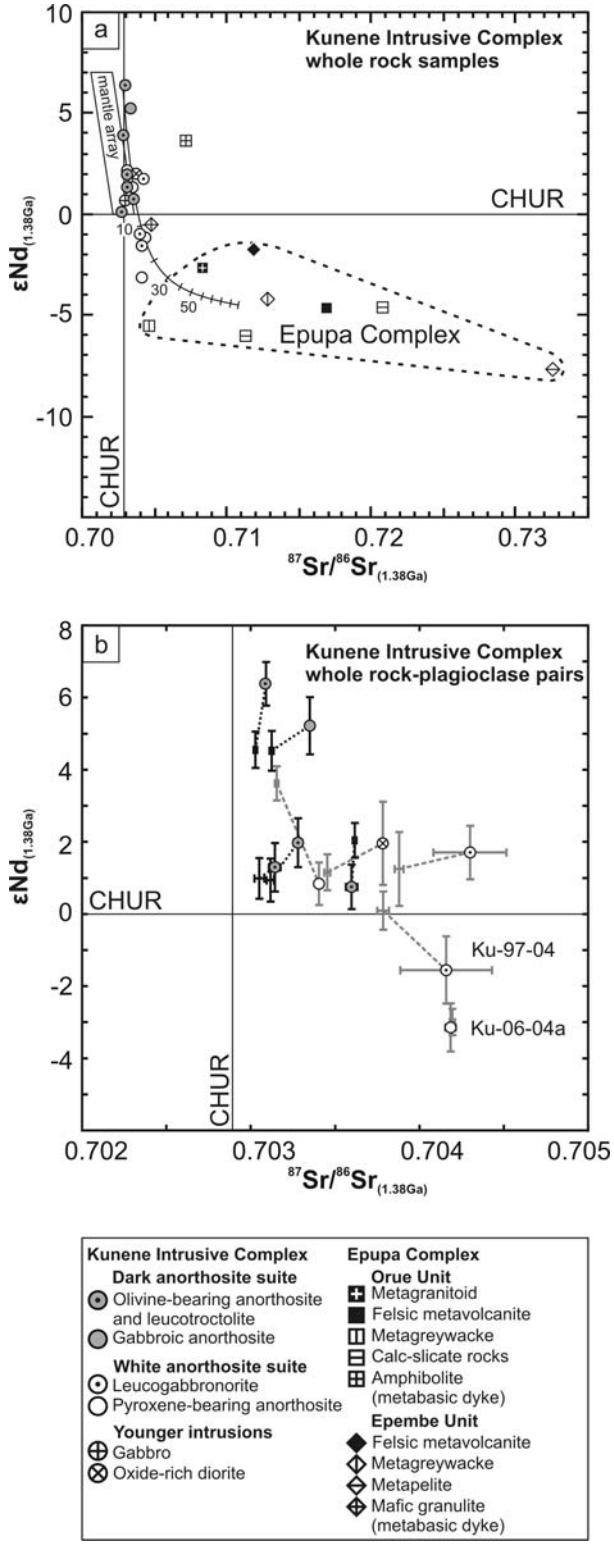

Fig. 4.4. (a) Sr-Nd isotopic composition of anorthosites and EC basement rocks at the time of KIC formation. The metabasic dykes have been excluded from the Epupa Complex field. Mesoproterozoic mantle array is estimated from the depleted mantle models of DePaolo (1981) and Goldstein et al. (1984). Ticks on the mixing curve (grey line) represent 10 % increments of contamination of the parental melt by local crust. (b) Sr-Nd isotopic composition of KIC rocks and plagioclase separates (white anorthosite: grey; dark anorthosite: black). Whole rock analyses are indicated by appropriate symbols and connected by a dashed line to the corresponding plagioclase. Pyroxene analyses are omitted for clarity. Errors of the age correction were calculated from analytical uncertainties of the individual measurements and an estimated uncertainty of the intrusion age of ± 20 Ma.

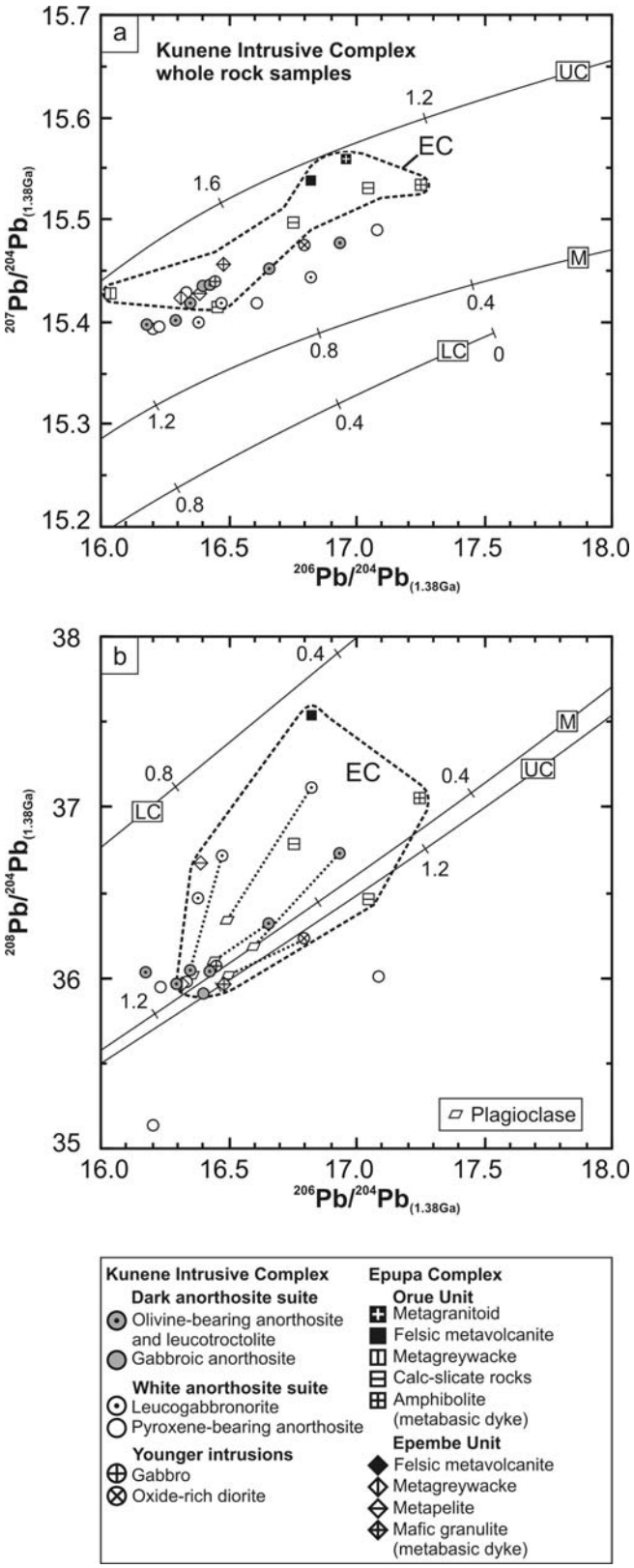

Fig. 4.5. Pb isotopic composition of anorthosites and EC basement rocks at the time of KIC formation. Ratios of highly altered EC samples were omitted for clarity. Plagioclase analyses are shown only where they differ clearly from the corresponding whole rock. Model evolution of mantle (M), lower crust (LC) and upper crust (UC) from Zartman & Doe (1981). Ticks represent 400 Ma model age increments.

4.4.3.2 Epupa Complex

$^{87}Sr/^{86}Sr_{(1.38\ Ga)}$ isotopic ratios of the felsic orthogneisses range from 0.70664 to 0.71687, with negative $\varepsilon Nd_{(1.38\ Ga)}$ values of -1.7 to -4.6 (Fig. 4.4a). The intercalated paragneisses yield $^{87}Sr/^{86}Sr_{(1.38\ Ga)}$ 0.70470 – 0.73254 and $\varepsilon Nd_{(1.38\ Ga)}$ -3.2 to -7.7. Calculated Nd-model ages, according to a depleted mantle source, range from 2.0 to 2.2 Ga and 2.1 to 2.5 Ga, respectively. The amphibolite facies metabasic dyke of the Orue Unit has $^{87}Sr/^{86}Sr_{(1.38\ Ga)}$ 0.70725 and $\varepsilon Nd_{(1.38\ Ga)}$ +3.6, whereas the granulite facies metabasic dyke of the Epembe Unit displays $^{87}Sr/^{86}Sr_{(1.38\ Ga)}$ of 0.70481 and $\varepsilon Nd_{(1.38\ Ga)}$ -0.5.

The $Pb_{(1.38\ Ga)}$ isotopic composition of the EC samples is highly variable. In the $^{206}Pb/^{204}Pb$ vs. $^{207}Pb/^{204}Pb$ diagram (Fig. 4.5a), the felsic orthogneisses plot close to the 1.38 Ga upper crust model composition (Zartman & Doe, 1981). The paragneisses fall below this model curve and overlap in parts with the anorthosites. Some samples display anomalously low $^{208}Pb/^{204}Pb_{(1.38\ Ga)}$ values that reflect overcorrection of in-situ Pb growth. These data indicate loss of U and in particular Pb during later metamorphism and/or hydrothermal alteration.

4.5 Discussion

4.5.1 Isotope systematics

Assimilation and fractional crystallization processes during the formation of cumulate rocks may affect the initial isotopic composition of cumulus and late-stage phases. In general, short isochrons are sensitive to initial isotopic heterogeneity that may originate from wall rock assimilation or mixing, which in turn may result in deviation of the isochron age from the true age (cf. Romer, 2001). The internal isotope systematics of anorthosites may provide a fingerprint for initial isotopic heterogeneity among the magmatic minerals and their possible alteration during later post-cumulus processes, which may result in significant scatter around the regression line in isochron diagrams or marked deviation of the apparent age of short isochrons from the U-Pb zircon age.

The Sm-Nd isotope data of the majority of the dark anorthosite bulk rocks and mineral separates define a 1342 ± 68 Ma regression line (Fig. 4.6a). Three samples and corresponding plagioclase separates plot above this regression line and were excluded. The Pb-Pb isotope composition of all dark anorthosites and their mineral separates, on the other hand, fits to a 1389 ± 12 Ma regression line (Fig. 4.6b). The resulting calculated internal isochron ages for dark anorthosites range from 1317 ± 65 to 1401 ± 52 Ma. The white anorthosites display even higher scatter and do not fit to a regression line, except for one pyroxene-bearing white anorthosite sample with an internal plagioclase-whole rock-orthopyroxene Sm-Nd isochron of 1357 ± 49 Ma (Fig. 4.6a). Despite the large age uncertainties, which are mainly due to the limited spread of the data, the obtained ages correlate well with the U-Pb zircon age of 1385 ± 25 Ma (Drüppel et al., 2000) determined for a pyroxene-bearing anorthosite from

Namibia. The overlap of internal isochron ages with the U-Pb zircon age indicates both a closed system and a relatively homogenous initial composition among phases of individual samples. In contrast, the deviation of some younger isochron ages (i.e. 1317 ± 65 Ma) from the true emplacement age may reflect a heterogeneous initial composition or minor open-system behaviour of these samples. However, the closed system behaviour of most samples together with petrographic and U-Pb isotopic evidence (Drüppel et al., 2007) clearly demonstrate that the KIC was not affected by later prograde amphibolite facies metamorphism at 1340 - 1320 Ma, as suggested by Seth et al. (2005).

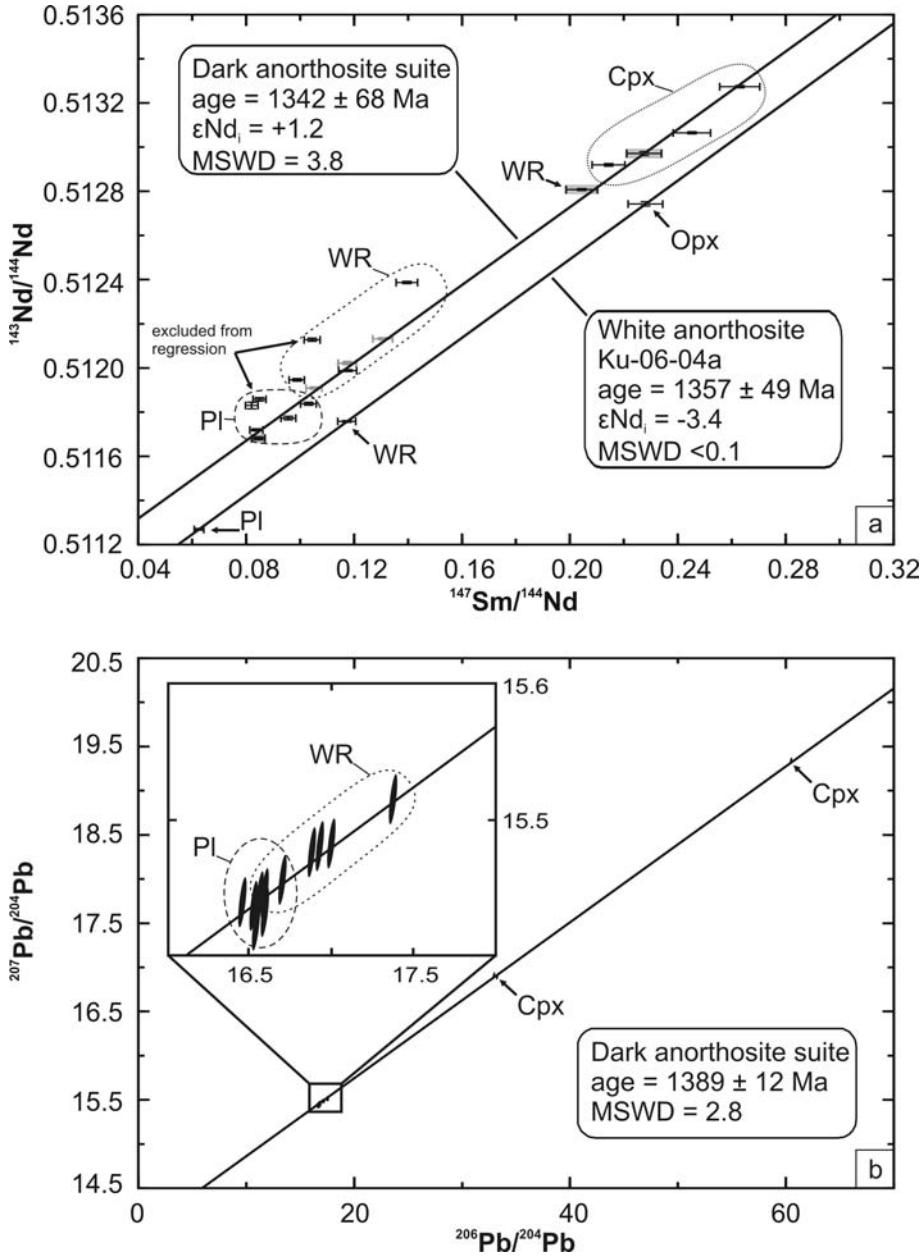

Fig. 4.6. (a) Sm-Nd isotope systematic of the dark anorthosite suite (including data of Drüppel et al., 2007: grey symbols and oxide-rich diorite: grey boxes) and a pyroxene-bearing white anorthosite (Ku-06-04a). (b) Pb-Pb isotope systematic of the dark anorthosite suite. Assigned Pb isotope ratio errors (2σ) are 0.1 % of measured values with an error correlation of 0.9. The regression lines were calculated using the Isoplot 3.00 software of Ludwig (2003).

The Rb-Sr isotope data of both anorthosite varieties from Namibia, however, do not define isochrons. This behaviour was also noted for other Proterozoic massif-type anorthosites (e.g. Ashwal et al., 1998; Evans et al., 1999). Instead, the low Rb/Sr ratios of most samples resulted in very limited in-situ growth of ^{87}Sr, thus indicating that initial heterogeneities ($^{87}Sr/^{86}Sr$: 0.7028 – 0.7043) among melt compositions are preserved.

4.5.2 Source of the parental magma

A fundamental question on anorthosite petrogenesis is whether they originate from mantle-derived high-aluminous basaltic parental magmas (Ashwal, 1993; Emslie et al., 1994; Mitchell et al., 1995; Scoates & Frost, 1996; Morse, 2006) or ferrodioritic melts (Vander Auwera et al., 1998, 2006; Longhi, 2005), produced by melting of foundered mafic crust (Duchesne et al., 1999; Schiellerup et al., 2000; Shumlyanskyy et al., 2006). Size and composition of Proterozoic massif-type anorthosites like the KIC require the extraction of large quantities of intermediate plagioclase over a restricted temperature-pressure interval from a huge magma reservoir. Moreover, the parental magma must produce olivine- and orthopyroxene-normative compositions. The Sr-Nd-Pb isotope systems provide reliable constraints on the source characteristics and crustal contamination processes that occurred during the formation of cumulate rocks like the Proterozoic massif-type anorthosites (e.g. Ashwal, 1993; Emslie & Hegner, 1993; Scoates & Frost, 1996).

In the KIC intra-mineral isotope systematic reveals that later alteration was minor or absent (see discussion above), and hence the isotopic composition of mineral and rock samples reflects source and contamination process characteristics. When calculated to the intrusion age of the anorthosites, the white anorthosite suite displays a range in $^{87}Sr/^{86}Sr_i$ from 0.70312 to 0.70430 and εNd_i +2.1 to -3.1. In contrast, the dark anorthosite suite shows lower $^{87}Sr/^{86}Sr_i$ values with a smaller range from 0.70284 to 0.70360 and higher εNd_i values from +6.4 to +0.8 at nearly the same ε-range. The calculated initial Pb isotopic composition of the dark anorthosite suite overlaps with that of the white anorthosite suite and in parts also with that of the EC rocks.

The dark anorthosites show the highest initial $^{143}Nd/^{144}Nd$ values and no petrographic evidence for crustal contamination and, therefore, represent the closest estimate for the composition of the primitive parental melt. The range of the three most primitive samples in εNd_i from +6.4 to +3.8 with corresponding $^{87}Sr/^{86}Sr_i$ from 0.70295 to 0.70335 overlap with the compositional range of typical depleted upper mantle of $\varepsilon Nd_{(1.38\ Ga)}$ +7.0 to +4.8; (De Paolo, 1981; Goldstein et al., 1984). This corresponds to the characteristics of rocks derived from the Proterozoic mantle beneath the southern Congo Craton, such as a metabasic dyke of the EC, that shows primitive REE pattern (Fig. 4.3a), an $\varepsilon Nd_{(1.38\ Ga)}$ value of +3.6 (Fig. 4.4a) and a $\delta^{18}O$ value of 5.7 ‰ (Gleißner et al., 2010). In contrast, most of the white anorthosites display a more enriched trace element and isotopic composition which suggests contribution of crustal material.

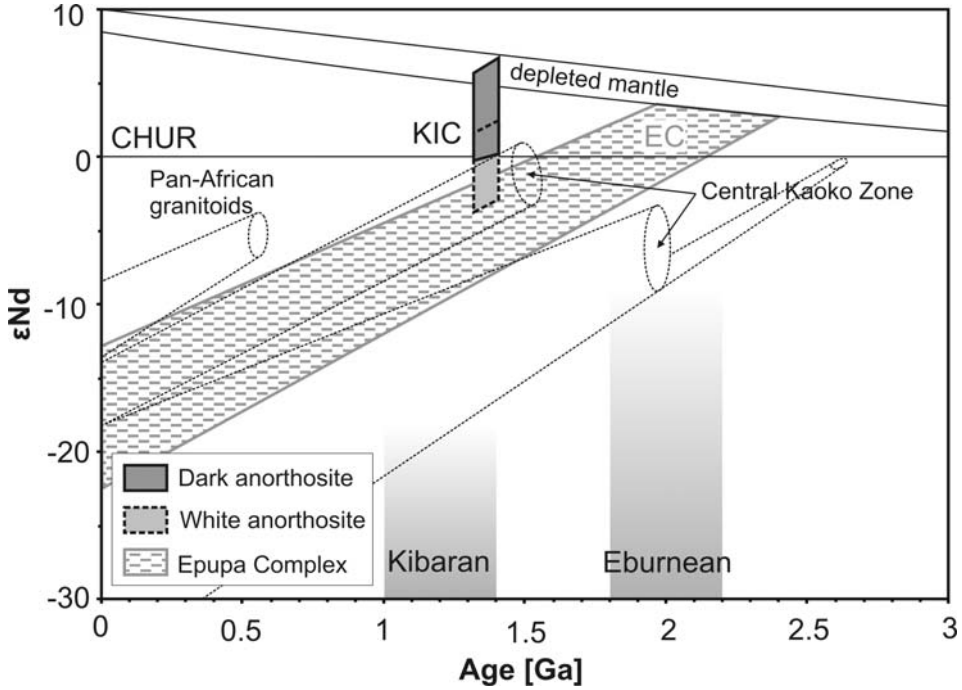

Fig. 4.7. Nd evolution diagram for high-grade metamorphic and unmetamorphosed rocks of NW Namibia. Age interval of the intrusion of the Kunene Intrusive Complex is taken from Drüppel et al. (2000) and Mayer et al. (2004). The Nd isotopic composition of EC rocks is similar to that of Proterozoic rocks of the central Kaoko zone (Kröner et al. 2004) which are amalgamated with reworked Neoarchean rocks and intruded by younger Pan-African granitoids (Franz et al., 1999; Seth et al., 2002), in the structurally complex Kaoko belt to the south of the EC (Fig. 1). Isotopic evolution of depleted mantle is calculated for the models proposed by DePaolo (1981) and Goldstein et al. (1984). Age ranges for the Eburnean and Kibaran event are taken from De Carvalho et al. (2000) and De Waele et al. (2008).

The initial Pb isotopic compositions of both anorthosite varieties are unrelated to the Nd and Sr isotopic composition. The range does not necessarily constrain a heterogeneous composition of their parental melts, but reflects the isotopic signature of the contaminants. Typical mantle sources have 50 to 100 times less Pb than crustal sources (e.g. Zartmann & Doe, 1981; McDonough & Sun, 1995; Rudnick & Fountain, 1995). Thus even minor contamination by crustal material may superimpose the Pb isotopic composition of the assimilated rocks onto the mantle-derived melt. The alternative interpretation, that the evolved Pb isotopic composition reflects an enriched upper mantle source, similar to a HIMU mantle, may be difficult to reconcile with the distinctly positive εNd values of the dark anorthosites. Furthermore, the relatively low $^{87}Sr/^{86}Sr$ values of the KIC anorthosites argue also against other enriched mantle compositions.

Regarding the cumulate origin of massif-type anorthosites, the size of the KIC indicates a huge and comparably homogeneous parental melt volume. Partial melting of dry mafic crust would require an extremely huge source region of relatively homogeneous composition to provide enough melt for the 18,000 m^2 anorthosite massif, which is likely to result in lower crustal collapse. Furthermore, it seems unlikely that fluid-absent melting of any mafic precursor in the lower crust could produce a melt that is parental to the dry olivine-bearing leucotroctolites of the KIC, although experimental data for this

specific rock type are not available. Apart from these considerations, the strongly depleted εNd_i values of the most primitive dark anorthosites of the KIC suggest an Nd isotopic composition even beyond the depleted mantle evolution which is unlikely for lower crustal precursors (Fig. 4.7). Thus, available data indicate the upper mantle as the only source region that can provide melt of primitive composition that is hot enough for extensive assimilation of crustal material and that is of appropriate volume to fractionate the observed volume of plagioclase cumulates.

4.5.3 Crustal contamination

Regarding the intrusion of many massif-type anorthosites at middle-upper crustal depths (see Ashwal, 1993 for a review) it seems rather unlikely that any mantle-derived parental melt escaped contamination during ascent through the crust. Isotope and trace element data on the composition of plagioclase and whole rocks are particularly useful for constraining the characteristics and timing of crustal assimilation (Mitchell et al., 1995; Scoates & Frost, 1996; Peck & Valley, 2000).

4.5.3.1 The contaminants

Petrographic and isotopic data demonstrate that the white anorthosites were subject to significant crustal contamination. The presence of crustal xenoliths (Figs. 2b and 2c) further shows that part of the crustal material was assimilated as solid bulk rocks. The overall crustal isotopic composition of the older white anorthosites points to contamination with isotopically evolved crustal material (>Mesoproterozoic in age) during an early stage of the anorthosite formation. Assimilation of isotopically evolved crustal material is also indicated by Nd model ages of 1.8 - 2.5 Ga that are significantly older than the intrusion age of 1.38 Ga. The Pb isotopic composition is consistent with older contaminants, but does not show the distinctive high $^{208}Pb/^{204}Pb$ at low $^{206}Pb/^{204}Pb$ relation that arises from old U depletion and would represent evidence for assimilation of old lower crustal components (Fig. 4.5).

The rocks of the dark anorthosite suite display mantle-like Sr and Nd isotopic composition. The large range in εNd_i values (Fig. 4.4a) and the coincidence of their Pb isotopic composition with that of the contaminated white anorthosites (Fig. 4.5) suggest that minor contamination also affected the dark anorthosites. The overall lower amount of crustal contamination of the younger dark anorthosites, which mainly intruded the central part of the white anorthosite massif, most likely arises from the use of the same magma conduit as the slightly older white anorthosite. The highest εNd_i values of +6.4 to +3.8 were found in samples in the central massive part of the KIC. The εNd_i values of +0.1 to +2.3 of samples from the intrusions near the southern margin of the complex, including small leucotroctolite bodies (Drüppel et al., 2007) and younger gabbroic and dioritic intrusions, suggest that these smaller marginal bodies underwent a more pronounced interaction with crustal material.

The continuous array from the primitive dark anorthosites towards the white anorthosites in the Sr-Nd isotope diagram (Fig. 4.4a) demonstrates that both evolved from a common melt composition and indicates that the assimilated material had a crustal isotopic signature and higher Nd/Sr ratios than the parental magma of the anorthosites. Identical εNd values of whole rock and mineral separates demonstrate that crustal contamination occurred prior to plagioclase and pyroxene crystallization in those samples (Fig. 4.4b). Others which display lower εNd values of whole rocks compared to the corresponding plagioclase clearly indicate late crustal contamination of intercumulus melt after plagioclase crystallization. Some observed higher εNd values of whole rocks might reflect replenishment events, as suggested by Gleißner et al. (2010), based on the large-scale oscillatory zoning in anorthite content of cumulus plagioclase. However, the εNd_i values of cumulus whole rocks and corresponding plagioclase of most individual samples are similar and hence rule out a simple late stage contamination of a crystal mush at the intrusion level.

Potential lower to middle crustal contaminants are the rocks of the bordering EC. The Nd model ages of EC felsic orthogneisses (2.0 – 2.2 Ga) meet the upper range of Paleoproterozoic zircon protolith ages from the literature (Tegtmeyer & Kröner, 1985; Seth et al., 2003, 2005) and demonstrate that the EC evolved during Eburnean times from relatively juvenile material (Fig. 4.7). The older Nd model ages of the EC metasediments (2.1 – 2.5 Ga) are consistent with their derivation from older, presumably early Paleoproterozoic precursors. Indeed, the Pb isotopic composition of the EC rocks is consistent with the Paleoproterozoic model ages and shows no evidence for old U depletion (Fig. 4.5). From the presence of andradite xenocrysts (Fig. 4.2b; Drüppel et al., 2007) and the overlap in $^{208}Pb/^{204}Pb$ values, calc-silicate rocks and metapelites seem to represent likely contaminants of the leucogabbronorites in the KIC (Fig. 4.5b). Both units of the EC were subject to partial melting via biotite-dehydration melting (Brandt et al., 2007; Brandt & Klemd, 2008). The high trace element contents in cumulus plagioclase of the white anorthosite (Gleißner et al., 2010) suggest that these melts or similar lower crustal partial melts interacted with the primitive parental melt of the KIC anorthosites.

4.5.3.2 Contamination model

In order to estimate the amount of material assimilated by the KIC parental melt and elucidate characteristics of the contaminated melt, we calculated mixing with possible crustal contaminants. The potential contaminants, the high-grade metamorphic rocks of the EC, display significantly higher trace element concentrations (except for Sr) when compared to the primitive parental melt of the anorthosites of the KIC (Fig. 4.8a). The Nd isotopic composition (this study) and the oxygen isotope data of separated plagioclase (Gleißner et al., 2010) can be used as proxy for the bulk mixing of primitive parental melt with a crustal contaminant. A general trend is observed ranging from depleted

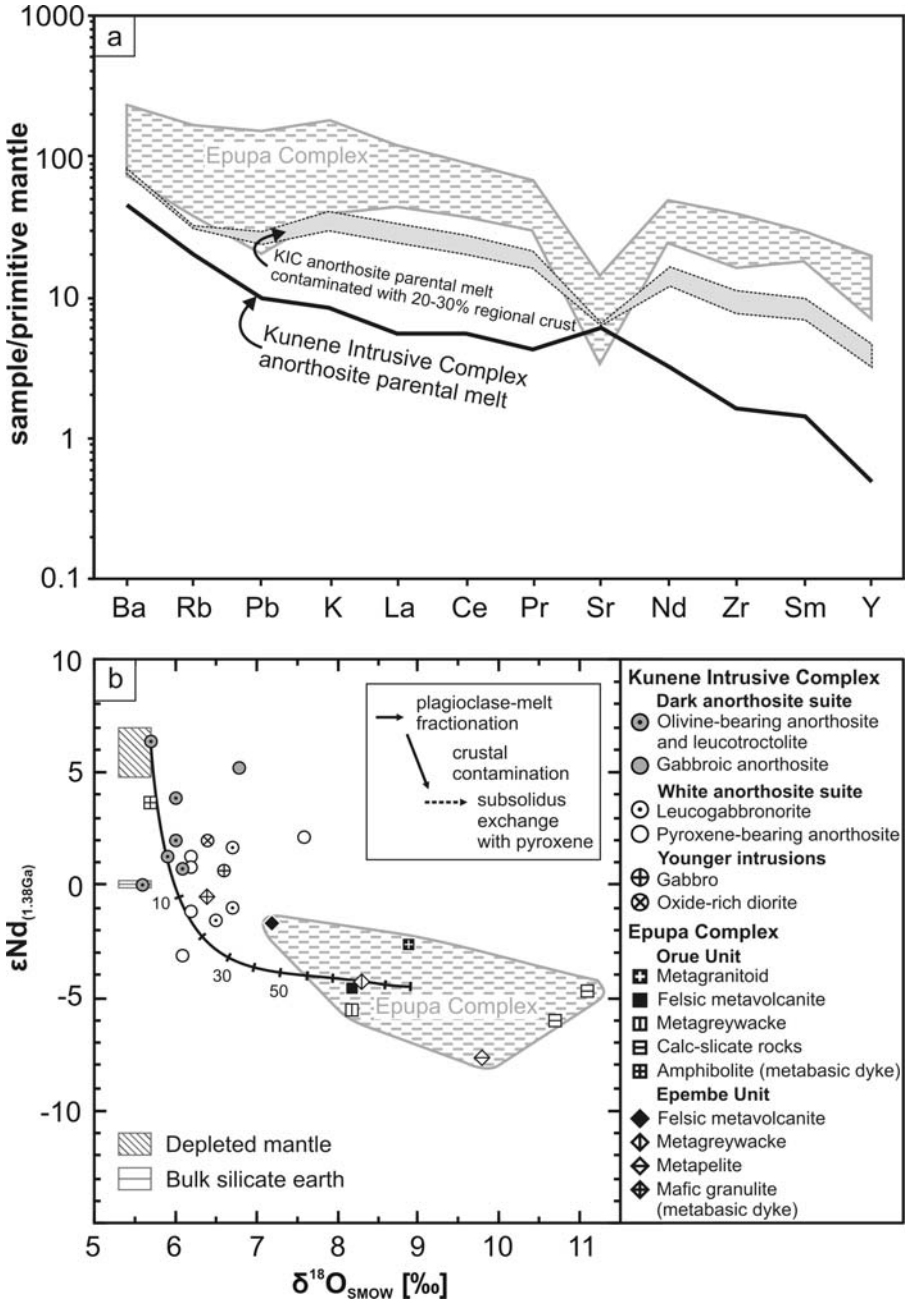

Fig. 4.8. (a) Trace element composition of primitive and contaminated parental melt of the Kunene Intrusive Complex anorthosites together with crustal rocks of the Epupa Complex. The concentration of trace elements in the primitive parental melt was deduced from plagioclase as described in Gleißner et al. (2010). Contamination with average Orue Unit crust elevates the trace element concentration of the melt except for Sr. The composition of local crust was estimated as average of our data from the Orue Unit of the Epupa Complex. (b) O-Nd isotopic composition of the Kunene Intrusive Complex anorthosites and possible crustal contaminants of the Epupa Complex. Displayed are $\varepsilon Nd_{(1.38\ Ga)}$ whole rock values (this study) with corresponding plagioclase $\delta^{18}O$ values of the anorthosites and whole rock $\delta^{18}O$ values of the EC samples (Gleißner et al., 2010). The metabasic dykes have been excluded from the Epupa Complex field. The range of mantle compositions is taken from Eiler (2001), DePaolo (1981) and Goldstein et al. (1984). Ticks on the mixing curve represent 10 % increments of contamination of the parental melt by local crust. Inset shows schematically the influence of isotope fractionation and crustal contamination. Plagioclase-melt fractionation affects mainly the oxygen isotope composition whereas crustal contamination has a stronger influence on the Nd isotopic composition of the anorthosites. Deviation of some of the data to higher δ18O values is attributed to subsolidus exchange with pyroxene (Gleißner et al., 2010).

mantle-like composition of the dark anorthosites towards more evolved, crustal-like values of the white anorthosites (Fig. 4.8b).

For the white anorthosite suite of the KIC crustal contamination prior to plagioclase crystallization is evident from petrographic indicators like zircon inclusions in plagioclase (Fig. 4.2b), trace element and oxygen isotope composition of plagioclase (Gleißner et al., 2010) and its isotopic composition (this study). Calculated assimilation of average EC crust yields a mixing hyperbola with pronounced effect on the Nd isotope composition (Fig. 4.8b). A crustal contribution 10 - 30 % to the primitive parental melt could thus explain both the oxygen and neodymium isotopic compositions of the white anorthosites. Such an assimilation of average EC crust would shift the trace element concentrations to higher values (except for Sr) and would produce a melt with considerable crustal characteristics (Fig. 4.8a). The dark anorthosites, on the other hand, apparently experienced crustal contamination of less than 10 % and largely preserved the isotope characteristics of a depleted mantle (Fig. 4.8b).

Using trace element zoning patterns of plagioclase and intercumulus phases of leucogabbronorite, Gleißner et al. (2010) furthermore suggested a subsequent crustal contamination of the residual melt after plagioclase fractionation. The more radiogenic Sr and Pb isotopic compositions of many whole rocks compared to their corresponding plagioclase (e.g. leucogabbronorite Ku-97-04; Figs. 4b and 5b) corroborate such a secondary process of late contamination. For both scenarios (i.e. contamination prior and after fractional crystallization of plagioclase) the contrasting trace element contents of the mantle-derived parental melt and crustal rocks will significantly alter the Nd isotopic composition of the magma. The lower Sr content of crustal rocks compared to both, the parental melt and cumulus plagioclase of the anorthosites, would have a much smaller effect on the Sr isotopic signature of the magma, whereas the Pb isotopic signature would be entirely dominated by the Pb-rich crust or its partial melts. This interpretation is in good agreement with the calculated mixing proportions in the Sr-Nd isotope diagram (Fig. 4.4a) and the overall crustal Pb isotope composition (Fig. 4.5), which reflect time integrated values of the latter processes.

4.5.4 Comparison with other Proterozoic massif-type anorthosites

The large variation in εNd_i and a comparatively small range in $^{87}Sr/^{86}Sr_i$ observed for anorthosites of the KIC is in agreement with the results from other massif-type anorthosite occurrences of the World, i.e. Laramie Complex (Geist et al., 1990, Mitchell et al., 1995; Scoates & Frost, 1996), the Horse Creek Complex (Frost et al., 2000), the Nain Complex (Emslie et al., 1994) and the Rogaland Complex (Demaiffe et al., 1986; Schiellerup et al., 2000). According to most authors, the Sr-Nd array reflects different amounts of contamination as well as variations in age and isotopic composition of the assimilated crustal rocks (e.g. Geist et al., 1990; Emslie et al., 1994; Mitchell et al., 1995; Scoates & Frost, 1996; Frost et al., 2000). Our calculations for different contamination scenarios of the anorthosites of the KIC have shown that the smaller range in Sr isotopic compositions reflects the

higher Sr concentration of the primitive parental magma of the anorthosites, whereas crustal contamination yields a more pronounced effect on the Nd isotopic composition of the anorthosites. Further contamination of the residual melt after fractional crystallization of the plagioclase may lead to the contrastingly higher variation in $^{87}Sr/^{86}Sr_i$ values, but lower variation in εNd_i as observed in the chemically evolved rocks associated with massif-type anorthosites (Geist et al., 1990; Emslie et al., 1994; Scoates et al., 1996; Bolle et al., 2003).

If present, olivine-bearing anorthosites and leucotroctolites of the unmetamorphosed massif-type anorthosites always represent the most primitive Nd isotopic compositions (Fig. 4.9a; Emslie et al., 1994; Scoates & Frost, 1996). This observation is in accordance with the least extent of crustal contamination and hence provides the most reasonable estimates of parental melt compositions. For the KIC, which comprises a particularly large volume of olivine-bearing anorthosites, their composition clearly points to a depleted mantle-derived parental melt.

The Nd and Pb isotopic composition of Proterozoic massif-type anorthosites depends largely on the crustal residence time of the contaminants. The anorthosites of the KIC were contaminated with relatively young (Paleoproterozoic) crustal rocks. Accordingly, they display positive to moderately negative initial εNd values (Fig. 4.9a) and corresponding upper crustal Pb isotopic composition (Fig. 4.9b) like the massif-type anorthosites of the Labreville (Owens et al., 1994) and the Rogaland Complex (Weis, 1986). In contrast, the anorthosites of the Nain Complex display negative initial εNd values and significantly less radiogenic Pb isotopic compositions in accordance with Archean lower crustal contaminants (Ashwal, 1993; Emslie et al., 1994). The comparison between massif-type anorthosites of different cratons demonstrate that Sr-Nd-Pb isotope can resolve source characteristics of their parental melt if the age and composition of the crust (the potential contaminant) are considered.

4.6 Conclusions

The Kunene Intrusive Complex comprises two major anorthosite varieties which intruded the Epupa Complex basement during the same igneous event, but display distinct petrographic and geochemical characteristics. The older white anorthosite suite consists of pyroxene-bearing andesine-type anorthosite and leucogabbronorite and displays isotopic and trace element characteristics consistent with its derivation from mantle-derived parental melt that was subject to crustal contamination during an early stage of its evolution. The Sr-Nd isotopic signature of subsequently intruded olivine-bearing labradorite-type anorthosite and leucotroctolite of the dark anorthosite suite provides evidence for their origin from depleted upper mantle. The continuous Sr-Nd array from depleted mantle composition to crustal-like values together with increasing crustal characteristics in the trace element pattern of the KIC anorthosites strongly support an origin from mantle-derived melts with variable degrees of crustal contamination, but argue against an origin by a crustal melting process.

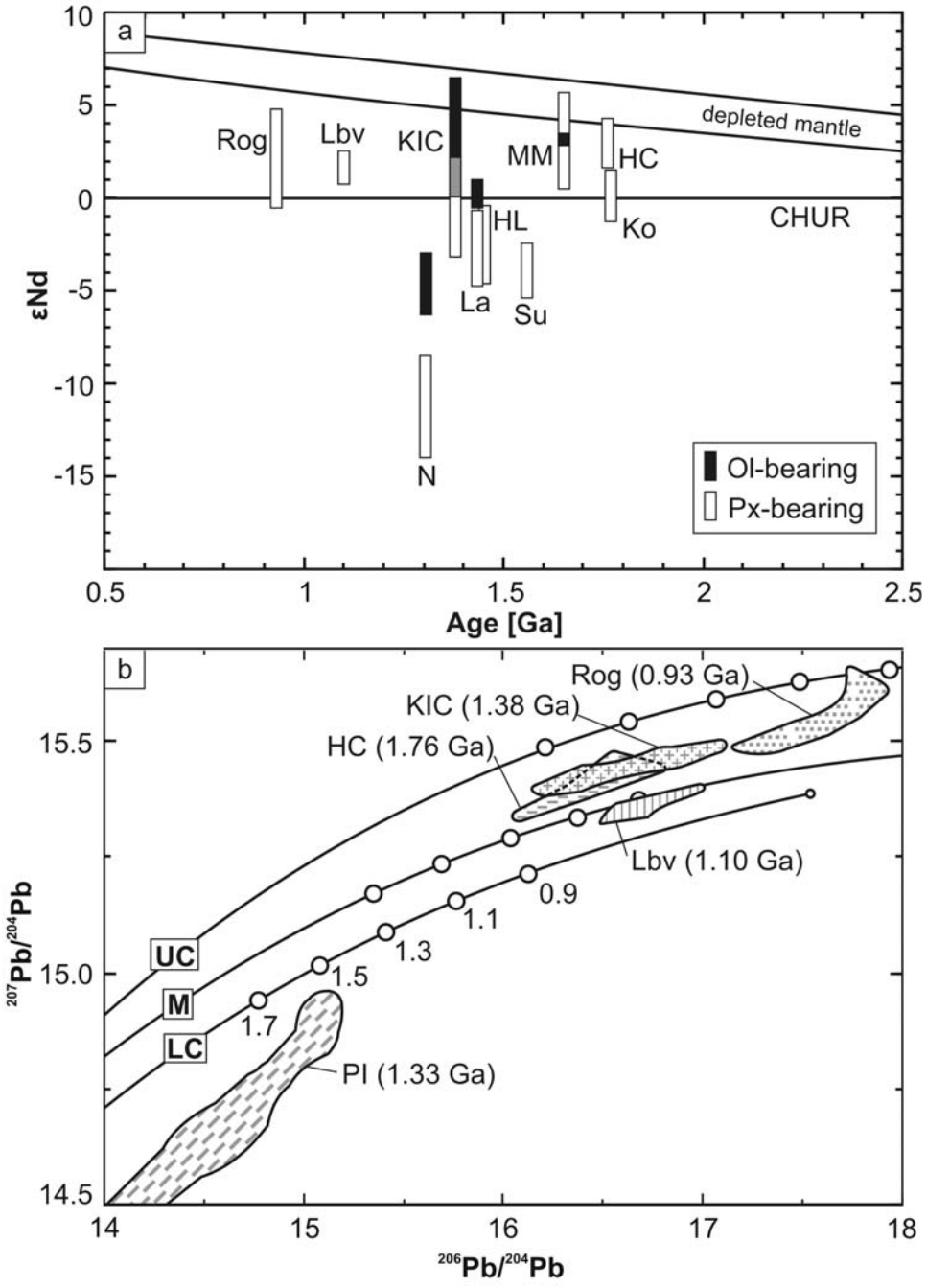

Fig. 4.9. (a) Initial Nd isotopic composition of unmetamorphosed massif-type anorthosite complexes. Anorthosite complexes: HC, Horse Creek (n=7; Frost et al., 2000); Ko, Korosten (n=7; Shumlyanskyy et al., 2006); MM, Mealy Mountains (n=3; Ashwal et al., 1986); Su, Suwałki (n=9; Wiszniewska et al., 2002); HL, Harp Lake (n=4; Ashwal et al., 1986); La, Laramie (n=27; Geist et al., 1990; Mitchell et al., 1995; Scoates & Frost, 1996); N, Nain (n=29; Emslie et al., 1994); Lbv, Labrevielle (n=4; Owens et al., 1994); Rog, Rogaland (n=35; Schiellerup et al., 2000; Demaiffe et al., 1986); depleted mantle: DePaolo (1981) and Goldstein et al. (1984). (b) Initial Pb isotopic composition of representative massif-type anorthosite complexes. Anorthosite complexes: HC, Horse Creek (n=6; Frost et al., 2000); PI, Paul island of the Nain Complex (Ashwal, 1993); Lbv, Labreville (n=4; Owens et al., 1994); Rog, Rogaland Complex (n=17; Weis, 1986; Schärer et al., 1996); Pb isotopic model evolution of the mantle and the crustal reservoir: Zartman & Doe (1981).

The Nd and Pb isotope data of both anorthosite varieties indicate variable addition of Paleoproterozoic crustal material at different stages of the igneous evolution of the KIC. Potential contaminants are the bordering amphibolite to granulite facies metamorphic volcano-sedimentary successions of the Epupa Complex that were formed during the Eburnean (1.8 - 2.2 Ga) and experienced a relatively short crustal residence time at the time of anorthosite formation. The contrast in trace element contents between the primitive mantle-derived parental magma of the KIC and the crustal contaminants of the EC yields distinct signatures for Sr, Nd and Pb during fractional crystallization and mixing. The Sr isotopic composition of the parental magma of the KIC is largely controlled by the high Sr content of the primitive melt and early cumulus plagioclase. The Nd and Pb budget of the magma, on the other hand, was significantly lower than Sr. Consequently, the isotopic composition of Nd provides as a good indicator for an increasing amount of wall-rock assimilation, whereas the Pb isotopic signature is entirely dominated by the crustal signature.

Similar Sr-Nd-Pb isotope characteristics can be observed in other unmetamorphosed massif-type anorthosites. The timing of fractional crystallization, magma recharge as well as the age of the crustal contaminant account for the variability within and among individual complexes. For instance, preferential assimilation of young crustal rocks yields anorthosites with positive εNd values, whereas assimilation of old crustal rocks yields lower and negative εNd values for the same extent of contamination. In general, source characteristics of massif-type anorthosite parental melts will be best established from the isotopic composition of olivine-bearing lithologies, as they represent the least contaminated composition.

Chapter 5

Osmium isotopes and highly siderophile element fractionation in the massif-type anorthosites of the Mesoproterozoic Kunene Intrusive Complex, NW Namibia

Autoren: Philipp Gleißner[1], Kirsten Drüppel[2], Harry Becker[2].

[1]Technische Universität Berlin, Institut für Angewandte Geowissenschaften, Ackerstr. 71-76, 13355 Berlin

[2]Freie Universität Berlin, Institut für Geologische Wissenschaften, Malteserstr. 74-100, 12249 Berlin

Eingereicht zur Veröffentlichung bei: Chemical Geology, Elsevier

Eigenanteil:
Probennahme gemeinsam mit Dr. Kirsten Drüppel, selbständige Dünnschliffuntersuchung und EMP-Analytik, selbständige Mineralseparation für die Iostopengeochemischen Untersuchungen, Durchführung der Laborarbeiten und Massenspektrometrie unter Anleitung von Prof. Dr. Harry Becker, Auswertung und Interpretation der Ergebnisse gemeinsam mit Prof. Dr. Harry Becker und Dr. Kirsten Drüppel, selbständige Ausarbeitung der Publikation.

Abstract

The behaviour of highly siderophile elements (HSE) during differentiation of mafic melts and formation of cumulate rocks in the crust is little understood, mostly because abundances of some of these elements are very low and reliable data is scarce. Data on massif-type anorthosites and associated Fe-Ti ore from the Mesoproterozoic Kunene Intrusive Complex (NW Namibia), indicate the effects of fractional crystallization, crustal contamination, cumulate formation and post-cumulus re-equilibration on the distribution of the highly siderophile elements and the osmium isotopic composition of the anorthositic cumulate rocks.

Anorthosites and Fe-Ti ore of the Kunene Intrusive Complex are characterized by low concentrations and strongly fractionated chondrite-normalized patterns of the highly siderophile elements. The abundance of highly siderophile elements is dominated by Fe-Ti oxides and traces of sulfides. The osmium isotopic composition and highly siderophile elements distribution of the anorthosites are consistent with their derivation from a mantle-derived parental magma that was subject to fractionation of mafic minerals and variable extent of crustal contamination during its igneous evolution. Under conditions of the anorthosite formation Re behaves as a compatible element in fractionating titanomagnetite. The other highly siderophile elements are incorporated to a lower extend into the Fe-Ti oxides. During post-cumulus re-equilibration of Fe-Ti oxides Re is preferentially incorporated in magnetite whereas Pt displays preference for ilmenite.

5.1 Introduction

Massif-type anorthosite complexes, that commonly form huge intrusions composed of plagioclase cumulate rocks with minor volumes of associated mafic and granitic suites, are characteristic features of the Proterozoic crust (Ashwal, 1993; Scoates & Mitchell, 2000). In many anorthosite complexes locally restricted Fe-Ti ore bodies occur as irregular lenses, pods and dykes which can reach economic importance. Despite extensive investigation, no general agreement has been reached on the origin of both, the massif-type anorthosites and the related Fe-Ti ore bodies.

For the formation of massif-type anorthosites two major petrogenetic models have been proposed. According to the mantle-source model, massif-type anorthosites originate by plagioclase fractionation from a mantle-derived high-Al basaltic parental melt, after extensive fractionation of mafic minerals and variable crustal contamination (e.g. Ashwal, 1993; Scoates & Mitchell, 2000). A lower crustal source of Proterozoic massif-type anorthosites has been suggested on the basis of phase equilibria and fractional crystallization modelling of designated Al-rich parental melt compositions (Longhi et al., 1999; Longhi, 2005) and crustal Os isotopic composition of sulfides and oxides in anorthosites and associated Fe-Ti ores (Morgan et al., 2000; Schiellerup et al., 2000). According to the latter model,

intracrustal melting of mafic lower crust is triggered by downthrusting of tongues of crustal material along lithospheric-scale weakness zones (Duchesne et al., 1999), leading to the formation of ferrodioritic parental melts (Vander Auwera et al., 1998). For the formation of associated Fe-Ti ore bodies, increasing consensus exists in their interpretation as result of fractional crystallization of Fe-Ti oxides, silicates and apatite accompanied by density driven crystal sorting during accumulation (e.g. Specik et al., 1988; Charlier et al., 2006).

Isotope data of lithophile trace elements were often considered ambiguous or conflicting in resolving the enduring problem of anorthosite source regions (Duchesne et al., 1999; Longhi et al., 1999; Morgan et al., 2000; Schiellerup et al., 2000). Mantle melting and crystal fractionation of mafic to intermediate magmas, on the other hand, produce high Re/Os ratios that evolve towards very radiogenic Os isotope compositions in only a few million years. Therefore, initial Os isotopic data on anorthosites may constrain the involvement of relatively young mafic crust in anorthosite petrogenesis that may be undetectable using other isotopic systems such as Rb-Sr, Sm-Nd and Th-U-Pb (Schiellerup et al., 2000; Hart et al., 2002). In recent years, abundance distributions of highly siderophile elements (platinum group elements + Re + Au) and Os isotope composition of crustal rocks have received increasing attention and were used to constrain source characteristics of magmatic precursor rocks (e.g. Puchtel & Humayun, 2000; Dale et al., 2008), magmatic differentiation (e.g. Rehkämper et al., 1999; Bézos et al., 2005; Pitcher et al., 2009) and crustal contamination of mantle-derived mafic to intermediate magmas (e.g. Hart et al., 2002). Re-Os studies of sulfides and oxides from the Suwałki and Rogaland anorthosites and related Fe-Ti ore bodies reveal radiogenic initial Os isotopic compositions (Morgan et al., 2000; Schiellerup et al., 2000; Loeppke & Hannah, 2004). Both Morgan et al. (2000) and Schiellerup et al. (2000) concluded that crustal contamination of a mantle-derived magma requires unrealistic crustal compositions and contamination ratios, and therefore suggest direct melting of a mafic source region in the lower crust. In contrast, Hannah & Stein (2002) proposed a process of either bulk or selective sulfide assimilation followed by partitioning of Os into an immiscible sulfide liquid, similar to the formation of sulfide deposits in layered intrusions, leading to decoupling of Os isotopic and Nd, Sr, Pb isotopic systems.

The Mesoproterozoic Kunene Intrusive Complex (Angola/Namibia) experienced no metamorphic overprint after its emplacement (Ashwal & Twist, 1994; Morais et al., 1998; Mayer et al., 2004; Drüppel et al., 2007; Gleißner et al., in press) and hence allows a direct study of the magmatic processes active during its formation. As shown recently by Drüppel et al. (2007) and Gleißner et al. (2010) the overall trace element and O-Sr-Nd-Pb isotopic composition of the anorthosites is in agreement with their formation via assimilation and fractional crystallization from mantle-derived parental magma. Massive Fe-Ti ore bodies occur in the anorthosites and display microtextures and compositions indicative for their formation by fractional crystallization and accumulation of titanomagnetite (Franke et al., 2009).

Os isotope and highly siderophile element (HSE) data of anorthosites and associated Fe-Ti ore of the Kunene Intrusive Complex provide insights into HSE fractionation during fractional crystallization of mafic melts and hence into the petrogenesis of massif-type anorthosite. In order to gain information on source characteristics and early magmatic evolution we measured HSE concentrations and Os isotope composition of primitive and crustally contaminated anorthositic rocks and Fe-Ti ore of the Kunene Intrusive Complex. Additional data on mineral separates from these samples shed new light on the factors controlling HSE fractionation in fractionated mafic magmas and during post-magmatic re-equilibration of Fe-Ti oxides.

5.2 The Kunene Intrusive Complex: geological setting, previous work and sample selection

The approximately 18,000 km^2 Kunene Intrusive Complex (KIC) extends from NW Namibia into SW Angola (Fig. 5.1) and is one of the largest massif-type anorthosite intrusions of the world (Ashwal & Twist, 1994). The anorthositic rocks intruded high-grade metamorphic basement of the Epupa Complex (EC) at the southern margin of the Congo Craton during the Mesoproterozoic (Morais et al., 1998). In NW Namibia the EC mainly comprises Paleoproterozoic upper amphibolite facies volcano-sedimentary successions and locally restricted ultrahigh-temperature granulite facies terranes (Brandt et al., 2007). The rocks of the north-eastern EC, including our study area, are overlain by undeformed Neoproterozoic sediments of the Damara Supergroup (Brandt et al., 2007) and demonstrate that both EC and KIC were not deformed during the Pan-African orogeny.

In the Namibian part of the KIC, two anorthosite varieties were distinguished, a tectonized and altered pale ‘white anorthosite’ and a weakly to non altered ‘dark anorthosite’ (Menge, 1998; Drüppel et al., 2001, 2007). The white anorthosite suite mainly comprises pyroxene-bearing anorthosite and leucogabbronorite with well developed cumulate textures. Trace element zoning patterns of plagioclase demonstrate that the older white anorthosite was derived by simultaneous fractional crystallization of plagioclase, pyroxene and Fe-Ti oxides (Gleißner et al., 2010). Trace element and isotopic data suggest that crustal contamination of the primitive parental melt took place prior and during fractional crystallization of plagioclase (Gleißner et al., in press).

The younger dark anorthosite intruded as sheet-like bodies in the centre of the white anorthosite massif and typically contains xenoliths of the white anorthosite (Drüppel et al., 2007). The dark anorthosite suite mainly consists of leucotroctolite, olivine-bearing anorthosite and minor gabbroic anorthosite. The generally fresh and massive rocks display homogeneous cumulate textures. They evolved by fractional crystallization of plagioclase, olivine and Fe-Ti oxides at magmatic temperatures and experienced less crustal contamination than the white anorthosites (Gleißner et al., 2010). The

initial Nd isotopic composition of primitive leucotroctolite constrains the derivation of the parent melt from depleted upper mantle (Gleißner et al., in press).

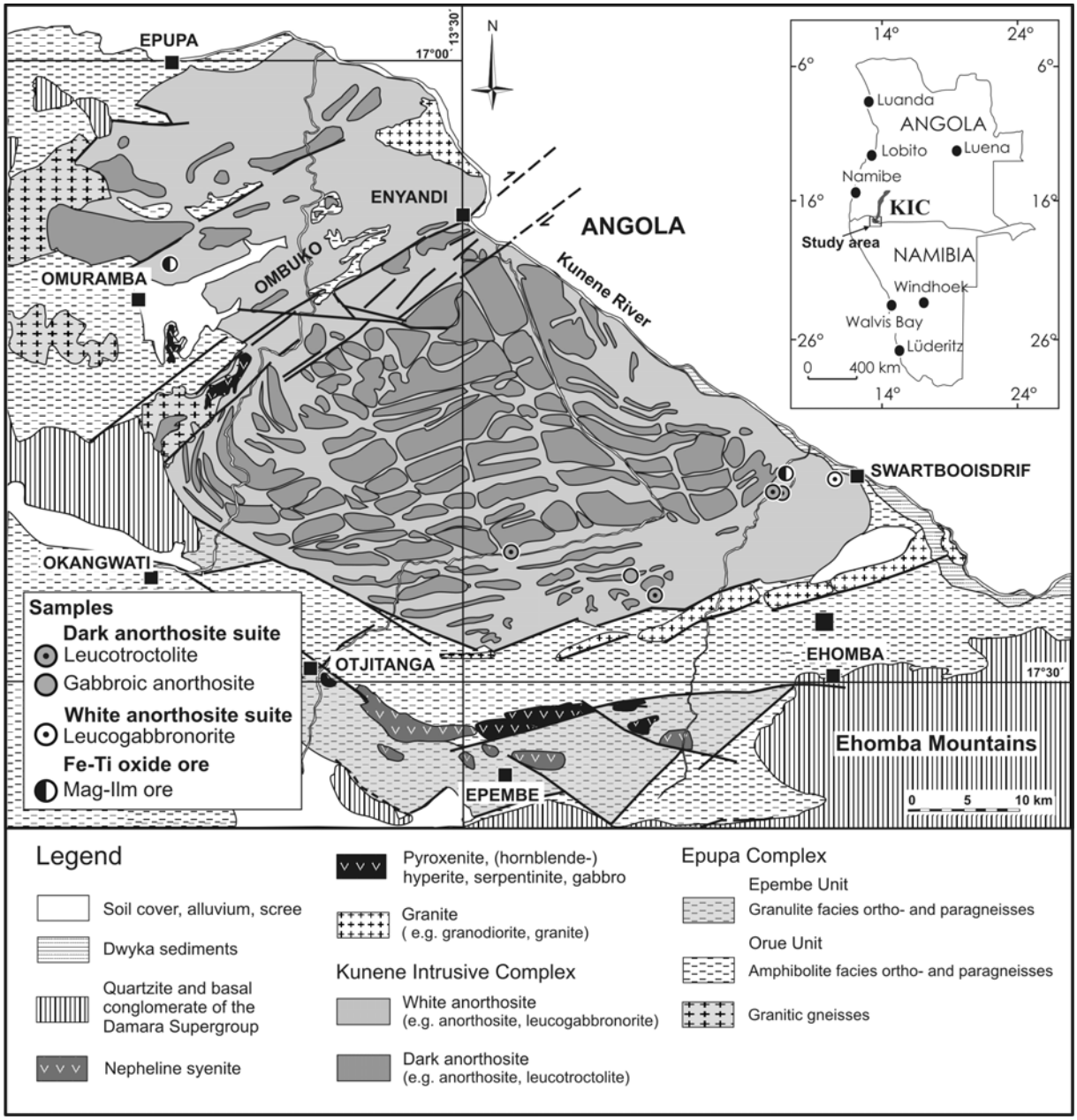

Fig. 5.1. Geological map of the southern Kunene Intrusive Complex (KIC) and the adjacent Epupa Complex in NW Namibia. Map after Menge (1998), modified by Brandt et al. (2007) and Drüppel et al. (2007). Locations of samples used for Os isotope and HSE analysis are indicated. Inset shows location of the Kunene Intrusive Complex in SW Angola and NW Namibia.

The Fe-Ti ore bodies in our study area are oval shaped and up to 80 m in diameter and restricted to the white anorthosite (von Seckendorff et al., 2000; Drüppel et al., 2007). The bodies mainly comprise coarse magnetite-ilmenite ore with minor silicate phases (von Seckendorff et al., 2000; Franke et al., 2009). Fe-Ti oxide microtextures and compositions indicate that they have been formed by

accumulation of titanomagnetite, together with minor ilmenite and orthopyroxene (Franke et al., 2009).

A U-Pb zircon age of 1385 ± 25 Ma dates the intrusion of the dark anorthosite suite in NW Namibia (Drüppel et al., 2000). The U-Pb zircon age of 1376 ± 2 Ma of a syenodiorite (Drüppel et al., 2007) and the radiogenic isotope systematics of anorthositic rocks (Gleißner et al., in press) reveal that both anorthosite suites and the coeval felsic rocks were emplaced during the same magmatic event. The rocks of the KIC experienced no metamorphic overprint after its emplacement and hence display well preserved magmatic phases and textures (Ashwal & Twist, 1994; Morais et al., 1998; Drüppel et al., 2001, 2007; Mayer et al., 2004).

On the basis of major, trace element and other isotope data a set of 8 whole rock samples, including four leucotroctolites and one gabbroic anorthosite of the dark anorthosite suite, one leucogabbronorite of the white anorthosite suite and two Fe-Ti ore samples were chosen (see Fig. 5.1 for sample locations) for the analysis of osmium isotope and HSE composition. The leucotroctolites are the major constituent of the dark anorthosite suite and yielded the most primitive olivine, whole-rock geochemical and isotopic composition in the KIC (Gleißner et al., 2010, in press), and thus could provide insights into the composition of the uncontaminated melt. The gabbroic anorthosite sample is interpreted as a late stage cumulate from the primitive magma related to the leucotroctolites. Leucogabbronorite of the white anorthosite suite, which displays isotopic evidence for significant crustal contamination (Gleißner et al., 2010, in press), was analysed to gain information on the effect of crustal contamination on the HSE during the early stage of anorthosite formation. Samples of associated Fe-Ti ores were analyzed in order to elucidate their origin and relation to the anorthosite formation. Mineral separates of one sample from each unit were analysed to study HSE distribution during fractional crystallization and later post-cumulus re-equilibration.

5.3 Analytical techniques

Electron microprobe analysis and scanning electron imaging of Fe-Ti oxides was performed on a Cameca Camebax and a Hitachi S-2700 instrument at the Zentraleinrichtung für Elektronenmikroskopie, Technische Universität Berlin. Mineral analyses were performed with an accelerating voltage of 15 kV, a beam current of 13 nA and an electron beam of 2.5 µm in diameter. Natural and synthetic standards were used for instrument calibration. Scanning electron imaging was done with an accelerating voltage of 15 - 20 kV and a beam current of 500 nA. Sulfur analyses of whole rock samples were done by gas chromatography using an elementar vario ELIII instrument at the Institut für Ökologie, Technische Universität Berlin.

For the analysis of HSE and Os isotope composition, the whole rock material was crushed and visually unaltered pieces were powdered in an agate mill. Mineral separation was done by standard

magnetic separation techniques and hand-picking under a binocular microscope. Finally the mineral separates were powdered in an agate mortar.

The sample digestion, chemical separation and mass spectrometry work was done at the geochemical laboratory of the Freie Universität Berlin. An average amount of 2 g for anorthosite whole rocks, 1 g for Fe-Ti ore and 1 g for mineral separates (except for sulfide were 20 mg were used) were weighted into quartz glass digestion vessels. For the analysis of Os, Ir, Ru, Pt, Pd and Re concentrations a mixed ^{185}Re–^{190}Os spike solution for high Re/Os samples and a ^{191}Ir–^{99}Ru–^{194}Pt–^{105}Pd spike solution were added (Fischer-Gödde et al., 2010). Sample digestion was carried out in a high-pressure asher (HPA-S, Anton Paar™) using 7.5 - 9.0 ml reverse aqua regia at 100 bar/320°C for 12 hours. After digestion the liquid showed usually a yellow colour and the remaining slush was grey with minor precipitated ferric iron compounds stuck to the glass. Sulfides and oxides were digested easily in the reverse aqua regia whereas the silicate phases may have digested only partially.

Osmium was separated by solvent extraction from reverse aqua regia into CCl_4, back extraction into HBr and followed by micro-distillation for 2 - 3 h at 85°C (Birck et al., 1997). The purified Os was loaded in HBr on baked Pt-filaments and covered with $Ba(OH)_2$ solution. The isotopic composition was measured as OsO_3^- by negative thermal ion mass spectrometry (NTIMS) using a Thermo-Finnigan™ Triton instrument. Signals were detected using the electron multiplier (SEM) in pulse counting mode. Measured ratios were corrected for interferences from isobaric OsO_3^- molecules. A mass fractionation correction following Boelrijk (1968) for the sample spike mixture was applied to the oxide corrected values. Repeated measurement of the UMD Os standard solution yield $^{187}Os/^{188}Os$ = 0.1140 ± 0.0001 (2σ, n = 8). Replicate analyses of sample powder of three bulk rocks and different grain size fractions of minerals of the same three samples were done to evaluate the reproducibility of whole rock analyses and the influence of sulfide inclusions in magnetite and ilmenite separates.

Rhenium, Ir, Ru, Pt, Rh, Pd and Au were separated from the aqua regia by cation exchange chromatography using pre-cleaned Eichrom™ AG50 W-X8 (100 - 200 mesh) resin. In order to recover Rh and Au, a technique modified from the method described in Fischer-Gödde et al. (2010) was used. The sample was three times taken to near dryness with HCl and dissolved in 0.5M HCl-40 % acetone before loading onto the column, which was equilibrated with the same solution. The HSE were eluted with 0.5M HCl-40 % acetone. Before ICP-MS analysis of Re, Ir, Pt and Au the acetone was evaporated. To avoid interferences from Cd isotopes on Pd, a clean up procedure with Eichrom AG50 W-X8 (100 - 200 mesh) resin in 0.2M HCl was carried out with the remaining solution after Re, Ir, Pt and Au measurement. The eluted solution was evaporated to near dryness and dissolved with 0.28M HNO_3 for ICP-MS analysis of Ru, Rh, Pd, Ir and Pt.

Isotopic ratios of the HSE were measured by sector-field inductively coupled plasma mass spectrometry on a Thermo-Electron™ Element-XR instrument. The sample was introduced with a conventional Scott-type glass spray chamber for Re, Ir, Pt and Au analysis, whereas an Aridus membrane desolvator was used for Ru, Rh, Pd, Ir and Pt. Signals were detected in low resolution

mode with secondary electron multiplier operating in pulse counting mode. We measured the following isotope masses for the concentration calculation: 99, 101, 102, 104 (Ru), 103 (Rh), 105, 106, 108, 110 (Pd), 185, 187 (Re), 191, 193 (Ir), 194, 195, 196, 198 (Pt), 197 (Au). Additional elements were analysed to monitor isobaric interferences (Cd, Os and Hg isotopes) or potentially interfering oxide species (Sr, Y, Zr, Mo, Yb, Lu, Hf and Ta). Oxide formation (CeO^+/Ce^+) was ~10 % for the Scott-type glass spray chamber and ~2 % during measurement with the Aridus membrane desolvator. The masses of HSE were integrated for 45 ms and those of the monitors for 10 ms during each scan (300 scans in total). The internal precision of measured isotopic ratios ranged from 1 – 10 % (2σ), depending on signal intensity.

Background correction was carried out according to measured acid blank solutions at the start and after every second sample solution throughout every measurement session. Instrumental mass fractionation was determined and corrected by comparison to a standard solution with roughly chondritic HSE ratios and ~1 ppb Ir. Our measurements reveal that Os and Cd were effectively removed by the Os solvent extraction and Cd cleanup procedures and isobaric interferences on ^{187}Re and ^{106}Pd were negligible. To avoid interferences from Hg isotopes we used the $^{194}Pt/^{195}Pt$ ratio for the concentration calculation. In Fe-Ti oxide samples significant Zr and Hf signals were detected. Isotopic ratios of Pd and Pt suggest that interferences from Zr or Hf oxides were insignificant.

Rhenium, Ir, Ru, Pt and Pd concentrations were determined by isotope dilution. For monoisotopic Rh and Au, a combined internal-external standardization technique was used, similar to that described by Meisel et al. (2003) and Fischer-Gödde et al. (2010). The measured abundance of ^{195}Pt was used as internal standard, because Pt tends to be more abundant than for example Ir, and ^{195}Pt provides the best reproducibility. Rhodium and Pt show coincident elution curves during column chemistry, and their recoveries were >95 % (Fischer-Gödde et al. 2010). The relative concentrations of Rh, Au and Pt were calibrated by comparison with the external standard solution.

Through the course of this study, total analytical blanks (TAB) had an average $^{187}Os/^{188}Os$ of 0.21 ± 0.02 with a concentration of 1.5 ± 0.02 pg Os (n = 5) and 18 ± 8 pg Re, 0.8 ± 0.4 pg Ir, 2.4 ± 1.2 pg Ru, 17 ± 8 pg Pt, 22 ± 8 pg Pd, 32 ± 16 pg Au, 2.3 ± 1.2 pg Rh (n = 4). Uncertainties applied to blank corrections are 2σ, or in the case of larger scatter assumed to be 50 % of measured values. Blank corrections were usually below 20 % but occasionally reach 60 %. The average blank contribution to the measured values is relatively high. To account for these blank contributions we calculated the limit of detection as well as the uncertainties of concentration values and isotopic ratios according to the uncertainty of average blank values used for correction. Details about TAB and uncertainty calculation are reported in appendix A.2.10.

5.4 Results

5.4.1 Petrography, mineral chemistry and geochemistry of the anorthosite and the Fe-Ti ore samples

Anorthositic rocks of the KIC display well-preserved primary magmatic assemblages and textures. Major and trace element data of anorthositic rocks and Fe-Ti ore are listed in Table 5.1. Detailed petrographical and geochemical features have been previously described by von Seckendorff et al. (2000), Drüppel et al. (2001, 2007), Franke et al. (2009) and Gleißner et al. (2010, in press). Therefore we only give a short summary with focus on Fe-Ti oxide and sulfide minerals.

A characteristic feature of the KIC anorthosites is the dominance of coarse-grained plagioclase, showing adcumulate to mesocumulate texture. Rocks of the white anorthosite suite display the igneous mineral assemblage of cumulus plagioclase (An_{39-64}) ± cumulus orthopyroxene (X_{Mg}: 0.57 – 0.72) + interstitial ortho- and clinopyroxene (X_{Mg}: 0.57 – 0.78) + ilmenite ($Ilm_{82-95}Pyr_{3.7-14}Hem_{0.7-3.6}$) ± magnetite ($Mag_{96-99}Ulv_{0.5-3.5}Chr_{0.0-1.7}$) ± amphibole ± biotite ± apatite ± sulfide. Ilmenite and magnetite occur as µm-sized inclusions in cumulus plagioclase and also as mm-sized interstitial grains (Fig. 5.2a). Leucogabbronorite of the white anorthosite suite display the highest content of oxide minerals (up to 14 wt.%) and accessory sulfides. The µm-sized, subhedral, pyrite and chalcopyrite grains are either included in ilmenite, or occur in interstices between plagioclase and ilmenite grains (Fig. 5.3a). Xenocrysts of andradite-rich garnet occur in the interstices between cumulus plagioclase within leucogabbronorite and suggest contamination of the parental melt with calc-silicate gneisses of the country rock (Drüppel et al., 2007).

The dark anorthosites display the primary magmatic assemblage of cumulus plagioclase (An_{53-65}) + olivine (Fo_{56-74}) + interstitial ortho- and clinopyroxene (X_{Mg}: 0.64 – 0.74) + ilmenite ($Ilm_{88-98}Pyr_{0.6-13}Geik_{0.0-9.7}Hem_{0.2-4.4}$) ± magnetite ($Mag_{97-99}Ulv_{0.0-2.5}Chr_{0.0-2.7}$) ± biotite. In leucotroctolite, µm-sized ilmenite inclusions in plagioclase and olivine point to the early crystallisation of Fe-Ti phases (Fig. 5.2b). Larger, mm-sized, anhedral, coarse-grained ilmenite, magnetite and subordinated spinel ($Hc_{56-82}Spl_{16-43}Mag_{1.9-3.3}$) occur in the interstices (Fig. 5.3b). Their complex exsolution features are interpreted as result of re-equilibration of primary titanomagnetite. The composition of coexisting ilmenite-magnetite pairs indicates re-equilibration at ~700°C under oxygen fugacities close to FMQ (Drüppel et al., 2001). Gabbroic anorthosite displays a well-preserved cumulate texture with euhedral plagioclase laths and interstitial clinopyroxene, interpreted as late stage cumulate with abundant residual melt (Fig. 5.2c). Larger sulfide grains are absent in the dark anorthosites.

The Fe-Ti ore bodies are mainly composed of granular, coarse magnetite ($Mag_{77-99}Ulv_{0.4-16}Chr_{0.3-0.6}$) and subordinate ilmenite ($Ilm_{78-89}Pyr_{1.8-3.0}Geik_{5.1-14}Hem_{2.9-6.4}$) together with minor spinel ($Hc_{30-40}Spl_{40-56}Mag_{7-11}$) and subordinate orthopyroxene (Franke et al., 2009).. Abundant granular and lamellar exsolution of ilmenite from coarse-grained magnetite (Fig. 5.2d) is interpreted as result of re-

equilibration of cumulus titanomagnetite (Franke et al, 2009). Pleonaste inclusions in ilmenite, along and parallel to the grain boundary with magnetite, as well as in the interstices are interpreted as resulting from the exsolved Al-spinel component of the magnetite (Fig. 5.3c). Sulfides are extremely scarce in the Fe-Ti ore samples. Von Seckendorff et al. (2000) reported occasionally pyrite and chalcopyrite as inclusions in ilmenite. The Fe-Ti oxide micro textures and composition indicates that they have been formed at temperatures above 800°C and oxygen fugacities close to FMQ, whereas post-cumulus re-equilibration of Fe-Ti oxide compositions took place down to ~670°C (Franke et al., 2009).

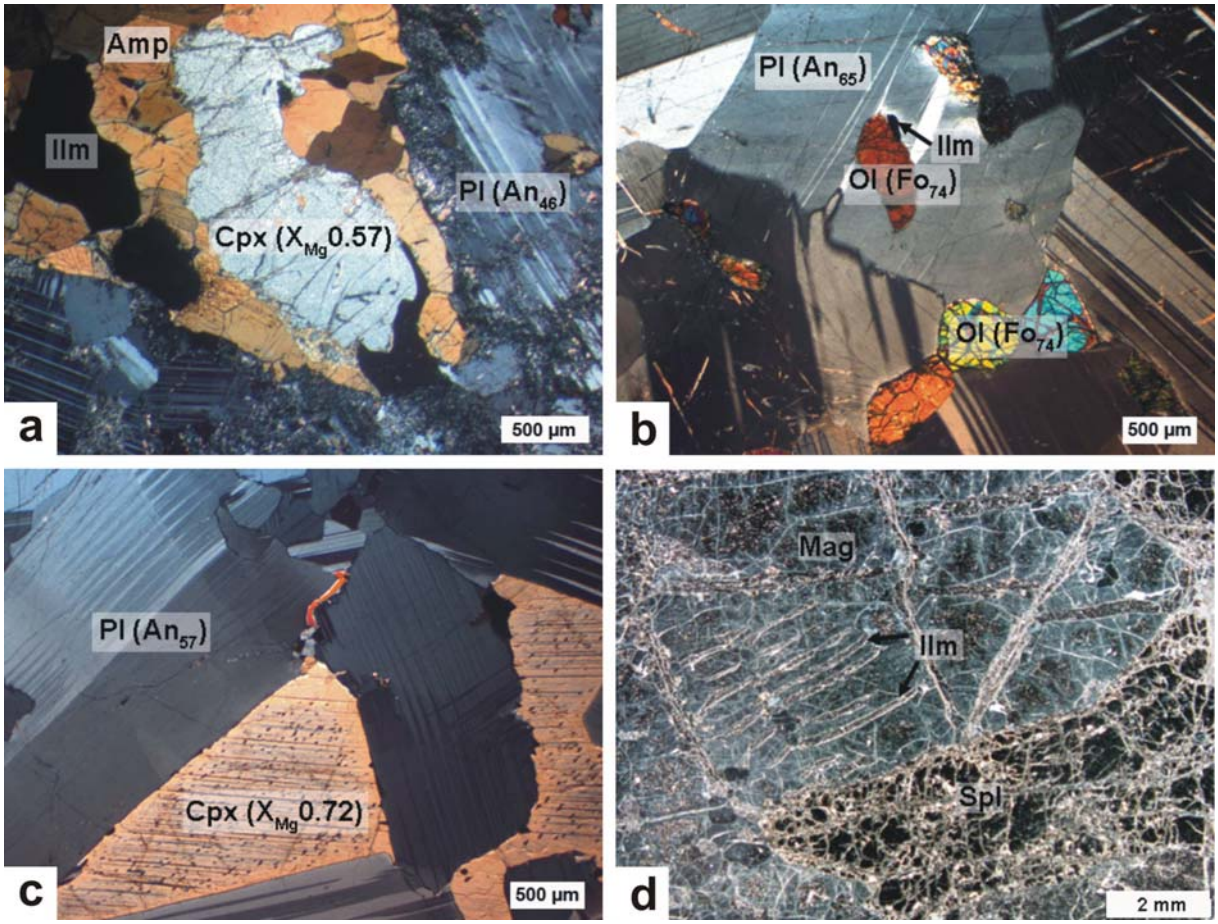

Fig. 5.2. Thin sections microphotographs of anorthositic rocks of the (a) white anorthosite suite, (b-c) dark anorthosite suite and Fe-Ti ore (d). Microphotographs a-c cross-polarized light and d reflected light. (a) Interstitial clinopyroxene, ilmenite and amphibole in leucogabbronorite (Ku-97-04). (b) Olivine and ilmenite included in plagioclase in leucotroctolite (Ku-98-228). (c) Late clinopyroxene, with Fe-Ti oxide exsolutions, filling the interstitial spaces between cumulus plagioclase in gabbroic anorthosite (Ku-06-72). (d) Coarse-grained magnetite displaying abundant ilmenite lamellae adjacent to subhedral spinel (Ku-06-57d).

Anorthosites and Fe-Ti ore samples of the KIC are cumulate rocks (Drüppel et al., 2007; Franke et al., 2009). However, the overall amount of cumulus phases and residual liquid varies between the rock types. In the dark anorthosites the residual liquid is represented mainly by the interstitial clinopyroxene (Gleißner et al., 2010). The abundance of clinopyroxene increases from the

leucotroctolite (0 - 9 wt.%) towards the gabbroic anorthosite (15 wt.%). At the same time, the proportion of oxides in the gabbroic anorthosite is low (3 wt.%) and oxides are entirely enclosed by clinopyroxene. This mode of occurrence suggests that the oxides crystallized from the residual liquid or after its entrapment. In the leucogabbronorite of the white anorthosite suite clinopyroxene was a cumulus phase. In these rocks, the trace element composition of late magmatic phases like amphibole and apatite indicate the presence of interstitial liquid that displays evidence of crustal contamination (Gleißner et al., 2010). The residual liquid between the cumulus phases of Fe-Ti ores was most likely expelled efficiently during compaction (Franke, 2009) and hence they represent the highest relative abundance of cumulus minerals (i.e. titanomagnetite).

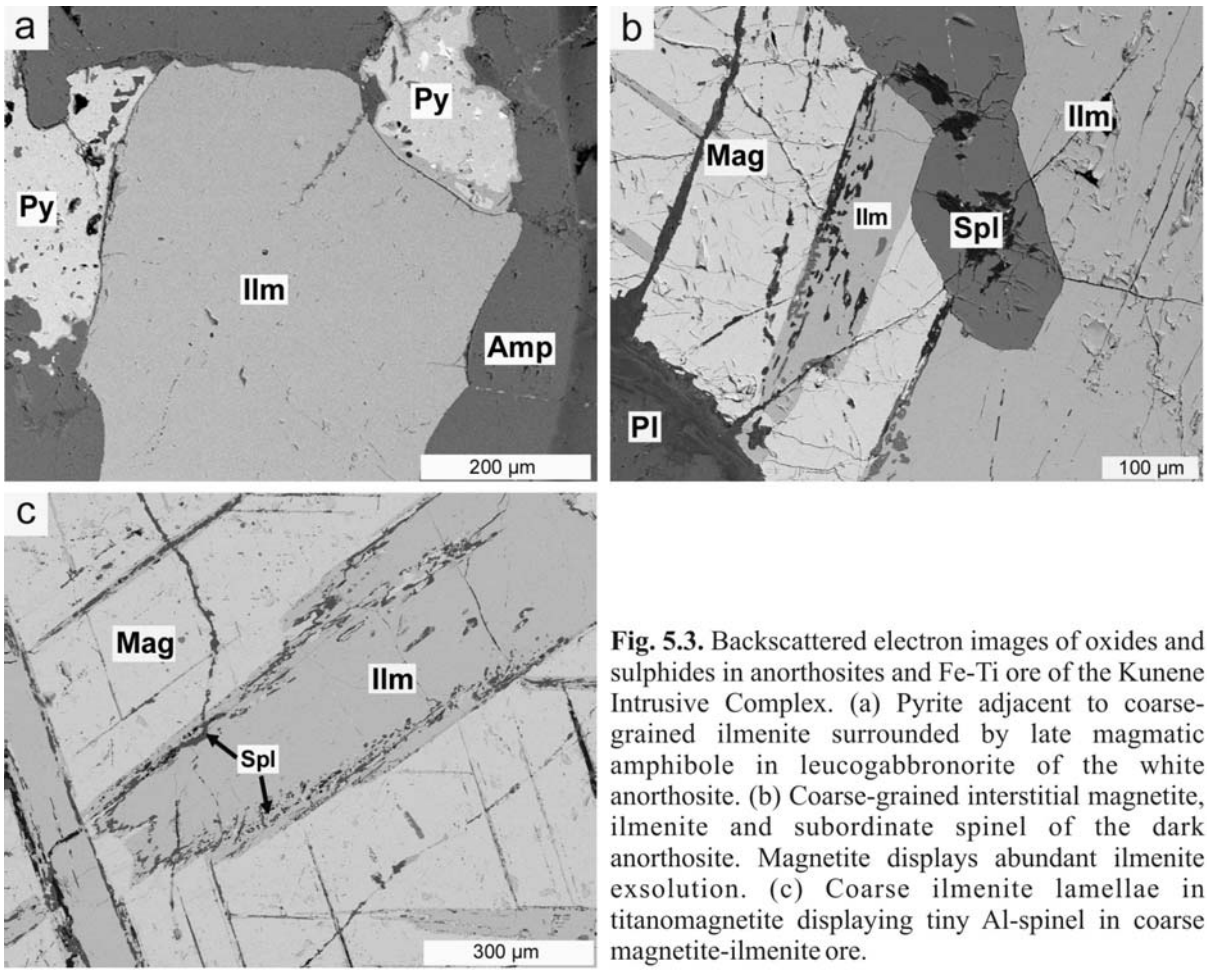

Fig. 5.3. Backscattered electron images of oxides and sulphides in anorthosites and Fe-Ti ore of the Kunene Intrusive Complex. (a) Pyrite adjacent to coarse-grained ilmenite surrounded by late magmatic amphibole in leucogabbronorite of the white anorthosite. (b) Coarse-grained interstitial magnetite, ilmenite and subordinate spinel of the dark anorthosite. Magnetite displays abundant ilmenite exsolution. (c) Coarse ilmenite lamellae in titanomagnetite displaying tiny Al-spinel in coarse magnetite-ilmenite ore.

The anorthositic rocks are generally rich in Al_2O_3, CaO, FeO_T and MgO, reflecting high amounts of cumulus plagioclase and variable abundance of Fe-Mg silicates and Fe-Ti oxides. Significant enrichment in trace elements in the whole rocks is attributed to the abundance of particular mineral species e.g. plagioclase (Ba, Sr), olivine (Ni), clinopyroxene (Cr), and Fe-Ti oxides (V). The chemical composition of the ore samples is dominated by the high modal abundance of magnetite and ilmenite,

and thus the ores are enriched in transition elements like V, Cr, Ni and Zn (Franke et al, 2009). Minor SiO_2 and MgO in the ores testify to the occurrence of Fe-Mg silicates.

Sulfur abundances of the whole rocks were determined to assess the role of sulfides as possible HSE host minerals. The KIC cumulate rocks yield low concentrations of 19 - 184 ppm in the dark anorthosites and 72 and 123 ppm in the Fe-Ti ore. A significantly higher concentration of 1412 ppm was measured in the pyrite-bearing leucogabbronorite of the white anorthosite.

Table 5.1. Major and trace element data of analysed anorthositic rocks and Fe-Ti ore of the Kunene Intrusive Complex.

	Dark anorthosite					White anorthosite	Fe-Ti ore	
Rock type	LT[G]	LT[G]	LT[D]	LT[D]	GA[G]	LGN[D]	Mag-Ilm ore[F]	Mag-Ilm ore[F]
Sample	Ku-06-07	Ku-06-69	Ku-98-125	Ku-98-228	Ku-06-72	Ku-97-04	Ku-06-57d	Ku-06-66a
[wt.%]								
SiO_2	48.5	48.9	44.7	49.6	51.4	43.9	0.74	7.55
TiO_2	0.15	0.30	2.08	0.10	0.29	4.24	18.4	15.5
Al_2O_3	24.3	23.7	21.4	26.7	24.0	15.9	7.40	4.29
Fe_2O_3	1.53	2.27	2.55	0.81	1.50	4.00	49.3	37.7
FeO	3.63	4.25	8.70	3.02	2.38	9.24	20.3	24.2
MnO	0.07	0.08	0.11	0.05	0.07	0.25	0.32	0.38
MgO	6.18	6.16	5.33	5.40	3.64	4.42	2.15	7.42
CaO	11.0	10.4	8.56	11.8	12.0	10.1	0.02	0.13
Na_2O	3.08	3.02	3.37	3.15	3.54	3.35	b.d.l.	b.d.l.
K_2O	0.22	0.30	0.47	0.17	0.35	1.27	b.d.l.	b.d.l.
P_2O_5	0.02	0.02	0.06	0.01	0.02	0.16	0.02	0.01
L.O.I.	1.16	1.15	1.41	0.23	0.480	1.61	1.36	2.82
Total	99.8	100.6	98.8	101.2	99.7	98.6	100.0	100.0
X_{Mg}	0.69	0.64	0.46	0.72	0.64	0.38	0.06	0.19
[ppm]								
V	n.a.	33	285	14	n.a.	296	2900	2360
Cr	34	33	133	22	277	36	1640	498
Ni	171	128	129	202	53	36	444	479
Zn	28	43	95	30	24	118	547	455
Ga	14	19	17	26	19	b.d.l.	56	41
Sr	426	427	602	553	450	447	b.d.l.	b.d.l.
Y	b.d.l.	b.d.l.	b.d.l.	b.d.l.	12	19	5.00	b.d.l.
Zr	b.d.l.	b.d.l.	27	b.d.l.	b.d.l.	104	47	41
Nb	b.d.l.	b.d.l.	b.d.l.	b.d.l.	b.d.l.	15	3	5
Ba	105	101	358	109	275	567	b.d.l.	b.d.l.
Yb	0.13	0.18	0.16	0.03	0.43	2.1	b.d.l.	n.a.
S	52(4)	108(4)	184(44)	38(26)	19(6)	1412(298)	72(18)	123(4)
Pl	An61	An61	An53	An65	An57	An46		
Ol/Cpx	Fo68	Fo64	Fo60	Fo74	#Mg72	#Mg57		
CIPW [wt.%]								
Plag	79	78	71	86	81	52	0	1
Ol	12	9	17	12	1	6	4	9
Px	5	9	0	1	15	20	0	0
Fe-Ti oxides	2	4	8	1	3	14	96	82

Major and trace element values taken from [D]Drüppel (2003), [F]Franke (2009) and [G]Gleißner et al. (in press). For sulphur analyses (this study) the uncertainties are given in parentheses at the 2σ level. Mineral chemistry data are average values taken from Gleißner et al. (2010). Rock types: LT, leucotroctolite; GA, gabbroic anorthosite; LGN, leucogabbronorite.

Table 5.2. Highly siderophile element concentration and Os isotope composition of anorthositic rocks, Fe-Ti ore and mineral separates of the Kunene Intrusive Complex.

sample	rock type/mineral (grain-size µm)[a]	Os [ppt]	^{192}Os [ppt]	com. Os[b] [ppt]	Ir [ppt]	Ru [ppt]	Rh [ppt]	Pt [ppt]	Pd [ppt]	Au [ppt]	Re [ppt]	^{187}Re/^{188}Os	^{187}Os/^{188}Os	^{187}Os/^{188}Os (1.38Ga)[c]	γOs (1.38Ga)[d]	$T_{(ch)}$ [Ga]
Dark anorthosite																
Ku-98-228	LT	2.69(5)	1.01(2)	2.48(4)	1.2(2)	2.4(6)	5(2)	28(2)	45(4)	88(20)	17(4)	33(9)	0.94(2)	0.2(1)	48	1.5
Ku-06-07	LT	5.41(5)	1.83(2)	4.48(4)	1.4(2)	11.9(6)	<4.5	51(2)	61(4)	226(17)	53(5)	58(5)	1.94(2)	0.58(6)	396	1.4
Ku-06-69	LT	2.22(5)	0.65(1)	1.60(4)	0.6(2)	<2.0	<4.5	50(2)	44(4)	384(17)	54(5)	185(17)	4.6(2)	0.3(2)	146	1.8
Ku-06-72	GA	2.27(5)	0.82(2)	2.06(5)	<0.55	<2.0	32(1)	<10.5	<13.5	<27	<10		1.11(3)			
Ku-98-125	LT	10.72(5)	2.97(1)	7.26(3)							263(4)	179(3)	4.08(3)	-0.08(4)*	-164*	1.3
Ku-98-125	LT	10.06(5)	2.51(1)	6.14(3)	2.5(2)	12.7(6)	6(1)	21(2)	29(4)	203(17)	231(4)	189(4)	5.53(5)	1.14(5)	872	1.7
	Mag (355-500)	7.3(2)	1.64(4)	4.0(1)							665(16)	1097(70)	11.5(7)	-14.0(9)*	-11993*	0.6
	Mag (250-355)	13.0(1)	1.33(1)	3.24(3)	<1.1	4(1)	<9	36(4)	56(8)	381(16)	1433(9)	3221(155)	39(2)	-36(2)*	-30704*	0.7
	Ilm (500-1000)	12.0(1)	3.02(2)	7.39(6)	<1.1	5(1)	<9	79(4)	29(4)	179(16)	644(9)	450(9)	5.73(8)	-4.7(1)*	-4109*	0.7
White anorthosite																
Ku-97-04	LGN	10.05(5)	0.705(4)	1.72(1)							563(5)	2392(107)	60(3)	5(2)	3982	1.5
Ku-97-04	LGN	n.d.			1.1(2)	<2.0	<4.5	47(2)	203(4)	273(17)	485(5)					
	Mag (500-1000)	24.9(1)	1.44(1)	3.51(1)							813(9)	1725(79)	76(3)	36(2)	30776	2.6
	Mag (355-500)	18.3(1)	1.03(1)	2.53(1)	1.3(4)	4(1)	<9	46(4)	68(7)	133(16)	590(8)	2045(137)	93(6)	46(3)	39060	2.7
	Ilm (500-1000)	11.5(1)	1.31(1)	3.21(3)							387(9)	840(41)	32(1)	12.4(8)	10469	2.2
	Ilm (500-1000)	11.8(2)	1.82(3)	4.45(8)							1250(19)	2346(195)	28(2)	-27(3)*	-22959*	0.7
	Ilm (355-500)	8.3(1)	0.86(1)	2.10(3)	<1.1	<4.0	<9	127(4)	36(8)	222(16)	331(9)	1571(162)	55(5)	18(3)	15568	2.1
	Py (355-500)	1062(4)	53.3(2)	130.3(5)							84591(395)	5413(313)	100(6)	-25(5)*	-21589*	1.1
	Py (355-500)	962(5)	40.3(2)	98.5(5)	1385(18)	3835(54)	743(1)	4185(180)	5070(360)	22922(15)	41458(405)	4969(553)	176(19)	60(12)	51171	2.1
Fe-Ti ore																
Ku-06-66a	Mag-Ilm ore	19.7(1)	2.07(1)	5.07(2)	<1.1	4(1)	<9	61(4)	66(7)	110(17)	665(8)	768(18)	28.5(6)	10.7(4)	8997	2.2
Ku-06-57d	Mag-Ilm ore	21.9(2)	2.89(3)	7.06(6)							1163(18)	1083(44)	24.8(9)	-0.3(7)*	-351*	1.4
Ku-06-57d	Mag-Ilm ore	20.3(1)	2.65(1)	6.48(3)	11.7(4)	<4.0	<9	35(4)	<27	138(16)	1262(10)	1114(24)	20.9(4)	-4.9(3)*	-4279*	1.1
	Mag (500-1000)	19.0(1)	1.50(1)	3.66(2)							1543(9)	2941(115)	50(2)	-18(2)*	-15773*	1.0
	Mag (500-1000)	18.3(1)	1.35(1)	3.30(2)	16.4(4)	7(1)	10(1)	51168(4)	39(7)	69(16)	1370(9)	3095(145)	58(3)	-14(2)*	-11867*	1.1
	Ilm (500-1000)	11.3(1)	1.48(1)	3.63(3)	1.2(4)	6(1)	5(1)	299(4)	62(4)	466(16)	546(9)	982(40)	24.9(9)	2.1(6)	1674	1.5
	Spl	8.9(1)	1.32(1)	3.22(4)	<1.1	370(1)	96(1)	155(4)	63(4)	118(16)	299(9)	614(31)	21.3(9)	7.1(6)	5926	2.0

All data are fractionation and blank corrected. Uncertainties are given in parentheses for the last decimal place at the 2σ level. n.d. not detected. Values '<' give the limits of detection. [a]Rock types: LT, leucotroctolite; GA, gabbroic anorthosite; LGN, leucogabbronorite. [b]Os concentration recalculated to ^{187}Os/^{188}Os=0.13. [c]The ^{187}Re decay constant of 1.666×10-11 y^{-1} and an intrusion age of 1.38 Ga (Drüppel et al., 2000) were used for calculation of initial values. [d]γOs calculated according to Shirey and Walker (1998 and references therein). *Negative values due to later open system behaviour.

5.4.2 Highly siderophile element abundances in anorthositic rocks and Fe-Ti ore

Highly siderophile element data of leucotroctolites, gabbroic anorthosite, leucogabbronorite, Fe-Ti ore and mineral separates are listed in Table 5.2. In general, the concentrations of Os, Ir, Ru and Rh are very low in all KIC rocks (lower ppt range). Higher absolute and relative concentrations were measured for Pt, Pd, Au and Re, but concentrations higher than 1 ppb are restricted to Re in the ore samples.

Four leucotroctolites of the dark anorthosite suite display a range of 1.6 - 7.3 ppt common Os, 0.6 - 2.5 ppt Ir, 2.4 - 12.7 ppt Ru, 21 - 51 ppt Pt, 29 - 61 ppt Pd, 88 - 384 ppt Au, 17 - 263 ppt Re (Fig. 5.4a-e). Rh is mostly below detection limit but yields 5 and 6 ppt in two samples. The chondrite-normalized patterns (Fig. 5.5a) display small negative Ir anomalies (Os_N/Ir_N: 2 - 3) and enrichment of Pt, Pd, Au and Re over Os, Ir and Ru (Pt_N/Os_N: 2 - 16; Re_N/Os_N: 83 - 454). The most primitive leucotroctolite sample (Ku-98-228) with the lowest content of oxide minerals (~1 wt.%) displays a HSE pattern almost parallel to typical gabbro values reported elsewhere (Dale et al., 2008). In contrast, an oxide-rich leucotroctolite (Ku-98-125; Ilm + Mag ~8 wt.%) is about one order of magnitude higher in Re (Fig. 5.5a). A gabbroic anorthosite of the dark anorthosite suite displays HSE abundances below the detection limit, except for Os and Rh (Fig. 5.5a).

The leucogabbronorite of the white anorthosite suite is characterized by significantly higher Pd (203 ppt) and Re (485 - 563 ppt) than the dark anorthosites (Fig. 5.4d). The chondrite-normalized pattern display increasing enrichment from Pt, Pd (Pt_N/Os_N: 14) to Re (Re_N/Os_N: 3949) over Os, Ir and Ru (Fig. 5.5b).

Abundances of the HSE in the Fe-Ti ore samples are similar to the range of the leucotroctolites, with the exception of higher Re in the ores (665 - 1262 ppt). Additionally, almost unaltered Mag-Ilm ore (Ku-06-57d) was found to be higher in Ir (11.7 ppt) than the anorthosites whereas Ir of martitized Mag-Ilm ore (Ku-06-66a) is below detection limit. The chondrite-normalized pattern display enrichment of Pt, Au and Re over Os, Ir and Ru (Pt_N/Os_N: 3 - 6; Re_N/Os_N: 1583 - 2349), similar to that of the oxide-rich leucotroctolite (Fig. 5.5b).

Fig. 5.4. (next page) Variation of highly siderophile elements in bulk rocks, magnetite, ilmenite and spinel of the Kunene Intrusive Complex. The Os concentration is displayed as common Os. The HSE concentrations in pyrite from leucogabbronorite are one to three orders of magnitude higher than in the oxides and its composition off scale is indicated with a grey arrow. Replicate analyses from the same bulk rock sample powder for Os and Re are encircled with a dotted line. Iron in (f) is measured FeO_T in oxides and FeO_T, corrected for iron in Mg-Fe silicates, in bulk rocks. Inset in (g) schematically illustrates the effect of Fe-Ti oxide accumulation and crustal contamination on S and Re content of anorthosites and Fe-Ti ore.

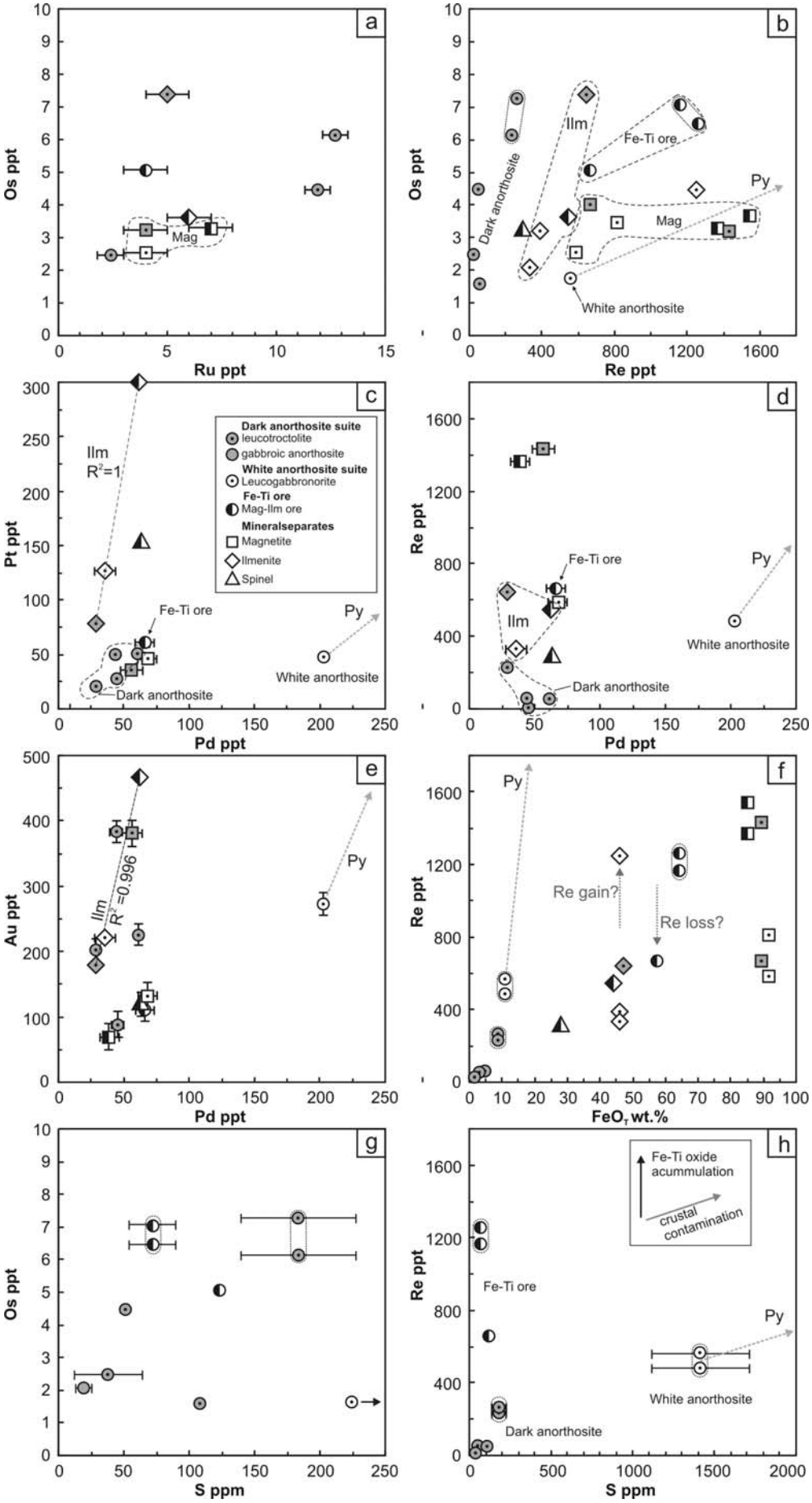
a
Os ppt
Ru ppt
Mag
b
Os ppt
Re ppt
Ilm
Fe-Ti ore
Py
Mag
Dark anorthosite
White anorthosite
c
Pt ppt
Pd ppt
Ilm
R²=1
Dark anorthosite suite
leucotroctolite
gabbroic anorthosite
White anorthosite suite
Leucogabbronorite
Fe-Ti ore
Mag-Ilm ore
Mineralseparates
Magnetite
Ilmenite
Spinel
Fe-Ti ore
Py
White anorthosite
Dark anorthosite
d
Re ppt
Pd ppt
Fe-Ti ore
Py
Ilm
White anorthosite
Dark anorthosite
e
Au ppt
Pd ppt
Ilm
R²=0.996
Py
f
Re ppt
FeO$_T$ wt.%
Py
Re gain?
Re loss?
g
Os ppt
S ppm
h
Re ppt
S ppm
Fe-Ti oxide acummulation
crustal contamination
Fe-Ti ore
Py
White anorthosite
Dark anorthosite

The Re/Os ratios increase consistently from 2 - 38 in the dark anorthosites to 131 - 195 in the Fe-Ti ore and to 327 in the leucogabbronorite of the white anorthosite (Fig. 5.4b). Comparison to the major element composition of the samples reveals a strong increase of Re with Fe content (Fig. 5.4f). A weak positive correlation with sulfur in the dark anorthosites and Fe-Ti ore was observed for Os but not for Re (Fig. 5.4g and h). No correlation of other HSE with lithophile major or trace elements (for instance Yb) was observed.

5.4.3 Highly siderophile element abundances of separated oxide and sulfide minerals

Oxide mineral separates from selected samples of the three rock suites (dark anorthosite, white anorthosite, Fe-Ti ore) display concentrations of Os, Ir and Ru in the same range like those of the corresponding bulk rocks, but are generally higher in Pt and Re. Like in the bulk rock analyses, Ir, Ru and Rh abundances in oxide separates are often below the detection limit (Table 5.2).

In all samples magnetite displays higher Re than ilmenite, whereas ilmenite displays higher Pt contents (Fig. 5.4b-d). Ilmenites from the three different rock suites display conspicuous correlations of Pt, Pd and Au contents but no correlation of these elements with Re seem to exist (Fig. 5.4c-e). Generally the Re/Os ratios increase in the order Spl < Ilm < Mag < Py (Fig. 5.4b).

In leucotroctolite of the dark anorthosite suite the oxides display slightly steeper chondrite-normalized patterns than the bulk rock and significantly lower Ir (below detection limit of ~1.1 ppt). Magnetite is higher in Pd, Au and Re when compared to ilmenite (Fig. 5.6a). In leucogabbronorite of the white anorthosite suite the oxides and bulk rock show almost parallel HSE patterns except for lower Pd in the oxides. Ilmenite also displays higher Pt than the bulk rock whereas Ir, Ru and Rh are below the detection limit. Pyrite yields two orders of magnitude higher HSE concentrations than the oxides but displays a relatively unfractionated chondrite-normalized pattern except for a depletion in Os and a strong increase of Re and Au (Fig. 5.6b). Magnetite is the major constituent of the Fe-Ti ore sample and its chondrite-normalized HSE patterns are almost parallel to the bulk rock except for very high Pt in one case (51 ppb). Ilmenite displays a similar pattern but with significantly lower Pt and Ir (Os_N/Ir_N: 2). Spinel is a minor constituent of the ores (~5 wt.%) and shows strong enrichment in Ru (370 ppt) and Rh (96 ppt) but Ir below detection limit (Fig. 5.6c).

5.4.4 Os isotope compositions

Re-Os concentrations and Os isotopic compositions of leucotroctolites, gabbroic anorthosite, leucogabbronorite, Fe-Ti ore and mineral separates are given in Table 5.2. The measured $^{187}Os/^{188}Os$ ratios increase from the dark anorthosites (0.94 ± 2 to 5.53 ± 5), towards the Fe-Ti ore (20.9 ± 4 to 28.5 ± 6) and the white anorthosite (60 ± 3). Replicate analysis of the bulk rock sample powder of two samples yield similar concentrations (Fig. 5.4b) but differ in isotopic composition by 20 - 30 % (Fig.

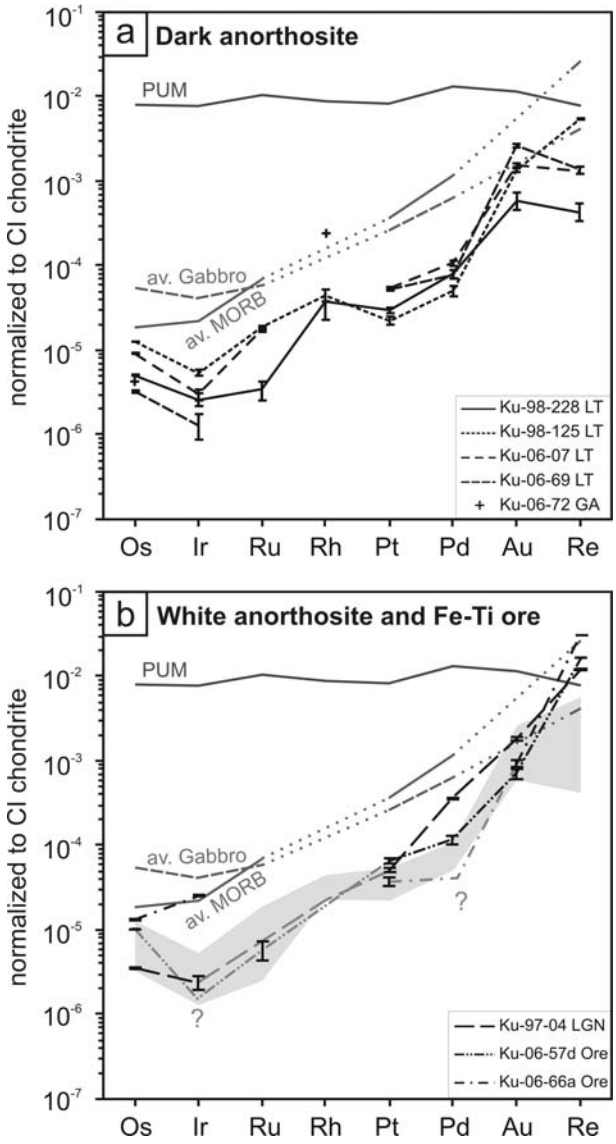

Fig. 5.5. Highly siderophile element abundances of bulk rocks normalized to chondrite values (Fischer-Gödde et al., 2010). Elements are listed in the order of increasing incompatibility during magmatic fractionation. (a) Leucotroctolite and gabbroic anorthosite of the dark anorthosite suite. (b) Leucogabbronorite of the white anorthosite and associated Fe-Ti ore. The shaded field in (b) outlines the range of leucotroctolite from (a). For comparison the composition of the primitive upper mantle (Becker et al., 2006; Fischer-Gödde et al., in press) and the average MORB and oceanic gabbro values (Dale et al., 2008; 2009) are displayed.

5.7). This scatter indicates heterogeneity of the sample powder or underestimation of analytical uncertainty. However, the $^{187}Os/^{188}Os$ values are generally consistent with their measured Re/Os and corroborate a strong difference between the three units. The dark anorthosites and one Fe-Ti ore sample fall close to a reference line through a chondritic initial $^{187}Os/^{188}Os$ at 1.38 Ga, whereas the white anorthosite sample and the other Fe-Ti ore sample plot above this line. Bulk rock errorchrons (Isoplot Model 3, Ludwig, 2003) for the whole sample suite and the dark anorthosite suite yield dates of 1438 ± 300 Ma and 1440 ± 660 Ma and initial $^{187}Os/^{188}Os$ ratios of 0.6 ± 4.8 and 0.3 ± 1.6,

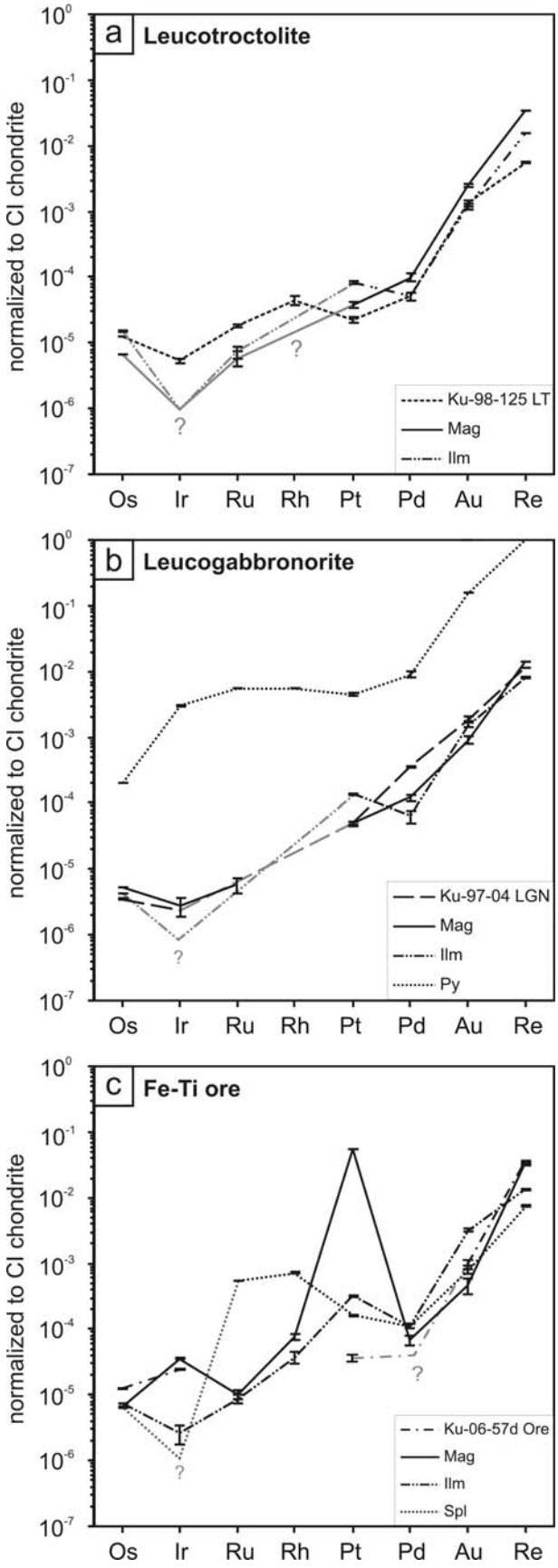

Fig. 5.6. Highly siderophile element abundances of bulk rock and mineral separates normalized to chondrite values (Fischer-Gödde et al., 2010). (a) Leucotroctolite of the dark anorthosite suite. (b) Leucogabbronorite of the white anorthosite suite. (c) Fe-Ti ore.

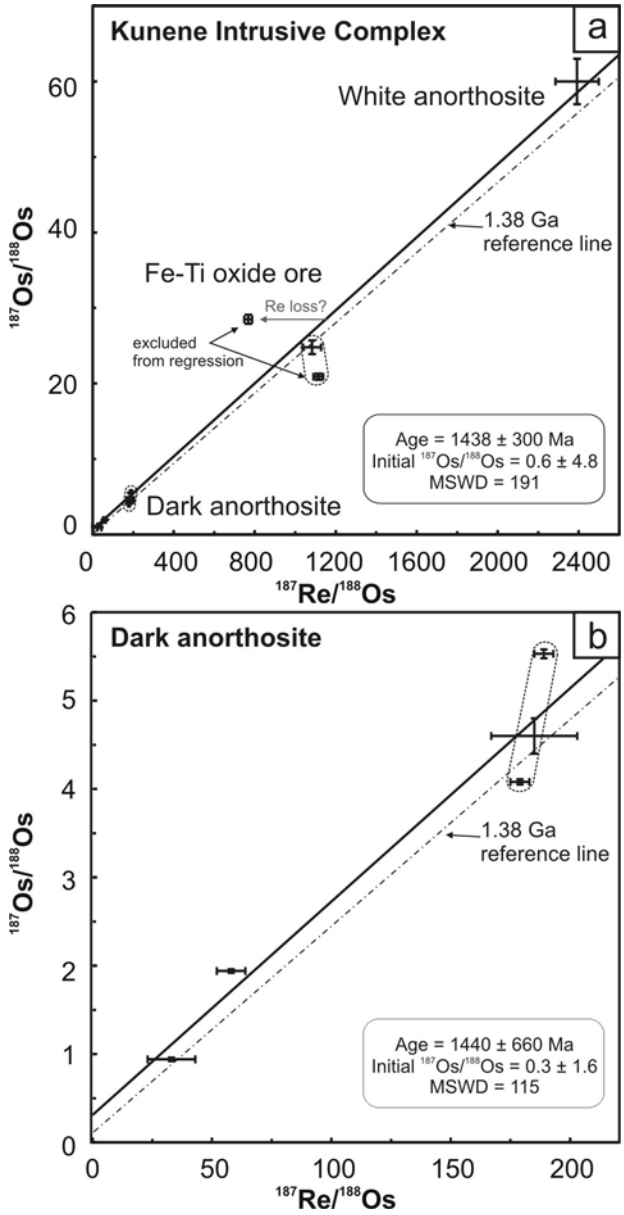

Fig. 5.7. Re-Os isotope systematics for bulk rocks analysed in this study. (a) Dark anorthosite, white anorthosite and Fe-Ti ore. (b) Dark anorthosite. The regression lines were calculated using the Isoplot 3.00 software of Ludwig (2003). Also shown for reference is a 1.38 Ga reference line with a chondritic (=uncontaminated mantle) initial Os isotope composition. Replicate analyses from the same bulk rock sample powder are encircled with a dotted line.

respectively (Fig. 5.7a and b). Despite the large uncertainties, which are mainly due to the heterogeneities within the sample set and the limited spread of the dark anorthosite data, the Re-Os dates agree with the U-Pb zircon age of 1385 ± 25 Ma obtained for an anorthosite sample from Namibia (Drüppel et al., 2000).

In contrast, internal Re-Os isotope systematics of minerals are disturbed and presumably reflect post-magmatic redistribution of Re and Os. Ilmenite and magnetite of a leucotroctolite of the dark anorthosite suite fall below the 1.38 Ga reference line and define a 674 ± 160 Ma errorchron date (Fig. 5.8a); whereas in leucogabbronorite of the white anorthosite suite, the analyses display substantial

scatter (Fig. 5.8b). In Fe-Ti ore the magnetite falls below the chondritic reference line whereas the spinel plots above. Together with the bulk rock these samples define an 873 ± 250 Ma errorchron date (Fig. 5.8c).

The measured $^{187}Os/^{188}Os$ (and Re/Os) of mineral separates increase in the order spinel, ilmenite, magnetite and, if present, pyrite. The Os isotopic composition of ilmenite is generally close to the bulk rock composition. Analyses of different grain-size fractions of magnetite and ilmenite yield no systematic differences in Os and Re concentrations and Re/Os ratios. One ilmenite sample from pyrite-bearing leucogabbronorite displays a high Re concentration (Fig. 5.7f) and Re/Os ratio but the lowest $^{187}Os/^{188}Os$ ratio (Fig. 5.8b). Hence, the measured Re and Os values can not be attributed to the presence of abundant pyrite inclusions in the oxides.

5.5 Discussion

5.5.1 Re-Os isotope systematics

Internal Re-Os isotope systematics of the samples demonstrates that the Re-Os isotopic system has been reset at the mineral scale. In leucotroctolite and the Fe-Ti ore sample the measured values are consistent with final equilibration of Os isotopic composition between the phases at ~670 - 870 Ma. Since the KIC is apparently unmetamorphosed (Drüppel et al., 2007) with the internal Sm-Nd isotopic compositions being undisturbed (Gleißner et al., in press) we suggest that these dates reflect closure of the Re-Os distribution between Fe-Ti oxides. Similar relations were found in the Voisey's Bay sulfide deposit where mineral isochron ages postdate whole rock isochron and U-Pb ages by ~300 Ma (Lambert et al., 2000). In the leucogabbronorite sample, the non-isochronous behaviour of most mineral separates suggests Re mobility during later alteration. Minerals such as magnetite and pyrite, plotting above the 1.38 Ga reference line may have lost some Re (Fig. 5.8b).

Most anorthosite whole rock analyses fall on to or close to the reference line through chondritic initial $^{187}Os/^{188}Os$ at 1.38 Ga and hence, indicate closed system behaviour at the sample scale. The dark anorthosite whole rock errorchron date of 1440 ± 660 Ma coincides with the U-Pb zircon age of 1385 ± 25 Ma (Drüppel et al., 2000). The uncertainty of 660 Ma most likely results from initial heterogeneities in Os isotopic composition among the samples, as indicated by a significant range in initial εNd from +6 to 0 (Gleißner et al., in press). The Os isotopic composition of Fe-Ti ores is consistent with preferential incorporation of Re in titanomagnetite during magmatic fractionation. Ore sample Ku-06-57d plots on the 1.38 Ga reference line, and thus corroborates the interpretation that anorthosites and Fe-Ti oxide cumulates evolved during the same magmatic event from a similar magma composition, although the range in $^{187}Re/^{188}Os$ ratios observed in Fe-Ti ore indicate some post-magmatic mobility of Re.

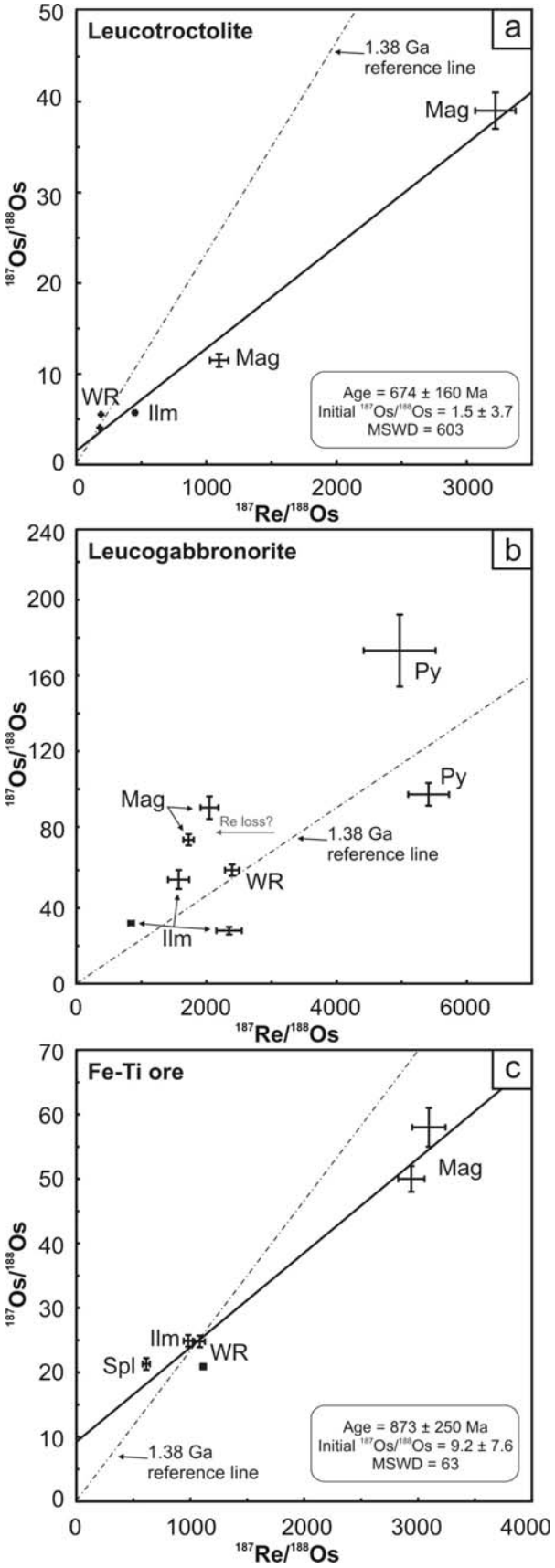

Fig. 5.8. Re-Os isotope systematics of bulk rock and corresponding mineral separates. (a) Leucotroctolite of the dark anorthosite suite. (b) Leucogabbronorite of the white anorthosite suite. (c) Fe-Ti ore. Also shown for reference is a 1.38 Ga reference line with a chondritic (=uncontaminated mantle) initial Os isotope composition.

The high $^{187}Re/^{188}Os$ ratios in all samples lead to large corrections for in-situ growth of ^{187}Os and result in high uncertainties of initial $^{187}Os/^{188}Os$. The negative initial γOs values for many mineral separates indicate disturbance of the Re-Os isotope system and do not permit calculation of reliable initial isotopic composition or model ages. The dark anorthosite whole rock analyses, when calculated to the intrusion age of the anorthosites, displays a range in $^{187}Os/^{188}Os$ from 0.2 ± 0.1 to 1.14 ± 0.05 (γOs_i 48 to 872) and Os model ages of 1.4 - 1.8 Ga. The leucogabbronorite of the white anorthosite yields significantly higher initial $^{187}Os/^{188}Os$ of 5 ± 2 (γOs 3982).

5.5.2 Source characteristics

The initial Os isotope composition of the KIC anorthosites ranges from $^{187}Os/^{188}Os$ 0.2 ± 0.1, overlapping with mantle compositions, to very radiogenic vales of 5 ± 2. Osmium isotope data from other anorthosites massifs are available for the Rogaland Anorthosite Complex (Schiellerup et al., 2000), the Suwałki Anorthosite Complex (Morgan et al., 2000) and several Proterozoic layered intrusions (Fig. 5.9). Although the origin of massif-type anorthosites is still matter of debate, layered intrusions are interpreted as mantle-derived mafic melts and the observed range in initial Os isotopic compositions is attributed to interaction with enriched subcontinental mantle (Richardson & Shirey, 2008) or the continental crust (Ripley et al., 1999; Sproule et al., 2002; Day et al., 2008; O'Driscoll et al., 2009). The Os isotope composition of the dark anorthosites of the KIC and the available data of other massif-type anorthosites are within the range of layered intrusions that were affected by crustal contamination during their emplacement in the crust (Ripley et al., 1999; Lambert et al., 2000; Sproule et al., 2002). The initial osmium isotope compositions of sulfide deposits and host rocks in layered intrusions reflect either bulk or selective contamination of the primitive melts involving highly radiogenic crustal sulfide, followed by liquid immiscibility of sulfide melts and equilibration with the magma column (Lambert et al., 2000; Sproule et al., 2002). During the formation of sulfur undersaturated massif-type anorthosites like the KIC exsolution of sulfide liquid probably does not occur and the observed range in Os isotopic compositions reflects directly the composition of the crustally contaminated magmas. However, the sulfide-enriched leucogabbronorite of the white anorthosite suite exceeds the usual range of initial γOs observed for Proterozoic igneous rocks, implying a different process or significantly higher assimilation ratio and/or more radiogenic composition of the contaminants. Von Seckendorff et al. (2000) argued for a sulfidation of Fe-Ti oxides due to metasomatic overprint for anorthosites in contact with mantle-derived carbonatite and alkali syenite dykes in the southeastern KIC. The leucogabbronorite sample of this study display high abundances of sulfide when compare to other white and dark anorthosites but its initial highly radiogenic isotopic composition of γOs = 3982 reveals that the Os content is mainly of crustal origin.

Comparison of the Os isotopic data with the isotopic composition of lithophile trace elements, reveals that KIC anorthosites define a trend of decreasing initial εNd with strongly increasing initial

$^{187}Os/^{188}Os$ from the dark anorthosites towards the white anorthosite (Fig. 5.10). The leucotroctolite samples of the dark anorthosite suite fall into the Nd isotopic compositional field of depleted mantle, and overlap in uncertainty with the Os isotopic composition of the mantle at 1.38 Ga. Leucogabbronorite of the white anorthosite falls close to the estimated compositional field of felsic orthogneisses and paragneisses of the Paleoproterozoic Epupa Complex as the possible contaminants. The data are in accordance with contamination of mantle-derived parental melt by crustal material with highly radiogenic Os, unradiogenic Nd and high Nd/Os ratios. The alternative interpretation that the Os isotopic composition reflects melting of a mafic lower crustal source, as suggested for the Rogaland and Suwałki massif-type anorthosites (Morgan et al., 2000; Schiellerup et al., 2000), seems not likely for the KIC since the most primitive leucotroctolite sample overlap in uncertainty with the composition of the mantle (Fig. 5.10).

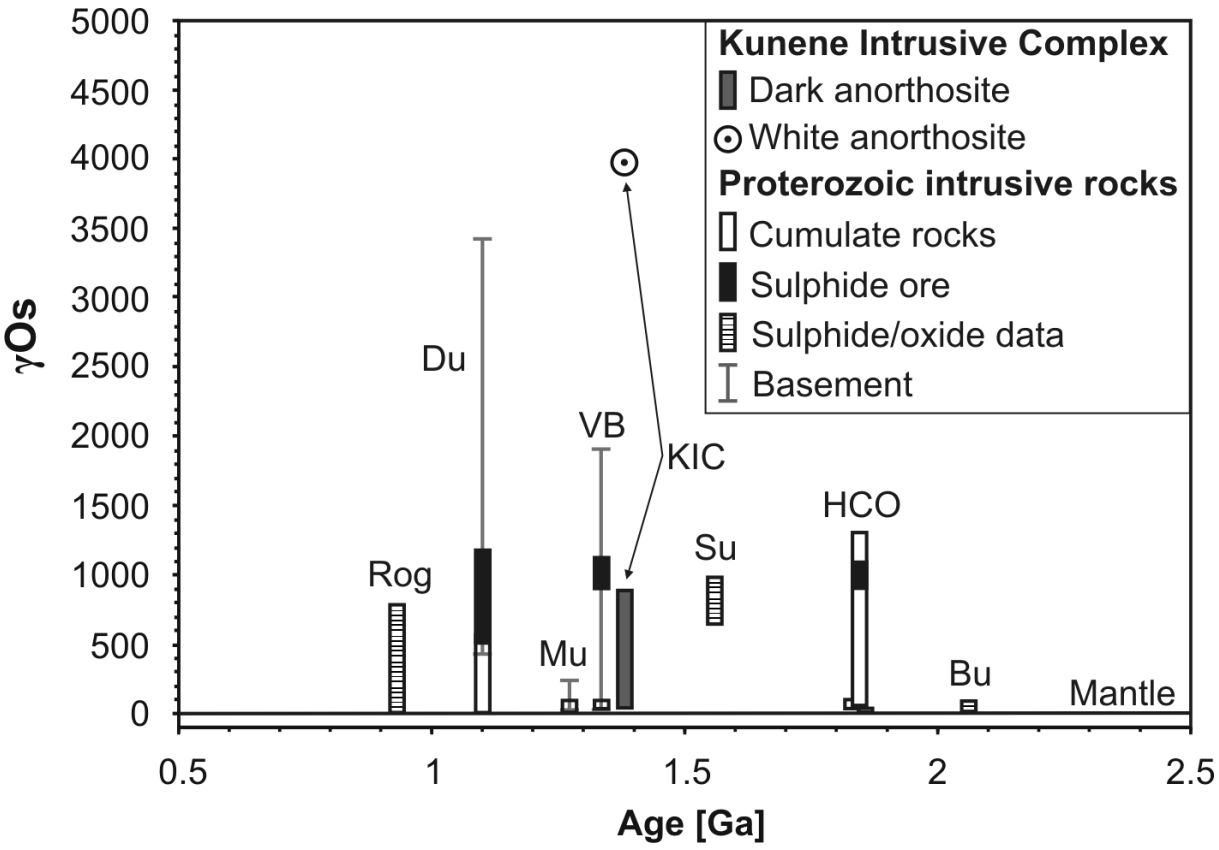

Fig. 5.9. Os isotopic composition of Proterozoic massif-type anorthosites and Proterozoic layered intrusions. Shown is the observed range of the initial isotopic composition in γOs notation. Massif-type anorthosites: Su Suwałki (Morgan et al., 2000); KIC Kunene Intrusive Complex (this study); Rog Rogaland Complex (Schiellerup et al., 2000). Layered intrusions: Bu Bushveld (Richardson & Shirey, 2008 and references therein); HCO layered intrusions in the Halls Creek orogen (Sproule et al., 2002); VB Voisey's Bay (Lambert et al., 2000); Mu Muskox (Day et al., 2008); Du Duluth (Ripley et al., 1999).

5.5.3 Crustal contamination

The range in the initial Os and Nd isotopic composition of the anorthosites of the KIC indicates increasing contamination with crustal material from the less evolved dark to the more evolved white anorthosites. The radiogenic Os isotopic composition and the presence of trace amounts of sulfide in the leucogabbronorite of the white anorthosite suite with highly radiogenic initial $^{187}Os/^{188}Os$ suggest the involvement of old crustal material with at least minor proportions of sulfide. The upper crust-like Nd isotopic composition and high concentrations of lithophile trace elements (Gleißner et al., 2010) of this sample are in agreement with bulk assimilation of crustal material.

Quantitative modelling of crustal contamination in sulfide-undersaturated melts is complex for three reasons (Sproule et al., 2002): 1) Os and Re concentrations of both, parental melt and crustal contaminant are poorly constrained. Recalculation of HSE contents in the melt from measured concentrations in magmatic phases is hampered by unknown partition coefficients and element redistribution during cooling. 2) Concentrations and Re/Os of the melt may change during igneous evolution, as for instance during fractional crystallization of chromite and associated HSE-bearing phases (O'Driscoll et al., 2009), although this does not change the Os isotopic composition of the melt during closed system fractionation. 3) Selective assimilation of crustal sulfide may lead to an overestimation of the amount of crustal contamination.

For a tentative approach and comparison to previous estimates it seems reasonable to assume that the crustal contamination is a binary mixing process and that no sulfide segregated from sulfur undersaturated magma. The Os isotope composition of the initial uncontaminated melt of the KIC is assumed to be close to that of the contemporaneous mantle. The Os isotopic composition of the Epupa Complex was estimated according to its Nd mantle separation ages of 2.0 - 2.5 Ga (Gleißner et al., in press) and $^{187}Re/^{188}Os$ ratios of 50 - 150, as reported for felsic crustal rocks (Peucker-Ehrenbrink & Blum, 1998; Saal et al., 1998; Ripley et al., 1999; Lambert et al., 2000; Day et al., 2008).

Our calculation is based on $Os_{melt}/Os_{contaminant}$ ratios, because of the difficulty to estimate absolute concentrations. The fractionated HSE patterns of the anorthosites suggest early fractionation of mafic minerals, and later fractionation of Fe-Ti oxides (see section 5.5.5). Such a fractionated melt should contain significantly lower Os than primitive mantle-derived melts. If we assume a $Os_{melt}/Os_{contaminant}$ ratio of 0.33 for the mixture and an average $^{187}Re/^{188}Os$ value of 150 for the assimilated crust, less than 10 % and ~30 % crustal contamination are obtained for the most radiogenic dark anorthosite and the white anorthosite of the KIC, respectively (Fig. 5.10). Similar contamination ratios were obtained using trace element and Nd-O isotope data (Gleißner et al., 2010, in press).

Despite the uncertainties of this approach, two important conclusions can be drawn. First, an early fractionation event which possibly lowered the Os concentration of the primitive magma should make the Os isotopic composition of the remaining melt much more sensitive to crustal contamination. Secondly the contaminant in the KIC was highly radiogenic implying high $^{187}Re/^{188}Os$. Although

basement samples have not been analyzed in the present study, high $^{187}Re/^{188}Os$ of >100 were observed for felsic gneisses from different localities (see Fig. 3 of Hannah & Stein, 2002). For a better understanding and more detailed modelling of interaction between mantle-derived melt and the crust, further work is required on Re-Os and HSE systematics in crustal rocks and how partial melting of such rocks affects HSE budgets of partial melts (i.e. potential crustal contaminants) and their residues.

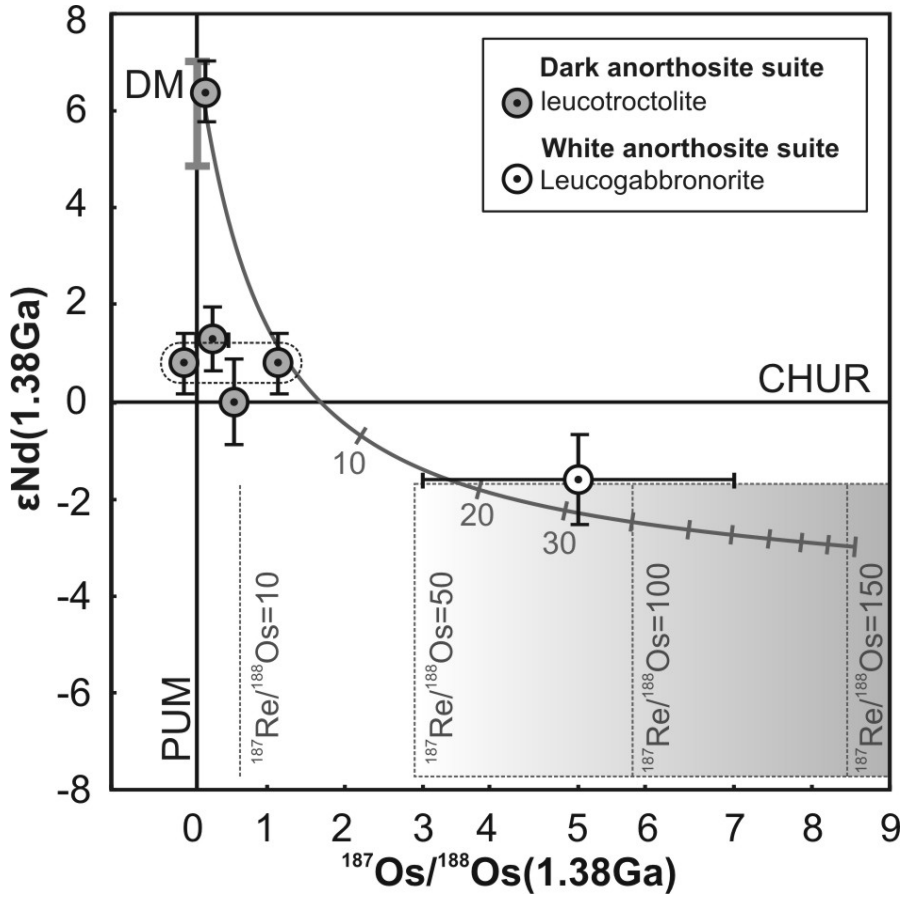

Fig. 5.10. Os and Nd isotopic composition of anorthositic rocks of the Kunene Intrusive Complex and Epupa Complex basement rocks at the time of anorthosite formation. Nd isotope data taken from Gleißner et al. (in press). The composition of the depleted mantle is taken from DePaolo (1981), Goldstein et al. (1984) and Meisel et al. (2001). The Os isotopic composition of the Epupa Complex (shaded field) is estimated according to Nd model ages of 2.0 - 2.5 Ga (Gleißner et al., in press) and $^{187}Re/^{188}Os$ ratios of 50 - 150. Ticks on mixing curve represent 10 % increments of contamination of the parental melt with Epupa Complex crust.

5.5.4 HSE partitioning during fractional crystallization and post-cumulus re-equilibration of Fe-Ti oxides

The HSE are commonly enriched in metals and sulfides. In absence of those phases their solubility and partitioning behaviour in oxide and silicate phases are believed to govern the geochemistry of the HSE in magmatic systems (Capobianco et al., 1994; Righter et al., 2004). Relatively few HSE

abundance data have been published for natural oxide minerals like magnetite and Al-spinel and almost no data for ilmenite exists so far. Some previous studies of natural samples indicate that in mafic to silicic magmatic rocks, magnetite appears to be an important host of Re (Righter et al., 1998; Shirey & Walker, 1998; Hart et al., 2002).

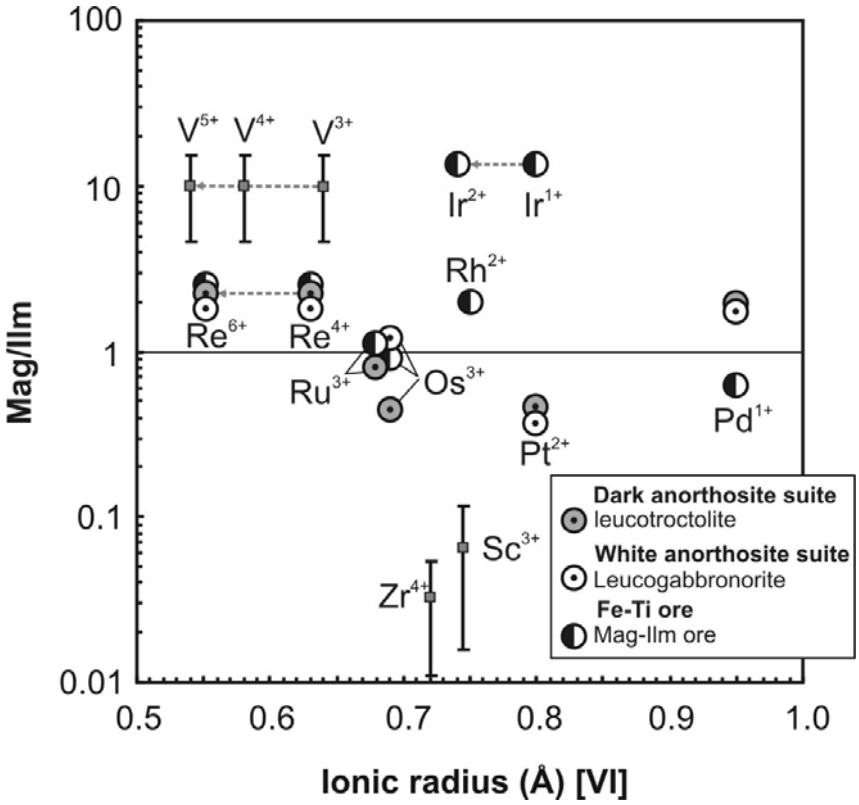

Fig. 5.11. Ionic radius versus relative distribution of highly siderophile elements between magnetite and ilmenite in anorthositic rocks and Fe-Ti ore of the Kunene Intrusive Complex. The ionic radius in octahedral coordination (Shannon, 1976) is displayed according to their dominant valence state at oxygen fugacity close to FMQ (compiled by Ertel et al., 2008). The ionic radii of Os^{3+}, Ir^{1+}, Ir^{2+} and Pd^{1+} were extrapolated from the data of Shannon (1976) for the higher oxidation states. Additionally, LA-ICP-MS data for transition elements of Franke (2009) and Gleißner et al. (2010) are shown for comparison. The squares and error bars give the average value and range for the LA-ICP-MS data of the anorthosites and Fe-Ti ore. The ionic radii of redox-sensitive elements like Re and V are displayed for different valence states.

In several studies of Re-Os and HSE in oxide minerals it has been shown that small sulfide inclusions in oxides dominate or at least contribute to the measured concentrations of these elements (e.g. Morgan et al., 2000; Barnes et al., 2004). In samples of the present study, sulfides were observed as common accessories of leucogabbronorite, while only trace amounts occur in the Fe-Ti ores, and no sulfides were observed in leucotroctolite of the dark anorthosite suite. From mass balance calculations for HSE abundances in bulk rocks and mineral separates and the general increase of Os with the sulfur content of the whole rocks we suspect the presence of a small amount HSE-rich sulfide phase disseminated in the rocks. Separated oxides show different concentrations and distinct relative enrichments and depletions of HSE when compared to the whole rocks. We therefore assume that our

HSE abundance data on oxide minerals represent mostly intrinsic HSE concentrations with only minor contribution from sulfides or other inclusion phases. In leucogabbronorite, separated pyrite differs significantly from the HSE patterns of the oxide minerals, in particular by having lower Os/Ir. Here, neither the concentration of HSE (Fig. 5.4) nor the Os isotopic composition (Fig. 5.8b) would support the notion that pyrite inclusions dominate the HSE budget of magnetite and ilmenite separates.

The internally disturbed Re-Os isotope systematics of the samples (see discussion above) suggests redistribution of Re and maybe Os and other HSE during subsolidus re-equilibration of Fe-Ti oxides. The distribution of HSE between magnetite and ilmenite separates of the three rock suites allows some general inferences (Fig. 5.11). Palladium and Re display consistent preference for magnetite over ilmenite (Mag/Ilm = 1.8 - 2.5) whereas Pt is more abundant in ilmenite (Mag/Ilm ~0.4), with magnetite of the Fe-Ti ore as a notable exception. Unlike the other samples the latter is lower in Pd and much higher in Pt than corresponding ilmenite. The high Pt value (51 ppb) exceeds the whole rock value, of which magnetite is the major constituent, by three orders of magnitude. The chondrite-normalized pattern of the bulk rock and ilmenite also display enrichment of Pt, indicating that the presence of an unknown Pt-rich micro-phase is likely (Fig. 5.6c).

Platinum, which in basaltic melt is dominantly divalent (Ertel et al., 2008 and references therein), has an ionic radius only slightly larger than Fe^{2+} and therefore most likely substitutes in octahedral Fe^{2+} positions. In ilmenite the Fe^{2+} octahedral position is enlarged due to adjustment of the anions away from the layers with the larger cations (Waychunas, 1991) and substitution therefore should be facilitated. The correlation of divalent Pt with monovalent Au and Pd in ilmenite of three different rock types (Fig. 5.4c-e) may indicate coupled substitution of Pt^{2+} and the large Au^{1+} ion, whereas the slightly smaller Pd^{1+} does not fit so well to the structure. No correlation of these elements with Re occurs for the oxide minerals, indicating a different substitution mechanism for Re.

Rhenium in the bulk rocks is correlated with Fe, which in turn reflects the modal proportion of oxides (Fig. 5.4f), hence, suggesting compatible behaviour of Re in fractionating Fe-Ti oxides (e.g. titanomagnetite). This is in good accordance with experimental results. At oxygen fugacities close to FMQ, Re is found to exist mainly in tetravalent state and having a partitioning behaviour similar to Ti^{4+} (Mallmann & O'Neill, 2007). Thus, during post-cumulus re-equilibration, Re is expected to partition into the ilmenite structure like Zr^{4+} or Sc^{3+}. However, like V^{4+} which is similar in size and charge to Re^{4+} and Ti^{4+}, Re is hosted mainly in magnetite (Fig. 5.11). Magnetite occurs also in the more differentiated lithologies of most layered mafic intrusions. It is often markedly enriched in V in those horizons where it first appears as a cumulate phase (Frost & Lindsley, 1991 and references therein). Equal partitioning of V between magnetite and ilmenite was observed for Fe-Ti ore from the Suwałki massif-type anorthosite (Speczik et al., 1988). The preferred incorporation of Re and V in magnetite instead of ilmenite in the Kunene anorthosite complex may be related to their electronegativity similar to Fe and higher than Sc and Zr. Alternatively or in combination with the

electronegativity they can be better accommodated to the larger size of the octahedral position in magnetite when compared to the ilmenite structure.

The interpretation of Os, Ir, Ru and Rh distribution is limited by the low concentrations and unknown amount of sulfide inclusions. Regarding the magnetite/ilmenite distribution Os^{3+} and Ru^{3+} are similar in size and charge (Fig. 5.11) and seem to partition almost equally between magnetite and ilmenite, whereas Ir^{1+} is found mainly in magnetite.

The coarse-grained Al-spinel of the Fe-Ti ore is interpreted as result of exsolution from high-Al magnetite and textural coarsening (Franke, 2009). The high concentrations of Ru and Rh imply their preferred incorporation in the Al-spinel structure, and confirm experimental work by Capobianco et al. (1994). Rh^{2+} is similar in size to divalent transition metals like Co and Zn which are preferentially incorporated in spinel (Franke et al., 2009). The observed fractionation of Ru from Os during spinel exsolution from magnetite, although similar in size and charge in trivalent state, might imply a more reduced valence state of Ru^{2+} and ionic radius similar to Rh^{2+}.

5.5.5 HSE fractionation during magmatic evolution of the KIC

In the previous section we discussed the influence of post-cumulus redistribution of HSE among oxide phases in individual samples. The Re-Os isotope systematics of the whole rock samples, however, indicate that almost no redistribution of Re and Os at the bulk sample scale occurred (see discussion above). Hence the HSE budget of the bulk rocks is assumed to reflect the distribution in cumulate minerals and variable amounts of trapped liquids. All anorthositic rocks of the Kunene Intrusive Complex display strongly fractionated chondrite-normalized HSE patterns. As indicated by the data on mineral separates, these HSE patterns reflect the composition of the cumulus phases and their formation from highly fractionated melt compositions (Figs. 5.5 and 5.6).

The abundance of HSE in basaltic rocks depends on melting processes and degree of melting of the source (e.g. Rehkämper et al., 1999; Bézos et al., 2005; Ballhaus et al., 2006; Mallmann & O'Neill, 2007; Dale et al., 2008; Righter et al., 2008) and subsequent reactive infiltration during transport in the mantle and fractional crystallization in the crust (e.g. Becker et al., 2001; Puchtel & Humayun, 2001; 2004; Pitcher et al., 2009). During fractional crystallization of olivine and chromite, Os, Ir, and Ru behave compatibly in sulfide undersaturated basaltic melts under reducing conditions (~FMQ), whereas Rh, Pt, Pd, Re, and Au are incompatible and tend to be enriched in the residual liquid until sulfide saturation is reached (e.g. Barnes et al., 1985; Puchtel & Humayun, 2000, 2001, Righter et al., 2004; Brenan et al., 2005; Day et al., 2008; Pitcher et al., 2009). Early-magmatic fractional crystallization of olivine, chromite and inclusions of platinum group metals and alloys would effectively deplete Os, Ir and Ru from the mafic parental melt and would also be in accordance with the mantle source model of anorthosite petrogenesis. Early fractionation of olivine and chromite also

seems to be the reason for the intermediate magnesium numbers and low chromium contents of massif-type anorthosites (e.g. Ashwal, 1993).

The most conspicuous feature of most KIC chondrite-normalized HSE patterns is the strong enrichment of Re compared to other incompatible HSE, such as Pd and Au, in particular in the white anorthosite (Fig. 5.5). On the other hand, the weak enrichment of Re in leucotroctolite with the least modal abundance of oxides (Ku-98-228) suggests that the Re enrichment over Pd and Au may be no feature of the parent melt, but may be controlled by the abundance of cumulus oxides. From its correlation with the bulk Fe content we argue for compatible behaviour of Re in fractionating titanomagnetite (see section 5.5.4). The oxide-rich leucotroctolite and the Fe-Ti ore samples display strong enrichment of Re whereas in the gabbroic anorthosite, which may have crystallized from melt after significant plagioclase and Fe-Ti oxide fractionation, Re is below the detection limit (10 ppt). This interpretation is in good accordance with the results of Righter et al. (1998) who suggested magnetite control on Re abundances in reduced sulfide-undersaturated magmatic systems.

All leucotroctolites display nearly parallel chondrite-normalized HSE patterns and negative Ir anomalies (Fig. 5.5a). The constant trace of this anomaly in almost al oxide mineral separates (Fig. 5.6) argues for a generally higher incompatibility of Ir in the accumulating oxide assemblage. From the obvious discrepancy in charge and ionic radius, differences in partition behaviour between the smaller Os^{3+} and Ru^{3+} ions and the larger Ir^{1+} seem likely (Fig. 5.11).

According to previous studies (e.g. Barnes et al., 1985; Puchtel & Humayun, 2001; Bézos et al., 2005) sulfide segregationis the main cause of PGE depletion in mafic magmas during differentiation. Based on closed system fractionation in the Kiglapait intrusion, Scoates & Mitchell (2000) argue that sulfide-saturation occurs late in the crystallization history of high-Al basaltic magmas. In the KIC, which may have developed from a high-Al basalt precursor magma, the low fO_2 (Drüppel et al., 2001) and fS_2 (von Seckendorff et al., 2000) that prevailed during magmatic evolution are unfavourable for early sulfide saturation (see discussion in Righter et al., 1998). The measured sulfur contents are low in the leucotroctolites of the dark anorthosite (38 - 184 ppm) but demonstrate that at least a small amount of sulfides occur and contribute significantly to the HSE budget (see section 5.5.4). The extremely low sulfur and HSE concentrations in gabbroic anorthosite (Fig. 5.4g) argue for fractionation of a sulfide component prior to entrapment of the residual melt in the cumulates.

Sulfides are present in the white anorthosite suite where sulfide saturation possibly occurred during increase of fO_2 and fS_2 after crustal contamination of the parental melt. The higher S content together with high Pd and Re accompanied by the highly radiogenic initial $^{187}Os/^{188}Os$ ratio of the leucogabbronorite may indicate assimilation of sulfide-bearing crustal material (Fig. 5.4h). On the other hand the observed chondrite-normalized HSE pattern of pyrite displays a similar enrichment of Re like the oxides. Together with the anomalously low Os/Ir ratio this argues against a primary magmatic pattern of the separated pyrite. Von Seckendorff et al. (2000) argued for the replacement of igneous pyrrhotite by pyrite during contemporaneous sulfidation and oxidation of Fe-Ti oxides in the

white anorthosites. The HSE were possibly incorporated selectively (according to local availability and oxidation conditions) into pyrite during such a post-magmatic processes.

5.6 Conclusions

The highly siderophile element abundances and osmium isotope composition of anorthositic rocks and Fe-Ti ores of the Kunene Intrusive Complex place constraints on source and magmatic evolution of the parental melt. The Os isotope composition of leucotroctolite of the dark anorthosite suite overlaps within uncertainty with that of the contemporaneous mantle, suggesting that the source of the parental melt was most likely the mantle. Chondrite-normalized HSE abundances of anorthositic bulk rocks and oxide mineral separates display fractionated patterns that are considered to reflect crystallization from a melt composition that previously was subject to fractional crystallization of mafic minerals (possibly including platinum group minerals). The Os concentration of the differentiated melt was lower than commonly invoked for primitive mantle-derived melts and made the Os isotopic composition very sensitive to crustal contamination. A leucogabbronorite sample, which was subject to a larger extent of crustal contamination, displays higher content of S, Pd and Re and a highly radiogenic initial Os isotope composition, consistent with assimilation of crustal material.

From the observed fractionation patterns and high $^{187}Re/^{188}Os$ ratios, contamination ratios of <10 % for the dark anorthosites and ~30 % for the white anorthosites have been calculated, consistent with results from trace element, stable and lithophile radiogenic isotope modelling. Similar radiogenic initial Os isotopic compositions were observed in other massif-type anorthosites and indicate that variable interaction with middle to upper crust may be a general process during the evolution of anorthosite complexes.

The abundance of HSE in the KIC rocks is dominated by Fe-Ti oxides and traces of sulfides. Rhenium in the anorthosites and especially in the related Fe-Ti ore is mainly controlled by the modal proportion of Fe-Ti oxides. The observed correlation with iron suggests compatible behaviour of Re in fractionating titanomagnetite which seem to play an important role in affecting the Re budget of mafic magmas. The chondrite-normalized HSE patterns of leucotroctolite of the dark anorthosite suite display conspicuous negative Ir anomalies which, together with similar anomalies in the oxides, most likely reflect higher incompatibility of Ir than Os and Ru in the fractionating oxide assemblage.

The Os isotopic composition of the associated Fe-Ti ores is consistent with the observed preferred incorporation of Re in fractionating titanomagnetite and indicate both, contemporaneous and consanguineous relation of the ores with the hosting anorthosites. During post-cumulus re-equilibration of the Fe-Ti oxides in anorthosites and Fe-Ti ore Re displays preference for magnetite whereas Pt partitions mainly into ilmenite.

Chapter 6
Summary and conclusion

6.1 Summary of the results from petrographic, chemical and isotope analysis

Two successively emplaced anorthosite varieties have been recognized in the Mesoproterozoic Kunene Intrusive Complex. The older white anorthosite suite consists of pyroxene-bearing anorthosite and leucogabbronorite associated with Fe-Ti ores, whereas the younger dark anorthosite suite is dominated by olivine-bearing anorthosite and leucotroctolite. Through the course of this study, the anorthositic rocks of the Kunene Intrusive Complex were characterized for their mineral chemical, isotope, major and trace element compositions. The outcome of this study is briefly summarized in the following paragraphs.

6.1.1 The white anorthosite suite

The samples of the white anorthosite suite display the magmatic mineral assemblage of cumulus plagioclase (An_{39-64}) ± cumulus orthopyroxene (X_{Mg} 0.57 – 0.72) + interstitial ortho- and clinopyroxene (X_{Mg} 0.57 – 0.78) + ilmenite ($Ilm_{82-95}Pyr_{3.7-14}Hem_{0.7-3.6}$) ± magnetite ($Mag_{96-99}Ulv_{0.5-3.5}Chr_{0.0-1.7}$). Late magmatic biotite and amphibole may surround pyroxene and Fe-Ti oxides and contain euhedral inclusions of apatite. Occasionally, accessory zircon and sulfides occur. Anorthositic rocks of the white anorthosite suite are rich in Al_2O_3 (15 – 30 wt.%), CaO (8 – 14 wt.%), Na_2O (2 – 5 wt.%) and Sr (400 – 800 ppm), reflecting high amounts of cumulus plagioclase. Variable abundance of Mg-Fe silicates and Fe-Ti oxides result in variations of FeO_T (1 – 11 wt.%) and MgO (0.1 – 8 wt.%) with X_{Mg} values between 0.34 and 0.72.

The rocks of the white anorthosite suite are enriched in incompatible lithophile trace elements like Ba, Sr and the LREE. Chondrite-normalized REE patterns display an enrichment of LREE over MREE (La_N/Sm_N 1.9 – 6.5) and HREE (La_N/Yb_N 8.2 – 30.6), and positive europium anomalies (Eu/Eu* 2.0 – 7.0), typical to plagioclase cumulate rocks.

Plagioclase display irregular oscillatory zoning in major elements with a variation of the anorthite content of less than 3 mol.%. The trace element budget is characterized by high Sr contents (600 – 1100 ppm) and variable concentrations of incompatible trace elements. In general, the chondrite-normalized REE patterns of plagioclase display enrichment of LREE (La_N/Sm_N 5 – 22) and strong positive europium anomalies (Eu/Eu* 13 – 27). The crystals display zoning in trace element content with increasing concentrations from core to rim and toward adjacent medium-sized plagioclase. The trace element record of the interstitial phases reflects much of the evolution of the magma during

plagioclase fractionation (e.g. negative europium anomalies) and contamination (absence of europium anomalies).

The oxygen isotopic compositions of separated plagioclase of the white anorthosite suite range from 6.2 to 6.8 ‰ $\delta^{18}O$. The initial isotopic composition of lithophile trace elements of bulk rocks and separated plagioclases overlaps with mantle values and reveal increasing crustal influence in the order of strontium ($^{87}Sr/^{86}Sr$ 0.7031 – 0.7043), neodymium ($^{143}Nd/^{144}Nd$ 0.5110 – 0.5107; εNd +2.1 to -3.1), and lead ($^{206}Pb/^{204}Pb$ 16.21 – 17.09). The highly siderophile element abundances of a leucogabbronorite sample of the white anorthosite suite display a fractionated chondrite-normalized pattern with enrichment of P-PGE over I-PGE (Pt_N/Os_N 14) and high Pd and Re (Re_N/Os_N 3949). The initial osmium isotopic composition is highly radiogenic ($^{187}Os/^{188}Os$ 5 ± 2; γOs +3982).

6.1.2 The dark anorthosite suite

The dark anorthosites display the primary magmatic assemblage of cumulus plagioclase (An_{53-65}) + olivine (Fo_{56-74}) + interstitial ortho- and clinopyroxene (X_{Mg} 0.64 – 0.74) + ilmenite ($Ilm_{88-98}Pyr_{0.6-13}Geik_{0.0-9.7}Hem_{0.2-4.4}$) ± magnetite ($Mag_{97-99}Ulv_{0.0-2.5}Chr_{0.0-2.7}$) ± biotite. Al_2O_3 and CaO contents are generally higher than those of the most white anorthosite and increase with X_{Mg} from the white towards the dark anorthosite suite, reflecting higher anorthite content of plagioclase and the predominance of Mg-rich olivine over pyroxene in the dark anorthosites. Concentrations of incompatible trace elements such as K, Sr, Ba and Zr, on the other hand, are generally lower in the dark anorthosite suite.

The dark anorthosites display lower absolute trace element concentrations except for Ni, attributed to the abundance of olivine. The chondrite-normalized REE patterns also show enrichment of LREE over MREE (La_N/Sm_N 2.1 – 4.3) and HREE (La_N/Yb_N 3.2 – 29.4), and positive europium anomalies (Eu/Eu* 3.3 – 7.1).

The majority of plagioclase is characterized by large-scale wavy oscillatory zoning with variations in the anorthite content of up to 5 mol.%. Plagioclase of the dark anorthosite suite has lower Sr contents (400 – 750 ppm) and a lower concentration of incompatible trace elements than that of the white anorthosite. The chondrite-normalized REE patterns display enrichment of LREE over M+HREE (La_N/Sm_N 3 – 10) and positive europium anomalies (Eu/Eu* 7 – 18). All plagioclases show decreasing Sr concentrations from coarse towards medium-grained crystals by a factor of ~5, consistent with its compatible behaviour during plagioclase crystallization. Negative europium anomalies in interstitial clinopyroxene reflect their cystallization from intercumulus liquid after extensive plagioclase fractionation.

The oxygen isotope composition of separated plagioclase of the dark anorthosite suite ranges from 5.6 to 6.2 ‰ $\delta^{18}O$ and overlap with typical mantle values. The initial isotopic composition of bulk rocks and separated plagioclases fall in the compositional field of strongly depleted to undepleted

mantel for strontium and neodymium ($^{87}Sr/^{86}Sr$ 0.7028 – 0.7036; $^{143}Nd/^{144}Nd$ 0.5112 – 0.5109; εNd +6.4 to +0.8) and close to upper crustal values for lead ($^{206}Pb/^{204}Pb$ 16.18 – 16.94). The highly siderophile element abundances of leucotroctolites of the dark anorthosite suite also display fractionated chondrite-normalized pattern but lesser enrichment of P-PGE and Re over I-PGE (Pt_N/Os_N 2 – 16; Re_N/Os_N 83 – 454). The initial osmium isotopic composition ranges from $^{187}Os/^{188}Os = 0.2 \pm 0.1$ (γOs +48) to 1.14 ± 0.06 (γOs +872). The value of the most primitive leucotroctolite overlaps in uncertainty with the composition of the mantle.

6.2 Origin and nature of the parental melt

The source of the parental melts is critical for petrogenetic modeling and further interpretation of Proterozoic anorthosites. The importance of source and composition of the parental melts for tectonic and crystallization modeling was stressed by many authors (Ashwal, 1993, 2004; Scoates, 2004, 2008; Longhi, 2005; Morse, 2006) and has major influence on outstanding interpretations of the 'anorthosite problem' especially in the context of changing tectono-thermal conditions in the mantle-crust system through time.

In the Kunene Intrusive Complex two successively emplaced anorthosite varieties have been recognized. The most conspicuous difference between the two anorthosite varieties is the occurrence of olivine in the dark anorthosites in contrast to the prevalence of orthopyroxene in the white anorthosites in combination with the occurrence of apatite and OH-bearing phases. In correlation with the change in anorthite content of the plagioclase from labradorite-type (dark anorthosite) to andesine-type (white anorthosite) these data indicate a significant change in composition of the magma from which the two anorthosite varieties crystallized. In the present study advantage is taken of this circumstance to characterize chemical features and isotopic compositions of their magmas and to elucidate their source and composition.

6.2.1 The source of the parental melt

The dark anorthosites of the KIC show no major petrographic evidence for crustal contamination and display the highest initial $^{143}Nd/^{144}Nd$ and the lowest $\delta^{18}O$ values and, therefore, represent the closest estimate for the composition of the primitive parental melt. The oxygen isotope composition of separated plagioclase is particularly suitable for constraining the character of the parental melt and hence their source because only minor fractionation occurs during crystallization of plagioclase from the melt. The data of the dark anorthosite suite reflect melt values of ~5.3 to 5.8 ‰ $\delta^{18}O$, which perfectly overlap with those of unmetasomatized mantle (Fig. 3.8). Plagioclase of the white anorthosite suite display higher values (>6.2 ‰ $\delta^{18}O$) and imply the influence from a crustal reservoir. When compared to published data on massif-type anorthosites, the range the KIC plagioclase $\delta^{18}O$

values overlap with the range of plagioclase of the Rogaland Complex (Fig. 6.1). The even higher values of some anorthosites of northern America (e.g. Marcy of the Adirondack Mountains and Morin) are interpreted to result from large crustal input from supracrustal components including metasediments (Morrison & Valley, 1988; Peck & Valley, 2000).

The characteristics of the mantle-source can be derived from the isotopic record of lithophile trace elements of the anorthosites in more detail. The observed interval in $^{143}Nd/^{144}Nd_i$ from 0.5112 to 0.5111 (εNd_i +6.4 to +3.8) of the most primitive dark anorthosite samples falls in the compositional range of typical depleted mantle. The deviation from $^{143}Nd/^{144}Nd$ values expected in a chondritic uniform reservoir (CHUR) corresponds to a mantle source which has been progressively depleted in lithophile elements through time. According to the crust-mantle evolution models of DePaolo (1981) and Goldstein et al. (1984) such values are typical to upper mantle that was subject to previous melt extraction. Along with the oxygen isotope composition, the observed Nd isotopic composition is the strongest argument for a mantle origin of the anorthosites. The strongly depleted initial values of the most primitive dark anorthosites make remelting of an older lower crustal source very unlikely (see discussion in section 4.5.2).

The alternative model that the source region of the parental melts of massif-type anorthosites lies in the lower crust, deduced mainly from phase equilibria and fractional crystallization modelling of designated parental melt compositions (Vander Auwera et al., 1998, Longhi et al., 1999), received backing from two recent studies of the Os isotope compositions of sulfides and oxides in anorthosites. Schillerup et al. (2000) and Morgan et al. (2000) reported crustal initial Os isotopic compositions from the Rogaland (Norway) and the Suwałki (Poland) anorthosite complexes. Both concluded that crustal contamination of a mantle-derived magma requires unrealistic crustal compositions and contamination ratios and therefore suggest direct melting of a mafic source region in the lower crust, supporting the crustal tongue melting model of Duchesne et al. (1999). The osmium isotopic compositions of the KIC anorthosites combined with the abundances of highly siderophile elements reveal that initial crustal values do not necessarily imply a crustal origin of the rock suite. Nonetheless, the very low abundance of Os in the anorthosites and the uncertain Os isotopic composition of crustal rocks inhibit better characterization of the mantle source and crustal contaminants from these data.

The new isotope and trace element data of the dark and white anorthosite suite of the Kunene Intrusive Complex demonstrate that they originate from a mantle-derived parental melt that was subject to variable amounts of crustal contamination. Consistently, the isotope compositions of oxygen, strontium, neodymium and osmium range from mantle-like values in the dark anorthosite suite towards more crustal-like vales in the white anorthosite suite. At the same time the overall concentrations of lithophile incompatible trace elements increase in the bulk rocks as well as in the cumulus plagioclases (a feature that only in parts originate from the crystal-chemical control on the partition of trace elements). All observed features are consistent with crustal contamination of an initially mantle-derived parental melt. The crustal contamination was dominant in the early stage of

KIC magmatism and hence had led to the formation of the white anorthosite, which displays significant crustal characteristics. The characteristics of the slightly younger dark anorthosite suite are consistent with its formation from an olivine-normative melt that had mantle isotopic composition and received less crustal additions. Anorthosite formation in the KIC can therefore be interpreted as a mantle-derived crust-forming process without the need for large-scale melting of a lower crustal source. Conformably, the isotopic record of both anorthosite suites clearly demonstrates that the source of their primary melt was the upper mantle.

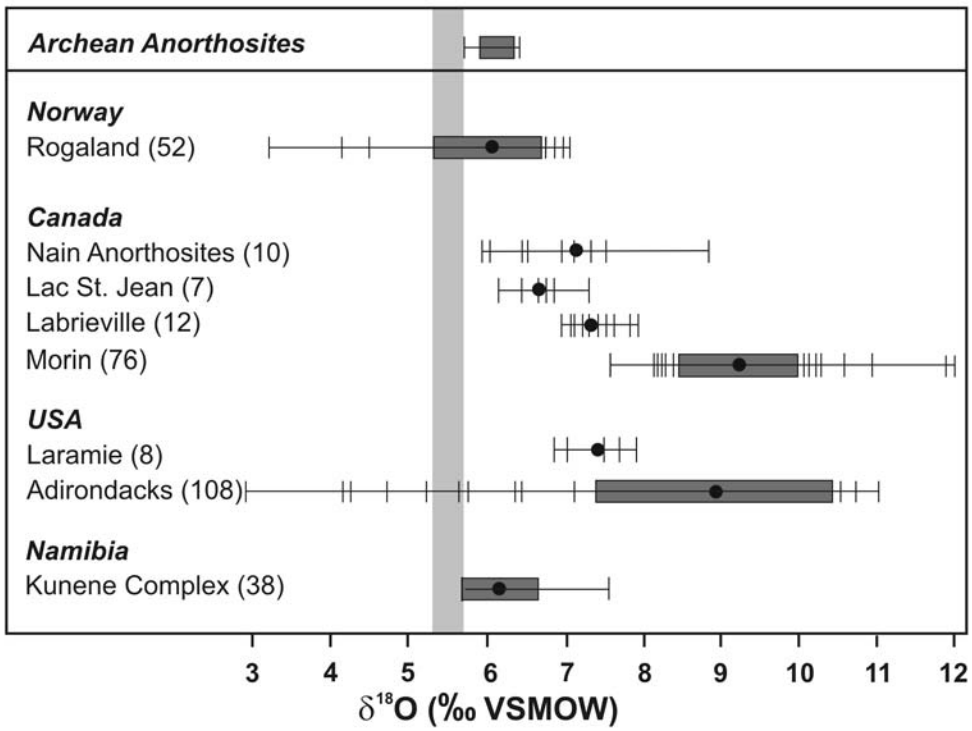

Fig. 6.1. Compilation of $\delta^{18}O$ whole-rock and plagioclase values for Proterozoic anorthosites (modified after Peck & Valley, 2000). Values in parentheses are the number of analyses, filled circles give average values. Shaded rectangle encloses ± 1σ in data sets n >12. The shaded bar illustrates the range of mantle values after Eiler (2001). Archean anorthosites, which as a group have uniform $\delta^{18}O$ values in equilibrium with mantle melts, are shown for reference (Peck & Valley, 2000 and references therein).

6.2.2 The composition of the parental melt

The composition of the parental melt is relevant to any discussion about the magmatic evolution of anorthosites and possible consanguineous rocks. High-Al dykes and marginal rocks of several anorthosite massifs were interpreted to represent chilled parental melt compositions. Major element data of these designated parental melts of massif-type anorthosites are shown in Figure 6.2. Displayed are values of anorthositic dykes of the Nain Complex, interpreted as hyperfeldspatic liquids (Wiebe, 1990), primitive and evolved ferrodiorites of the Rogaland Complex (Vander Auwera et al., 1998) and the Nain Complex (Emslie et al., 1994) which are believed to represent chilled melt compositions, and

olivine-normative high-Al basaltic dykes of the Harp Lake, Nain and Laramie Complex, considered to represent younger samples of the parental melt (Scoates & Mitchell, 2000). Recent experimental work on these proposed parental melt compositions reveal that the phase equilibria of anorthositic dykes do not represent crystallised melt compositions (Fram & Longhi, 1992). The experimental liquidus equilibria of proposed parental melt compositions like ferrodiorite (primitive jotunite) and synthetic high-Al gabbro fall on opposite sides of a thermal divide on the plagioclase + pyroxene liquidus surface (Longhi et al., 1999). The authors conclude that mantle-derived melts can not produce the full range of troctolitic-noritic to troctolitic-gabbroic mineral assemblages observed in anorthosite massifs without extensive low-pressure granite assimilation and proposed a mafic lower crustal source.

None of the KIC younger intrusions or dyke compositions fit to the compositional fields of proposed parental melts. Moreover, as discussed in section 1.1.6 the composition of the parental melt is not accessible from the composition of the anorthosites itself. However, element ratios like Fe/Mg of the parental melt can be estimated from the composition of Fe-Mg silicates. The X_{Mg} of olivine of the dark anorthosite suite ranges from 0.55 to 0.74 which should be in equilibrium with melt X_{Mg} of 0.30 - 0.49 using fractionation coefficients of Ulmer (1989) and Toplis (2005). Since variations in liquidus temperature and pressure do not alter the partition of Fe and Mg between melt and olivine significantly, the results constrain the X_{Mg} for a large range of crystallization depths (Fig. 6.2). Despite the uncertainties of this approach it demonstrates that primitive ferrodioritic melts (X_{Mg} 0.34 - 0.40) can not fractionate the entire range of observed compositions of olivine in the dark anorthosites. The X_{Mg} range of high-Al basaltic dykes (0.43 - 0.63; Scoates & Mitchell, 2000), observed in many anorthosite complexes, on the other hand, overlaps with values calculated for melt in equilibrium with the most Mg-rich olivine of the KIC (Fig. 6.2) and most other massif-type anorthosites (see Fig. 3.5). Although, positive strontium and europium anomalies of many high-Al basaltic dykes (Scoates & Mitchell, 2000; see also Fig. 3.10) demonstrate that they contain a significant amount of cumulus plagioclase and do not represent pure initial melt compositions.

Assuming an overall tholeiitic to calc-alkaline fractional crystallization trend of the KIC parental melt, the composition can be tentatively estimated at ~15 - 17 wt.% Al_2O_3 and X_{Mg} of ~0.5. The younger gabbro and troctolite intrusions in the KIC (described in section 3.5.3) are Al-rich (17 - 22 wt.% Al_2O_3) but their high X_{Mg} of 0.69 - 0.72 (Fig. 6.2) and positive europium anomalies (Eu/Eu* = 1.6) reveal that they contain huge amounts of cumulus clinopyroxene or olivine and significant cumulus plagioclase. Hence these rocks, although primitive in chemical and isotopic composition, can not be interpreted as primitive parental melt equivalents.

In section 3.8.2 a different approach was used to assess information about the parental melt. The trace element compositions of cumulus phases were measured by in situ LA-ICP-MS analysis. By the use of appropriate mineral-melt partition coefficients (Green & Pearson, 1987; Bindemann et al., 1998) the trace element abundances were then inverted to concentrations of the melt they crystallized from. This method is unable to yield major element compositions of the original melt but gives an

estimate of the trace element composition, which provides important information about the magma source as well as previous fractional crystallization and crustal contamination processes.

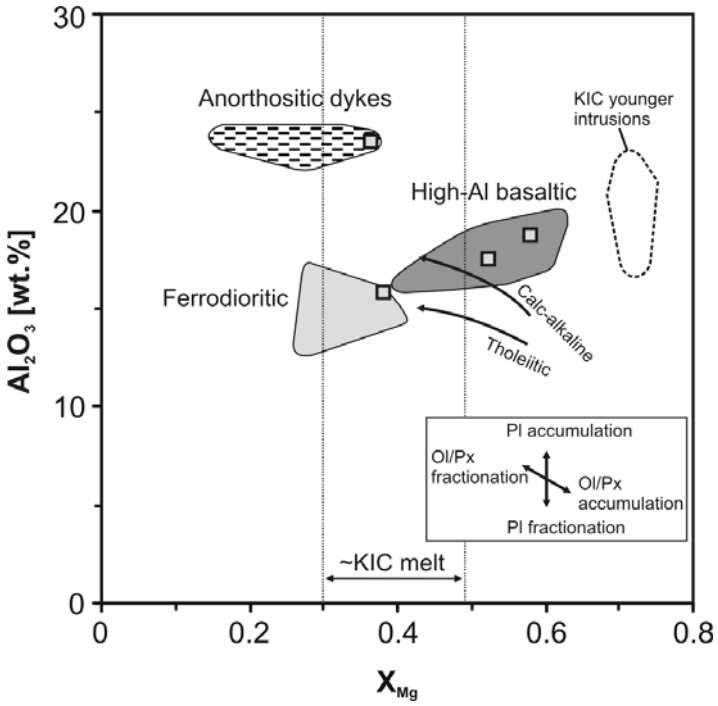

Fig. 6.2. X_{Mg} (Mg/(Mg+Fe)) versus Al_2O_3 for designated parental melt compositions of Proterozoic massif-type anorthosites from the literature (Wiebe, 1990; Emslie et al., 1994; Mitchell et al., 1995; Vander Auwera et al., 1998; Scoates & Mitchell, 2000). Rectangles indicated inferred parental melt compositions used for experiments (Fram & Longhi, 1992; Longhi et al., 1999; Vander Auwera et al., 2000). The X_{Mg} value of crystallizing Fe-Mg silicates is always higher then that of the melt and X_{Mg} of the whole rock is therefore used as a fractionation index. The estimated X_{Mg} range of melt in equilibrium with the olivine of the dark anorthosite suite (KIC) is indicated by dotted lines (see text for explanation). The compositional field of younger high-Al intrusions (troctolites and gabbros) of the KIC is displayed for comparison. The effect of fractional crystallization or accumulation of olivine, pyroxene and plagioclase on the composition of the melt is indicated by arrows. Two general fractionation trends of mafic melts are shown for comparison.

Plagioclase is an early liquidus phase in the anorthosites of the KIC and provides important information on the abundance of trace elements in the parental magma. Ilmenite is the dominant Fe-Ti oxide of both anorthosite varieties and gives additional information about the concentrations of elements excluded from plagioclase (like Nb and Ta). The reconstructed concentrations and ratios of trace elements significantly differ between the two anorthosite varieties and demonstrate that they did not form from the same magma composition. The white anorthosites crystallized from a melt with higher overall trace lithophile element abundance and higher enrichment in LREE when compared to the HREE. The primitive mantle-normalized trace element patterns of this magma are characterized by negative Rb and Sr anomalies, a feature inherited from the assimilated crustal material (see Fig. 4.8). Nb/Ta ratios range from 11.5 to 13.0 and are in good agreement with crustal values of ~11 - 13 (Green, 1995; Barth et al., 2000). The dark anorthosites, on the other hand, crystallized from a melt which shows significantly lower trace element concentrations and a flat primitive mantle- normalized

pattern without accentuated anomalies. The Nb/Ta ratios range from 14.5 to 20.5 overlapping with mantle values of ~17.5 - 17.8 (Green, 1995; McDonough & Sun, 1995).

When compared to designated parental melt compositions, the estimated trace element compositions of the white and dark anorthosite melt display similarities with ferrodioritic (jotunite) and high-Al gabbroic compositions, respectively (see Fig. 3.10). Values calculated from plagioclase of the primitive dark anorthosites, however are more suitable for the calculation of the parental melt composition, since these rocks experienced only minor crustal contamination. It can hence be concluded that the parental melt of the anorthosites was broadly basaltic in composition. In case of the white anorthosites crustal contamination and fractional crystallization produced an evolved melt with ferrodiorite affinities.

6.3 The magmatic evolution and the role of crustal contamination

The magmatic evolution of the KIC needs to be evaluated carefully to understand the processes which connect the primary mantle-derived melt with the high-Al basaltic parental melt and finally with the composition of the exposed plagioclase cumulate rocks. The Al-rich nature and intermediate X_{Mg} values of the melt parental to the anorthosites of the KIC (see section 6.2.2) imply major differentiation processes prior to their formation. Despite the fact that true melt compositions are not preserved, the cumulate nature of the anorthosites suggest that fractional crystallization further changed the melt composition during their formation. The decrease in anorthite component of plagioclase and X_{Mg} of mafic silicates in parts reflects this trend of increasing differentiation. The trace element record of cumulus and interstitial phases further provide important insights into changing melt compositions during assimilation fractional crystallization processes. In order to investigate the genetic relation between the two anorthosite varieties contamination models need to be tested to evaluate the role of crustal contamination in the magmatic evolution of the parental melt.

6.3.1 Fractional crystallization

Plagioclase fractionation and accumulation is a widely accepted petrogenetic process for Proterozoic massif-type anorthosites (e.g. Ashwal, 1993, Duchesne et al., 1999). In contrast, the igneous evolution prior to plagioclase accumulation is still misty. This is mainly because there is no phase that continuously records the entire fractionation process. Moreover, the lithophile trace elements, recorded in cumulus plagioclase, are not very sensitive to prior fractionation of Fe-Mg silicates and oxides. In addition, fractionation coefficients strongly depend on temperature and major element composition of the crystallizing phase which in turn is strongly dependent on the composition of the parental melt and thus the source of the primary melt of the anorthosites.

From the whole set of trace elements the abundance of highly siderophile elements in anorthosites provides the most reliable information about fractionation processes that occurred prior to plagioclase saturation. Although the abundance of HSE is generally low in the KIC rocks, their concentrations can be measured via the isotope dilution technique. The HSE concentrations in the melt cannot be calculated from the abundances in the anorthosites directly, however the fractionated chondrite-normalized patterns, with extremely low I-PGE and increasing abundances towards P-PGE and Re, of bulk rocks and separated oxides are indicative for a strongly fractionated melt (see Fig. 5.5). Such a composition is in accordance with extensive fractionation of olivine, chromite, and/or platinum group minerals (PGM) under relative reducing conditions (~FMQ) from a basaltic to picritic melt. A further outcome of early fractionation of olivine and chromite are intermediate magnesium numbers and low chromium contents, as observed in many massif-type anorthosites (e.g. Ashwal, 1993).

The onset of plagioclase crystallization and its subsequent accumulation to form the anorthosites, offer the first direct insights into the magmatic processes. Their major and trace element compositions provide a record of physical and chemical fluctuations in the parental magma (see Fig. 2.7). The observed large-scale wavy oscillatory zoning of plagioclase is consistent with repeated changes in melt composition (see Appendix A.2.5). Such changes can reflect repeated replenishment with hotter and less differentiated melt or movement of crystallizing plagioclase in a huge magma reservoir. The relative constant variability in anorthite content supports the assumption of a magma chamber which achieves addition of mantle-derived melt. The derivation of anorthosites from a hyperfeldspatic liquid can not completely be denied from the present dataset, but is expected to result in progressively decreasing anorthite content of plagioclase upon fractional crystallization. This process, however, is not in accordance with the observed patterns of plagioclase from the KIC.

The lithophile trace element record of cumulus plagioclase and interstitial phases reveals crustal contamination of the melt both prior and during plagioclase fractionation in the white anorthosite suite. In the dark anorthosite suite the trace element composition of cumulus plagioclase reflect less LREE enriched (more primitive) melt compositions. The trace element budget of its interstitial phases evidences crystallization from the residual intercumulus liquid (see Fig. 3.7). Crustal contamination in an early stage of magmatic evolution is also in good agreement with the radiogenic and stable isotope composition of the two anorthosite varieties. Contamination with broadly quartzofeldspatic material (either gneiss or its partial melt) leads to increasing oxygen and silica activities of the evolved magma. The coupled nature of silica activity and oxygen fugacity drives the melt composition from olivine normative towards orthopyroxene + magnetite normative, faster than simple fractional crystallization would do. Hence olivine-bearing labradorite-type anorthosites and pyroxene-bearing andesine-type anorthosites in the KIC (and maybe also in other massif-type anorthosites) are not related by a fractionation but a contamination process.

Contemporaneous fractional crystallization of plagioclase with Fe-Ti oxides (most likely titanomagnetite) is evident from a decreasing vanadium content of the melt, recorded by plagioclase

trace element zoning profiles (see Fig. 3.6). The Fe-Ti ore present in the white anorthosite suite of the KIC display coarse-grained cumulus textures and mainly comprise strongly exsolved titanomagnetite and minor ilmenite and hercynite spinel. According to Franke (2009) and Franke et al. (2009) they represent titanomagnetite cumulates that evolved from fractional crystallization, gravitational crystal sorting and compaction during later deformation. Accordingly, the V concentrations of these ores are high (0.2 - 0.3 wt.%). Even though the exposed Fe-Ti oxide ore bodies are most likely not derived from titanomagnetite fractionation of their immediate bordering anorthosites, they may represent products of a similar fractionation process. These assumptions in parts are supported by the Os isotopic composition of the Fe-Ti ore and high abundance of Re which seems to behave as a compatible trace element in fractionating titanomagnetite (see Figs. 5.7 and 5.4).

6.3.2 Crustal contamination

One of the most important points in most published petrogenetic models for massif-type anorthosites is the discussion whether chemical and isotopic heterogeneities reflect crustal contamination or source heterogeneity. Composition and isotope data provide valuable information on source, composition, and magmatic evolution of the parental melt but also on the interaction of the melt with crustal material. For the KIC, Drüppel et al. (2007) reported petrographic evidence for assimilation of crustal material in leucogabbronorite of the white anorthosite suite (see Figs. 3.3b and 4.2b). The distribution of lithophile and highly siderophile trace elements and isotope data of this study reveal numerous evidence and details on the crustal contamination processes (summarized in section 6.2.1). However, regarding the proposed crustal contamination of an initially mantle-derived parental melt, it is necessary to explain why the isotopic composition of O, Sr and Nd unquestionably reflect the mantle origin whereas Pb and Os do not.

The calculation of lithophile trace element abundances of the melts together with the isotopic composition of anorthosites and potential contaminants enable us to estimate the amount of crustal contamination of the parental melt (see Fig. 4.8). In Chapter 4 the major impact of the reservoir composition of the parental melt and the crustal contaminant, and the influence of fractional crystallization on the mixing relations between mantle-derived melt and crustal material are demonstrated. The effect of these processes on the isotopic composition of a two-component mixture is shown in Figure 6.3. The Sr isotopic composition of the magma of the KIC is largely controlled by the high Sr content of the parental melt and early plagioclase accumulation. The Nd budget of the magma was significantly lower than that of Sr and the isotopic composition of Nd hence provides a good indicator for increasing crustal contamination. The Pb isotopic signature of a contaminated melt, on the other hand, is entirely dominated by the high Pb concentrations of the crust when compared to the extremely low contents of the mantle-derived parental melt.

For Os the calculation of original melt concentrations is not possible but the highly fractionated HSE patterns point to very low concentrations of Os in both the parental and the evolved melt. Nonetheless, based on some reasonable assumptions derived from the abundance of HSE in anorthositic rocks and oxide minerals of the KIC (see discussion in section 5.5.3), a qualitative calculation of the effect of crustal assimilation on the Re-Os system can be made (see Fig. 5.11). The main outcome of this approach is that the huge Os isotopic contrast between white and dark anorthosite suite of the KIC can be ascribed to a crustal contamination of the same amount as previously calculated from the abundance and isotopic composition of lithophile elements (section 4.5.3).

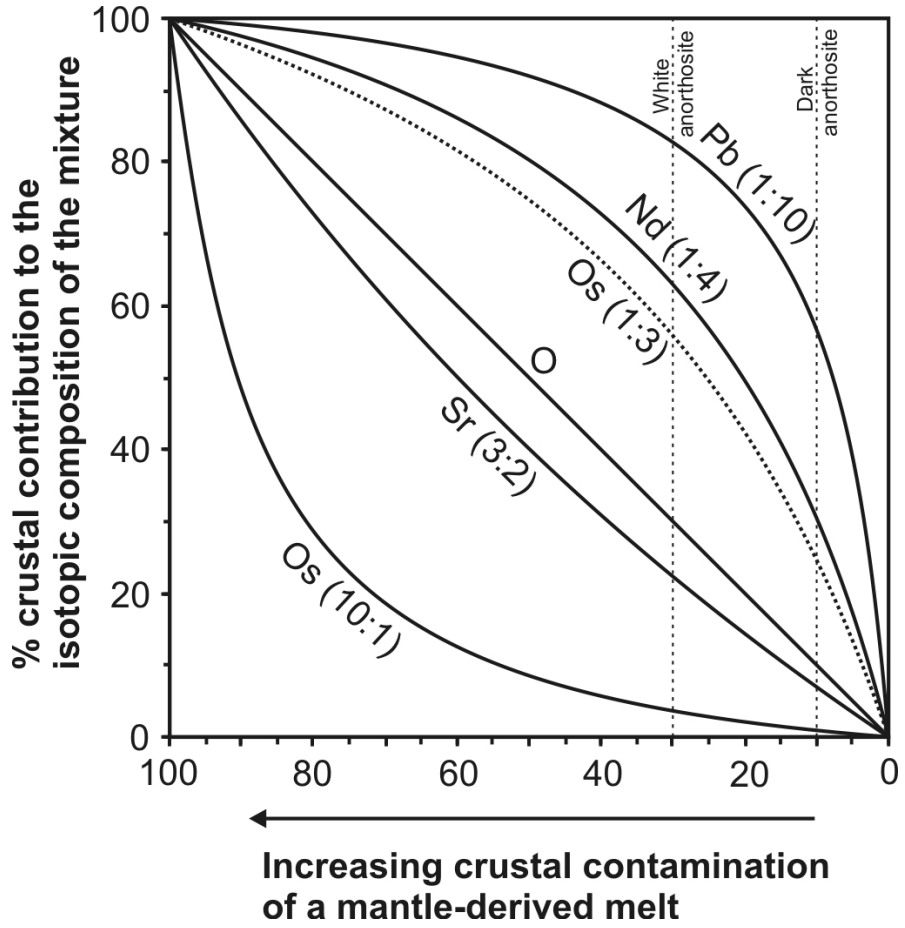

Fig. 6.3. Schematic mixing model for the impact of crustal contamination on the isotopic composition of a mantle-derived melt. The ratio of average trace element concentration in the mantle-derived melt and the crustal contaminant is given in parenthesis (taken from Chapter 4). All common rocks and melts span a narrow range in oxygen concentration and therefore mixing proportions of isotopically distinct components contribute equaly to the chemistry of the magma. Two mixing lines for osmium are shown, one assuming broadly basaltic osmium concentrations of the parental melt (solid line) and the second one accounting for lower osmium concentration due to prior fractional crystallization of mafics and platinum group minerals from the magma (dotted). The vertical lines display the calculated maximum contamination for the white and dark anorthosite suite of the Kunene Intrusive Complex (taken from Chapter 4).

Previous studies on the Os isotopic composition of massif-type anorthosites assumed that if the anorthosites are derived from a mantle source, the parental melt has to be broadly basaltic in composition (Morgan, et al., 2000; Schiellerup et al., 2000). For the calculation of subsequent crustal contamination, Os concentrations typical to basalts elsewhere were hence taken for calculation (Fig. 6.3). The new data on HSE abundance in anorthosites of the KIC suggest that this assumption was maybe wrong. The composition of the parental melt was likely basaltic but due to previous fractional crystallization of mafics (and maybe also PGM) the Os concentration was significantly lower than that suggested by these authors. Following this, the isotopic composition of the parental melt was much more sensitive to the highly radiogenic crustal Os during subsequent contamination. In the KIC this resulted in a huge initial Os isotopic contrast between highly contaminated white anorthosite suite and less contaminated dark anorthosite suite (see Fig. 5.11). When compared to the isotopic composition of the lithophile trace elements, the impact of contamination on the Os isotopic composition was probably similar to that for Nd but lower than that for Pb which is entirely dominated by the crust (Fig. 6.3).

6.4 A possible petrogenetic model for the Kunene Intrusive Complex

This study is mainly concerned with the source and composition of the parental melt of the KIC and its magmatic evolution. Hence, the proposed petrogenetic model for the Kunene Intrusive Complex mainly focuses on these aspects. However, the source and composition of the parental melt to massif-type anorthosites is as much a tectonic question as a petrological one (Ashwal, 2004). From the location of the KIC at the southern margin of the Congo Craton, in strike with the Kibaran Belt of Tanzania Mayer et al. (2004) argued that its emplacement reflect a significant thermal event predating the separation of the Congo and Kaapvaal Cratons. In contrast, recent paleogeographic reconstructions favor the interpretation that both cratons evolved independently during the Mesoproterozoic (Johnson et al., 2005). Moreover, the I- and S-type magmatism in the Kibaran Belt is syntectonic (Ernst et al., 2008; De Waele et al., 2008) whereas the KIC intruded more than 100 Ma after the last recorded metamorphic overprint and is therefore regarded as anorogenic (Drüppel et al., 2009). The emplacement of the KIC and the associated granitic rocks at the southern margin of the Congo Craton are part of long-lasting Mesoproterozoic mantle-derived igneous activity between 1.4 and 1.1 Ga in this region and might be related to the successive break-up of a 1.8 - 1.5 Ga continent (Drüppel et al., 2009).

The age relation of mantle-derived rocks in the study area, summarized in Drüppel et al. (2009), indicate that the anorthosites appear at the very beginning of episodic long-lived magmatic activity, reflecting a within plate setting or possibly the start of a continental rifting. Based on the retrograde cooling path inferred for ultrahigh-temperature metamorphic rocks (970 ± 40°C/9.5 ± 2 kbar) of the Epupa Complex, Brandt et al. (2003) discussed a possible tectonic scenario in which the granulite

facies metamorphism might have taken place related to collision tectonics and a subsequent decompression due to extensional collapse of the tectonically thickened crust. The formation of the peak-metamorphic assemblages of the granulite facies metamorphism took place between 1.52 and 1.45 Ga (Seth et al., 2003). According to the geobarometric results of Brandt et al. (2003) a minimal crustal thickness of 30 – 35 km can be concluded for this time. The anorthosites of the KIC intruded at 1.38 Ga in the already stabilized craton. The crustal thickness at this time is assumed similar to the time of granulite facies metamorphism.

The isotopic data of this study demonstrate that the source of the primary melt of the KIC was the mantle. A mantle origin of the anorthosites invalids the crustal tongue melting model of Duchesne et al. (1999) although the isotopic record of the KIC and many other anorthosite complexes demonstrates that the crust significantly contributed to the magma compositions (e.g. Scoates & Frost, 1996, Peck & Valley, 2000). According to these considerations and the new data of this study, the in the following a possible petrogenetic model is proposed for the KIC, which is based on the general model of Ashwal (1993) and the thermobarometric evolution of the KIC (Drüppel et al., 2001) and the metamorphic evolution of the Epupa Complex (Brandt et al., 2003, 2007; Brandt & Klemd 2008): The formation of the Kunene Intrusive Complex anorthosites started with partial melting of a depleted upper mantle composition (see section 6.2.1), like spinel-lherzolite to harzburgite. The partial melts coalesced to form a huge magma chamber at the crust-mantle boundary (Fig. 6.4a). Exposed examples for the regional lower crustal rocks are granulite facies rocks of basement surrounding the KIC. This volcano-sedimentary sequence was subject to partial melting during ultrahigh-temperature metamorphism between 1.52 and 1.45 Ga (Brandt et al., 2007). The emplacement of hot, mantle-derived primary melt of the anorthosites at ~1.38 Ga hence induced only minor partial melting of the restitic lower crustal rocks but assimilation of small proportions of crustal material from the roof seems possible.

Upon cooling this primary melt starts to crystallize olivine and Cr-spinel. These dense phases sink to the bottom of the magma chamber resulting in a lowering of Mg and Cr contents of the melt and hence explaining the low abundances of the elements in the anorthosites of the KIC. According to the observed HSE abundances of KIC rocks, the melt also looses the majority of its I-PGE during that stage (see section 5.5.5). The melt also becomes progressively enriched in aluminium to form a high-Al basaltic parental melt. Diapirs of the high-Al basaltic and variably contaminated magma rise upwards into the middle crust. This ascent was most likely channeled through pre-existing lithospheric fault zones (Fig. 6.4b).

Further contamination with crustal material took place during ascent and emplacement into the volcano-sedimentary sequence of the Orue Unit (section 6.3.2). The presence of calc-silicate rocks in the Orue Unit together wit the preservation of calc-silicate xenoliths in the white anorthosites reveal that bulk rock assimilation took place in the intrusion level. Furthermore, the Orue Unit was subject to biotite-dehydration melting and the partial melts of such processes possibly also interacted with the parental melt to produce an evolved melt. The final emplacement level at ~7 kbar is constrained from

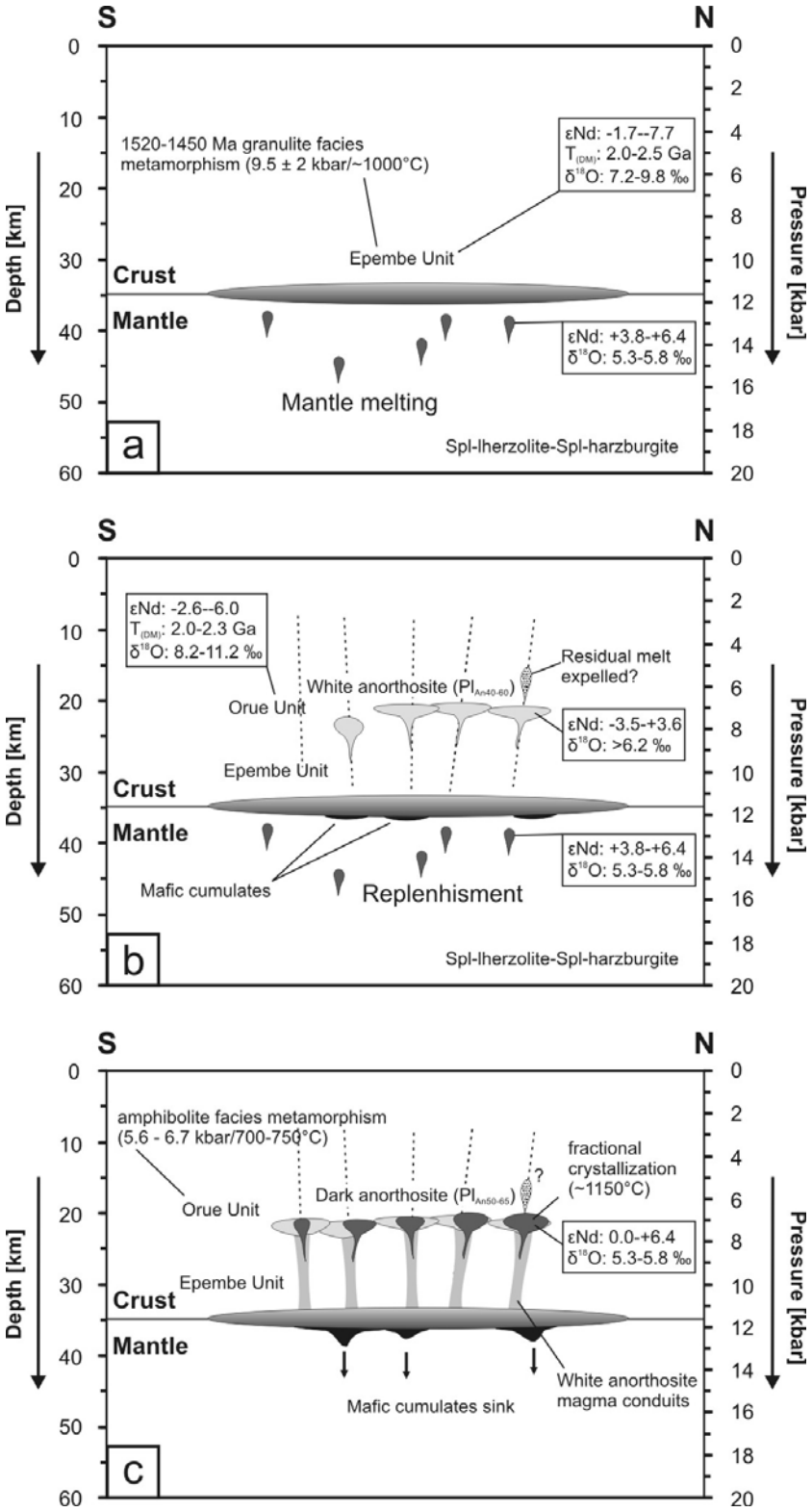

Fig. 6.4. Schematic model for the petrogenesis of the anorthosites of the Kunene Intrusive Complex. (a) Partial melts of depleted mantle coalesce in a deep seated magma chamber. (b) After fractionation of mafic phases and early crustal contamination the melt ascend as diapirs along previous weakness zones into the lower-middle crust to form the white anorthosite massive. Further crustal contamination took place during ascent and at the emplacement level. (c) Replenishment of the deep seated magma chamber produces a less contaminated melt that ascends along the same conduits. The magma intrudes in the centre of the white anorthosite and form the dark anorthosite suite.

thermobarometric studies on late crystallized amphibole and Grt-Opx-Qtz assemblages around olivine of the dark anorthosite suite (Drüppel et al., 2001). This is further supported by the presence of a narrow reaction zone of undeformed Grt-Crd-Sil rocks, which record the contact thermal effect induced by the emplacement of the anorthosites (Brandt et al., 2003).

Regarding the anorthosite formation, there is no convincing evidence for the onset of plagioclase fractionation and flotation in the deep seated magma chamber and later diapiric ascent as a crystal mush followed by adcumulus growth. The observed large-scale wavy oscillatory zoning of plagioclase is consistent with repeated changes in melt composition but does not reveal evidence for true polybaric crystallization (see section 6.3.1). Therefore, the plagioclase crystallization process probably took place in a lower pressure range than previously thought. On the other hand oxygen isotope composition and trace elements in plagioclase indicate that its crystallization took place prior and during crustal contamination, a process that most likely occurred during ascent and at the final emplacement level. A possible scenario would be plagioclase that crystallized in the intrusion level whereas the residual melt was largely expelled into higher levels during compaction. This interpretation also accounts for plagioclase accumulation and the minor presence of other phases but is difficult to reconcile due to the absence of such residual melts at the present level of exposure.

Prior to the formation of the dark anorthosite suite, the deep seated magma chamber was subject to replenishment with primitive melt from the upper depleted mantle. After olivine and Cr-spinel fractionation a second generation of melt diapirs ascended through the same conduits which previously were used by the white anorthosite diapirs (Fig. 6.4c). The lower availability of crustal partial melts and/or assimilation of previously formed mantle melt-crust mixing zones resulted in lower amount of crustal contamination in the younger dark anorthosite suite. Hence the dark anorthosites crystallized from more primitive melt and preserved much of the initial isotopic composition of the mantle-derived parental melt. At the emplacement level the dark anorthosites intruded in the centre of the white anorthosite massif, which at this time was probably not fully consolidated. The diapiric ascent and emplacement channelled by older magma conduits resulted in the ridge-like appearance of the dark anorthosites within the massif of the white anorthosites.

The formation of the Fe-Ti ore bodies in the KIC is interpreted as fractional crystallization and accumulation of titanomagnetite (Franke, 2009; Franke et al., 2009). The HSE pattern and Os isotope composition of the Fe-Ti ore reveal that their origin is related to the formation of the anorthosites. The emplacement of such dense cumulate rocks into the white anorthosite is possible either as remobilized cumulates or probably related to in-situ crystallization of mainly plagioclase, magnetite and pyroxene from an intrusive melt diapir.

The emplacement of the dark anorthosite suite was followed by subsolidus re-equilibration of the plutonic body during cooling and uplift (700 - 800°C/ 6.2 kbar). The intrusion of the associated granitoids occurred at similar pressures of 6.5 kbar (Drüppel et al., 2009). The emplacement of the anorthosites and felsic rocks between 1385 ± 25 Ma (Drüppel et al., 2000) and 1376 ± 2 Ma (Drüppel

et al., 2007) was followed by upper amphibolite facies metamorphism of the nearby Orue Unit of the Epupa Complex at 5.5 - 6.7 kbar and 700 - 750°C (Brandt & Klemd, 2008).

The later post-magmatic regional history is characterized by nearly isobaric cooling of the KIC and uplift of the granulite facies Epembe Unit along subvertical ductile shear zones (Brandt et al., 2003). Ultramafic rocks located along these shear zones are probably related to the formation of the KIC and may represent ultramafic cumulates from former lower crust magma chambers. The same shear zones channelled the 1220 Ma nepheline-syenites that belong to the long-lasting mantle-derived igneous activity in NW-Namibia (Drüppel et al., 2009). Undeformed Neoproterozoic sediments (845 - 545 Ma) of the Damara Supergroup overlay the Epupa Complex and demonstrate that the region was not metamorphosed during the Pan-African orogeny.

References

Andersen, T., Griffin, W. L. (2004). Lu-Hf and U-Pb isotope systematics of zircon from the Storgangen intrusion, Rogaland Intrusive Complex, SW Norway: implications for the composition and evolution of Precambrian lower crust in the Baltic Shield. Lithos 73, 271-288.

Ashwal, L. D. (1993). Anorthosites. Minerals and Rocks Series 21. Springer-Verlag, Berlin.

Ashwal, L. D. (2004). Origin of anorthosites: petrological and tectonic considerations. Joint Annual Meeting, Program with Abstracts, V51E-04.

Ashwal, L. D., Hamilton, M. A., Morel, V. P. I., Rambelson, R. A. (1998). Geology, petrology and isotope geochemistry of massif-type anorthosites from southwest Madagascar. Contributions to Mineralogy and Petrology 133, 389-401.

Ashwal, L. D., Twist, D. (1994). The Kunene Complex, Angola/Namibia: a composite massif-type anorthosite complex. Geological Magazine 131, 579-591.

Ashwal, L. D., Wooden, J. L., Emslie, R. F. (1986). Sr, Nd, and Pb isotopes in Proterozoic intrusives astride the Grenville Front in Labrador: implications for crustal contamination and basement mapping. Geochimica et Cosmochimica Acta 50, 2571-2585.

Ballhaus, C., Bockrath, C., Wohlgemuth-Ueberwasser, C., Laurenz, V., Berndt, J. (2006). Fractionation of the noble metals by physical processes. Contributions to Mineralogy and Petrology 152, 667-684.

Barnes, S.-J., Naldrett, A. J., Gorton, M. P. (1985). The origin of the fractionation of platinum-group elements in terrestrial magmas. Chemical Geology 53, 303-323.

Barnes, S-J., Maier, W. D., Ashwal, L. D. (2004). Platinum-group element distribution in the Main Zone and Upper Zone of the Bushveld Complex, South Africa. Chemical Geology 208, 293-317.

Barth, M. G., McDonough, W. F., Rudnick, R. L. (2000). Tracking the budget of Nb and Ta in the continental crust. Chemical Geology 165, 197-213.

Becker, H., Shirey, S. B., Carlson, R. W. (2001). Effects of melt percolation on the Re–Os systematics of peridotites from a Paleozoic convergent plate margin. Earth and Planetary Science Letters 188, 107–121.

Becker, H., Horan, M. F., Walker, R. J., Gao, S., Lorand, J. P., Rudnick, R. L. (2006). Highly siderophile element composition of the Earth's primitive upper mantle: constraints from new data on peridotite massifs and xenoliths. Geochimica et Cosmochimica Acta 70, 4528-4550.

Bézos, A., Lorand, J. P., Humler, E., Gros, M. (2005). Platinum-group element systematics in Mid-Oceanic Ridge basaltic glasses from the Pacific, Atlantic, and Indian Oceans. Geochimica et Cosmochimica Acta 69, 2613-2627.

Bindemann, I. N., Davis, A. M., Drake, M. J. (1998). Ion microprobe study of plagioclase-basalt partition experiments at natural concentration levels of trace elements. Geochimica et Cosmochimica Acta 62, 1175-1193.

Birck, L., Roy-Barman, M., Capmas, F. (1997). Re–Os isotopic measurements at the femtomole level in natural samples. Geostandards Newsletter 21, 19–28.

Black, R., Liégeois, J. (1993). Cratons, mobile belts, alkaline rocks and continental lithospheric mantle: the Pan-African testimony. Journal of the Geological Society, London 150, 89–98.

Blundy, J. D., Wood, B. J. (1991). Crystal-chemical controls on the partitioning of Sr and Ba between plagioclase feldspar, silicate melts, and hydrothermal solutions. Geochimica et Cosmochimica Acta 55, 193-209.

Blundy, J. D., Wood, B. J. (2003). Partitioning of trace elements between crystals and melts. Earth and Planetary Science Letters 210, 383-397.

Boelrijk, N. A. I. M. (1968). A General formula for double isotope dilution analysis. Chemical Geology 3, 323-325.

Bolle, O., Demaiffe, D., Duchesne, J. C. (2003). Petrogenesis of jotunitic and acidic members of an AMC suite (Rogaland anorthosite province, SW Norway): a Sr and Nd isotopic assessment. Precambrian Research 124, 185-214.

Bowen, N. L. (1917). The problem of the anorthosites. Journal of Geology 25, 209-243.

Brandt, S. (2003). Metamorphic evolution of ultrahigh-temperature granulite facies and upper amphibolite facies rocks of the Epupa Complex, NW Namibia. Dr. rer. Nat. thesis, University of Würzburg.

Brandt, S., Klemd, R. (2008). Upper-amphibolite facies partial melting of paragneisses from the Epupa Complex, NW Namibia, and relations to Mesoproterozoic anorthosite magmatism. Journal of metamorphic Geology 26, 871-893.

Brandt, S., Will, T. M., Klemd, R. (2007). Magmatic loading in the Proterozoic Epupa Complex, NW Namibia, as evidenced by ultrahigh-temperature sapphirine-bearing orthopyroxene–sillimanite–quartz granulites. Precambrian Research 153, 143-178.

Brenan, J. M., McDonough, W. F., Ash, R. (2005). An experimental study of the solubility and partitioning of iridium, osmium and gold between olivine and silicate melt. Earth and Planetary Science Letters 237, 855-872.

Buddington, A. F. (1939). Adirondack igneous rocks and their metamorphism. Geological Society of America Memoir 7, 343 p.

Capobianco, C. J., Hervig, R. L., Drake, M. J. (1994). Experiments on crystal/liquid partitioning of Ru, Rh and Pd for magnetite and hematite solid solutions crystallized from silicate melt. Chemical Geology 113, 23-43.

Cawthorn, R. G., Ashwal, L. D. (2009). Origin of anorthosite and magnetitite layers in the Bushveld Complex, constrained by major element compositions of plagioclase. Journal of Petrology 50, 1607-1637.

Charlier, B., Duchesne, J. C., Vander Auwera, J. (2006). Magma chamber processes in the Tellnes ilmenite deposit (Rogaland Anorthosite Province, SW Norway) and the formation of Fe–Ti ores in massif-type anorthosites. Chemical Geology 234, 264-290.

Charlier, B., Skår, Ø., Korneliussen, A., Duchesne, J. C., Vander Auwera, J. (2007). Ilmenite composition in the Tellnes Fe–Ti deposit, SW Norway: fractional crystallization, postcumulus evolution and ilmenite–zircon relation. Contributions to Mineralogy and Petrology 154, 119-134.

Cherniak, D. J. (2003). REE diffusion in feldspar. Chemical Geology 193, 25-41.

Clayton, R. N., Mayeda, T. K. (1963). The use of bromine pentafluoride in the extraction of oxygen from oxides and silicates for isotopic analysis. Geochimica et Cosmochimica Acta 27, 43-52.

Corrigan, D. Hanmer, S. (1997). Anorthosite and related granitoids in the Grenville orogen: A product of convective thinning of the lithosphere? Geology 25, 61-64.

Dale, C. W., Burton, K. W., Pearson, D. ., Gannoun, A., Alard, O., Argles, T. W., Parkinson, I. J. (2009). Highly siderophile element behaviour accompanying subduction of oceanic crust: Whole rock and mineral-scale insights from a high-pressure terrain. Geochimica et Cosmochimica Acta 73, 1394-1416.

Dale, C. W., Luguet, A., Macpherson, C. G., Pearson, D. G., Hickey-Vargas, R. (2008). Extreme platinum-group element fractionation and variable Os isotope compositions in Philippine Sea Plate basalts: tracing mantle source heterogeneity. Chemical Geology 248, 213–238.

Day, J. M., Pearson, D. G., Hulbert, L. J. (2008). Rhenium-osmium isotope and platinum-group element constraints on the origin and evolution of the 1.27 Ga Muskox Layered Intrusion. Journal of Petrology 49, 1255-1295.

De Carvalho, H., Alves, P. (1990). Gabbro-Anorthosite Complex of SW Angola/NW Namibia. Inst. Inv. Cientifica Tropical, Série de Ciências da Terra, Communicações 2, pp. 1–66.

De Carvalho, H., Tassinari, C., Alves, P.H., Guimarães, F., Simões, M. C. (2000). Geochronological review of the Precambrian in western Angola: links with Brazil. Journal of African Earth Sciences 31, 383-402.

Deer, W. A., Howie, R. A., Zussman, J. (1992). An introduction to the rock-forming minerals.-2nd ed. Pearson Education Limited, Essex.

Demaiffe, D., Javoy, M. (1980). $^{18}O/^{16}O$ ratios of anorthosites and related rocks from Rogaland Complex (SW Norway). Contributions to Mineralogy and Petrology 72, 311-317.

Demaiffe, D., Weis, D., Michot, J., Duchesne, J. C. (1986). Isotopic constraints on the genesis of the Rogaland Anorthositic suite (southwest Norway). Chemical Geology 57, 167-179.

DePaolo, D. J. (1981). Neodymium isotopes in the Colorado Front Range and crust-mantle evolution in the Proterozoic. Nature 291, 193-196.

DePaolo, D. J. (1981). Trace element and isotopic effects of combined wallrock assimilation and fractional crystallization. Earth and Planetary Science Letters 53, 189-202.

DePaolo, D. J., Wasserburg, G. J. (1976). Nd isotopic variations and petrogenetic models. Geophysical Research Letters 3, 249-252.

De Waele, B., Johnson, S. P., Pisarevsky, S. A. (2008). Paleoproterozoic to Neoproterozoic growth and evolution of the eastern Congo Craton: its role in the Rodinia puzzle. Precambrian Research 160, 127-141.

Dobmeier, C. (2006). Emplacement of Proterozoic massif-type anorthosite during regional shortening: evidence from the Bolangir anorthosite complex (Eastern Ghats Province, India). International Journal of Earth Sciences 95, 543–555.

Drüppel, K. (2003). Petrogenesis of the Mesoproterozoic anorthosite, syenite and carbonatite suites of NW Namibia and their contribution to the metasomatic formation of the Swartbooisdrif sodalite deposits. Dr. rer. Nat. thesis, University of Würzburg.

Drüppel, K., Gleißner, P., Romer, R. L., Gerdes, A. (2009). Long-lived Mesoproterozoic magmatic activity in Namibia Insights to the origin and evolution of anorogenic igneous suites. Geochimica et Cosmochimica Acta 73/13, Suppl. 1, A306.

Drüppel, K., Hoefs, J., Okrusch, M. (2005). Fenitizing processes induced by ferrocarbonatite magmatism at Swartbooisdrif, NW Namibia. Journal of Petrology 46, 377-406.

Drüppel, K., Littmann, S., Okrusch, M. (2000). Geo- und isotopen-chemische Untersuchungen der Anorthosite des Kunene-Intrusiv-Komplexes (KIC) in NW-Namibia. Berichte der Deutschen Mineralogischen Gesellschaft. Beiheft zum European Journal of Mineralogy 12, 37.

Drüppel, K., Littmann, S., Romer, R. L., Okrusch, M. (2007). Petrology and isotope geochemistry of the Mesoproterozoic anorthosite and related rocks of the Kunene Intrusive Complex, NW Namibia. Precambrian Research 156, 1-31.

Drüppel, K., von Seckendorff, V., Okrusch, M. (2001). Subsolidus reaction textures in anorthosites of the Kunene Intrusive Complex, NW Namibia. European Journal of Mineralogy 13, 289-309.

Duchesne, J. C. (1984). Massif anorthosites: another partisan review. In: Brown, W. S. (ed) Feldspars and Feldspathoids. N.A.T.O. (North Atlantic Treaty Org.)-A.S.I. (Adv. Stud. Inst.), Ser. No. C137, Reidel, Dordrecht, 411-433.

Duchesne, J. C. (1999). Fe-Ti deposits in Rogaland anorthosites (South Norway): geochemical characteristics and problems of interpretation. Mineralium Deposita 34, 182-198.

Duchesne, J. C., Liégois, J. P., Vander Auwera, J., Longhi, J. (1999). The crustal tongue melting model and the origin of massive anorthosites. Terra Nova 11, 100-105.

Eiler, J. M. (2001). Oxygen isotope variations of basaltic lavas and upper mantle rocks. Reviews in Mineralogy & Geochemistry 43, 319-364.

Eiler, J. M., Valley, J. W., Baumgartner, L. P. (1993). A new look at stable isotope thermometry. Geochimica et Cosmochimica Acta 57, 2571-2583.

Emslie, R. F. (1978). Anorthosite massifs, rapakivi granites, and late Proterozoic rifting of north America. Precambrian Research 7, 61-98.

Emslie, R. F. (1985). Proterozoic anorthosite massifs. In: Tobi, A. C. & Touret, J. L. (ed) The deep Proterozoic crust in the North Atlantic Provinces. N.A.T.O. (North Atlantic Treaty Org.)-A.S.I. (Adv. Stud. Inst.) Ser. No. C158, Reidel, Dordrecht, 39-60.

Emslie, R. F., Hamilton, M. A., Thériault, R. J. (1994). Petrogenesis of a Mid-Proterozoic Anorthosite-Mangerite-Charnockite-Granite (AMCG) Complex: isotopic and chemical evidence from the Nain Plutonic Suite. Journal of Geology 102, 539-558.

Emslie, R. F., Hegner, E. (1993). Reconnaissance isotopic geochemistry of anorthosite-mangerite-charnockite-granite (AMCG) complexes, Grenville Province, Canada. Chemical Geology 106, 279-298.

Ernst, R. E., Wingate, M. T. D., Buchan, K. L., Li, Z. X. (2008). Global record of 1600-700 Ma Large Igneous Provinces (LIPs): implications for the reconstruction of the proposed Nuna (Columbia) and Rodinia supercontinents. Precambrian Research 160, 159-178.

Ertel, W., Dingwell, D. B., Sylvester, P. J. (2008). Siderophile elements in silicate melts – a review of the mechanically assisted equilibration technique and the nanonugget issue. Chemical Geology 248, 119-139.

Evans, R. J., Ashwal, L. D., Hamilton, M. A. (1999). Mafic, ultramafic, and anorthositic rocks of the Tete Complex, Mozambique: petrology, age, and significance. South African Journal of Geology 102, 153-166.

Farquhar, J., Chacko, T., Frost, B. R. (1993). Strategies for high-temperature oxygen isotope thermometry: a worked example from the Laramie Anorthosite Complex, Wyoming, USA. Earth Planetary Science Letters 117, 407-422.

Fischer-Gödde, M., Becker, H., Wombacher, F. (2010). Rhodium, gold and other highly siderophile element abundances in chondritic meteorites. Geochimica et Cosmochimica Acta 74, 356-379.

Fischer-Gödde, M., Becker, H., Wombacher, F., (in press). Rhodium, gold and other highly siderophile elements in orogenic peridotites and peridotite xenoliths. Chemical Geology. doi: 10.1016/j.chemgeo.2010.11.024

Fram, M. S., Longhi, J. (1992). Phase equilibria of dikes associated with Proterozoic anorthosite complexes. American Mineralogist 77, 605-616.

Franke, H., Drüppel, K., Brätz, H. (2009). Formation of anorthosite-related Fe-Ti deposits, Namibia. Geochimica et Cosmochimica Acta 73/13, Suppl. 1, A394.

Franke, H. (2009). Petrogenese von Ilmenit-Magnetit-Erzkörpern im anorthositischen Kunene-Intrusiv-Komplex, NW Namibia. Diploma Thesis, Technische Universität Berlin, 131 pp.

Franz, L., Romer, R. L., Digeldey, P. D. (1999). Diachronous Pan-African granulite-facies metamorphism (650 Ma and 550 Ma) in the Kaoko belt, NW Namibia. European Journal of Mineralogy 11, 167-180.

Frost, C. D., Chamberlain, K. R., Frost, B. R., Scoates, J. S. (2000). The 1.76-Ga Horse Creek anorthosite complex, Wyoming: a massif anorthosite emplaced late in the Medicine Bow orogeny. Rocky Mountain Geology 35, 71-90.

Frost, B. R., Lindsley, D. H. (1991). Occurrence of iron-titanium oxides in igneous rocks, in: Lindsley, D. H. (ed), Oxide minerals: Petrologic and magnetic significance. Reviews in Mineralogy 25, 433-468.

Geist, D. J., Frost, C. D., Kolker, A. (1990). Sr and Nd isotopic constraints on the origin of the Laramie Anorthosite Complex, Wyoming. American Mineralogist 75, 13-20.

Gleißner, P., Drüppel, K., Romer, R. L. (in press). The role of crustal contamination in massif-type anorthosites, new evidence from Sr-Nd-Pb isotopic composition of the Kunene Intrusive Complex, NW Namibia. Precambrian Research. doi: 10.1016/j.precamres.2010.11.004

Gleißner, P., Drüppel, K., Taubald, H. (2010). Magmatic evolution of anorthosites of the Kunene Intrusive Complex, NW Namibia: evidence from oxygen isotope data and trace element zoning. Journal of Petrology 51, 897-919.

Goldstein, S. L., O'Nions, R. K., Hamilton, P. J. (1984). A Sm-Nd isotopic study of atmospheric dusts and particulates from major river systems. Earth and Planetary Science Letters 70, 221-236.

Green, T. H. (1995). Significance of Nb/Ta as an indicator of geochemical processes in the crust-mantle system. Chemical Geology 120, 347-359.

Green, T. H., Pearson, N. J. (1987). An experimental study of Nb and Ta partitioning between Ti-rich minerals and silicate liquids at high pressure and temperature. Geochimica et Cosmochimica Acta 51, 55-62.

Grove, L. G., Baker, M. B., Kinzler, R. J. (1984). Coupled CaAl-NaSi diffusion in plagioclase feldspar: experiments and applications to cooling rate speedometry. Geochimica et Cosmochimica Acta 48, 2113-2121.

Hannah, J. L., Stein, H. J. (2002). Re-Os model for the origin of sulfide deposits in anorthosite-associated intrusive complexes. Economic Geology 97, 371-383.

Halama, R., Waight, T., Markl, G. (2002). Geochemical and isotopic zoning patterns of plagioclase megacrysts in gabbroic dykes from the Gardar Province, South Greenland: implications for crystallisation processes in anorthositic magmas. Contributions to Mineralogy and Petrology 144, 109-127.

Harris, C., Pronost, J. M., Ashwal, L. D., Cawthorn, R. G. (2005). Oxygen and hydrogen isotope stratigraphy of the Rustenburg Layered Suite, Bushveld Complex: constraints on crustal contamination. Journal of Petrology 46, 579-601.

Hart, G. L., Johnson, C. M., Shirey, S. B., Clynne, M. A. (2002). Osmium isotope constraints on lower crustal recycling and pluton preservation at Lassen Volcanic Center, CA. Earth and Planetary Science Letters 199, 269-285.

Holten, T., Jamtveit, B., Meakin, P. (2000). Noise and oscillatory zoning of minerals. Geochimica et Cosmochimica Acta 64, 1893-1904.

Horn, I., Hinton, R. W., Jackson, S. E., Longerich, H. P. (1997). Ultra-trace element analysis of NIST SRM 616 and 614 using Laser Ablation Microprobe-Inductively coupled Plasma-Mass Spectrometry (LAM-ICP-MS): a comparison with Secondary Ion Mass Spectrometry (SIMS). Geostandards Newsletter 21, 191-203.

Huber, W., 2003. Basic calculations about the limit of detection and its optimal determination. Accreditation and Quality Assurance 8, 213-217.

Hunt, T. S. (1863). In: Logan, W. E., Murray, A. Hunt, T. S., Billings, E. (eds) Geology of Canada: Report of Progress from its Commencement to 1863. Geological Survey of Canada, 983 p.

Johnson, S. P., Rivers, T., De Waele, B. (2005). A review of the Mesoproterozoic to early Palaeozoic magmatic and tectonothermal history od south-central Africa: implications for Rodinia and Gondwana. Journal of the Geological Society, London 162, 433-450.

Kasemann, S., Meixner, A., Rocholl, A., Vennemann, T., Schmitt, A., Wiedenbeck, M. (2001). Boron and oxygen isotope composition of certified reference materials NIST SRM 610/612, and reference materials JB-2G and JR-2G. Geostandards Newsletter 25, 405-416.

Kretz, R. (1983). Symbols for rock-forming minerals. American Mineralogist 68, 277-279.

Kolker, A. (1982). Mineralogy and geochemistry of Fe–Ti oxide and apatite (nelsonite) deposits and evaluation of the liquid immiscibility hypothesis. Economic Geology 77, 1146-1148.

Köstlin, E. C. (1974). The Kunene basic complex, northern South West Africa. In: Kröner, A. (ed), Contributions to the Precambrian Geology of Southern Africa, vol. 15. University of Cape Town Bulletin, Capetown, 123–135.

Köstlin, E. C. (1967). The geology of part of the Kunene basic complex, Kaokovel; South West Africa. Unpublished M.Sc. Thesis, University of Cape Town.

Kröner, S., Konopásek, A., Kröner, A., Passchier, C. W., Poller, U., Wingate, M. T. D., Hofmann, K. H. (2004). U-Pb and Pb-Pb zircon ages for metamorphic rocks in the Kaoko Belt of Northwestern Namibia: A Paleo- to Mesoproterozoic basement reworked during the Pan-African orogeny. South African Journal of Geology 107, 455-476.

Kushiro, I. (1980). Viscosity, density, and structure of silicate melts at high pressure, and their petrological application. In: Hargraves, R. B. (ed) Physics of magmatic processes. Princeton, NJ: Princeton University Press, 93-120.

Lambert, D. D., Foster, J. G., Li, C., Naldrett, A. J. (2000). Re-Os Isotope Systematics of the Voisey's Bay Ni-Cu-Co magmatic sulfide system, Labrador, Canada: II. Implications for parental magma chemistry, ore genesis, and metal redistribution. Economic Geology 95, 867-888.

Loeppke, N., Hannah, J. (2004). Re-Os systematics in Fe-Ti oxides from Proterozoic anorthosite complexes. Geological Society of America /Abstracts with Programs 36, 508.

Longhi, J. (2005). A mantle or mafic crustal source for Proterozoic anorthosites? Lithos 83, 183-198.

Longhi, J., Vander Auwera, J., Fram, M. F., Duchesne, J. C. (1999). Some phase equilibrium constraints on the origin of Proterozoic (massif) Anorthosites and related rocks. Journal of Petrology 40, 339-362.

Ludwig, K. R. (2003). Isoplot 3.00: A geochronological toolkit for Microsoft Excel. Berkeley Geochronology Center Special Publication No. 4.

Lundmark, A. M., Corfu, F. (2008). Late-orogenic Sveconorwegian massif anorthosite in the Jotun Nappe Complex, SW Norway, and causes of repeated AMCG magmatism along the Baltoscandian margin. Contributions to Mineralogy and Petrology 155, 147-163.

Maier, W. D., Teigler, B., Miller, R. (2008). The Kunene anorthosite complex and its satellite intrusions. In Miller, R. Mc. G. (ed) The Geology of Namibia, Geological Survey of Namibia, 9-1 - 9-18.

Mallmann, G., O'Neil, H. St. C. (2007). The effect of oxygen fugacity on the partition of Re between crystals and silicate melt during mantle melting. Geochimica et Cosmochimica Acta 71, 2837-2857.

Mayer, A., Hofmann, A. W., Sinigoi, S., Morais, E. (2004). Mesoproterozoic Sm-Nd and U-Pb ages for the Kunene Anorthosite Complex of SW Angola. Precambrian Research 133, 187-206.

Markl, G. (2001). REE constraints on fractionation processes of massive-type anorthosites on the Lofoten Islands, Norway. Mineralogy and Petrology 72, 325-351.

Markel, G., Frost, R. (1999). The origin of anorthosites and related rocks from the Lofoten Islands, Northern Norway: II. Calculation of parental liquid compositions for anorthosites. Journal of Petrology 40, 61-77.

Markl, G., Frost, B. R., Bucher, K. (1998) The origin of anorthosites and related rocks from the Lofoten islands, northern Norway. I. Field relations and estimation of intrinsic variables. Journal of Petrology 39, 1425-1452.

McDonough, W. F., Sun, S. (1995). The composition of the Earth. Chemical Geology 120, 223-253.

Meisel, T., Walker, R. J., Irving, A. J., Lorand, J-P. (2001). Osmium isotopic compositions of mantle xenoliths: a global perspective. Geochimica et Cosmochimica Acta 65, 1311-1323.

Meisel, T., Fellner, N., Moser, J. (2003). A simple procedure for the determination of platinum group elements and rhenium (Ru, Rh, Pd, Re, Os, Ir, and Pt) using ID-ICP-MS with an inexpensive on-line matrix separation in geological and environmental materials. Journal of Analytical Atomic Spectrometry 18, 720-726.

Menge, G. F. W. (1998). The antiformal structure and general aspects of the Kunene Complex, Namibia. Zeitschrift der Deutschen Geologischen Gesellschaft 149, 433-448.

Miller, J. D., Weiblen, P. W. (1990). Anorthositic rocks of the Duluth Complex: examples of rocks formed from plagioclase crystal mush. Journal of Petrology 31, 295-339.

Mitchell, J. N., Scoates, J. S., Frost, C. D. (1995). High-Al gabbros in the Laramie Anorthosite Complex, Wyoming: implications for the composition of melts parental to Proterozoic anorthosite. Contributions to Mineralogy and Petrology 119, 166-180.

Morais, E., Sinigoi, S., Mayer, A., Mucana, A., Miguel, L. G., Rufino Neto, J. (1998). The Kunene gabbro-anorthosite Complex: preliminary results based on new field and chemical data. African Geoscience Review 5, 485-498.

Morgan, J. W., Stein, H. J., Hannah, J. L., Markey, R. J., Wiszniewska, J. (2000). Re-Os study of Fe-Ti-V oxide and Fe-Cu-Ni sulfide deposits, Suwałki Anorthosite Massif, northeast Poland. Mineralium Deposita 35, 391-401.

Morrison, J., Valley, J. W. (1988). Contamination of the Marcy Anorthosite Massif, Adirondack Mountains, NY: petrologic and isotopic evidence. Contributions to Mineralogy and Petrology 98, 97-108.

Morse, S. A. (1973). The feldspar/magma density paradox. In Morse, S. A. (ed) The Nain Anorthosite Project, Labrador: Field Report 1972. Amherst, MA: University of Massachusetts at Amherst, 113-116.

Morse, S. A. (1982). A partisan review of Proterozoic anorthosites. American Mineralogist 67, 1087-1100.

Morse, S. A. (2006). Labrador massif anorthosites: chasing the liquids and their source. Lithos 89, 202-221.

Morse, S. A., Nolan, K. M. (1984). Origin of strongly reversed rims on plagioclase in cumulates. Earth Planetary Science Letters 68, 485-498.

Mukherjee, A., Das, S. (2002a). Anorthosites, granulites and the supercontinent cycle. Gondwana Research 5, 147-156.

Mukherjee, A., Das, S. (2002b). The plagioclase-magma density paradox re-examined and the crystallization of Proterozoic anorthosites: a discussion. Journal of Petrology 43, 1975-1978.

Nolan, K. M., Morse, S. A. (1986). Marginal rocks resembling the estimated bulk composition of the Kiglapait Intrusion. Geochimica et Cosmochimica Acta 50, 2381-2386.

O'Connor, Y-L., Morrison, J. (1999). Oxygen isotope constraints on the petrogenesis of the Sybille intrusion of the Proterozoic Laramie Anorthosite Complex. Contributions to Mineralogy and Petrology 136, 81-91.

O'Driscoll, B., Day J. M. D., Daly, S., Walker, R. J., McDonough, W. F. (2009). Rhenium–osmium isotopes and platinum-group elements in the Rum Layered Suite, Scotland: implications for Cr-spinel seam formation and the composition of the Iceland mantle anomaly. Earth and Planetary Science Letters 286, 41-51.

O'Hara, M. J. (1977). Geochemical evolution during fractional crystallization of a periodically refilled magma chamber. Nature 314, 503-507.

Owens, B. E., Dymek, R. F., Tucker, R. D., Brannon, J. C., Podosek, F. A. (1994). Age and radiogenic isotopic composition of a late- to post-tectonic anorthosite in the Grenville Province: the Labreville massif, Quebec. Lithos 31, 189-206.

Pearce, N. J. G., Perkins, W. T., Westgate, J. A., Gorton, M. P., Jackson, S. E., Neal, C. R., Chenery, S. P. (1997). A compilation of new and published major and trace element data for NIST SRM 610 and NIST SRM 612 glass reference materials. Geostandards Newsletter 21, 115-144.

Pearson, D. G., Woodland, S. J. (2000). Solvent extraction/anion exchange separation and determination of PGEs (Os, Ir, Pt, Pd, Ru) and Re-Os isotopes in geological samples by isotope dilution ICP-MS. Chemical Geology 165, 87-107.

Peck, W. H., Valley, J. W. (2000). Large crustal input to high $\delta^{18}O$ anorthosite massifs of the southern Grenville Province: new evidence from the Morin Complex, Quebec. Contributions to Mineralogy and Petrology 139, 402-417.

Peucker-Ehrenbrink, B., Blum, J. D. (1998). Re-Os isotope systematics and weathering of Precambrian crustal rocks: Implications for the marine osmium isotope record. Geochimica et Cosmochimica Acta 62, 3193-3203.

Philpotts, A. R. (1981). A model for the generation of massif-type anorthosites. Canadian Mineralogist 19, 233-353.

Pitcher, L., Helz, R. T., Walker, R. J., Piccoli, P. (2009). Fractionation of the platinum-group elements and Re during crystallization of basalt in Kilauea Iki Lava Lake, Hawaii. Chemical Geology 260, 196-210.

Puchtel, I., Humayun, M. (2000). Platinum group elements in Kostomuksha komatiites and basalts: Implications for oceanic crust recycling and core-mantle interaction. Geochimica et Cosmochimica Acta 64, 4227-4242.

Puchtel, I., Humayun, M. (2001). Platinum group element fractionation in a komatiitic basalt lava lake. Geochimica et Cosmochimica Acta 65, 2979-2993.

Rehkämper, M., Halliday, A. N., Fitton, J. G., Lee, D. C., Wieneke, M., Arndt, N. T., 1999. Ir, Ru, Pt, and Pd in basalts and komatiites: New constraints for the geochemical behaviour of the platinum-group elements in the mantle. Geochimica et Cosmochimica Acta 63, 3915-3934.

Richardson, S. H., Shirey, S. B. (2008), Continental mantle signature of Bushveld magmas and coeval diamonds. Nature 453, 910-914.

Righter, K., Campbell, A. J., Humayun, M., Hervig, R. L. (2004). Partitioning of Ru, Rh, Pd, Re, Ir, and Au between Cr-spinel, olivine, pyroxene and silicate melts. Geochimica et Cosmochimica Acta 68, 867-880.

Righter, K., Chesley, J. T., Caiazza, C. M., Gibson, E. K., Ruiz, J. (2008). Re and Os concentrations in arc basalts: the roles of volatility and source region fO_2 variations. Geochimica et Cosmochimica Acta 72, 926-947.

Righter, K., Chesley, J. T., Geist, D., Ruiz, J. (1998). Behavior of Re during magma fractionation: an example from Volcán Alcedo, Galápagos. Journal of Petrology 39, 785-795.

Ripley, E. M., Lambert, D. D., Frick, L. R. (1999). Re-Os, Sm-Nd, and Pb isotopic constraints on mantle and crustal contributions to magmatic sulfide mineralization in the Duluth Complex. Geochimica et Cosmochimica Acta 62, 3349-3365.

Romer, R. L. (2001). Lead incorporation during crystal growth and the misinterpretation of geochronological data from low-$^{238}U/^{204}Pb$ metamorphic minerals. Terra Nova 13, 258-263.

Romer, R. L., Hahne, K. (2010). Life of the Rheic Ocean: scrolling through the shale record. Gondwana Research 17, 236-253.

Rudnick, R. L., Fountain, D. M. (1995). Nature and composition of the continental crust: A lower crustal perspective. Review of Geophysics 33, 267-309.

Saal, A. E., Rudnick, R. L., Ravizza, G. E., Hart, S. R. (1998). Re-Os isotope evidence for the composition, formation and age of the lower continental crust. Nature 393, 58-61.

Schärer, U., Wilmart, E., Duchesne, J. C. (1996). The short duration and anorogenic character of anorthosite magmatism: U-Pb dating of the Rogaland complex, Norway. Earth and Planetary Science Letters 139, 335-350.

Schiellerup, H., Lambert, D. D., Prestvik, T., Robins, B., McBride, J. S., Larsen, R. B. (2000). Re-Os isotopic evidence for a lower crustal origin of massif-type anorthosites. Nature 405, 781-784.

Scoates, J. S. (2000). The plagioclase-magma density paradox re-examined and the crystallization of Proterozoic anorthosites. Journal of Petrology 41, 627-649.

Scoates, J. S. (2002). The plagioclase-magma density paradox re-examined and the crystallization of Proterozoic anorthosites: a reply. Journal of Petrology 43, 1979-1983.

Scoates, J. S. (2008). The parent magmas to Proterozoic anorthosites. GAC-MAC Joint Annual Meeting, Program with Abstracts, 155.

Scoates, J. S., Chamberlain, K. R. (1997). Orogenic to post-orogenic origin for the 1.76 Ga Horse Creek Anorthosite Complex, Wyoming, USA. The Journal of Geology 105, 331-343.

Scoates, J. S., Frost, C. D. (1996). A strontium and neodymium isotopic investigation of the Laramie anorthosites, Wyoming, USA: implications for magma chamber processes and the evolution of magma conduits in Proterozoic anorthosites. Geochimica et Cosmochimica Acta 60, 95-107.

Scoates, J. S., Frost, C. D., Mitchell, J. N., Lindsley, D. H., Frost, B. R. (1996). Residual-liquid origin for a monzonitic intrusion in a mid-Proterozoic anorthosite complex: The Sybille intrusion, Laramie anorthosite complex, Wyoming. GSA Bulletin 108, 1357-1371.

Scoates, J. S., Mitchell, J. N. (2000). The evolution of troctolitic and high Al basaltic magmas in Proterozoic anorthosite plutonic suites and implications for the Voisey`s Bay massive Ni-Cu sulfide deposit. Economic Geology 85, 677-701.

Seth, B., Armstrong, R. A., Brandt, S., Villa, I. M., Kramers, J. D. (2003). Mesoproterozoic U-Pb and Pb-Pb ages of granulites in NW Namibia: reconstructing a complete orogenic cycle. Precambrian Research 126, 147-168.

Seth, B., Armstrong, R. A., Büttner, A., Villa, I. M. (2005). Time constraints for Mesoproterozoic upper amphibolite facies metamorphism in NW Namibia: a multi-isotopic approach. Earth and Planetary Science Letters 230, 355-378.

Seth, B., Jung, S., Hoernes, S. (2002). Isotope constraints on the origin of Pan-African granitoid rocks in the Kaoko belt, NW Namibia. South African Journal of Geology 105, 179-192.

Seth, B., Kröner, A., Mezger, K., Nemchin, A. A., Pidgeon, R. T., Okrusch, M. (1998). Archaean to Neoproterozoic magmatic events in the Kaoko belt of NW Namibia and their geodynamic significance. Precambrian Research 92, 341-363.

Shannon, R. D. (1976). Revised effective ionic radii and systematic studies of interatomic distances in halides and chalcogenides. Acta Crystallographica 32, 751-767.

Shirey, S. B., Walker, R. J. (1998). The Re-Os isotope system in cosmochemistry and high-temperature geochemistry. Annual Review of Earth and Planetary Sciences 26, 423–500.

Shumlyanskyy, L., Ellam, R. M., Mitrokhin, O. (2006). The origin of basic rocks of the Koroston AMCG complex, Ukrainian shield: Implication of Nd and Sr isotope data. Lithos 90, 214-222.

Silva, L. C. (1972). O Maciqu Gabbro-Anorthositico do S.W. de Angola. Ciências Naturzis 17, 253-277.

Silva, Z. C. G. (1992). Mineralogy and cryptic layering of the Kunene anorthosite complex of SW Angola and Namibia. Mineralogical Magazine 56, 319–327.

Simpson, E. S. W., Otto, J. D. T. (1960). On the Precambrian anorthosite mass of southern Angola. International Geological Congress 13, 216-227.

Slejko, F. F., Demarchi, G., Morais, E. (2002). Mineral chemistry and Nd isotopic composition of two anorthositic rocks from the Kunene complex (South western Angola). Journal of African Earth Sciences 35, 77–88.

Speczik, S., Wiszniewska, J., Diedel, R. (1988). Minerals, exsolution features and geochemistry of Fe-Ti ores of the Suwałki District (North-East Poland). Mineralium Deposita 23, 200-210.

Sproule, R. A., Lambert, D. D., Hoatson, D. M. (2002). Decoupling of the Sm-Nd and Re-Os isotopic systems in sulphide-saturated magams in the Halls Creek Orogen, Western Australia. Journal of Petrology 43, 375-402.

Streckeisen, A. (1976). To each plutonic rock its proper name. Earth-Science Reviews 12, 1-33.

Steiger, R. H., Jäger, E. (1977). Subcommission on geochronology: convention on the use of decay constants in geo- and cosmochronology. Earth and Planetary Science Letters 36, 359–362.

Sun, S., McDonough, W. F. (1989). Chemical and isotopic systematic of oceanic basalts: implications for mantle composition and processes. In: Saunders, A. D. & Norry, M. J. (eds.) Magmatism in the Ocean Basins. Geological Society Special Publications 42, 313-345.

Taylor, H. P. (1968). The oxygen isotope geochemistry of igneous rocks. Contributions to Mineralogy and Petrology 19, 1-71.

Taylor, H. P. (1980). The effects of assimilation of country rocks by magmas on $^{18}O/^{16}O$ and $^{87}Sr/^{86}Sr$ systematics in igneous rocks. Earth and Planetary Science Letters 47, 243-254.

Taylor, S. R., McLennan, S. M. (1985). The continental crust: its composition and evolution. Blackwell Scientific, Boston, 312 p.

Taylor, S. R., Campbell, I. H., McCulloch, M. T., McLennan, S. M. (1984). A lower crustal origin for massif-type anorthosites. Nature 311, 372-374.

Tegtmeyer, A., Kröner, A. (1985). U-Pb zircon ages for granitoid gneisses in northern Namibia and their significance for Proterozoic crustal evolution of Southwestern Africa. Precambrian Research 28, 311-326.

Tollari, N., Barnes, S. J., Cox, R. A., Nabil, H. (2008). Trace element concentrations in apatites from the Sept-Îles Intrusive Suite, Canada - Implications for the genesis of nelsonites. Chemical Geology 252, 180-190.

Toplis, M. J. (2005). The thermodynamics of iron and magnesium partitioning between olivine and liquid: criteria for assessing and predicting equilibrium in natural and experimental systems. Contributions to Mineralogy and Petrology 149, 22-39.

Vander Auwera, J., Longhi, J., Duchesne, J. C. (1998). A liquid line of decent of the jotunite (hypersthene monzodiorite) suite. Journal of Petrology 39, 439-468.

Vander Auwera, J., Longhi, J., Duchesne, J. C. (2000). The effect of pressure on D_{Sr} (plag/melt) and D_{Cr} (opx/melt): implications for anorthosite petrogenesis. Earth Planetary Science Letters 178, 303-314.

Vander Auwera, J., Weis, D., Duchesne, J. C. (2006). Marginal mafic intrusions as indicators of downslope draining of dense residual melts in anorthositic diapirs? Lithos 89, 329-352.

Valley, J. W., Kitchen, N., Kohn, M. J., Niendorf, C. R., Spicuzza, M. J. (1995). UWG-2, a garnet standard for oxygen isotope ratios: strategies for high precision and accuracy with laser heating. Geochimica et Cosmochimica Acta 59, 5223-5231.

Valley, J. W., O'Neil, J. R. (1982). Oxygen isotope evidence for shallow emplacement of Adirondack anorthosite. Nature 300, 497-500.

Vermaak, C. F. (1981). Kunene Anorthosite Complex. In: Hunter, D. F. (ed) Precambrian of the southern hemisphere. Elsevier Amsterdam, 882 p.

von Seckendorff, V., Drüppel, K., Okrusch, M., Cook, N. J., Littmann, S. (2000). Oxide-sulphide relationships in sodalite-bearing metasomatites of the Epembe-Swartbooisdrif Alkaline Province, north-west Namibia. Mineralium Deposita 35, 430-450.

Ulmer, P. (1989). The dependence of the Fe^{2+}-Mg cation-partitioning between olivine and basaltic liquid on pressure, temperature and composition An experimental study to 30 kbars. Contributions to Mineralogy and Petrology 101, 261-273.

Waychunas, G. A. (1991). Crystal chemistry of oxides and oxyhydroxides, in: Lindsley, D.H. (ed), Oxide minerals: Petrologic and magnetic significance. Reviews in Mineralogy 25, 11-68.

Weis, D. (1986). Genetic implications of Pb isotopic geochemistry in the Rogaland anorthositic complex (southwest Norway). Chemical Geology 57, 181-199.

Wiebe, R. A. (1980). Anorthositic magmas and the origin of Proterozoic anorthosite massifs. Nature 286, 564-567.

Wiebe, R. A. (1990). Evidence for unusually feldspathic liquids in the Nain complex, Labrador. American Mineralogist 75, 1-12.

Wiebe, R. A. (1992). Proterozoic anorthosite complexes. In: Condie, K. C. (ed) Proterozoic crustal evolution. Elsevier, 215-261.

Wilmart, E., Pineau, F., Réjou-Michel, A., Duchesne, J. C. (1994). Fluid transfer in anorthosites and related rocks from Rogaland (Southwest Norway): Evidence from stable isotopes. Earth and Planetary Science Letters 125, 55-70.

Wilson, A. D. (1960). The micro-determination of ferrous iron in silicate minerals by a volumetric and a colorimetric method. The Analyst 85, 823-827.

Windley, B. F. (1993). Proterozoic anorogenic magmatism and its orogenic connections. Journal of the Geological Society, London 150, 39-50.

Wisniewska J., Claesson, S., Stein, H. J., Vander Auwera, J., Duchesne, J. C. (2002). The north-eastern Polish anorthosite massifs: petrological, geochemical and isotopic evidence for a crustal derivation. Terra Nova 14, 451-460.

Zartman, R. E., Doe, B. R. (1981). Plumbotectonics – the model. Tectonophysics 75, 135-162.

Zhao, Z-F., Zheng, Y-F. (2003). Calculation of oxygen isotope fractionation in magmatic rocks. Chemical Geology 193, 59-80.

Zheng, Y-F. (1991). Calculation of oxygen isotope fractionation in metal oxides. Geochimica et Cosmochimica Acta 55, 2299-2307.

Zheng, Y-F. (1993). Calculation of oxygen isotope fractionation in anhydrous silicate minerals. Geochimica et Cosmochimica Acta 57, 1079-1091.

Geological map of Namibia 1:250,000 Sheet 1712-Swartbooisdrif (2002). Geological Survey of Namibia, Windhoek